



Titre: Morphology of ethylene-propylene-diene terpolymer/polypropylene
Title: (EPDM/PP) blends and their thermoplastic vulcanizates

Auteur: Prashant Bhadane
Author:

Date: 2005

Type: Mémoire ou thèse / Dissertation or Thesis

Référence: Bhadane, P. (2005). Morphology of ethylene-propylene-diene
terpolymer/polypropylene (EPDM/PP) blends and their thermoplastic vulcanizates
Citation: [Thèse de doctorat, École Polytechnique de Montréal]. PolyPublie.
<https://publications.polymtl.ca/7549/>

 **Document en libre accès dans PolyPublie**
Open Access document in PolyPublie

URL de PolyPublie: <https://publications.polymtl.ca/7549/>
PolyPublie URL:

**Directeurs de
recherche:**
Advisors:

Programme: Non spécifié
Program:

UNIVERSITÉ DE MONTRÉAL

MORPHOLOGY OF ETHYLENE-PROPYLENE-DIENE
TERPOLYMER/POLYPROPYLENE (EPDM/PP) BLENDS AND THEIR
THERMOPLASTIC VULCANIZATES

PRASHANT BHADANE
DÉPARTEMENT DE GÉNIE CHIMIQUE
ÉCOLE POLYTECHNIQUE DE MONTRÉAL

THÈSE PRÉSENTÉE EN VUE DE L'OBTENTION
DU DIPLÔME DE PHILOSOPHIAE DOCTOR
(GÉNIE CHIMIQUE)
DÉCEMBRE 2005

© Prashant Bhadane, 2005.



Library and
Archives Canada

Bibliothèque et
Archives Canada

Published Heritage
Branch

Direction du
Patrimoine de l'édition

395 Wellington Street
Ottawa ON K1A 0N4
Canada

395, rue Wellington
Ottawa ON K1A 0N4
Canada

Your file Votre référence

ISBN: 978-0-494-16982-7

Our file Notre référence

ISBN: 978-0-494-16982-7

NOTICE:

The author has granted a non-exclusive license allowing Library and Archives Canada to reproduce, publish, archive, preserve, conserve, communicate to the public by telecommunication or on the Internet, loan, distribute and sell theses worldwide, for commercial or non-commercial purposes, in microform, paper, electronic and/or any other formats.

The author retains copyright ownership and moral rights in this thesis. Neither the thesis nor substantial extracts from it may be printed or otherwise reproduced without the author's permission.

AVIS:

L'auteur a accordé une licence non exclusive permettant à la Bibliothèque et Archives Canada de reproduire, publier, archiver, sauvegarder, conserver, transmettre au public par télécommunication ou par l'Internet, prêter, distribuer et vendre des thèses partout dans le monde, à des fins commerciales ou autres, sur support microforme, papier, électronique et/ou autres formats.

L'auteur conserve la propriété du droit d'auteur et des droits moraux qui protègent cette thèse. Ni la thèse ni des extraits substantiels de celle-ci ne doivent être imprimés ou autrement reproduits sans son autorisation.

In compliance with the Canadian Privacy Act some supporting forms may have been removed from this thesis.

Conformément à la loi canadienne sur la protection de la vie privée, quelques formulaires secondaires ont été enlevés de cette thèse.

While these forms may be included in the document page count, their removal does not represent any loss of content from the thesis.

Bien que ces formulaires aient inclus dans la pagination, il n'y aura aucun contenu manquant.


Canada

UNIVERSITÉ DE MONTRÉAL

ÉCOLE POLYTECHNIQUE DE MONTRÉAL

Cette thèse intitulée :

MORPHOLOGY OF ETHYLENE-PROPYLENE-DIENE
TERPOLYMER/POLYPROPYLENE (EPDM/PP) BLENDS AND THEIR
THERMOPLASTIC VULCANIZATES

présentée par : BHADANE Prashant

en vue de l'obtention du diplôme de : Philosophie Doctor

a été dûment acceptée par le jury d'examen constitué de :

M. PATIENCE Gregory S., Ph.D., président

M. FAVIS Basil D., Ph.D., membre et directeur de recherche

M. HUNEAULT Michel A., Ph.D., membre et codirecteur de recherche

M. DUBOIS Charles, Ph.D., membre

M. COLE Kenneth, Ph.D., membre

Dedicated

To

my father Arun, my mother Nirmala,

and my wife Vidya

ACKNOWLEDGEMENTS

I would like to express my heartfelt gratitude to my research and thesis director Professor Basil D. Favis for providing me an opportunity to study under his supervision. Indeed, I am very indebted to him for his guidance, motivation and help throughout my study at the École Polytechnique de Montréal. I am also very thankful to him for his kind affection during the painful and difficult times, when my father deceased, towards me and my family. His encouragement inspired me to go through all the difficulties in the research. His accurate, practical and realistic attitude toward scientific research will certainly hold positive influences on my career and personal life.

I would also like to thank my research co-director Michel Huneault, as well as Michel Champagne, and Florin Tofan for their expertise, cooperation, and kind understanding throughout this work. They were indeed there to help me whenever I needed them.

I would like to express my sincere gratitude to the other Professors and technical staff of the Chemical Engineering department at the École Polytechnique de Montréal and at the Industrial Materials Institute, Boucherville, for their help in different aspects.

I would also like to thank my colleagues Jianming, Pei Lian, Pierre, Nick, Xavier, Joel, Kiril, other friends Ramin, Maryam, Sho Koh, and best pals Shashank, Kanchan, Mayur, Adinath, Atul, Sandeep for their friendship, help and cooperation during my study. My thanks also go to Unde sir for his efforts, faith, and able guidance,

my sister Manisha, and uncles Ashok (motha-mama), and Mukund (nana-mama). At this time, I also remember my niece, Priyal, for her love.

Finally, I would like to say more than thanks to my mother, Nirmala, and father, Arun, who took innumerable pain for me, not only during this research work but through all of my life, and to my beloved wife, Vidya, for her love, caring, faith, patience and encouragement which are indispensable in accomplishment of my study. I am also grateful to God for simply 'everything'.

RÉSUMÉ

Le développement de la continuité des phases et des morphologies co-continues est fortement influencé par la nature de l'interface dans les mélanges immiscibles de polymères. Généralement, les interfaces peuvent être définies comme étant binaires compatibles, binaires incompatibles ou ternaires compatibles. Cette thèse porte sur l'étude de la morphologie, le développement de la continuité et de la co-continuité dans les mélanges de polymères ayant une basse tension interfaciale, c'est-à-dire les mélanges avec une interface de type binaire compatible. L'effet de la réticulation dynamique sur la continuité et la co-continuité est aussi examiné.

La très basse tension interfaciale dans les systèmes EPDM/PP rend ces mélanges intéressants pour de telles investigations. La valeur de la tension interfaciale obtenue par l'équation de la moyenne harmonique entre ces deux polymères est estimée à 0.3 mN/m lors de la mise en forme à 190°C. Des mélanges de EPDM/PP avec un rapport de viscosité variant de 0.1 à 17.0, un rapport d'élasticité variant de 0.1 à 29 et une contrainte en cisaillement de la matrice variant de 11.7 kPa à 231.4 kPa ont été préparés à l'état fondu dans un mélangeur interne. Il a été montré que les phases de ces mélanges sont complètement immiscibles après refroidissement.

Dans les mélanges EPDM/PP possédant un rapport de viscosité faible ou moyen (de 0.2 à 5.0), la microscopie électronique à balayage (SEM) et la microscopie à force atomique (AFM) ont montré que la phase dispersée est distribuée très uniformément et forme de très petits domaines de quelques centaines de nanomètres de diamètres. Contre

toute attente, en dissolvant sélectivement la matrice, il a été montré que la phase dispersée dans ces mélanges existe sous la forme de nano fibres de quelques 50-200 nm de diamètre. Une analyse du temps de rupture des fibres suivant la théorie de Tomotika supporte également la présence de fibres dispersées très stables.

En augmentant la composition de la phase mineure, il a été montré que ces fibres coalescent à partir d'un certain point et permettent le développement de la continuité. Dès lors, le système atteint la co-continuité par la coalescence fibre-fibre. Le développement de la continuité pour les deux constituants du mélange est étudié. Dans toutes ces expériences, lorsqu'il est nécessaire de dissoudre la phase PP sans dissoudre la phase EPDM, la phase EPDM est initialement réticulée par irradiation après l'étape de mélange. Un développement de la continuité hautement symétrique et identique par rapport à la composition médiane est observé pour ces mélanges à bas et moyens rapports de viscosité. En fait, une courbe maîtresse unique pour le développement de la continuité peut être obtenue pour ces mélanges. Il est aussi observé que la taille des particules est indépendante du rapport de viscosité, mais qu'elle varie significativement lorsque la contrainte en cisaillement varie par un facteur 8.

Contrairement à d'autres mélanges ayant une faible tension interfaciale, les mélanges EPDM/PP démontrent des seuils de percolation élevés, un développement de la continuité retardé, une zone de co-continuité relativement étroite suivant la composition (sur environ 20%), et démontrent un haut niveau de coalescence. Les mélanges EPDM/PP démontrent donc plusieurs caractéristiques morphologiques de

mélanges partiellement miscibles, malgré le fait que l'analyse des températures de transition vitreuse montre que ces matériaux sont complètement immiscibles après la préparation et le refroidissement des mélanges. Comme les caractéristiques morphologiques dominantes des mélanges sont formées durant l'étape de mélange, ces résultats indiquent que les mélanges sont partiellement miscibles durant l'étape de mélange. Cependant, ils deviennent complètement immiscibles durant l'étape de refroidissement subséquente. Le refroidissement des mélanges est donc suffisamment rapide pour permettre de préserver l'empreinte de cette miscibilité partielle au niveau de la morphologie des mélanges.

Cependant, si on augmente encore davantage le rapport de viscosité ($p = 11$ et 17), la morphologie des mélanges EPDM/PP subit de grandes modifications. Pour ces mélanges, la phase dispersée est constituée d'une variété de structures morphologiques inaccoutumées, incluant des fibres nanométriques stables, de très grosses particules, des particules partiellement coalescées, ainsi que de nombreuses particules interconnectées par des fibres de diamètres nanométriques. Cette combinaison inusitée de plusieurs types de morphologies donne lieu à une nouvelle structure co-continue de particules partiellement coalescées et de particules interconnectées par des fibres stables. Ainsi, les mélanges ayant un rapport de viscosité élevé sont caractérisés par des seuils de percolation à plus faible concentration que pour les mélanges dont les rapports de viscosité sont faibles ou intermédiaires. On observe alors un développement rapide de la continuité de la phase dispersée et la co-continuité est atteinte à des concentrations de phase mineure plus faibles que prévues.

L'érosion lente de la surface de la phase EPDM, de viscosité élevée pendant l'opération de mélange à l'état fondu, est à l'origine de ces structures morphologiques inhabituelles. Généralement, les phénomènes d'érosion se produisent très rapidement, de sorte que leur étude précise pendant l'opération de mélange est difficilement envisageable. Par ailleurs, la majorité des études se concentrent sur la morphologie finale du mélange, lorsqu'un état stationnaire est atteint après plusieurs minutes de mélange. En raison de la très faible tension interfaciale dans les systèmes EPDM/PP, les mélanges ayant des rapports de viscosité très élevés nous donnent l'opportunité unique d'examiner les phénomènes d'érosion, qui persistent sur de longues durées pendant l'opération de mélange à l'état fondu. De tels phénomènes d'érosion apparaissent parce que la contrainte transférée par la matrice (faible viscosité) ne suffit pas à déformer complètement et à désintégrer les particules de la phase dispersée (viscosité élevée). Néanmoins, si la contrainte transférée par la matrice est supérieure à une valeur critique, alors localement la viscosité de la matière à la surface d'une particule de haute viscosité diminue. La surface de la particule devient alors beaucoup moins visqueuse que le cœur en raison d'un effet rhéofluidifiant du matériau. Dans une telle situation, la particule ne peut garder plus longtemps la matière à la surface, de sorte que celle-ci commence à se retirer de la surface. La matière érodée forme alors des fibres nanométriques extrêmement stables en raison de la très faible tension interfaciale entre les composants du mélange et de la très haute viscosité de la phase dispersée.

Afin d'expliquer ce phénomène d'érosion qui dépend de la concentration de la phase dispersée, nous proposons un nouveau mécanisme, basé sur la dynamique des

collisions, de la coalescence et de la séparation des particules. Pour ce type d'érosion, les deux particules de forte viscosité s'interpénètrent partiellement, à l'origine d'une coalescence partielle à la surface des particules après collision. Cependant, en raison de la viscosité élevée des gouttelettes et sous l'influence du cisaillement, les gouttelettes partiellement coalescées se retirent par la suite chacune de leur côté. La séparation des gouttelettes entraîne la formation d'une ou de plusieurs fibres stables entre les particules là où elles étaient précédemment en contact. En tenant compte de l'augmentation du nombre de collisions pour des concentrations de phase dispersée plus élevées, le mécanisme proposé indique que le processus d'érosion est dramatiquement accéléré et permet ainsi de maintenir la co-continuité sur de longues durées de mélange.

Les mélanges co-continus avec des rapports de viscosité de 0.7 et 5.0 montrent, après réticulation, que le réseau initial co-continu de la phase EPDM non réticulée (réseau α) se transforme en un réseau beaucoup plus fin d'EPDM réticulé (réseau β). Les images à haute résolution sont obtenues avec une nouvelle technique d'analyse de la morphologie. Cette méthode consiste à préparer la surface des échantillons par gravure avec un faisceau ionique focalisé (FIB), suivie d'une analyse de la topographie de la surface avec un microscope à force atomique fonctionnant en mode dynamique (« Tapping Mode Atomic Force Microscope », TMAFM). Il est montré que les taux de gravures ioniques du PP et de l'EPDM sont significativement différents. Dès lors, ce traitement mène à un contraste topographique entre les différentes phases lorsque la surface est subséquentement analysée au TMAFM. Cette technique permet d'observer clairement la phase dispersée à une taille aussi petite que 100 nm. Puisque les taux de

gravure de la phase EPDM non réticulée et de la phase EPDM réticulée sont similaires, la phase EPDM non réticulée est sélectivement extraite à l'aide d'un solvant afin d'augmenter le contraste topographique entre les phases. Cette nouvelle combinaison de méthodes permet de clairement distinguer le polypropylène, de même que les phases EPDM non réticulée et réticulée.

Les micrographies et l'intégrité des échantillons après la mesure du contenu en EPDM réticulé suggèrent un haut niveau d'interconnectivité dans le réseau β . Il est suggéré que ce réseau β est produit suite à une différence de viscosité entre les phases EPDM non réticulée et réticulée. Au fur et à mesure que la phase EPDM réticulée se sépare de la phase non réticulée, un effet d'étalement se produit. La réticulation dynamique, dès lors, modifie significativement la morphologie co-continue.

Il est montré que le réseau α initial maintient sa continuité tout au long du processus de réticulation et que la taille des pores de ce réseau diminue au cours de la réticulation. De plus, après extraction de la phase non réticulée, aucune trace de la phase réticulée n'est trouvée dans le matériau extrait. Comme la réaction de réticulation est très rapide, ces résultats indiquent que la réaction de réticulation se déroule initialement sur l'enveloppe externe de la phase EPDM et procède graduellement vers le centre.

ABSTRACT

Phase continuity development and co-continuous morphologies are highly influenced by the nature of the interface in immiscible polymer blends. Broadly, the interfaces can be classified as binary compatible, binary incompatible, and ternary compatible type. This thesis evaluates morphology, continuity development and cocontinuity in polymer blends of low interfacial tension, i.e. binary compatible type of interface. The effect of dynamic crosslinking on the continuity and cocontinuity is also examined.

Besides considerable commercial significance, an ultra-low interfacial tension between ethylene-propylene-diene terpolymer (EPDM) and polypropylene (PP) makes this system an ideal model for such investigations. Using the harmonic mean equation, the value of interfacial tension between these materials is estimated to be 0.3 mN/m at a melt blending temperature of 190°C. Overall, EPDM/PP blends of viscosity ratios from 0.1 – 17.0, elasticity ratios from 0.1 – 29, and matrix shear stresses from 11.7 – 231.4 kPa were prepared by melt mixing in an internal mixer. The blend components are shown to be completely immiscible with each other after cooling from the melt.

In EPDM/PP blends of low to medium viscosity ratios (0.2 – 5.0), using scanning electron microscopy (SEM) and atomic force microscopy (AFM) it is shown that the dispersed phase is distributed very uniformly and forms very fine domains, only of a few hundred nanometers in diameter. Contrary to current belief, by selectively dissolving the matrices it is shown that the dispersed phase in this blend system actually

exists in the form of stable nano-fibers of about 50-200 nm in diameter. An analysis of thread break-up times from Tomotika theory also supports the notion of highly stable dispersed fiber formation.

With an increase in composition of minor phase, these fibers are shown to coalesce at crossover points to develop continuity. Thus, the system achieves cocontinuity by fiber-fiber coalescence. The continuity development for both the blend components is studied. In all these experiments, whenever it was necessary to dissolve the PP phase without dissolving the EPDM phase, the EPDM phase was irradiation crosslinked after melt blending. A highly symmetrical and identical continuity development with respect to mid-composition is observed at these low to medium viscosity ratios. In fact, a single master curve for the continuity development can be drawn for these blends. The particle sizes are also observed to be insensitive to the variations in viscosity ratio; however, an 8-fold variation in the shear stress has an effect.

Contrary to other low interfacial tension systems, however, the blends demonstrate artificially high percolation thresholds, delayed continuity development, maintain cocontinuity over very small (only over 20) composition units, and demonstrate high coalescence. EPDM/PP blends, thus, demonstrate several of the morphological features of a partially miscible system, despite the fact that the glass transition temperatures indicate these materials are completely immiscible after melt mixing and cooling. Since the dominant morphological features of the blend are

established during melt blending, these results indicate that the blends were partially miscible during melt blending but become fully phase separated upon cooling. The quenching of the blends from the melt is clearly rapid enough to preserve the imprint of that partial miscibility on the blend morphology after cooling.

A further increase in the viscosity ratio (11 and 17), however, is shown to have a dramatic effect on all aspects of the morphology in EPDM/PP blends. The dispersed phase in these blends is demonstrated to coexist in a variety of unusual morphological structures, including: isolated stable nano-fibers, very large particles, partially coalesced particles, and numerous particles interconnected by nano-fibers. This unusual combination of variety of morphologies leads the blend to a novel cocontinuous structure of partially coalesced particles and particles interconnected by stable fibers. Consequently, compared to the low to medium viscosity ratio blends, the high viscosity ratio blends unexpectedly demonstrate early percolation thresholds, rapid continuity development, and attain cocontinuity at lower than expected compositions of the minor phase.

The slow surface erosion of high viscosity EPDM phase during melt blending is shown to be responsible for the generation of these unusual morphological structures. Typically the time scale for erosion phenomena are so small, that they have defied study in the mixing environment itself and typical blend morphology studies almost always examine the final steady-state morphology obtained after several minutes of mixing. The combination of very low interfacial tension and very high viscosity ratios of these

EPDM/PP systems provide a unique opportunity to examine erosion phenomena persisting over longer time scales during melt mixing. In high viscosity ratio blends such erosion phenomenon occurs because the stress transferred by the low viscosity matrix is insufficient to completely deform and disintegrate the high viscosity particles in the blend. Nevertheless, if the stress transferred by the matrix is more than a critical value then the local viscosity of the material on the surface of a large high viscosity particle drops. The shear stress does not get transferred to the core because of the high viscosity of the droplet. Thus, the surface of the particle becomes much less viscous than its core because of the shear thinning of the material. Under such circumstances, the particle can no longer sustain material at the surface and starts giving away this material. The eroded material is shown to form extremely stable nano-fibers because of the ultra-low interfacial tension between the blend components and very high viscosity of the fiber material.

In addition, a new concentration-dependent erosion mechanism based on particle collision-coalescence-separation dynamics is proposed. In this type of erosion the two particles of highly viscous material partially penetrate each other, causing partial coalescence at the surface of the particles, after collision. However, due to the high viscosity of the droplets and under the influence of shear the partially coalesced droplets recoil. The separation draws stable nano-fiber(s) between the particles, since the particles were coalesced at the surface before separation. Based on increased particle-particle collisions at higher compositions, the proposed mechanism is shown to

dramatically accelerate the erosion process and maintain cocontinuity over prolonged periods of mixing.

On dynamically crosslinking the cocontinuous morphologies in 0.7 and 5.0 viscosity ratio blends, the high resolution images, surprisingly, indicate that a non-crosslinked co-continuous EPDM phase (α -network) transits to a much finer network of crosslinked EPDM (β -network). The high resolution images are obtained by a novel technique of morphology investigation involving focused ion beam (FIB) etching of the sample surface followed by topological investigation of the sample surface using tapping mode atomic force microscopy (TMAFM). It is shown that the FIB ion etching rate of EPDM and PP is distinctly different. Thus, this treatment leads to a topological contrast between the phases when subsequently analyzed by TMAFM. The technique allows for the clear observation of phases as small as 100 nanometers. Since the ion etching rates of non-crosslinked and crosslinked EPDM are similar, the non-crosslinked EPDM phase is selectively removed from the sample by solvent dissolution to create an additional topological contrast. This novel combination of techniques allows for the clear distinction of polypropylene as well as non-crosslinked and crosslinked EPDM phases in the blend.

The micrographs and the sample integrity after gel content measurement suggest a high level of interconnectivity in the β -network. It is suggested that this β -network is produced as a result of the viscosity mismatch between non-crosslinked and crosslinked EPDM created due to crosslinking. As the crosslinked material pulls away from the

non-crosslinked material under dynamic melt mixing conditions, it creates a smearing effect. The dynamic crosslinking, therefore, dramatically modifies the cocontinuous morphology.

It is shown that the initial α -network maintains its continuity and demonstrates a diminished pore diameter as crosslinking proceeds. Furthermore, when the non-crosslinked material is extracted no crosslinked phase is found to be present in the extract. As the crosslinking reaction rate is very high, these results indicate that the crosslinking proceeds initially at the outer envelope of the EPDM phase and works its way towards the center.

CONDENSÉ EN FRANÇAIS

L'objectif de cette thèse est d'effectuer une étude détaillée de la morphologie des mélanges à l'état fondu dans un mélangeur interne du terpolymère éthylène-propylène-diène / polypropylène (EPDM/PP) et de leurs vulcanisés thermoplastiques (TPV). En particulier, cette thèse porte sur l'étude du développement de la continuité et de la co-continuité dans les mélanges de polymères caractérisés par une tension interfaciale très faible, et sur l'effet de paramètres fondamentaux tels que les rapports de viscosité et d'élasticité. Les mélanges non réticulés ont été étudiés de manière approfondie, notamment la caractérisation des structures co-continues. Ensuite, l'influence de la vulcanisation dynamique sur la morphologie co-continue a été examinée, en réticulant la phase élastomère du mélange grâce au monomère diène de l'EPDM.

L'utilisation de trois EPDM ayant des viscosités de Mooney différentes et de deux polypropylènes de poids moléculaires très différents pour les mélanges a permis de faire varier les rapports de viscosité et d'élasticité. Au total, des mélanges EPDM/PP de rapports de viscosité entre 0.1 et 17.0, de rapports d'élasticité entre 0.1 et 29, et de contraintes de cisaillement pour la matrice entre 11.7 et 231.4 KPa, ont été préparés. En utilisant l'équation de la moyenne harmonique, la valeur de la tension interfaciale entre ces deux matériaux a été estimée à 0.3 mN/m, pour une température de mélange de 190°C. L'estimation expérimentale de la tension interfaciale par la méthode du fil

cassant a été entreprise mais n'a pas donné les résultats escomptés en raison de la valeur extrêmement faible de celle-ci.

La miscibilité entre les composants du mélange a été déterminée en mesurant la température de transition vitreuse des mélanges comprenant les composants de plus bas poids moléculaires, c'est-à-dire EP 1 et PP 2, par analyse thermo-mécanique dynamique (DMTA) à la température ambiante. Les résultats indiquent que les mélanges EPDM/PP sont complètement immiscibles sur toute la gamme de composition. Comme la teneur en éthylène est très semblable pour tous les EPDM utilisés dans ce travail, on peut supposer par extrapolation que tous les autres mélanges effectués à partir de polymères de plus hauts poids moléculaires sont complètement immiscibles après refroidissement à partir de l'état fondu.

Le développement de la morphologie de l'EPDM a été étudié en dissolvant la phase dispersée EPDM à la température ambiante. Les micrographies ont été obtenues par microscopie électronique en balayage (SEM) et par microscopie à force atomique (AFM). La taille des phases a été quantifiée par analyse d'image sur les micrographies. Par ailleurs, la dissolution de la phase matrice a permis de déterminer la structure tridimensionnelle de la phase dispersée. Le développement de la continuité et la région de co-continuité ont été déterminés par gravimétrie après dissolution sélective. Lorsqu'il était nécessaire de dissoudre la phase PP sans dissoudre pour autant la phase EPDM, les mélanges ont été réticulés par irradiation après l'opération de mélange à l'état fondu.

Les mélanges ayant un rapport de viscosité de faible à moyen, de 0.2 à 5.0, indiquent que la phase dispersée, aux faibles concentrations, est distribuée très finement et uniformément à travers la phase matrice. En moyenne, la taille des phases a été estimée à 50-200 nm en diamètre. À l'encontre de la conviction répandue que la phase dispersée existe sous la forme de gouttelettes sphériques dans ce système de polymères, l'étude de la dissolution de la matrice montre que la phase dispersée est en fait présente sous la forme de fibres stables ayant un diamètre extrêmement petit. Une telle morphologie est supportée par la théorie de Tomotika, lorsqu'on calcule les durées nécessaires à la rupture de fils de diamètres semblables.

En augmentant la concentration, ces fibres coalescent lorsqu'elles se rencontrent pour développer la continuité et la co-continuité suivant le comportement proposé pour les systèmes binaires compatibles. Lorsque le rapport de viscosité varie de 0.7 à 5.0, on observe peu d'effet sur la taille des phases, la forme de la phase dispersée, le % de continuité, la région de co-continuité. Cependant une variation d'un facteur 8 en contrainte de cisaillement de la matrice affecte les dimensions des particules. Ces mélanges sont caractérisés par un développement de la continuité vraiment symétrique par rapport à la composition 50/50.

Bien qu'ils suivent la plupart des caractéristiques des systèmes binaires compatibles, ces mélanges présentent de nombreuses particularités inattendues telles que : seuil de percolation artificiellement élevé, développement de la continuité retardé, co-continuité à des concentrations de la phase mineure plus élevées que prévues, et ainsi

une gamme plus étroite de co-continuité, et une coalescence élevée avec la composition. Ces caractéristiques sont typiques des systèmes partiellement miscibles. Étant donné que ces caractéristiques morphologiques dominantes se développent pendant l'opération de mélange, les résultats suggèrent que les mélanges sont partiellement miscibles à l'état fondu. Néanmoins, en raison de la nature cristalline du PP, les phases partiellement miscibles sont forcées de se séparer complètement au cours du refroidissement à l'issue de l'opération de mélange, comme le révèlent les températures de transition vitreuse mesurées sur les échantillons trempés. Clairement, la trempe des mélanges à partir de l'état fondu est suffisamment rapide pour préserver une empreinte de la miscibilité partielle à l'état fondu sur la morphologie du mélange après refroidissement.

Pour des rapports de viscosité plus élevés, entre 11 et 17, on observe en revanche des modifications importantes de la morphologie des mélanges. En plus de nano-fibres stables isolées, la phase dispersée se présente aussi sous la forme de larges particules, de particules partiellement coalescées et de particules interconnectées par des nano-fibres. Cette combinaison inhabituelle d'une variété de morphologies permet d'obtenir une nouvelle structure co-continue constituée de particules partiellement coalescées et de particules interconnectées par des fibres stables. Les mélanges ayant des rapports de viscosité élevés sont ainsi caractérisés par des seuils de percolation à des concentrations plus faibles, un développement rapide de la continuité, et atteignent la co-continuité à des concentrations en phase mineure plus faibles que prévues. Comparés

aux mélanges de rapports de viscosité faibles et moyens, ces mélanges démontrent une plus large mais asymétrique région co-continue.

Cette variété de morphologies générées est le résultat d'un lent procédé d'érosion de la surface de la phase EPDM de viscosité élevée. Les études sur la morphologie des mélanges examinent presque toujours la morphologie à l'état stationnaire obtenue après plusieurs minutes de mélange. Les durées pour parvenir à l'état stationnaire sont souvent si petites qu'elles empêchent l'étude de la morphologie à un état transitoire. Cependant, des mélanges ayant des rapports de viscosité élevés et une tension interfaciale extrêmement faible offrent une occasion unique d'examiner de tels phénomènes.

Lorsque le rapport de viscosité est élevé, le procédé d'érosion de la surface d'une particule prend place parce que la contrainte transférée par la matrice de faible viscosité est insuffisante pour déformer totalement et désintégrer les particules de haute viscosité. Cependant, si la contrainte transférée par la matrice est supérieure à un seuil critique, alors la viscosité locale de la matière à la surface d'une large particule diminue. La contrainte de cisaillement, cependant, ne peut être transférée au cœur de la particule en raison de la viscosité élevée de la gouttelette. Ainsi, la surface de la particule devient beaucoup moins visqueuse que le cœur en raison de l'effet rhéofluidifiant de la matière. Sous de telles circonstances, la particule ne peut plus soutenir la matière à sa surface qui commence à s'en aller. On observe alors que la matière érodée forme des nano-fibres extrêmement stables, dues à la tension interfaciale très faible entre les composants du

mélange et à la viscosité très élevée de la matière formant les fibres. La morphologie aux faibles concentrations n'est pas à l'état stationnaire, et le lent procédé d'érosion de la surface reste incomplet même après 30 minutes de mélange.

Pour des concentrations plus élevées, est proposé un nouveau mécanisme d'érosion dépendant de la concentration, basé sur la dynamique du phénomène collisions-coalescence-séparation des particules. Pour ce type d'érosion, les deux particules de forte viscosité se heurtent pendant l'opération de mélange et s'interpénètrent partiellement, à l'origine d'une coalescence partielle à la surface des particules après collision. Cependant, les gouttelettes partiellement coalescées s'étirent en raison de la viscosité élevée des gouttelettes, de tension interfaciale très faible et du cisaillement continu dans le mélangeur interne. La séparation des gouttelettes entraîne la formation d'une ou de plusieurs fibres stables entre les particules, là où elles étaient précédemment en contact. En tenant compte de l'augmentation du nombre de collisions pour des concentrations de phase dispersée plus élevées, le mécanisme proposé indique que le processus d'érosion est fortement accéléré et facilite ainsi la génération de fibres entre les deux particules se séparant sous les conditions de mélange dynamique, qui aide ainsi les mélanges à maintenir la co-continuité sur de longues durées de mélange.

Les morphologies co-continues pour les mélanges ayant des rapports de viscosité de 0.7 et 5.0 ont été réticulées à 50% et 100% en additionnant une quantité prédéterminée d'agent réticulant. Le degré de réticulation atteint pour chacun des mélanges est estimé en mesurant le contenu en gel. La morphologie des mélanges a été

analysée à l'aide d'une nouvelle méthode qui consiste à utiliser un faisceau ionique focalisé (FIB) pour préparer la surface d'analyse, puis à utiliser un microscope à force atomique en mode dynamique (TMAFM) pour étudier la topographie de surface. Il est montré que les taux de gravures ioniques du PP et de l'EPDM sont différents. Le traitement au FIB mène donc à un contraste topographique entre les phases lorsque la surface est subséquentement analysée au TMAFM. Le contraste généré par le traitement au FIB permet de mettre clairement en évidence des particules de la phase dispersée aussi petites que 100 nm de diamètre. Cette technique permet aussi de distinguer les particules d'oxyde de zinc dans le mélange.

Puisque les taux de gravure de l'EPDM non-réticulé et de l'EPDM réticulé sont semblables, la phase EPDM non réticulée est sélectivement extraite de l'échantillon à l'aide d'un solvant afin de créer un contraste topographique additionnel. Cette nouvelle combinaison de techniques permet de clairement distinguer le polypropylène, de même que les phases EPDM non réticulé et EPDM réticulé dans le mélange.

L'étude de l'EPDM non-réticulé a été effectuée par gravimétrie et par l'analyse de la taille des pores en utilisant la méthode d'adsorption d'azote (BET). La quantité de phase réticulée présente dans le solvant après extraction de la phase EPDM non réticulée est estimée en mesurant le poids de la membrane de filtration avant et après filtration.

Étonnamment, les résultats indiquent que la réticulation dynamique des morphologies co-continues (réseau α) mène à un réseau beaucoup plus fin d'EPDM

réticulé (réseau β). Les micrographies à haute résolution, combinées à l'intégrité de la structure des échantillons après la mesure du contenu en gel, suggèrent un haut niveau d'interconnectivité dans le réseau β . Le réseau α maintient également la co-continuité, mais la taille des pores diminue au fur et à mesure que la réaction de réticulation se déroule. Pour les rapports de viscosité étudiés, les résultats indiquent qu'il n'y pas de phase réticulée présente dans la phase EPDM non réticulée (réseau α). Puisque la vitesse de la réaction de réticulation est très rapide, ces résultats indiquent que la réticulation débute sur l'enveloppe externe de la phase EPDM et va progressivement vers le centre.

Le réseau β se développe dû à une différence de viscosité entre la phase EPDM réticulée et la phase EPDM non réticulée. Les micro-particules d'EPDM réticulé, en se détachant du réseau α , entraînent de l'EPDM non réticulé avec celles-ci. Ceci produit un effet d'étalement ayant comme conséquence de générer un réseau beaucoup plus fin. En se basant sur les micrographies et les autres résultats, un modèle du développement de la morphologie dans les mélanges EPDM/PP co-continus réticulés dynamiquement est présenté.

En se basant sur le travail de recherche effectué, plusieurs recommandations peuvent être formulées pour les travaux futurs.

Davantage de preuves devraient être présentées concernant la miscibilité partielle entre l'EPDM et le PP à la température de mélange. Pour ces travaux, une valeur juste de χ (paramètre d'interaction) sans l'effet de la deutération doit être

mesurée. Celle-ci peut être obtenue en prenant la racine carrée de la moyenne des carrés des deux valeurs de χ mesurées séparément, en effectuant la deutération d'un polymère à la fois. De plus, la morphologie dans le mélange fondu devrait être étudiée en échantillonnant de petites quantités de matériau directement dans le mélangeur interne et en gelant sur le champ la morphologie avec de l'azote liquide.

Davantage de preuves concernant la formation de nano-fibres dans les mélanges EPDM/PP à bas et moyens rapports de viscosité pourraient être amenées en enlevant tout d'abord couche par couche des tranches de matériau à l'aide du faisceau ionique focalisé (FIB), puis en analysant subséquemment la surface au SEM ou au AFM.

Pour les mélanges EPDM/PP avec des rapports de viscosité élevés et de faibles compositions en phase dispersée, i.e. dans les mélanges pour lesquels le phénomène d'érosion a été observé, le temps nécessaire pour atteindre la morphologie à l'équilibre et la morphologie à l'équilibre elle-même devraient être étudiés. Même si le développement de la continuité et de la morphologie pour un PP de faible viscosité dispersé dans une matrice EPDM de haute viscosité, i.e. dans les mélanges PP 1/EP 2 et PP 1/EP 3, ne devrait pas beaucoup différer de celui observé pour les mélanges à bas et à moyens rapports de viscosité, il est tout de même suggéré d'effectuer cette étude.

Concernant la partie de la vulcanisation dynamique, les prochaines études devraient porter sur la détermination des effets du degré de vulcanisation sur la miscibilité partielle entre les constituants du mélange lors du mélange et sur son rôle par

rapport au développement de la morphologie dans les thermoplastiques vulcanisés (TPV).

De plus, l'efficacité de l'agent réticulant envers l'EPDM et le PP doit être déterminée. La morphologie au tout début de la réticulation devrait être étudiée. Ce travail pourrait être effectué en additionnant une très petite quantité d'agent réticulant, avec différentes morphologies de départ, et aussi avec différents temps d'échantillonnage en gelant les échantillons prélevés directement de la chambre de mélange avec de l'azote liquide. Globalement, l'effet du degré de vulcanisation dynamique sur les différentes morphologies de départ doit être établi.

Davantage d'efforts sont nécessaires pour améliorer encore davantage le contraste entre les phases élastomères réticulées et non réticulées. Il est possible d'envisager soit une nouvelle technique, soit le développement d'un programme ou d'une méthode d'analyse des données de l'AFM permettant de distinguer de plus petites variations topographiques malgré la présence de pores profonds à la surface de l'échantillon après extraction sélective de la phase non réticulée. La forme et la taille des phases réticulées et non réticulées avec différents degrés de réticulation devraient aussi être étudiées. Pour obtenir des données plus précises concernant le diamètre des pores pour des mélanges réticulés dynamiquement, les mesures BET devraient être effectuées sur lyophilisés.

Les propriétés physiques, telles la résistance à l'impact, la résistance en traction, l'élongation à la rupture, etc., avant et après réticulation dynamique, devraient être mesurées.

Un des paramètres importants lors de la manufacture des TPV est la séquence d'addition des polymères et de l'agent réticulant. Les travaux futurs devraient étudier l'effet des différentes séquences d'addition et leurs effets sur la morphologie des mélanges.

La taille des phases et le diamètre des pores pour les systèmes à basse tension interfaciale sont connus pour être insensibles au rapport de viscosité, un phénomène qui à également été observé dans ce travail. Dès lors, un des principaux objectifs de ce travail, soit l'obtention de structures co-continues avec différentes tailles de pores, reste inachevé. Des structures co-continues avec différentes tailles de pores peuvent cependant être obtenues en variant la tension interfaciale entre les constituants du mélange. Différents TPV avec de plus hautes tensions interfaciales entre les phases, par exemple Nylon/élastomère, PET/élastomère, etc., devraient être mis en forme, de façon à pouvoir étudier l'effet de la vulcanisation dynamique sur la morphologie de ces mélanges.

Pour améliorer encore davantage les propriétés des TPV, il faudrait entreprendre l'étude des nanocomposites de TPV en leur additionnant des nano-argiles, des nanotubes de carbone, de la silice et d'autres charges.

TABLE OF CONTENTS

DEDICATION	IV
ACKNOWLEDGEMENTS.....	V
RÉSUMÉ.....	VII
ABSTRACT	XIII
CONDENSÉ EN FRANÇAIS.....	XIX
TABLE OF CONTENTS.....	XXX
LIST OF TABLES.....	XXXVII
LIST OF FIGURES.....	XXXVIII
LIST OF ANNEXES	XLV
NOMENCLATURE	XLVI
CHAPTER 1 : INTRODUCTION AND OBJECTIVES	1
1.1 Introduction	1
1.2 Objectives	5
CHAPTER 2 : LITERATURE REVIEW	8
2.1 Theory of droplet deformation and breakup.....	8

2.2 Coalescence in polymer blends	12
2.3 Percolation theory for the morphology development.....	16
2.4 Polymer blend morphologies.....	18
2.5 Continuity development and cocontinuity in polymer blends.....	21
2.5.1 Mathematical models for predicting the composition for phase inversion and cocontinuity.....	21
2.5.2 Methods for characterization of cocontinuous morphologies	28
2.5.2.1 SEM and image analysis.....	28
2.5.2.1.a Cocontinuity and cocontinuity balance	29
2.5.2.1.b Form factors.....	29
2.5.2.1.c Interfacial area to volume ratio and other methods	31
2.5.2.2 Atomic force microscopy (AFM)	33
2.5.2.3 BET and mercury porosimetry	34
2.5.2.4 Extraction gravimetric technique.....	36
2.5.3 Influence of various material related parameters on cocontinuity	37
2.5.3.1 Viscosity ratio, elasticity ratio, and composition	37
2.5.3.2 Interfacial tension	37
2.5.3.3 Interfacial modifier	43
2.5.4 Influence of processing related parameters on cocontinuity (miscellaneous variables affecting cocontinuity)	45
2.6 Literature related to EPDM/PP blends and their thermoplastic vulcanizates.....	53
2.6.1 History and introduction.....	53

2.6.2 Rheology of EPDM/PP blends	55
2.6.3 Morphology of EPDM/PP blends.....	56
2.6.4 Compatibilized EPDM/PP blend.....	63
2.6.5 Crystallization in EPDM/PP blends	65
2.6.6 Properties of EPDM/PP blends	66
2.6.7 Crosslinking systems	72
2.7 Conclusions of the literature review	76
2.8 Limitations of the previous work	79
CHAPTER 3 : ORGANIZATION OF THE ARTICLES.....	81
CHAPTER 4 : CONTINUITY DEVELOPMENT IN POLYMER BLENDS	
OF VERY LOW INTERFACIAL TENSION	87
4.1 Introduction	89
4.2 Experimental procedures	92
4.2.1 Materials	92
4.2.2 Rheological characterization	93
4.2.3 Melt blending	94
4.2.4 Irradiation crosslinking.....	95
4.2.5 Dynamic mechanical thermal analysis	96
4.2.6 Solvent extraction and gravimetry for % continuity	96
4.2.7 Characterization of phase morphology.....	97
4.2.8 BET measurement	98

4.2.9 Matrix dissolution.....	99
4.2.9.1 Complete matrix dissolution.....	99
4.2.9.2 Partial matrix dissolution.....	100
4.2.9.3 Complete matrix dissolution and the freeze drying.....	101
4.3 Results and discussions	102
4.3.1 Rheology	102
4.3.2 Interfacial tension and miscibility/immiscibility.....	104
4.3.3 Microstructure of EPDM/PP blends.....	107
4.3.3.1 EPDM minor phase	107
4.3.3.2 PP minor phase	115
4.3.4 Effect of EPDM composition on phase size.....	117
4.3.5 Effect of viscosity ratio and matrix viscosity on microstructure.....	118
4.3.6 Continuity development and cocontinuity.....	119
4.3.7 Morphological characteristics of partial miscibility.....	121
4.4 Conclusions	123

CHAPTER 5 : EROSION-CONTROLLED CONTINUITY DEVELOPMENT

IN HIGH VISCOSITY RATIO BLENDS OF VERY LOW

INTERFACIAL TENSION.....	129
5.1 Introduction	131
5.2 Experimental procedures	134
5.2.1 Materials.....	134

5.2.2 Rheological characterization	135
5.2.3 Melt blending	136
5.2.4 Irradiation crosslinking.....	136
5.2.5 Solvent extraction and gravimetry.....	137
5.2.6 Microtomy, scanning electron microscopy and image analysis.....	137
5.2.7 Pore diameter measurement	138
5.2.8 Matrix dissolution.....	139
5.3 Results and discussions	139
5.3.1 Rheology	139
5.3.2 Continuity development and cocontinuity.....	142
5.3.3 Microstructure of highly viscous EPDM in PP matrix.....	144
5.3.3.1 Erosion phenomenon	147
5.4 Conclusions	156

CHAPTER 6 : THE INFLUENCE OF DYNAMIC VULCANIZATION ON CO-CONTINUOUS MORPHOLOGY IN EPDM/PP

BLENDS.....	160
6.1 Introduction	164
6.2 Experimental procedures.....	166
6.2.1 Materials.....	166
6.2.2 Rheological characterization	167
6.2.3 Melt blending	167

6.2.4 Determination of gel content.....	169
6.2.5 Solvent extraction and gravimetry.....	169
6.2.6 Focused ion beam (FIB) sample preparation and atomic force microscopy (AFM)	170
6.2.7 BET nitrogen adsorption	171
6.3 Results and discussions	171
6.3.1 Rheology	171
6.3.2 Chemical crosslinking of EPDM.....	173
6.3.3 Microstructure of crosslinked blends	176
6.3.4 Effect of crosslinking on the continuity of non-crosslinked EPDM	183
6.3.5 Effect of crosslinking on pore diameter	186
6.3.6 Conceptual mechanism of morphology development in thermoplastic vulcanizates.....	187
6.4 Conclusions	189
CHAPTER 7 : GENERAL DISCUSSIONS.....	194
7.1 Dynamic crosslinking of the blends	194
7.2 Dynamic crosslinking of high viscosity ratio blends	196
CHAPTER 8 : CONCLUSIONS AND RECOMMENDATIONS	198
8.1 Conclusions	198
8.2 Recommendations	202
CHAPTER 9 : SCIENTIFIC CONTRIBUTIONS.....	206

REFERENCES	208
-------------------------	------------

ANNEXES	246
----------------------	------------

LIST OF TABLES

Table 2.1 :	Critical surface tension for different polymers at room temperature	59
Table 4.1 :	Characteristic properties of the materials	93
Table 4.2 :	Rheological property ratios at constant shear rate and constant shear stress	95
Table 4.3 :	Estimated fiber breakup times	114
Table 5.1 :	Characteristic properties of the materials	135
Table 5.2 :	Rheological property ratios at constant shear rate and constant shear stress	135
Table 6.1 :	Characteristic properties of the materials	167
Table 6.2 :	Rheological property ratios at constant shear rate and constant shear stress	168

LIST OF FIGURES

Figure 2.1 :	Critical capillary number for droplet breakup as a function of viscosity ratio in simple shear and elongational flow (Grace (1982)).....	9
Figure 2.2 :	Schematic presentation of the two dispersion mechanisms: on the left, the stepwise equilibrium mechanism of repeated breakup at Ca_{crit} , and on the right, the transient mechanism of thread breakup during extension. (Janssen et al. (1993)).....	10
Figure 2.3 :	Schematics of idealized shear-induced coalescence in Newtonian systems	12
Figure 2.4 :	Schematics of percolation theory (Hsu and Wu (1993)).....	17
Figure 2.5 :	Transmission electron micrographs for PMMA/PS blends at different blend compositions: (a) 90/10, (b) 50/50, (c) 30/70 (Steinmann et al. (2001)).....	18
Figure 2.6 :	Schematics for a cocontinuous structure in the binary blend of component A and B: On left, phase A is seen continuous after extraction of component B and the reverse situation is presented on the right (Gergen (1996))	19

Figure 2.7 :	Special types of polymer blend morphologies: (a) and (b) Composite droplet morphology (Virgilio et al. (2005) and Reignier et al. (2003)) (c) Ternary cocontinuous morphology, and (d) Inverted matrix morphology	20
Figure 2.8 :	Distribution of the two mean form factors depending on the blend composition (Steinmann et al. (2001))	31
Figure 2.9 :	Amount of interface per unit area of image as a function of blend composition (Galloway et al. (2002)).....	33
Figure 2.10 :	Schematic presentation of continuity development for different type of blend interfaces (Li et al. (2002)).....	38
Figure 2.11 :	Continuity development for different blend systems (Li et al. (2002))	39
Figure 2.12 :	Pore size as a function of minor phase composition for different blend systems (Li et al. (2002)).....	39
Figure 2.13 :	Continuity development in PMMA/PC blends (Marin et al. (2002))	41
Figure 2.14 :	Coalescence in PMMA/PC blends (Marin et al. (2002))	41

Figure 2.15 :	Glass transition temperatures of both the PMMA-rich and the PC-rich phases as a function of PMMA composition (Marin et al. (2002))	42
Figure 2.16 :	Continuity development in PMMA/PC blends after correction (Marin et al. (2002))	43
Figure 2.17 :	Effect of an interfacial modifier on continuity development in PS/HDPE blends (Bourry et al. (1998))	44
Figure 2.18 :	Continuity development in PS/PCL blends at different melt blending temperatures	47
Figure 2.19 :	The volume fraction at which a cocontinuous morphology once formed is stable against breakup into droplets as a function of the viscosity ratio of the blend components	50
Figure 2.20 :	Effect of vulcanized-rubber particle size on the mechanical properties of EPDM/PP TPVs.....	58
Figure 2.21 :	Morphology development for an 80/20 EPDM/PP TPV phase inversion	61
Figure 2.22 :	Vulcanization by phenolic curative resin	75

Figure 4.1 (a) : Complex viscosity of the pure materials as a function of shear rate at 190°C	103
Figure 4.1 (b) : Storage modulus of the pure materials as a function of shear rate at 190°C	104
Figure 4.2 : Glass transition temperatures for the EP 1/PP 1 blends as a function of EP 1 composition in the blend	106
Figure 4.3 : EPDM phase morphology development.....	109
Figure 4.4 : SEM micrographs of the dispersed EPDM phase after PP matrix dissolution	111
Figure 4.5 : SEM micrographs after partial PP matrix dissolution.....	112
Figure 4.6 : PP phase microstructure in EPDM matrix	116
Figure 4.7 : Average particle/pore diameters as a function of composition for EP 1/PP 2 blends	117
Figure 4.8 : Effect of viscosity ratio and shear stress on average particle/pore sizes as a function of composition.....	119
Figure 4.9 : Complete continuity development and cocontinuity diagram for EPDM/PP blends system (corrected for PP solubility in	

cyclohexane at room temperature, and EPDM solubility in xylene).....	120
Figure 5.1 (a) : Complex viscosity of the pure materials as a function of shear rate at 190°C	141
Figure 5.1 (b) : Storage modulus of the pure materials as a function of shear rate at 190°C	142
Figure 5.2 : Complete continuity development and cocontinuity diagram for EPDM/PP blends system (corrected for PP solubility in cyclohexane at room temperature, and EPDM solubility in xylene).....	143
Figure 5.3 : EPDM phase morphology development.....	145
Figure 5.4 (a) : Number average particle diameter as a function of EPDM composition in the blend	146
Figure 5.4 (b) : Volume average particle diameter as a function of EPDM composition in the blend	147
Figure 5.5 : Volume average diameter as a function of individual particle diameter at different EPDM compositions in the EP 3/PP 1 blends.....	148

Figure 5.6 :	SEM micrographs of the high viscosity dispersed EPDM phase after PP matrix dissolution	150
Figure 5.7 :	SEM micrographs of the continuous network of high viscosity EPDM phase obtained after complete matrix dissolution of the low viscosity PP matrix in 30 EP 3/70 PP 1 blend.....	151
Figure 5.8 :	Erosion in high viscosity ratio EPDM/PP blends.....	152
Figure 5.9 :	Schematics of single high viscosity particle surface erosion process – A big particle eroding to give out nanometer diameter fibers.....	154
Figure 5.10 :	Schematics of coalescence based conceptual particle collision- coalescence-separation type erosion of high viscosity EPDM phase.....	156
Figure 6.1 (a) :	Complex viscosity of the pure materials as a function of shear rate at 190°C	172
Figure 6.1 (b) :	Storage modulus of the pure materials as a function of shear rate at 190°C	173
Figure 6.2 :	Gel content as a function of crosslinking agent	174
Figure 6.3 :	Gel content as a function of EPDM composition.....	175

Figure 6.4 :	FIB micrographs.....	176
Figure 6.5 :	AFM micrographs after FIB sample preparation as well as topological height profiles of polypropylene, and non-crosslinked and crosslinked EPDM.....	179
Figure 6.6 :	AFM micrographs of 50 EP 1/50 PP 2 after FIB sample preparation at 0%, 50% and 100% EPDM crosslinking	182
Figure 6.7 (a) :	Effect of dynamic vulcanization on continuity	184
Figure 6.7 (b) :	Continuity of the non-crosslinked EPDM in the 50% crosslinked blend as a function of EPDM composition	185
Figure 6.8 :	Gravimetric analysis of the quantity of crosslinked EPDM material present in the continuous non-crosslinked EPDM	186
Figure 6.9 :	Effect of crosslinking on the pore diameter of non-crosslinked EPDM phase from BET	187
Figure 6.10 :	Schematics of the morphology development in a cocontinuous blend of EPDM/PP with dynamic crosslinking.....	189
Figure 7.1 :	Gel content in 50 EP 1/50 PP 2 blend before and after addition of the master batch	195
Figure 7.2 :	Gel content in high viscosity ratio blends	196

LIST OF ANNEXES

ANNEX I :	DETERMINATION OF THE AVERAGE SHEAR RATE IN AN INTERNAL MIXER	246
ANNEX II :	THEORETICAL ESTIMATION OF THE INTERFACIAL TENSION	252
ANNEX III :	DETERMINATION OF THE CRYSTALLINITY OF POLYPROPYLENE	255
ANNEX IV :	IRRADIATION CROSSLINKING OF THE POLYMERS	257
ANNEX V :	INVESTIGATION OF THE PP DISPERSED PHASE MORPHOLOGY IN AN EPDM MATRIX	264
ANNEX VI :	ESTIMATION AND APPLICATION OF CORRECTIONS.....	276

NOMENCLATURE

English letters:

a	area of adsorbed gas molecule
B	diameter of the thread
b	relative speed between rotors
Ca	capillary number
c	concentration
D_n, d_n	number average diameter
D_v, d_v	volume average diameter
d	pore diameter
ff	form factor
G	Gibbs free energy
G'	storage modulus
G''	loss modulus
H	heat of mixing
M_i	molecular weight of component 'i'
M_n	number average molecular weight
M_w	weight average molecular weight
M_T	total torque
m	consistency index
N	Avogadro's number, 6.02×10^{23} molecules/mol
N_1	first normal stress

N_2	second normal stress
n	flow index
P	pressure, perimeter of the domains
p	viscosity ratio
q	growth rate of the distortion
R	universal gas constant, radius of the droplet
R_e	equivalent inner radius
R_o	outside radius of the rotor
S	surface area, entropy of mixing
S_i	angular velocity of the rotors
T	torque, absolute temperature
T_g	glass transition temperature
t	time
t_b	thread breakup time
V	volume of the pores
V_M	molar volume
V_{ref}	reference volume
v_m	volume of gas required to form an adsorbed monomolecular layer
w	weight fraction
X_c, W	degree of crystallinity
x_i	mole fraction of component ' i '
x^p	polarity

Greek letters:

α	distortion amplitude
α_0	initial distortion amplitude
α -network	cocontinuous network of uncrosslinked elastomer phase
β -network	continuous network formed by crosslinked elastomer phase
γ, σ	interfacial tension, surface tension
γ_i^d	surface tension due to dispersion forces of component ' <i>i</i> '
γ_i^p	surface tension due to polar forces of component ' <i>i</i> '
$\dot{\gamma}$	shear rate
Δ	change in the property
δ	tangent delta, solubility parameter
η^*	complex viscosity
η_i	shear viscosity of component ' <i>i</i> '
η_d	viscosity of the dispersed phase
η_m	viscosity of the matrix phase
η_c	viscosity of the continuous phase
η_0	zero shear viscosity
$[\eta]$	intrinsic viscosity
θ	contact angle
λ	wavelength
λ_m	dominant wavelength

ρ	density
σ	shear stress
ϕ_i or φ_i	volume fraction of component ' <i>i</i> '
φ_c	percolation threshold composition
ϕ_i	cocontinuity index
$\varphi_{PI,i}$	composition of phase inversion of component ' <i>i</i> '
χ	interaction parameter
ψ	elasticity ratio
$\Omega(p,\lambda)$	complex function of viscosity ratio (<i>p</i>) and wavelength (λ)
ω	frequency

List of abbreviations:

AFM	atomic force microscopy
BET	Brunauer, Emmet and Teller nitrogen adsorption technique
DMTA	dynamic mechanical thermal analyzer
DSC	differential scanning calorimetry
ENB	ethylidene norbornene
EPDM	ethylene-propylene-diene terpolymer
EVA	ethylene-vinyl acetate rubber
FIB	focused ion beam
HDPE	high density polyethylene
IPN	interpenetrating polymer network
LCST	lower critical solution temperature
NBR	nitrile rubber
ODT	order-disorder temperature
PA	polyamides (nylons)
PB	polybutadiene rubber
PC	polycarbonate
PCL	poly(ϵ -caprolactone)
phr	parts per hundred rubber
PMMA	poly(methyl methacrylate)
PP	polypropylene
PS	polystyrene

SAN	polystyrene-co-acrylonitrile
SANS	small angle neutron scattering
SBR	styrene-butadiene rubber
SBS	styrene-butadiene-styrene copolymer
SD	spinodal decomposition
SEBS	styrene-ethylene-butylene-styrene copolymer
SEM	scanning electron microscopy
TEM	transmission electron microscopy
TMAFM	tapping mode atomic force microscopy
TPE	thermoplastic elastomers
TPV	thermoplastic vulcanizates
UCST	upper critical solution temperature
ZnO	zinc oxide

CHAPTER 1

INTRODUCTION AND OBJECTIVES

1.1 Introduction

The mixture of two or more polymers or copolymers is called a polymer blend. The basic concept, behind the preparation of polymer blends, is to gain additional mechanical or functional performance by mixing the base polymers. Polymer blends have gained tremendous commercial significance over the last 25 years, despite the fact that the first known patent in the field of polymer blends, awarded to Thomas Hancock, dates as far back as 1846. (Utracki, 1989).

Thermodynamically, like any other universal system, polymer blends are subject to the Gibbs rule for free energy of mixing. i.e.

$$\Delta G_{\text{mix}} = \Delta H_{\text{mix}} - T \cdot \Delta S_{\text{mix}}, \dots \dots \dots (1)$$

On substituting the Flory-Huggins expression for the combinatorial entropy and the Hildebrand-Scatchard-van Laar-type heat of mixing in the above equation (1), we get the classical expression for the Gibbs free energy of mixing for polymer blends, as follows,

$$\Delta G_{\text{mix}} = \frac{\chi RT}{V_{\text{ref}}} \phi_A \phi_B + RT \left[\frac{\rho_A \phi_A \ln \phi_A}{M_A} + \frac{\rho_B \phi_B \ln \phi_B}{M_B} \right] \dots \dots \dots (2)$$

where χ is the interaction parameter; V_{ref} is a reference volume that is usually taken as the molar volume of one of the repeat units in the system; R is the gas constant; T is the

absolute temperature; and ρ_i , ϕ_i , and M_i are respectively the density, volume fraction, and molecular weight of component 'i'.

As for any other system, a negative Gibbs free energy of mixing can result in spontaneous mixing and thus miscibility in polymer blends. However, the macromolecular nature of polymers significantly reduces the entropy of the mixing and its negative contribution to the Gibbs free energy. Therefore, without some specific preferred interactions between the components of polymer blends, spontaneous miscibility cannot be achieved. In some cases, miscibility between the blend components can be achieved by increasing the temperature of the system.

In addition to a negative Gibbs free energy of mixing, achieving miscibility also requires that the second derivative of Gibbs free energy, with respect to composition, at constant pressure and temperature must be positive. If this criterion of miscibility is not satisfied, then the metastable mixture of a polymer in a solvent, or in another polymer, separates into two phases. Either phase will contain both the blend components, but each phase will retain a higher composition of one of the blend components.

From the above discussion, it can be well understood that the vast majority of polymer blend systems are of the immiscible type. Although it is true that achieving miscibility can enhance some of the mechanical properties more than an immiscible blend, primarily due to the absence of weak interface between the blend components, achieving miscibility is not always the goal. In fact, immiscible type blends generate a discrete multiphase morphology which can be exploited for many different applications,

and can result in synergistic interactions which can also improve the properties by different mechanisms. For example, the dispersion of rubber particles in the matrix of a hard, brittle polymer can greatly enhance the impact properties of the matrix polymer by providing numerous sites for crack initiation and propagation. Stratified morphologies can be exploited for barrier properties; cocontinuous morphologies contribute fully towards the mechanical properties and offer many more functional properties. In some polymer blend systems, further in-situ chemical crosslinking (vulcanization) of dispersed phase morphologies can dramatically enhance the impact properties of the blend. If the same vulcanization is done for a higher elastomer content blend (about 70-80%), a material called a thermoplastic vulcanizate with an 'inverted matrix' type of morphology is formed. In this type of morphology, the major component forms the dispersed phase, whereas the minor component forms the matrix. This unique morphology enables these materials to attain the performance of a thermoset rubber and the processibility of a thermoplastic material.

The above discussion illustrates the importance of morphology in immiscible polymer blend systems. Each blend will show a unique type of morphology depending on various parameters, such as: composition, interfacial tension, viscosity ratio, elasticity ratio of the constituent polymers, processing parameters like shear rate, shear stress, temperature of blending, time of mixing, type of mixing equipment used for blending, the thermal history of the polymers, annealing, and also the type and the composition of the interfacial modifier, if present in the blend. In general, however,

polymer blend morphologies can be divided into two general classes: dispersed and cocontinuous.

Dispersion of droplets of the minor phase into the matrix of the major phase is the most common type of morphology, known as a dispersed droplet type morphology. However, depending on the various parameters, the minor phase can also be dispersed as fibers or sheets. Such types of morphologies are also called stratified morphologies. Generally, these types of morphologies are obtained below the percolation threshold composition and during the continuity development of the dispersed phase.

With an increase in the composition, both phases eventually become continuous throughout the blend, and it is impossible to define either a dispersed phase or a matrix. Such a blend morphology is called a cocontinuous morphology. Cocontinuous morphologies form highly interconnected and intertwining structures, and both blend phases remain fully continuous throughout the blend.

Other special types of morphologies reported in the literature include: subinclusion or composite droplet (droplet in droplet morphology), ternary cocontinuous, and inverted matrix morphologies.

The overwhelming majority of literature on polymer blends has focused on the study of binary immiscible dispersed phase morphologies and their properties. More recently, the binary and ternary immiscible cocontinuous morphologies, the subinclusion morphologies, and the inverted matrix type of morphologies are complex morphologies that are receiving more and more attention. They promise to be the future

of polymer blends. Thus, significant research is ongoing in understanding and developing the tools necessary for characterizing these morphologies.

Over the past few years, some researchers have made significant progress in understanding the development of these novel complex morphologies, particularly with respect to cocontinuous morphologies. Nevertheless, their work has only raised more challenging questions and produced more frontiers to be explored. The possibilities and the applications in this field appear limitless.

1.2 Objectives

Polypropylene (PP) is a very versatile polymer. Easy processing and extended applicability of PP has stimulated heavy growth of the PP industry worldwide. Today, the global production of PP is estimated at over 30 million tons. However, PP suffers due to its low impact strength, especially at lower temperatures. To overcome this weakness, PP is blended with various elastomers. Among other elastomers, ethylene-propylene-diene terpolymer (EPDM) has been found to be a very good impact modifier for PP.

The extremely low interfacial tension between EPDM and PP, estimated to be around 0.3 mN/m at 190 °C, allows for the very fine dispersion of the elastomer phase in the PP matrix. The elastomer phase provides a great number of sites for crack initiation and propagation on impact, thus increasing the impact strength of PP. The vulcanization of the fine dispersed phase can further increase the impact properties of the blend. The vulcanization of an EPDM-rich blend can produce the aforementioned

unique thermoplastic vulcanizate materials. Thus, the wide ranging composition dependent properties of the EPDM/PP blend satisfy the needs of various applications, thereby increasing the commercial importance of this blend system. Also, technologically, this system is one of the most studied blend systems in the polymer blend literature, yet very little fundamental knowledge concerning the morphology of these systems is available.

The combination of all these points, together with the ultra-low interfacial tension, makes this blend system an ideal model system for the study of morphology, continuity development, and cocontinuity of ultra-low interfacial tension blend systems.

The objectives of this study, therefore, include the systematic investigation of the morphological structures formed with the composition, with a particular emphasis on continuity development and cocontinuity. The study will also examine the effect of fundamental parameters such as viscosity and elasticity ratio on the continuity development and cocontinuity in these ultra-low interfacial tension blend systems. Due to the use of very different viscosity ratios, it is expected that the study will generate a wide scale of morphologies and cocontinuous structures.

The evolution of the inverted matrix type of morphology in the thermoplastic vulcanizates will also be examined in this study. This objective will be achieved by tracking the morphology change with the dynamic crosslinking (vulcanization) in the elastomer rich blends and by studying the effect of crosslinking on cocontinuity. This study should also enable us to establish the effect of crosslinking based on the initial

morphology, the scale of cocontinuous structures, and the viscosity ratio on the final inverted matrix type of morphology.

CHAPTER 2

LITERATURE REVIEW

During melt blending the minor phase in an immiscible polymer blend is deformable. Therefore, a wide range of sizes, from submicron to hundreds of microns, and shapes, such as: spherical, ellipsoidal, cylindrical, ribbon-like, cocontinuous or subinclusion types of morphologies, can be obtained under various melt-processing conditions. The final morphology obtained is a balance between deformation-disintegration phenomena and coalescence.

2.1 Theory of droplet deformation and breakup

Taylor (1932, 1934) extended the work of Einstein (1906) on diluted suspension of solid spheres in a Newtonian liquid, to a dispersion of Newtonian liquids suspended in another Newtonian liquid. He observed that when the radius of the drops is great enough or when the rate of distortion is high, the drops break up. He defined a Weber number which is today referred to as a capillary number (Ca). It is a ratio of the deforming stress $\eta_m \dot{\gamma}$ (matrix viscosity, η_m , times shear rate, $\dot{\gamma}$) imposed by the flow to interfacial forces σ/R , where σ is the interfacial tension and R is the radius of the droplet. Thus,

$$Ca = \eta_m R \dot{\gamma} / \sigma \dots\dots\dots (2.1)$$

If the capillary number is above a critical value, represented by Ca_{crit} , i.e. the deforming stress exceeds interfacial forces, the drop becomes unstable and finally

breaks. The drop break up process continues till the capillary number reduces below critical value, then the interfacial forces dominate over the deforming stress, and a steady drop shape evolves. Taylor predicted that no drop break up occurs above the viscosity ratio of 2.5. This result compares well with the experiment (Rumscheidt et al. (1961), Karam et al. (1968), Grace (1982)) where no drop breakup was observed above 4 viscosity ratio. Grace (1982) found that an elongational flow field is much more effective for droplet breakup, and the limiting viscosity ratio range is much greater than that for uniform shear flow. His results are summarized in Figure 2.1.

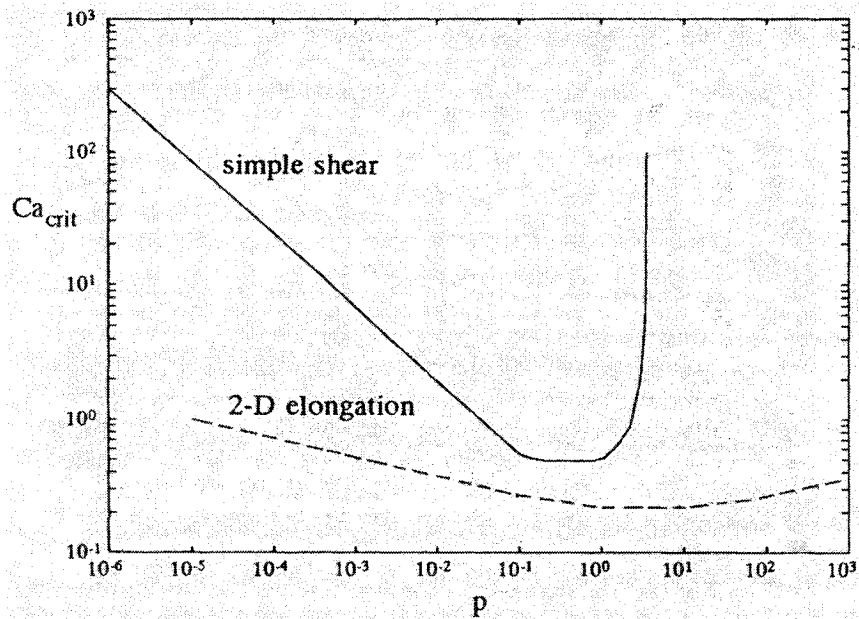


Figure 2.1: Critical capillary number for droplet breakup as a function of viscosity ratio in simple shear and elongational flow (Grace (1982))

Rumscheidt et al. (1961) observed different modes of deformation and burst for a spherical Newtonian drop in both shear and extensional flow. They found that two basic mechanisms are largely responsible for dispersing one liquid in another. One is

steady breakup or drop splitting and the other is the disintegration of a deformed fine thread into a series of fine droplets by a phenomenon called ‘capillary instability’ often observed under transient shear condition or after cessation of flow. Both of these mechanisms are schematically shown in Figure 2.2.

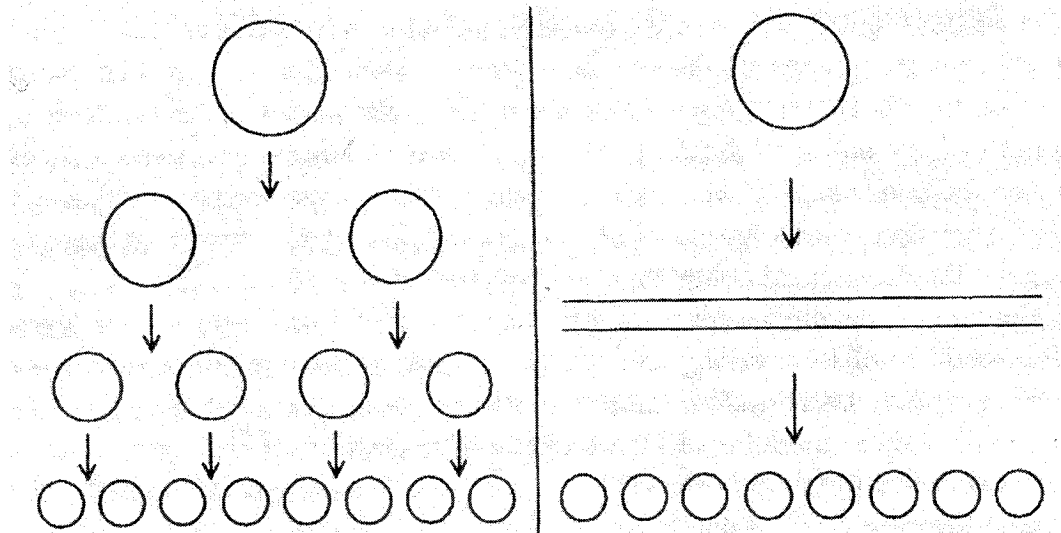


Figure 2.2: Schematic presentation of the two dispersion mechanisms: on the left, the stepwise equilibrium mechanism of repeated breakup at Ca_{crit} , and on the right, the transient mechanism of thread breakup during extension. (Janssen et al. (1993))

Extending Lord Rayleigh’s (1879) theory, Tomotika (1935) developed the following equation to determine the stability of a deformed cylindrical thread of Newtonian material in the matrix of another Newtonian material,

$$\alpha = \alpha_0 \cdot e^{qt} \dots\dots\dots (2.2)$$

where, α is an amplitude of distortion at time ' t ', α_0 is the initial distortion amplitude, and q is the growth rate of distortion given by,

$$q = \frac{\sigma \Omega(\lambda, p)}{2\eta_c R_0} \dots\dots\dots (2.3)$$

where, η_c is the matrix (continuous) phase viscosity, σ is interfacial tension, $\Omega(\lambda, p)$ is a dimensionless complex function of viscosity ratio (p) and observed wavelength of distortion (λ). For a given viscosity ratio (p) there will be one dominant wavelength (λ_m) at which the amplitude grows fastest, the distortion having this wavelength consequently causes the thread to breakup into droplets. Though the equation is developed for Newtonian systems, several authors have found a good correlation of the theory to non-Newtonian systems.

Tomotika estimated that for sinusoidal waves the smallest diameter of the thread reaches zero when amplitude (α) equals an average thread radius (\bar{R}), thus the value of amplitude at breakup is estimated to be $\alpha = 0.81 R_0$. By inserting this value and the value of initial amplitude of distortion (α_0), based on fluctuations of the interface caused by Brownian motion from the equation derived by Kuhn (1953), into the Tomotika equation, Elemans et al. (1986) derived an equation to predict the thread breakup time,

$$t_b = \left(\frac{\eta_c B}{\Omega(\lambda, p) \sigma} \right) \ln \left(\frac{0.8 B}{2 \alpha_0} \right) \dots\dots\dots (2.4)$$

where B is twice the radius of the thread. The equation shows that the fiber breakup time is inversely proportional to the interfacial tension, and hence the decrease in interfacial tension is expected to increase the fiber stability.

2.2 Coalescence in polymer blends

As already mentioned, the final morphology obtained is a balance between deformation-disintegration phenomena and coalescence. Several authors such as Coulaloglou et al. (1977), Allan et al. (1984), Chen et al. (1984), and Jeelani et al. (1991) have studied coalescence phenomena in binary Newtonian liquid mixtures. They found the contact time required for droplet coalescence increases with increase in droplet diameter, matrix viscosity, and the difference in density between the droplet and matrix phase. In general, the flow induced coalescence of two Newtonian liquid droplets can be modeled as a three step mechanism (Roland et al. (1984)) as shown in Figure 2.3,

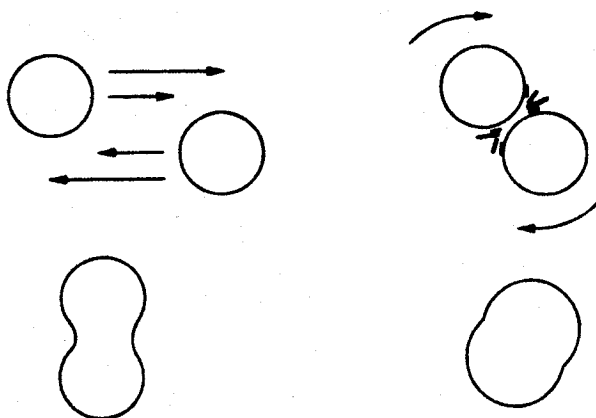


Figure 2.3: Schematics of idealized shear-induced coalescence in Newtonian systems

Firstly, two droplets come close to each other and the pair rotate in the shear field. The matrix phase film between the two droplets drains away (the film thickness decreases to a critical value and film ruptures) resulting in coalescence. Unlike gravity induced coalescence, where the drops have time to equilibrate, contact times in shearing flows are small. Therefore the film must drain out very quickly for a droplet pair to coalesce. The low viscosity matrix can thus be expected to promote coalescence in the blend.

Similar to kinetic models (Ziff (1986)), the modeling of drop sizes during mixing has been carried out using population balance concepts. Ramakrishna (1985) has given an excellent review of population balance modeling of drop sizes in all engineering fields. In Newtonian systems the collision frequency, i.e. the number of times that particles meet, has been modeled satisfactorily, but the coalescence probability, i.e. the probability that the meeting results in coalescence, is still very empirical (Muralidhar et al. (1988)). Coalescence probability in viscoelastic polymer systems is even less understood.

Interfacial mobility governs coalescence during mixing (van Gisbergen (1991)). A high polymer viscosity should give rise to a relatively immobile interface which should result in long drainage times for the intervening film. However, Elmendorp et al. (1986) found that polymers have a high coalescence probability during mixing and they concluded that polymers have fully mobile interfaces. Roland and Böhm (1984) found that increasing shear rates, which one would intuitively expect to decrease coalescence,

actually increased the amount of coalescence. Due to the different rheological behavior drop collision and film drainage in polymer blends are expected to be very different from the Newtonian systems. Elastic recoiling is expected to cause polymeric drops to separate during the initial step.

Several theories have been developed to interpret the coalescence effect. Based on the theory of Smoluchowski (1916, 1917), Tokita (1977) derived an expression for analysing the particle size of the dispersed phase in polymer blends considering composition as a variable. Tokita's theory is based on the fact that an equilibrium drop diameter originates from the continuous break up and coalescence of the dispersed particles. The total number of collisions per unit time (N_T) can be expressed as,

$$N_T = \frac{4n\phi_d\dot{\gamma}}{\pi} \dots\dots\dots (2.5)$$

where, n is the number of particles, ϕ_d is the volume fraction of the dispersed phase, and $\dot{\gamma}$ is the shear rate. Under the assumption that coalescence is proportional to the total number of collisions, the decrease in the number of particles with time (t) due to coalescence can be expressed as

$$\frac{dn}{dt} = -p_r N_T \dots\dots\dots (2.6)$$

where, p_r is the probability that a collision will result in a coalescence. On the other hand, the increase in the number of particles with mixing time due to the drop breakup can be given as,

$$\frac{dn}{dt} = n \left[\frac{\eta_m \dot{\gamma}^2}{E_{DK} + 6\sigma_{12}/d} \right] \dots\dots\dots (2.7)$$

where E_{DK} is the macroscopic bulk breaking energy, η_m is matrix phase viscosity, σ_{12} is the interfacial tension. At equilibrium, the rate of drop breakup and coalescence is equal; thus, from equations (2.6) and (2.7), the equilibrium drop size (d_{eq}) can be calculated as,

$$d_{eq} = \left(\frac{24 p_r \sigma_{12} \varphi_d}{\pi} \right) / \left(\eta_m \dot{\gamma} - \frac{4 p_r E_{DK} \varphi_d}{\pi} \right) \dots\dots\dots (2.8)$$

Equation (2.8) indicates that the equilibrium drop diameter increases with concentration, interfacial tension, and decreases with shear stress. Generally, this agrees with earlier work by Taylor. This particular theory is of interest because it includes the effect of composition, which is very critical, on phase size in its analysis.

Following a similar procedure to Tokita, Fortelny et al. (1989, 1993) proposed an equation to predict the equilibrium diameter of the dispersed phase,

$$r = r_c + \left(\frac{\sigma_{12} \alpha}{\eta_m f} \right) \varphi_d \dots\dots\dots (2.9)$$

where r_c is the critical droplet radius as calculated from Ca_{crit} ; α is the probability that droplets will coalesce after collision; f is the function of the Taylor capillary number Ca , and rheological properties of the system. This relationship, however, still contains several parameters which cannot be easily quantified for the blending of viscoelastic polymers.

2.3 Percolation theory for the morphology development

The term percolation for a statistical-geometry model was first introduced by Broadbent and Hammersley (1957). However, historically, the essence of percolation theory can be found in the theories of Flory, and Stockmayer, on how small branched molecules form larger and larger macromolecules if more and more chemical bonds are formed between the original molecules, i.e. polymerization process leading to gelation.

This theory divides a system, such as a polymer dissolved in a solvent, in an array of a defined lattice (triangular, honeycomb, square, etc) of N numbers. The fraction of defined lattices randomly contain the monomers of a polymer with probability p , and the other lattices contain solvent with probability $(1-p) \cdot N$. One can define a cluster as a group of neighboring lattices occupied by monomers having one side in common. Thus the original small monomers correspond to a lattice and the macromolecule to the cluster. Percolation theory mainly deals with the concept of the percolation threshold p_c at which an infinite connectivity of occupied sites first occurs, i.e. the network to percolating clusters, and the probability of finding such connectivity as a function of p .

The evolution of cocontinuous structures can be explained to some degree with the help of percolation theory, since it undergoes the transition from one minor phase randomly dispersed in the matrix of another polymer to high levels of interconnection with each other with increasing composition of the minor phase (schematics 2.4 (A),

(B) and (C)). Ultimately the system reaches the percolation threshold and forms the cocontinuous structure (schematic 2.4 (D)).

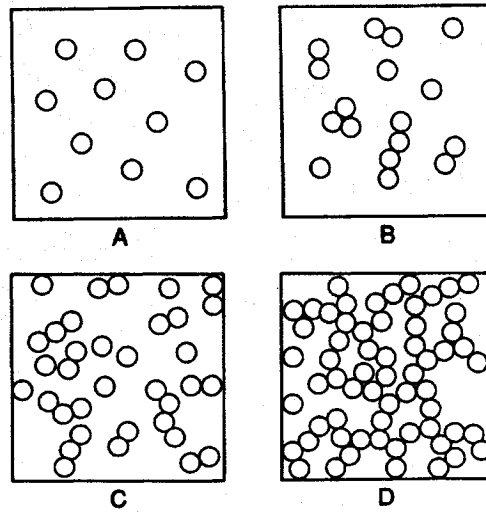


Figure 2.4: Schematics of percolation theory (Hsu and Wu (1993))

Through computer simulations (Monte Carlo method, series expansion, renormalization group technique and exact inequality), Stauffer (1980) showed that there is a qualitative difference of cluster structures above and below p_c and suggested that for the large clusters near the percolation threshold, p_c , the number average clusters n_s varies as,

$$n_s \approx s^{-\tau} f[(p - p_c) \cdot s^{\sigma}] \dots\dots\dots (2.10)$$

where, s is the number of sites; $f[(p - p_c) \cdot s^{\sigma}]$ is the scaling function; and τ , σ are the free exponents. Some researchers (Margolina et al., 1988, 1990; Hsu et al., 1993; Arends, 1992) have applied the percolation concept to interpret the change in mechanical properties in the transition region as function of morphology in polymer

blends, and they showed that percolation concepts could be successfully used to analyze the data and explain the transition.

But even today it is controversial whether the critical phenomena for gelation are described correctly by percolation theory and its assumption that chemical bonds are formed randomly (de Gennes (1976); Stauffer et al. (1982)).

2.4 Polymer blend morphologies

Dispersion of droplets of the minor phase into the matrix of the major phase is the most common type of morphology, known as a dispersed droplet type morphology. Figure 2.5 shows the transmission electron micrographs for poly(methyl methacrylate)/polystyrene (PMMA/PS) blends at different blend compositions.



Figure 2.5: Transmission electron micrographs for PMMA/PS blends at different blend compositions: (a) 90/10, (b) 50/50, (c) 30/70 (Steinmann et al. (2001))

The dispersed droplet type of morphology is clearly evident in micrographs (a) and (c). In micrograph (b) taken at the mid-composition level, though, it is impossible to define which phase is dispersed and which phase forms the matrix. Such a blend morphology is called a cocontinuous morphology. Cocontinuous morphologies form highly interconnected and intertwining structures, and both blend phases remain fully

continuous throughout the blend as schematically shown in Figure 2.6 for a binary mixture of component A and B.

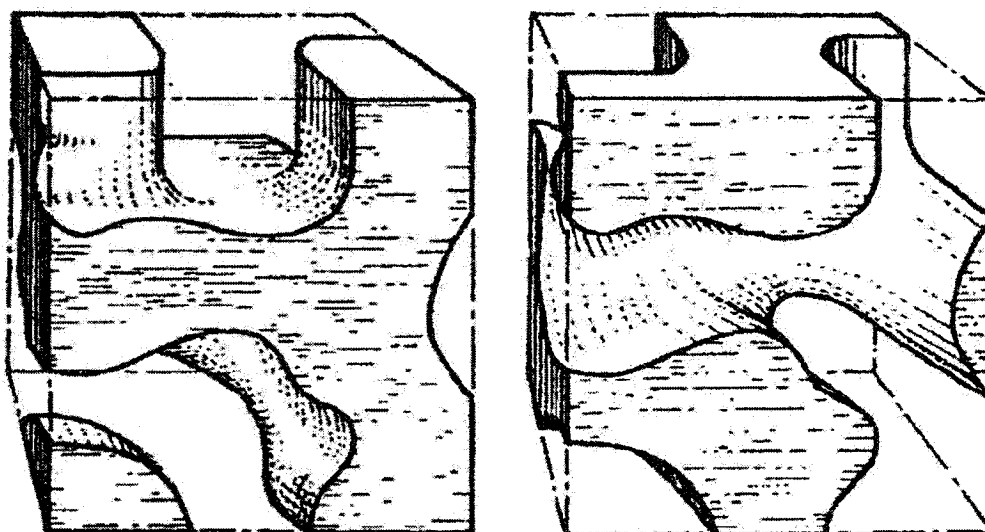


Figure 2.6: Schematics for a cocontinuous structure in the binary blend of component A and B: On left, phase A is seen continuous after extraction of component B and the reverse situation is presented on the right (Gergen (1996))

Moreover, some other special types of morphologies reported in the literature are shown in Figure 2.7. Subinclusion or composite droplet (droplet in droplet morphology) type morphology is seen in micrograph (a) obtained by tapping mode atomic force microscopy after focused ion beam etching of the sample (Virgilio et al. (2005)) and (b) obtained by scanning electron microscopy (SEM) after PMMA phase extraction (Reignier et al. (2003)). The micrographs demonstrate composite droplets of poly(methyl methacrylate) (PMMA) core and a polystyrene (PS) shell, dispersed in high density polyethylene (HDPE) matrix. Micrograph (c) schematically shows a ternary cocontinuous morphology. In this type of morphology, the minor component C is

located at the cocontinuous interface of component A and B. Micrograph (d) schematically shows inverted matrix type of morphology. In this type of morphology the blend component A forms the dispersed phase despite its higher concentration in the blend.

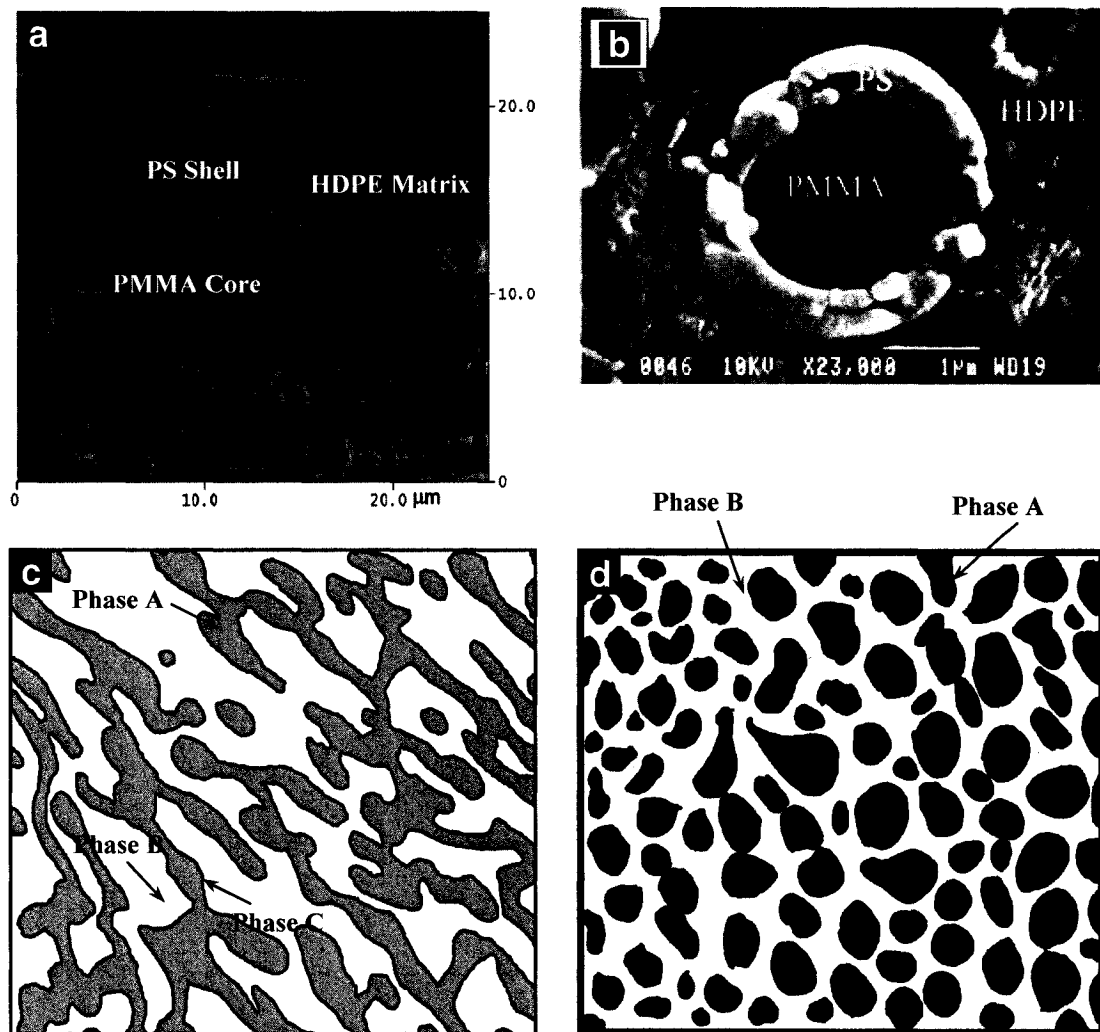


Figure 2.7: Special types of polymer blend morphologies: (a) and (b) Composite droplet morphology (Virgilio et al. (2005) and Reignier et al. (2003)) (c) Ternary cocontinuous morphology, and (d) Inverted matrix morphology

The aforementioned objectives of this thesis demand the study of the literature more specific to continuity development, cocontinuity, and ethylene-propylene-diene terpolymer/polypropylene (EPDM/PP) blends and their thermoplastic vulcanizate. Henceforth this chapter will provide literature more specifically related to aforementioned topics.

2.5 Continuity development and cocontinuity in polymer blends

2.5.1 Mathematical models for predicting the composition for phase inversion and cocontinuity

In the scientific literature significant efforts have been diverted towards predicting the composition for phase inversion (the composition at which the blend phases switch their role, i.e. the dispersed phase becomes the matrix and the former matrix becomes the dispersed phase) and more recently, for predicting the composition range over which cocontinuity exists. However, this traditional definition of phase inversion has some serious limitations. This definition could be true for systems with very high interfacial tension, but not for most polymer blend systems. Such polymer blends due to their very high viscosity and elasticity are known to display a composition range over which neither of the blend phases can be defined as a matrix or the dispersed phase, i.e. they are cocontinuous. In such a scenario it is impossible to define a single point of phase inversion. Therefore, there is a clear need to develop new terminology and a clear definition of phase inversion.

The mathematical models for predicting the composition of cocontinuity can be classified as basing their approach on viscosity ratio or on elasticity ratio. Some equations are also based on percolation theory, as well as Tomotika theory for capillary instabilities. In general, viscosity ratio based phase inversion models predict that the low viscosity material tends to form the matrix, while elasticity ratio based phase inversion models predict that the high elasticity material tends to form the matrix.

The idea of direct dependence of composition of phase inversion on the viscosity ratio was first given by Avgeropoulos et al. (1976). They used the torque ratio rather than viscosity ratio, which is convenient since such blends are often mixed in a torque rheometer or similar compounding machine. This idea of Avgeropoulos was generalized by Paul and Barlow (1980). The relationship was expressed in terms of the following equation by Jordhamo et al. (1986) and was later extended by considering the viscosity ratio of the material calculated at the actual shear rate of mixing by Miles and Zurek (1988).

$$\left. \begin{array}{l} \frac{\phi_1}{\phi_2} \cdot \frac{\eta_2}{\eta_1} \geq 1, \text{ phase 2 continuous} \\ \frac{\phi_1}{\phi_2} \cdot \frac{\eta_2}{\eta_1} \leq 1, \text{ phase 1 continuous} \\ \frac{\phi_1}{\phi_2} \cdot \frac{\eta_2}{\eta_1} \cong 1, \text{ dual phase continuity} \end{array} \right\} \dots\dots\dots (2.11)$$

where, ϕ_i is volume fraction at phase inversion and η_i is viscosity of the component i . Other authors, like Ho et al. (1990) and Everaert et al. (1999), modified the above equation usually with an exponent or another factor for the respective blend system to obtain a semi-empirical model and a better fit for their experimental results.

Purely based on the percolation theory, Lyngaae-Jørgensen and Utracki (1991) related the cocontinuity index Φ_1 , which represents the portion of the component that is a part of the percolation structure, with the volume fraction at the onset of cocontinuity Φ_{cr} and an exponent 0.45, which characterizes its increase beyond the onset composition.

$$\Phi_1 = k (\Phi - \Phi_{cr})^{0.45} \dots\dots\dots (2.12)$$

where, k is an empirical coefficient. For this equation, only knowledge of the critical volume fraction seems to be sufficient, however, it does not take into consideration any of the other important factors which play a crucial role in determining the composition for cocontinuity.

Based on the theory of capillary instabilities of Tomotika (1935) and assuming that the breakup times for both the phases of the blend should be equal for retention of two interpenetrating phases, Metelkin and Blekht (1984) developed the relation for phase inversion composition in terms of viscosity ratio,

$$\Phi_{2i} = \frac{1}{1 + f(\eta_1/\eta_2) \cdot (\eta_1/\eta_2)} \dots\dots\dots (2.13)$$

$$\text{where, } f(\eta_1/\eta_2) = \Omega_{1,2} \left(v_1, v_2, \frac{\eta_1}{\eta_2} \right) \frac{\ln(k_2/\alpha_{0,2})}{\ln(k_1/\alpha_{0,1})},$$

Ω is a function of the wavenumber, and v_i , k_i and $\alpha_{0,i}$ are respectively the wavenumber, characteristic of the type of breakup, and relative value of the critical amplitude of the

component 'i'. Φ_{2i} is the concentration of the second component above which it forms a continuous phase, as described by Metelkin and Blekht.

Utracki (1991) showed that under experimental conditions the $f(\eta_1/\eta_2)$ given by Metelkin and Blekht (1984) can be expressed as,

$$f(\eta_1/\eta_2) = 1 + 2.25 \log(\eta_1/\eta_2) + 1.81 [\log(\eta_1/\eta_2)]^2 \dots\dots\dots (2.14)$$

Luciani et al. (1996) considered that the phase continuity is governed by fiber stability and used Tomotika theory, similar to that of Metelkin and Blekht. They supposed that for a cocontinuous network to exist both the interpenetrating phases must have equal stability. In addition, they assumed that the two networks differ only in the diameters of their fiber but are made from the same number of fibers of same length. Therefore, they set the initial thread radius R_0 proportional to the square root of volume fraction. Thus these assumptions lead them to the following equation to determine the concentration for maximum continuity Φ_{11} ,

$$\Phi_{11} = \frac{(\eta_1/\eta_2)^2 \Omega^2(\eta_1/\eta_2)}{(\eta_1/\eta_2)^2 \Omega^2(\eta_1/\eta_2) + \Omega^2(\eta_2/\eta_1)} \dots\dots\dots (2.15)$$

where, $\Omega(\eta_1/\eta_2, \lambda)$ is a complex function, from Tomotika's equation, of both viscosity ratio and the observed wavelength of distortion λ .

Mostly all these equations predict the phase inversion composition with fair amount of accuracy when the viscosity ratio is near about unity, but as the viscosity

ratio increases these models predict too significant change in the phase inversion composition. For high viscosity ratio blends, based on intrinsic viscosity $[\eta]$, maximum packing volume fraction ϕ_m , and the relation given by Krieger and Dougherty for mono-dispersed hard spheres, Utracki et al. (1991) developed the following equation to predict the composition of phase inversion ϕ_{il} ,

$$\phi_{2I} = \frac{\phi_m + (1 - \phi_m)(\eta_1/\eta_2)^{1/[\eta]\phi_m}}{(\eta_1/\eta_2)^{1/[\eta]\phi_m} + 1} \dots\dots\dots (2.16)$$

For polymer blends ϕ_m is given as $\phi_m = 1 - \phi_c$, where ϕ_c is percolation threshold composition.

For predicting the composition range over which cocontinuity is observed, Willemse et al. (1998) proposed a semi-empirical relation by considering the minor phase of a fully cocontinuous blend as a dispersion of randomly oriented rods at their maximum packing density (i.e. the minimum volume fraction ($\phi_{d,cc}$) of the minor phase component for the formation of cocontinuity) in the major phase. Blending for a critical capillary number of one, the equation becomes,

$$\frac{1}{\phi_{d,cc}} = 1.38 + 0.0213 \left(\frac{\eta_m \dot{\gamma}}{\sigma} R_o \right)^{4.2} \dots\dots\dots (2.17)$$

where, η_m is matrix phase viscosity, $\dot{\gamma}$ is shear rate, σ is interfacial tension and R_o is initial radius of the droplet before deformation into a cylinder. This equation gives the lower limit of cocontinuity when applied to component 1 and upper limit for

cocontinuity when applied to component 2. Thereby, the composition range over which cocontinuity exists can be obtained by using this equation.

Assuming that the shape relaxation times of domains of components meet in a maximum at the phase inversion composition, Steinmann et al. (2002) derived the following relationship between the phase inversion composition and viscosity ratio,

$$\Phi_{2I} = \frac{1}{(\eta_1/\eta_2)^{1/z} + 1} \dots\dots\dots (2.18)$$

The parameter z is dependent on the blend system and must be determined experimentally from the phase inversion composition vs. viscosity ratio data for each particular system of interest.

Another approach based on elasticity ratio comes from a classical study of Van Oene (1972). In this study Van Oene developed an expression to describe an elastic contribution to the interfacial tension under dynamic conditions. He found that in the blends of PS/PMMA, a PMMA which had the largest second normal stress function (first normal stress function according to the current scientific notifications), was found to form droplets in the PS matrix. Addition of a low molecular weight PMMA to the same system resulted in stratification. Van Oene noted that when the discrete particles were smaller than 1 μm , the difference in morphology between complementary mixtures (i.e., stratification versus droplets) disappeared, indicating that the elastic contribution to interfacial tension was no longer dominant. Van Oene showed that the elastic contribution to the interfacial tension can result in a tendency for the phase of

higher elasticity to encapsulate the one with lower elasticity. He developed the following equation to determine the contribution of elasticity to the interfacial tension under dynamic conditions,

$$\sigma_{\text{eff}} = \sigma + \frac{d}{12} [(N_2)_d - (N_2)_m] \dots\dots\dots (2.19)$$

where σ_{eff} is the effective interfacial tension under dynamic conditions, σ is the static interfacial tension, d is the droplet diameter and N_{2d} and N_{2m} are the second normal stress functions of the dispersed and matrix phase, respectively.

Based on this concept and considering that the storage modulus G' or $\tan \delta$ represents the elasticity, Bourry and Favis (1998) proposed the following elasticity ratio based approach for predicting the phase inversion composition.

$$\frac{\phi_1}{\phi_2} = \frac{G'_2}{G'_1} \dots\dots\dots (2.20)$$

$$\frac{\phi_1}{\phi_2} = \frac{\tan \delta_1}{\tan \delta_2} \dots\dots\dots (2.21)$$

This simple elasticity and viscosity ratio based approach was inadequate to predict the phase inversion composition for the blends of Steinmann et al. (2001) prepared in a miniature single screw extruder. The results, however, were respected following a correlation based on elasticity ratios ($\Psi_{\text{eff}, G''}$) (at constant G''),

$$\phi_{PI} = -0.34 \log(\Psi_{\text{eff}, G''}) + 0.67 \dots\dots\dots (2.22)$$

Despite a wide range of models it still remains that none of the above mentioned equations accurately predict the composition of phase inversion or the composition range over which cocontinuity exists.

2.5.2 Methods for characterization of cocontinuous morphologies

Two dimensional photomicrographs obtained by scanning electron microscopy (SEM), transmission electron microscopy (TEM) and more recently by atomic force microscopy (AFM) can provide very good qualitative information about the morphology. However, the cocontinuous morphologies have a highly irregular, deformed, intertwining architecture in all three dimensions and therefore, two dimensional photomicrographs can be misleading in predicting such complex morphologies. Some scientists have been endeavoring to support the qualitative data from these micrographs with some statistical quantitative tools, while others are developing completely new characterization methods.

2.5.2.1 SEM and image analysis

SEM with subsequent image analysis is the most conventional approach for measurement of the domain size and distribution of the dispersed phase. However, it becomes laborious at best and impossible at worst to examine the cocontinuous morphologies by such a method. Some authors have suggested the use of statistical tools such as form factors, interfacial area etc. together with SEM micrographs for characterizing the cocontinuous morphologies.

2.5.2.1.a Cocontinuity and cocontinuity balance

Heeschen (1995) defined two new dimensionless and scale-invariant morphological parameters, namely ‘Cocontinuity’ and ‘Cocontinuity balance’ based on the area and convex area measurement of a cocontinuous blend. The idea was to measure the extent to which the phases of a polymer blend mutually surround each other.

In this method, Heeschen first digitized the images into a binary digital image. Then based on the pixel size and number of pixels he calculated the area occupied by each phase. He also calculated the convex area (the area per pixel multiplied by the total number of all pixels within the convex perimeter of the feature, where the convex perimeter is defined as the 32-sided equiangular polygon that circumscribes the feature) in a similar way. Then based on these areas he calculated several other different ratios and ultimately derived the two aforesaid morphological parameters. He observed that the calculated values agreed well with qualitatively observed morphology and impact energy values.

2.5.2.1.b Form factors

The form factor is a scale invariant parameter which represents the shape of finite domains in a two-dimensional image. It allows to distinguish quantitatively between spherical and cocontinuous morphologies. The form factor is defined as:

$$ff = 4 \pi \frac{A}{P^2} \dots\dots\dots (2.23)$$

where, A = Area and P = perimeter of the domains. Circular domains have a form factor of approximately 1, whereas the form factor of irregularly shaped domains can approach very small values.

Weis et al. (1998) and Steinmann et al. (2001) applied this technique to PMMA/PS blends. Steinmann et al. (2001) found that the form factor distribution is actually bimodal for cocontinuous morphologies. Thus, the form factor can be separated into a mean form factor of irregular domains, ff_{irr} ; and another mean form factor of circular domains, ff_c . The latter also includes fibrillar domains lying perpendicular to the cutting direction and not contributing to the cocontinuity. The minimum of the mean form factor of the irregularly shaped domains ff_{irr} then represents the maximum in cocontinuity and yields the phase inversion concentration and is shown in Figure 2.8. Thus, by means of image analysis of two dimensional SEM micrographs, the transition from a spherical morphology to cocontinuity can be characterized by the form factors.

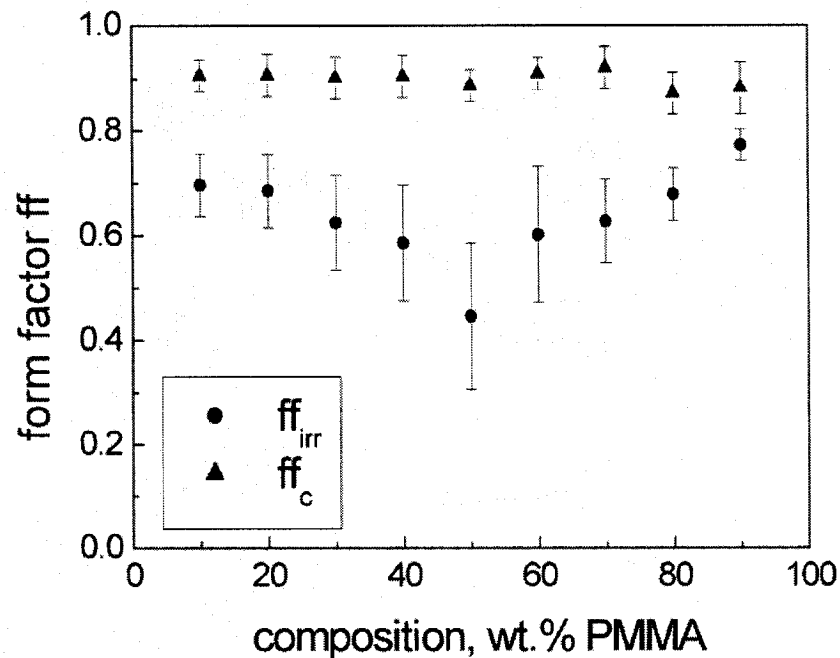


Figure 2.8: Distribution of the two mean form factors depending on the blend composition (Steinmann et al. (2001))

2.5.2.1.c Interfacial area to volume ratio and other methods

Several authors have used many different tools, developed in science for evaluating the mathematical morphology of images. Quintens et al. (1990, 1991) used the Chalkey parameter which estimates the volume-to-surface ratio of irregular features. Harrats et al. (1995, 2003) and Gubbles et al. (1995) used an “opening size granulometry distribution”, in which the total area of a number of circles that may be inscribed into the phase was related to the total area of the phase. Blacher et al. (1993) and Harrats et al. (1995) used multifractal analysis for determining the level of continuity. Dedecker et al. (1998) used interfacial area per volume unit of the minor

phase calculated from the total perimeter of the particles divided by their total area. Galloway (2002, 2004) measured the amount of interfacial area per unit volume and compared several different common techniques for measurements of continuity such as, solvent extraction, electrical conductivity, and rheology. This novel method operates by detecting edges within the images and using standard image processing operations to selectively eliminate false edges. They found that the interfacial area per unit volume exhibits maxima for blend compositions at the boundary between droplet and cocontinuous morphologies, as shown in Figure 2.9. They claimed that SEM with image analysis and solvent extraction provide the most quantitative information about the blend morphology and are the most powerful methods for characterizing the region of cocontinuity.

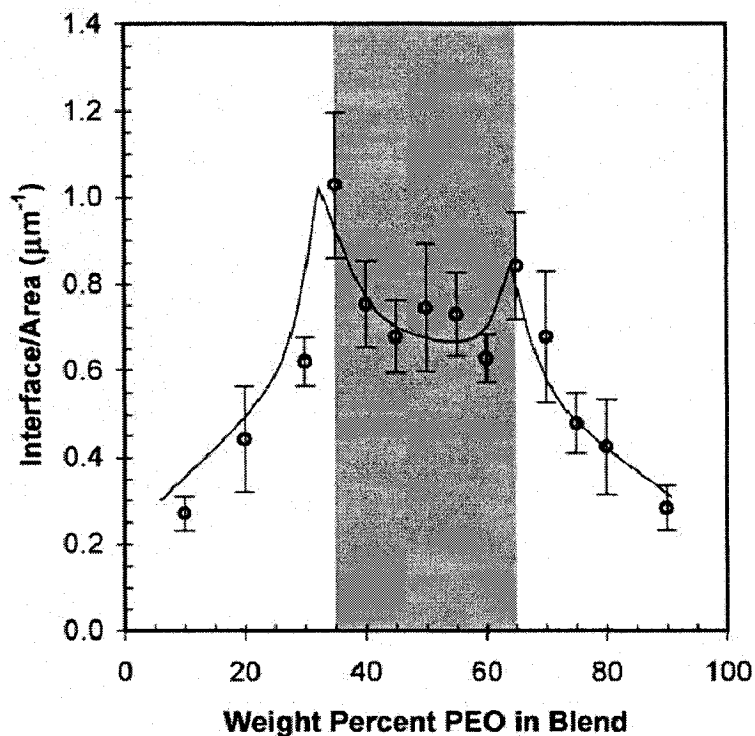


Figure 2.9: Amount of interface per unit area of image as a function of blend composition (Galloway et al. (2002))

2.5.2.2 Atomic force microscopy (AFM)

Atomic force microscopy is a novel microscopic technique, in which a cantilever beam with an Ångstrom sized tip scans the surface of a sample by physically contacting it. As it contacts the surface it gathers information on the topography of the surface, local properties at that point, chemical composition etc. In the field of polymer blends, that information can be used for detecting morphologies, especially in cases where microtomy, etching and staining techniques cannot be used.

More recently, a number of authors (Nysten et al. (1995), Galuska et al. (1997), Trifonova-Van Haeringen (1999), Chung et al. (2001), Tanem et al. (2003), Yerina et al. (2003), Ellul et al. (2004)) have applied AFM in various operating modes such as contact, lateral (friction), tapping, and force modulation in order to characterize complex morphologies. Virgilio et al. (2005) carried out tapping mode AFM on focused ion beam (FIB) etched ternary polymer blends of high density polyethylene/polystyrene/poly(methyl methacrylate) (HDPE/PS/PMMA). It was shown in that work that the three polymer components have different ion beam etching rates, which creates a topological contrast between the phases of the blends when viewed by TMAFM. The contrast levels obtained were so high that this approach allowed for the estimation of the PS interphase thicknesses from 100 to 200 nm depending on the PS/PMMA composition ratio.

2.5.2.3 BET and mercury porosimetry

Recently, Li et al. (2001) successfully applied two different techniques, BET (Brunauer, Emmet and Teller) nitrogen adsorption and the mercury porosimetry technique for analyzing cocontinuous polymer morphologies in all three dimensions.

In the BET technique, nitrogen gas is passed through the porous sample obtained after selective extraction of one of the blend components. The sample is brought to liquid nitrogen temperature by quenching the sample tube into liquid nitrogen. The nitrogen gas passing through the sample therefore condenses and adsorbs onto porous surface of the sample. The total volume of nitrogen gas adsorbed on the

surface is then measured. Then, assuming that the adsorption is a monomolecular layer, the surface area of the sample, S , is calculated from the following equation :

$$S = \frac{v_m \cdot N \cdot a}{V_M} \dots\dots\dots (2.24)$$

where, N is Avogadro's number, a is area of one adsorbed nitrogen molecule which is $16.2 \times 10^{-20} \text{ m}^2$, V_M = molar volume of the gas and v_m = volume of the nitrogen gas required to form monomolecular layer.

Two simplifying assumptions are made: (a) the pores in the sample are considered as interconnected cylinders and (b) only the surface of the pore wall is considered. In that way, the pore diameter, d , may be estimated by,

$$d = 4 \cdot \frac{V}{S} \dots\dots\dots (2.25)$$

where V is total volume of pore in the sample. Thus the surface area and pore diameter of the blend system can be measured by using the BET nitrogen adsorption technique.

The mercury porosimetry approach involves evacuation of all gas from the porous sample. Mercury is then introduced into a sample container while under vacuum. Finally, pressure is applied to force mercury into the porous sample. The mercury volume forced into the pores is usually monitored in a penetrometer containing the sample and filled with mercury. The experimental data treatment is based on the following Washburn equation,

$$P \cdot r = - 2 \sigma \cos \theta, \dots\dots\dots (2.26)$$

where, P is applied pressure, r is radius of the pore, σ is the interfacial tension (480 mN/m), and θ is the contact angle of mercury (140°). Thus the pore size and pore size distribution can be obtained from mercury porosimetry.

Unlike other techniques, both techniques use three dimensional samples, are very rapid, and are also less laborious. These techniques are powerful tools for the quantitative analysis of the cocontinuous morphologies.

2.5.2.4 Extraction gravimetric technique

Extraction gravimetry is a classical and simple technique for the determination of the percentage continuity of the minor phase. In the case of extraction gravimetry, the blend sample is weighed before and after selective solvent extraction of the dispersed phase. Then the % continuity of that dispersed phase is calculated using the following equation,

$$\% \text{ Continuity} = \frac{\text{Initial wt. of the sample} - \text{Final wt. of the sample}}{\text{Initial wt. of the sample} \times \text{wt. fraction of the extracted phase in the sample}} \times 100 \quad (2.27)$$

A number of authors have used this technique for the measurement of continuity and cocontinuity in polymer blend systems. The amount of swelling of the material and the availability of selective solvents are the limitations of this technique.

2.5.3 Influence of various material related parameters on cocontinuity

2.5.3.1 Viscosity ratio, elasticity ratio, and composition

Most of the literature on this topic has already been covered in section 2.5.1 which presented the mathematical models for predicting the composition for phase inversion and cocontinuity.

2.5.3.2 Interfacial tension

Interfacial tension is one of the most crucial parameters in determining the formation of cocontinuous structures in polymer blends. To identify the role of interfacial tension and its effect on continuity development and cocontinuity, Li et al. (2002) defined and examined three different types of blend interfaces. The first was a compatible binary interface (Type I), i.e. blends with low interfacial tension, comprised for example of high density polyethylene (HDPE)/styrene-ethylene-butylene-styrene (SEBS); the second was an incompatible binary interface (Type II), i.e. the blends with high interfacial tension, comprised for example of HDPE/polystyrene (PS); and the third was a compatible ternary interface (Type III), comprised for example of HDPE/PS compatibilized by SEBS. Based on the droplet and fiber lifetimes, Li et al. proposed that continuity develops by fiber-fiber coalescence in the case of low interfacial tension blends (Type I). It develops by droplet-droplet coalescence for the high interfacial tension blends (Type II) and by reduced droplet-droplet coalescence for the compatibilized blends (Type III).

Thus for low interfacial tension blends (Type I), they observed the onset of percolation and cocontinuity at low composition of dispersed phase. The cocontinuity is maintained over a wider composition range, and very little effect of composition on pore size of the blend is seen. The high interfacial tension (Type II) blends showed a delayed percolation threshold and attained cocontinuity at higher concentrations. These latter blends maintained cocontinuity over a smaller composition range and the pore size increased significantly with composition, as would be expected due to droplet-droplet coalescence. Because of an interfacial modifier at the interface, compatible ternary interface (Type III) showed even higher percolation thresholds and attained cocontinuity at even higher concentrations. Therefore, the region of cocontinuity was also narrowed further. All the features discussed are shown in Figure 2.10 through 2.12.

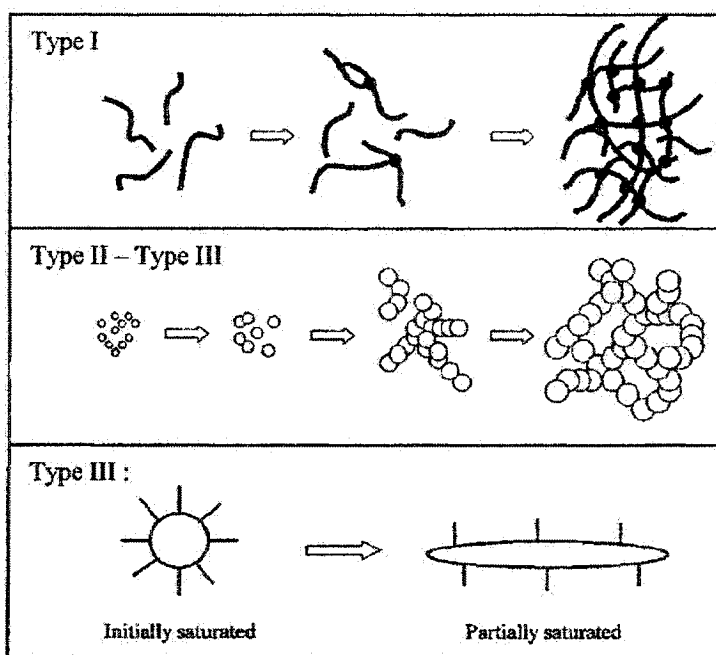


Figure 2.10: Schematic presentation of continuity development for different type of blend interfaces (Li et al. (2002))

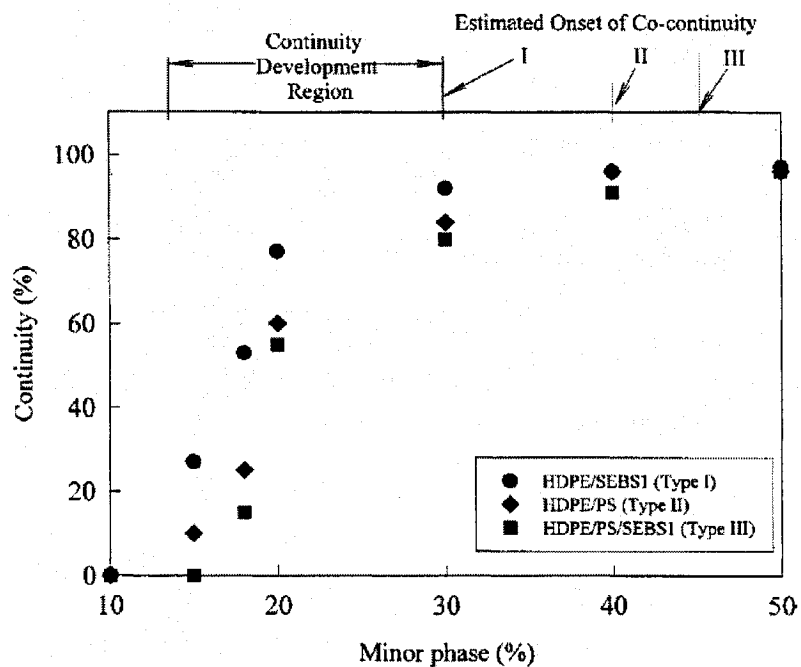


Figure 2.11: Continuity development for different blend systems (Li et al. (2002))

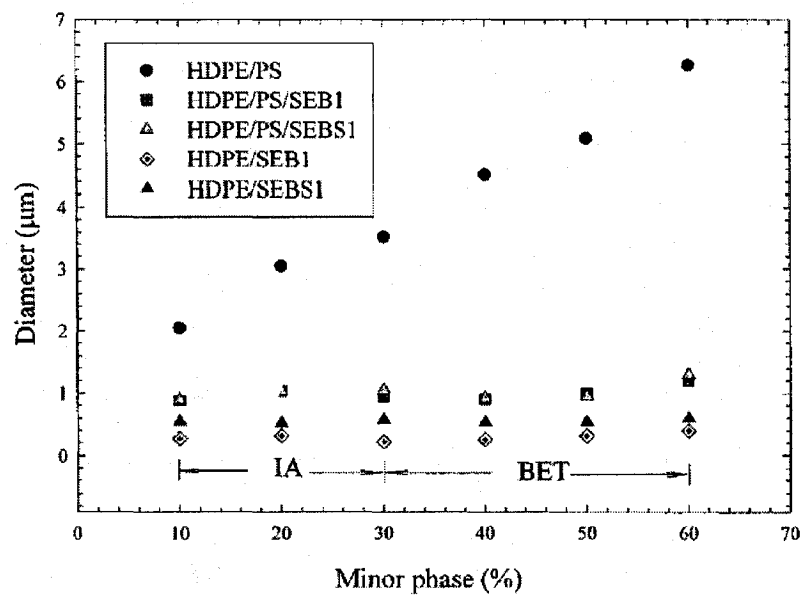


Figure 2.12: Pore size as a function of minor phase composition for different blend systems (Li et al. (2002))

Gubbels et al. (1995), Bourry et al. (1998), Chung et al. (1997), Willemse et al. (1998, 1999), Veenstra et al. (1999), and Steinmann et al. (2002) have also made similar observations for cocontinuous morphologies.

Marin et al. (2002) studied the co-continuous morphology development in partially miscible poly(methyl methacrylate) (PMMA)/polycarbonate (PC) blends. Both polymers are amorphous in nature and possess an interfacial tension of 0.6 mN/m. Due to the low value of the interfacial tension this blend system was expected to demonstrate the typical features of the binary compatible (Type I) blends, reported earlier by Li et al. (2002). However, due to the partial miscibility between the blend components these blends presented artificially high percolation thresholds, and attained cocontinuity at higher than expected compositions of the minor phase. Furthermore, these blends demonstrated significant coalescence effects as a function of dispersed phase composition as compared to the highly stable morphologies observed for fully immiscible binary blends of low interfacial tension. Both of these results are shown in Figure 2.13 and 2.14.

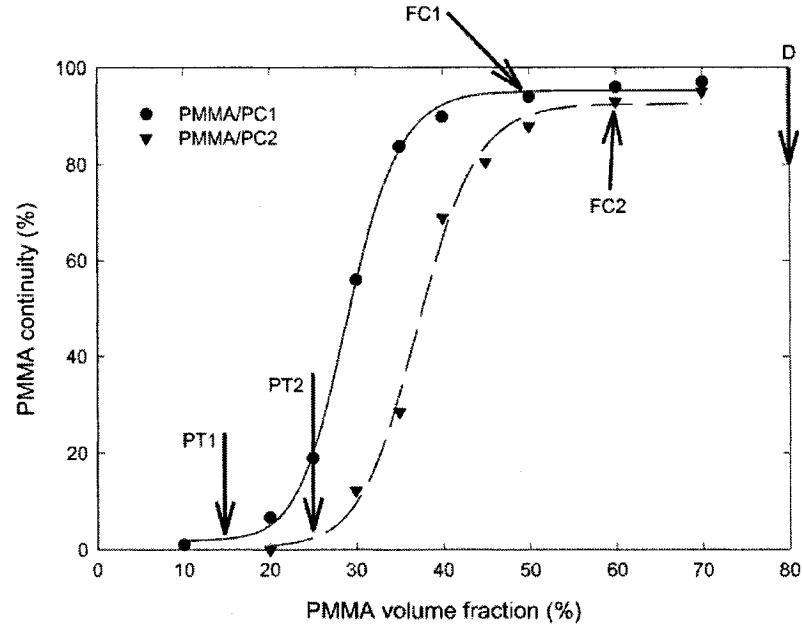


Figure 2.13: Continuity development in PMMA/PC blends (Marin et al. (2002))

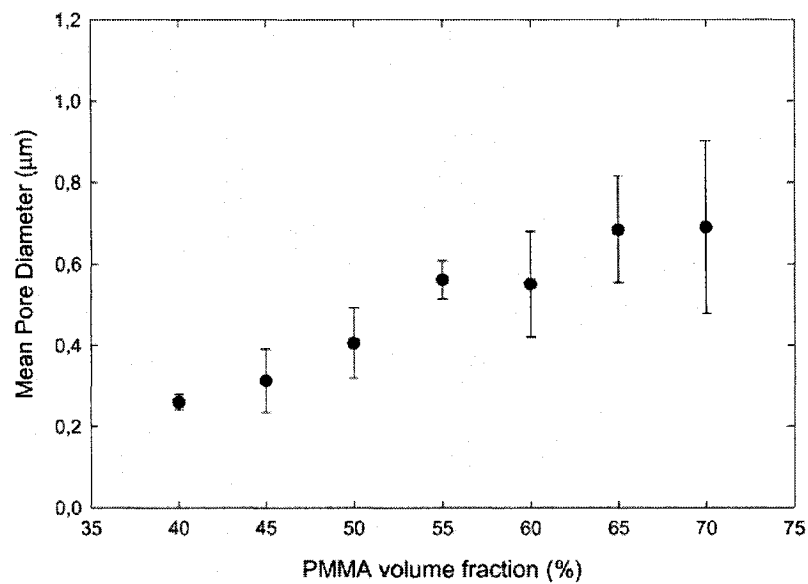


Figure 2.14: Coalescence in PMMA/PC blends (Marin et al. (2002))

The partial miscibility between the blend components was shown by measuring glass transition temperatures for both the PMMA-rich and the PC-rich phases at

different blend compositions using dynamic mechanical thermal analyzer (DMTA). The results are shown in Figure 2.15. The figure shows that the glass transition temperatures of PMMA and PC phases in the blend are shifting towards each other because of the partial miscibility.

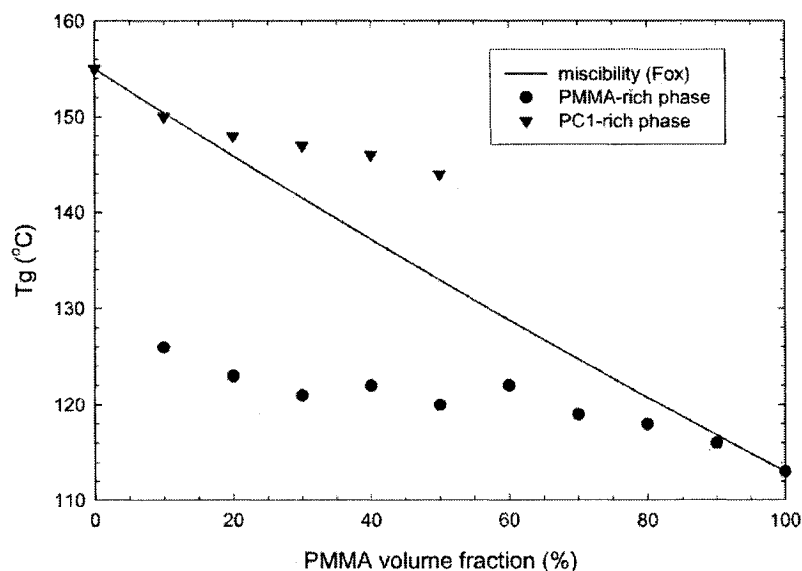


Figure 2.15: Glass transition temperatures of both the PMMA-rich and the PC-rich phases as a function of PMMA composition (Marin et al. (2002))

Marin et al. (2002) quantitatively estimated the extent of partial miscibility using the Fox equation and applied detailed correction to the gravimetric data by considering the blend as a mixture of a PMMA-rich phase with a PC-rich phase. By correcting the continuity and co-continuity data in this way they were able to demonstrate that indeed the blend showed all the principal features of a low interfacial tension system, as shown in Figure 2.16. They related the increase of phase size with increasing composition to a reduced miscibility of the PMMA/PC system.

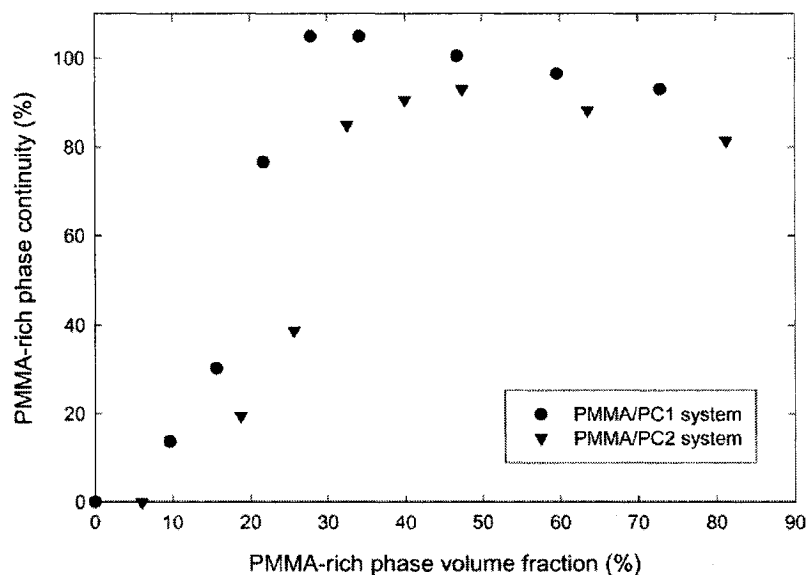


Figure 2.16: Continuity development in PMMA/PC blends after correction

(Marin et al. (2002))

2.5.3.3 Interfacial modifier

The effects of an interfacial modifier are fairly well understood for dispersed structures; however, they are much more complex during the formation of cocontinuous structures. As such, at the interface, compatibilizers are known to reduce the interfacial tension and prevent coalescence. Lower interfacial tension favors the formation and stability of cocontinuous structures. Reduced coalescence may hinder the cocontinuity formation, but once formed, it is known to increase network stability. However, on the other hand, the interfacial modifier also enhances interfacial viscosity, applied shear stress, and interfacial adhesion. These combined effects render the understanding of the effects of compatibilization on cocontinuous structure development difficult.

Most investigators have noted a composition-delayed formation and a narrower composition range of cocontinuity upon addition of an interfacial modifier. These observations cannot be explained by a reduced interfacial tension effect. On addition of SEBS interfacial modifier in PS/HDPE blends Bourry et al. (1998) and Li et al. (2002) noted a shift in the percolation threshold for PS particles to higher concentrations as shown in Figure 2.17, which ultimately narrowed the cocontinuity region. However, most experimental results reveal no influence on the position of the midpoint composition of cocontinuity upon addition of an interfacial modifier.

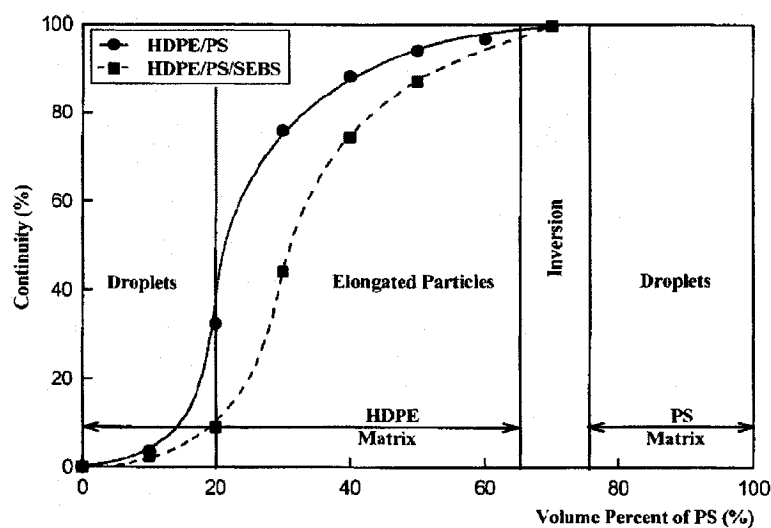


Figure 2.17: Effect of an interfacial modifier on continuity development in PS/HDPE blends (Bourry et al. (1998))

Several authors (e.g. Mekhilef et al. (1997) and Li et al. (2002)) show that the addition of the compatibilizer leads to much finer cocontinuous structures and reduces the coarsening of the structure during annealing. This is mainly due to the lower interfacial tension and higher stability against breakup.

Dedecker (1998) noted that the addition of copolymer transforms the cocontinuous morphology into a dispersed phase morphology. The time required to reach an equilibrium dispersed phase morphology, however, will depend upon the concentration of compatibilizer.

2.5.4 Influence of processing related parameters on cocontinuity (miscellaneous variables affecting cocontinuity)

Various processing related parameters are known to affect cocontinuity. These variables may be responsible for generating the cocontinuous structures (e.g. as a transitory morphology in early stages of melt mixing) or may affect the cocontinuous morphology generated during normal melt processing.

Sundararaj et al. (1995-1996) and Scott et al. (1994, 1995) did a significant work on morphology development during very early stages of melt blending. Their studies show that millimeter sized pellets of polymer quite gradually and rapidly reduce to micron sized structures. They found that the molten pellets are first stretched and folded into thin sheets under the combined influence of complex shear and elongation forces. These sheets reach a critical thickness and capillary wave instabilities lead to the formation of holes in the sheet. As mixing continues, the size and concentration of holes increase and the sheets break down into irregularly shaped particles or cylinders, and eventually reduce into spherical droplets via capillary instabilities. These authors observed the formation of a transitory cocontinuous structure during this sheet breakup process.

Sundararaj et al. (1996) observed the formation of a cocontinuous structure during phase inversion which was the result of melting point differences between the polymer blend components. During the early stages of mixing a minor component, which is expected to form the dispersed phase, melts and coats the major component pellets because of its lower melting point. As mixing continues, the major phase softens and forms the sheets, which eventually break up into irregularly shaped particles. These particles then coalesce around the minor phase to form the final matrix causing phase inversion. The author found the presence of a transitory cocontinuous structure during this phase inversion process and also noticed the trapping of small particles of major phase inside the minor phase as a result of this phase inversion process. Lee and Han (1999) also noted similar observations for blends prepared in the extruder.

Sarazin et al. (2005) observed important effects of the temperature of mixing on cocontinuity. They found for polystyrene/poly(ϵ -caprolactone) (PS/PCL) blends that the continuity develops rapidly and the blends become cocontinuous at lower compositions of minor phase as the temperature of blending is reduced. The results are shown in the Figure 2.18.

The temperature of melt blending is especially important in polymer blends containing elastomers which exhibit a melt yield stress, as shown by Veenstra et al. (1999). Elmendorp (1986) carried out several breaking thread experiments, including threads of fluids exhibiting a yield stress. He found that the breakup of such threads is prevented as long as the yield stress exceeds the pressure difference due to the

interfacial tension. In such case, the distortions will be unable to grow and the threads will remain stable. Due to this enhanced thread stability, very stable cocontinuous structures over a wide range of composition can be obtained.

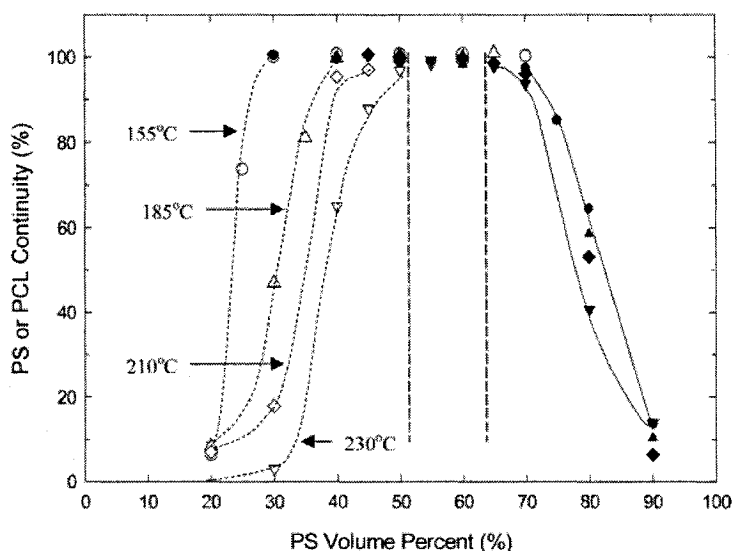


Figure 2.18: Continuity development in PS/PCL blends at different melt blending temperatures

Veenstra et al. (1999) prepared blends of polymers showing a melt yield stress and found that it is essential to process the block copolymer in a microphase-separated state, i.e. below its order-disorder temperature (ODT), in order to form stable cocontinuous structures over a very wide composition range. Blending in the single phase state, i.e. at higher temperatures where the copolymer does not exhibit a melt yield stress, leads to a narrower composition range of cocontinuity. Further it is found that annealing these cocontinuous morphologies below the ODT barely influences the composition range and coarseness level, whereas annealing above ODT increases the

domain size significantly or leads to a breakup into dispersed structures. This ultimately reduces the composition range of cocontinuity. Several other authors like Gergen et al. (1984,1996), Ho et al. (1990), Verhoogt et al.(1994), Li et al. (2002) have reported similar observations.

Other parameters such as higher shear rates and prolonged mixing times are also known to reduce cocontinuous structures into a dispersed droplet type of morphology. Ha et al. (1997) found that cocontinuity occurs over a wide composition range after mixing for a short time. An increase in the mixing time narrows the composition range of cocontinuity and finally reduces it to one point. He concluded that the final morphology is determined only by the volume fraction rather than by the viscosity ratio. Thus, the cocontinuity will occur only at a volume ratio of 50/50 and at all other compositions the minor phase will form spherical droplets after prolonged mixing times. Veenstra et al. (1999) also observed similar phenomenon after blending for longer times and at high shear rates.

- *Annealing*

Though interfacial tension is the main driving force behind coarsening of cocontinuous morphologies during static annealing, other parameters such as viscosity ratio and phase dimensions also play a very important role. On annealing, many authors such as Quintens et al. (1993), Mekhilef et al. (1997), Verhoogt et al. (1994), Willemse et al. (1999) have observed that cocontinuous morphologies breakup into dispersed phase morphologies upon static coarsening. Annealing, thus, effectively reduces the

composition range over which cocontinuity exist. Stone et al. (1986) showed that capillary type breakup mechanism occurs only in the case of highly extended fibers; otherwise fibers only retract to a spherical shape. The breakup time of these fibers also depends on the phase dimensions. At lower concentrations, the cocontinuous structure breaks up quickly and reduces to a dispersed phase morphology because of the thinner threads. Thus, there is a critical volume concentration ($\phi_{cc,stable}$) above which the cocontinuous structure does not breakup during annealing. Willemse et al. (1998) formulated an equation for calculating this critical concentration and its dependence on zero shear viscosity ratio of the blend components and is shown in Figure 2.19.

Veenstra et al. (2000) found that the static coarsening rate (dr/dt) of cocontinuous morphologies could be related to the interfacial tension and zero shear viscosity of the blend materials, as follows,

$$\frac{dr}{dt} = \frac{c \sigma}{\eta_e} \dots\dots\dots (2.28)$$

where, r is average thickness of network ligaments, c is a dimensionless factor, σ is the interfacial tension, and η_e is effective viscosity (weight average of the components zero shear viscosity).

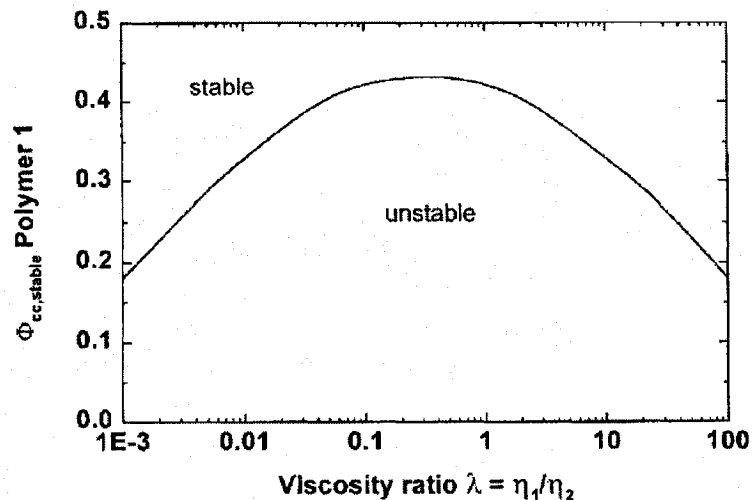


Figure 2.19: The volume fraction at which a cocontinuous morphology once formed is stable against breakup into droplets as a function of the viscosity ratio of the blend components

Using a conceptual model of cocontinuity based on thin and thick rods, very recently Yuan and Favis (2005) proposed that the driving force for the coarsening of cocontinuous morphologies during a quiescent annealing process is capillary pressure. The differences in capillary pressure throughout the cocontinuous structure result in a continuous merging of thin parts toward the thick ones.

The thick rods were treated as a cylindrical thread which cannot break up via capillary instability due to the numerous branches which continuously feed it. Thus, it was proposed that the rate of growth of the distortion amplitude ($d\alpha/dt$), taken from Tomotika analysis for capillary instabilities, can be directly related to the coarsening rate (dr/dt). Since α_0/R_0 (ratio of the initial distortion amplitude to the initial thread radius) was found to be constant for all studied cocontinuous systems, the coarsening

rates are controlled by the interfacial tension, the zero shear viscosity of the surrounding medium and Ω from Tomotika theory, as shown in following equation,

$$k = \alpha_o q = (\alpha_o / R_o) \frac{\sigma \Omega(\lambda, p)}{2 \eta_c} \dots\dots\dots (2.29)$$

where, k refers to the pore size growth rate (coarsening rate), α_o is the initial distortion amplitude, R_o is the initial thread radius, q is the growth rate, σ is the interfacial tension, $\Omega(\lambda, p)$ is the complex function from Tomotika equation, and η_c is the viscosity of the continuous phase. In other words, the more easily a thread of one phase breaks up according to Tomotika theory, the more readily a thread of that phase can grow and the faster the phase can coarsen on annealing.

This model explains all of the principal features observed in the coarsening of immiscible cocontinuous blends: (a) the linear time dependence, (b) the continuous coarsening over long timescales, (c) the influence of interfacial tension and zero shear viscosity, and (d) the actual coarsening rate itself.

The presence of an interfacial modifier at the interface of a cocontinuous blend is known to stabilize a cocontinuous morphology against annealing. Harrats et al. (1995) found that due to the direct location of copolymer at the blend interface, the copolymers are also able to prevent the coalescence of the emulsified microphases. However, in the absence of copolymer, the cocontinuous network rapidly disrupts into dispersed particles on heating the blends at 200°C for only a few minutes. They further

found that a tapered block copolymer is more efficient than the corresponding pure diblock for stabilizing the cocontinuous structure.

- *Effect of chemical crosslinking on cocontinuity*

Very little research has been done on the effect of selective chemical crosslinking (vulcanization) on the cocontinuity of a polymer blend. During the manufacturing of materials known as “Thermoplastic Vulcanizates”, the elastomer phase is selectively crosslinked in-situ. As a result of this chemical reaction the viscosity of the elastomer phase increases to a very high level which ultimately prevents its coalescence with the other elastomer particles. Thus the crosslinked elastomer particles remain dispersed in the matrix of another polymer even if it is present in much higher concentration than the other polymer and thus forms the inverted-matrix type of morphology. There are only some brief references in the literature suggesting the formation of a cocontinuous morphology during the transition of the matrix elastomer phase to the dispersed phase during selective chemical crosslinking. It is suggested that if one begins the selective chemical crosslinking of a cocontinuous elastomer phase it also ends up as a dispersed crosslinked elastomer phase in the matrix of the other polymer. Thus, selective chemical crosslinking appears to destabilize cocontinuous morphologies completely and reduce them to a dispersed phase morphology. This aspect will be discussed further later in this review in relation to EPDM/PP blends.

2.6 Literature related to EPDM/PP blends and their thermoplastic vulcanizates

2.6.1 History and introduction

EPDM/PP blends are commercially very important due to their composition dependent properties and the further improvement in the properties due to the selective crosslinking of the elastomer phase. Thermoplastic Vulcanizates (TPVs) have seen widespread use since their first commercial introduction by the Monsanto Company, under the trade name “Santoprene Thermoplastic Rubber”, in 1981. The dynamic vulcanization process, wherein the elastomer phase is in-situ crosslinked during melt mixing, was first discovered by Gessler et al. (1962) and by Holzer et al. (1966) independently, while attempting to improve the impact properties of PP through the partial vulcanization of halo butyl rubber with zinc oxide. However, the first commercial application was based on the patents by Fischer (1974) wherein the partial dynamic vulcanization of EPDM in a PP matrix was accomplished by limiting the amount of peroxide to maintain the thermoplastic processibility of the blend. Significant improvement in the properties of these blends was achieved by Coran and Patel (1978) by fully vulcanizing the rubber phase under dynamic shear, without affecting the thermoplasticity of the blend. This discovery was further advanced by Abdou-Sabet et al. (1982) through the use of preferred curatives to achieve improvement in elastomeric properties and flow characteristics, which have now aided the successful commercialization of this dynamic vulcanization technology.

Dynamic vulcanization differs from the more common static vulcanization in that vulcanization occurs during mixing or mastication of the composition being prepared. If enough of the thermoplastic resin is present in the molten state, as part of the composition being masticated, the mixture does not lose processibility as a result of vulcanization. This is true even when the rubber is fully cured. Thus products, elastomeric in nature yet with the processibility of thermoplastics, can be prepared.

Dynamic curing generates the same necessary crosslinks or three-dimensional polymer structures, as static cure. In dynamic curing, however, these structures are generated in small rubber particles dispersed in the non-crosslinked thermoplastic polymer matrix as a microgel. Partially crosslinked compositions give a modest improvement in material properties relative to non-crosslinked blends. Fully curing the rubber phase and controlling the rubber particles to a diameter of 1-2 μm or less, leads to a significant improvement in the material properties.

TPVs are also economically more attractive due to their well-known thermoplastic processibility as compared to the traditional multi-step thermoset rubber processing. The traditional rubber processing frequently consists of three steps: mixing, shaping, and vulcanization. Each step is known to be capital, labor and energy intensive. While significant progress has been made over the past years in reducing these costs with the advent of continuous cure extrusion lines and increased usage of injection molding, thermoset rubber processing still remains more expensive than thermoplastic processing because of the costs of mixing, vulcanization and the

production of non-recyclable scrap. Due to all these reasons TPVs have become very competent in the market and are still replacing many traditional thermoset rubber products. A better scientific understanding of the morphology of these products should engineer the new products with these materials.

2.6.2 Rheology of EPDM/PP blends

Many authors have noted that both EPDM and PP show typical shear-thinning behavior. Chung et al. (1997) have found that these materials follow the Cox-Merz empiricism, i.e. $\eta^*(\omega) = \eta(\dot{\gamma})$, complex viscosity in the rheometer is the same as shear viscosity.

Rheologically, TPVs behave in a similar fashion to highly filled polymer composites in shear flow. TPVs display highly pseudoplastic behavior, and thus provide unique processing characteristics that enable a TPV product to perform well in both injection molding and extrusion. The high viscosity at low shear rate provides better integrity, less die swell of the extrudate during extrusion. The low viscosity at high shear rate enables low injection pressure and less injection time. Therefore, the high-flow TPV not only aids in injection molding, but also provides lower backpressure for extrusion. The low die-swell characteristics of TPVs also give high precision for dimensional control during extrusion. The rheology of vulcanized EPDM/PP blends has been studied by Jain et al. (2000) and Chung et al. (1997). They found that the melt viscosity increases with increasing EPDM concentration and decreases with increasing intensity of the shear mixing for all compositions. In comparison to non-vulcanized

blends, dynamically vulcanized blends display higher viscosity and highly pseudoplastic behavior.

2.6.3 Morphology of EPDM/PP blends

Despite the structural similarity EPDM itself is not miscible with PP. Blends of EPDM/PP do not follow the logarithmic additivity rule of viscosity which is expressed as: $\ln \eta_{\text{blend}} = w_1 \ln \eta_1 + w_2 \ln \eta_2$, where: w_1 and w_2 are the weight fractions and η_1 and η_2 are the viscosity of the blend components in the melt state, respectively. However, instead of a linear increase in the torque (proportional to the viscosity), in all cases the torque was lower than the theoretical value. Arroyo et al. (2000) suggested, this can be attributed to the immiscibility of the components of the blend, as was previously also suggested by Utracki and Schlund (1987).

Yang et al. (1984) found that EPDM is more compatible with PP than the other rubbers. On solution blending of EPDM rubber, polybutadiene rubber (PB) and styrene-butadiene rubber (SBR) with PP, they found that phase separation was evident in all three rubbers. Only the shape, size, and the distribution of the particles vary with the type of rubber, with EPDM particles being the smallest (400 to 800 Å). Thus, the compatibility of PP varies in the order: EPDM > PB > SBR.

At lower compositions EPDM shows a spherical dispersed phase morphology. D'Orazio et al. (1991) found the number average particle diameter increases from 0.3 to 0.5 μm and the particle size distribution increases with the viscosity ratio. When the mixed polymers have similar melt viscosities, Danesi et al. (1978) and Karger-Kocsis et

al. (1984) found that the resultant morphology is very fine and the distribution of the minor component is very uniform. Lower ethylene content and low molecular weight also further favor a fine distribution of EPDM. When the components have different melt viscosities, the morphology of the resultant blend depends on whether the minor phase has a lower or higher melt viscosity than the major one. If the minor component has a lower viscosity, this component will be finely and uniformly dispersed with domains oriented in the extrusion direction. In contrast, the minor component will be coarsely dispersed, essentially in spherical domains, if its viscosity is higher than that of the major phase. The relative viscosities of the components determine the extent of deformation of the phases. When the viscosity of the minor component is equal to or lower than that of the major one, the dispersed component experiences the same extent of deformation which is imposed on the continuous phase. In contrast, if the viscosity of the minor component exceeds that of the major one, the deformation of the dispersed phase is always less than the deformation imposed on the continuous phase.

In the case of TPVs the optimum morphology should remain stable during the fabrication of the material into final parts, and during use. If the elastomer is fully vulcanized then it is easier to achieve all these criteria. According to Coran and Patel (1978), the vulcanization can be said to be complete if the cyclohexane extractibles are less than 3% of the weight of the rubber at 23°C, or if the crosslink density determined on the same monoolefin copolymer rubber is greater than about 7×10^{-5} moles per mL of rubber.

Another very crucial morphological factor in enhancing the mechanical properties of TPVs is the dispersed rubber particle size. Coran and Patel (1980) have demonstrated the importance of rubber particle size in TPVs. Figure 2.20 depicts the effect of the fully vulcanized dispersed phase particle size on the mechanical properties. Clearly, the ultimate properties are an inverse function of rubber particle diameter. When preparing TPVs, an emphasis should be placed on obtaining the lowest particle size.

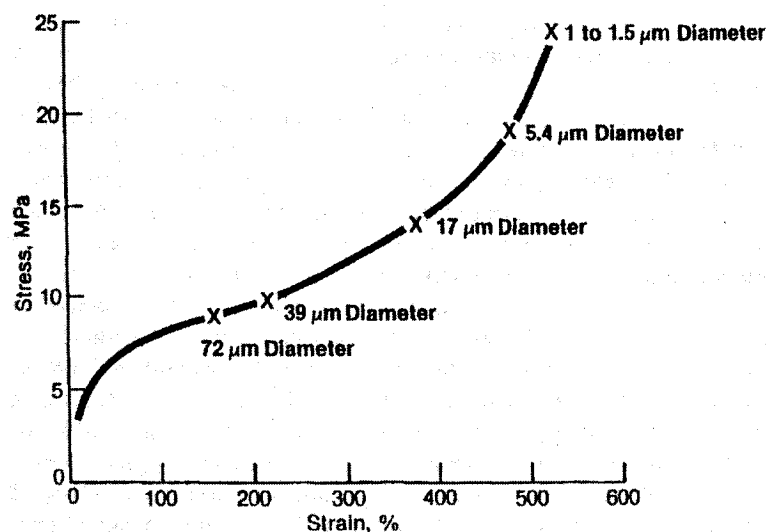


Figure 2.20: Effect of vulcanized-rubber particle size on the mechanical properties of EPDM/PP TPVs

Interfacial tension plays the most crucial role in determining the particle size. However the interfacial tension or critical surface tension (γ_c) itself is a function of the surface tension and polarity of the polymers. To evaluate the effect of interfacial tension on the blend morphology and properties, Coran and Patel (1981) used three different

polarity rubbers: ethylene-propylene-diene monomer (EPDM), ethylene-vinyl acetate rubber (EVA) and nitrile rubber (NBR) and four different polarity plastics: polypropylene (PP), polystyrene (PS), polystyrene-co-acrylonitrile (SAN) and nylon polyamides (PA).

The parameter γ_c correlates with the solubility parameter δ , and is also a measure of polarity. The reason for considering γ_c was that the difference ($\Delta\gamma_{SH}$) between γ_c for the soft phase material and that of the hard phase material might relate to interfacial surface energy. The values of γ_c were taken from the literature and are at room temperature. The values which were not available, were estimated on the basis of the correlation between solubility parameter δ and γ_c . The following Table 2.1 shows various values of γ_c for different polymers.

**Table 2.1: Critical surface tension for different polymers at room temperature
(Coran and Patel, (1981))**

Polymer	γ_c, mN/m	W_c	σ_H, MPa	E, Mpa
PP	28	0.63	30	660
PS	33	0.0	42	1550
SAN	38	0.0	58	1730
PA 1,1	31	0.25	43	850
PA 6,9	39	0.25	46	1250
PA 6,66	40	0.25	29	700
EPDM	28	0.0	-	3
EVA	34	0.0	-	3
NBR	39	0.0	-	3

They found that the smaller the difference of γ_c between the two phases, the lower the expected interfacial tension. During the early part of the vulcanization phase of the process, they found that the rubber became highly viscous and was forced to be the dispersed phase. Thus, a lower interfacial tension results in smaller rubber droplets, smaller cured rubber particles and better mechanical properties.

The viscosity ratio is another important parameter in determining the phase morphology of the blend. Abdou-Sabet and Patel (1991) found that at low compositions of EPDM, the EPDM/PP blend showed a dispersed phase morphology, irrespective of the viscosity ratio. As the composition increased the blend with a low viscosity ratio showed signs of cocontinuity at a composition of 40/60 EPDM/PP. In the case of the high viscosity ratio blend, the morphology was still predominantly a dispersed phase. At higher compositions both, low and high viscosity ratio, EPDM blends showed cocontinuity. At the 80/20 EPDM/PP composition, the PP appeared to be dispersed phase in an EPDM matrix for both viscosity ratio blends suggesting that phase inversion had already taken place. Karger-Kocsis et al. (1984) found contradictory results, the low viscosity ratio blends containing 20% EPDM showed the dispersed phase in the continuous PP matrix, and blends having a high viscosity ratio showed a co-continuous network at 20% EPDM. Karger-Kocsis explained that this might be due to the much smaller chance of destabilization or even breakup of the cylindrical threads during the blending process than for blends of a lower viscosity ratio value.

Abdou-Sabet and Patel (1991) explained that, for 80/20 EPDM/PP composition, PP is the minor component and is dispersed in the EPDM matrix. During dynamic vulcanization of such a blend, the EPDM and the PP have to undergo a phase inversion to maintain the thermoplasticity of the blend. In the initial stages of dynamic curing two cocontinuous phases are first generated and as the degree of crosslinking advances during mixing, the continuous rubber phase becomes elongated further and then breaks up into polymer droplets. As these droplets are forming, the PP becomes the continuous phase. This can be seen in the SEM micrographs of Figure 2.21, where the EPDM phase appears white and the PP black. The middle micrograph shows both phases to be cocontinuous. To confirm the dispersed phase morphology, since the rubber phase is quite dominant compared to the PP phase, Abdou-Sabet et al. (1991) diluted the composition to 20/80 EPDM/PP and then examined it by electron microscopy. The electron micrograph then definitely showed a dispersed-phase morphology.

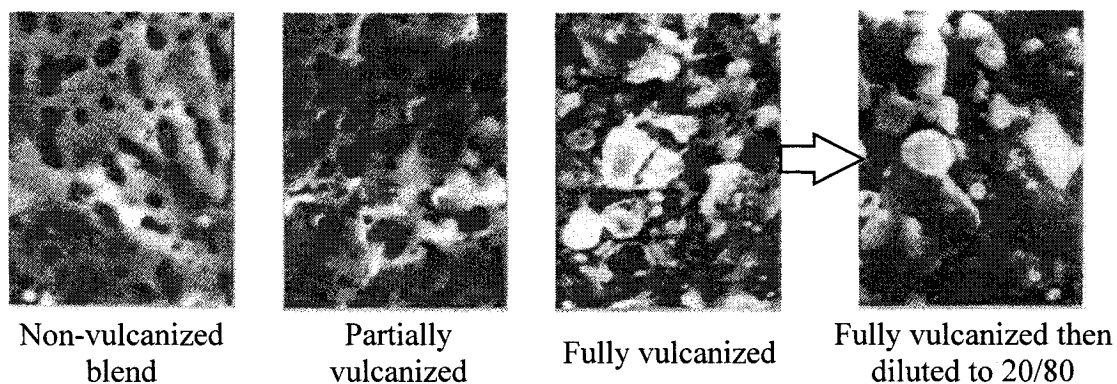


Figure 2.21: Morphology development for an 80/20 EPDM/PP TPV phase inversion (Abdou-Sabet et al. (1991))

They also noted that the low molecular EPDM requires higher amounts of curative to achieve similar crosslink densities and it showed a higher non-cured portion than the high molecular weight EPDM.

It is believed that the crosslinking of compatibilized blends should further increase the mechanical properties of the blend. However, not much scientific work is available on this topic. Kim et al. (1995) carried out the dynamic vulcanization by using dicumyl peroxide to control the miscibility in EPDM/PP blends which were already compatibilized by using sodium and zinc neutralized ionomers. From the rheology and crystallization studies of the compatibilized and vulcanized blends they suggested that the addition of ionomer and the application of dynamic vulcanization could create a synergy to improve the miscibility of PP and EPDM. The dynamically vulcanized EPDM and PP blend, with 15 wt% of Zn-ionomer and 1.0 phr dicumyl peroxide content, showed the most prominent thermoplastic IPN structure and enhanced miscibility of all the blends studied.

However, their conclusion seems very superficial. The above conclusion was drawn simply due to the observation of an increase in the viscosity of those blends. However, from the studies of Abdou-Sabet and others we can understand that the vulcanized blends of EPDM/PP actually behave like filled systems. This is to say, they show a higher viscosity than the non-vulcanized blends at low shear rate. After vulcanization the rubber transforms into a fine dispersed phase thermoset rubber in a

thermoplastic matrix. Thus, after vulcanization, the blend shows a heterophase morphology and will not induce miscibility in the TPV.

2.6.4 Compatibilized EPDM/PP blend

In EPDM/PP blends, the incompatibility of the blends is demonstrated by a poor interface and undesirable mechanical properties. One of the ways to control the morphology and improve the properties is through the use of “compatibilizers”, block or graft polymers that act as interfacial agents in polymer blends. There are two effects of the presence of the compatibilizer at the interface: the adhesion between the phases increases, and the interfacial tension between them decreases. As the interfacial tension decreases a finer dispersion of the phases can be achieved during intensive mixing. The smaller phase size along with the increased phase adhesion results in improved physical properties such as impact strength and tensile strength. A European patent by Tsujimoto et al. (1994) provides very good information and lists various compatibilizers that can be used to compatibilize EPDM/PP blends along with the methods to prepare them. Some of the copolymers used by Tsujimoto to compatibilize EPDM/PP blend includes styrene-butadiene-styrene (SBS), styrene-ethylene-butylene-styrene copolymers (SEBS) etc., epoxy-modified styrene-ethylene-butylene-styrene (EP-SEBS), maleic anhydride modified ethylene-propylene (MAH-EP), ethylene-glycidyl methacrylate-methyl acrylate terpolymer (E-GMA-AM) and maleic anhydride modified polypropylene (PP-MAH). Lohse et al. (1991) made a graft copolymer of PP and EPDM with iPP arms pendent from an EPDM backbone in a two step process. The EPDM is made in one

reactor and is then fed to a second in which iPP grows through the non-reacted double bonds of diene, forming the graft polymer. The formation of graft polymer is found to be greater than 50% and the addition of graft polymer reduced the average particle size by four times from 2 μm to 0.5 μm and doubled the low temperature impact strength. Kim et al. (1994, 2000) tried sodium (Na) and zinc (Zn) neutralized ionomers and a triblock copolymer of PP-g-MAH-co-PA 6,6-co-EPDM-g-MAH. Micrographs of ionomer compatibilized blends showed that the compatibilization is achieved at a 5 wt% concentration of Na-ionomer. The Zn-ionomer did not show any better compatibilization effect than the Na-ionomer. The triblock compatibilized blend showed the highest viscosity at a compatibilizer content of 0.5 wt.%, indicating that the most effective physical interlocking between the components occurs at this compatibilizer level. However, SEM micrographs of the cold impact fractured specimens did not show any notable difference in particle size with the compatibilizer content but increased the number of dispersed EPDM domains, and improved the uniformity of distribution of the EPDM domains. However both of their papers lacked the quantitative information and the micrographs did not show much variation in the particle size. Thus it is difficult to understand the effectiveness of these compatibilizers in compatibilizing EPDM/PP blend. Also the increase in properties was not significant, thus their efficiency does not seem to be good enough as a compatibilizer for EPDM/PP blends.

2.6.5 Crystallization in EPDM/PP blends

PP is a crystalline material and EPDM is an amorphous material in nature. For such blends, the morphology is very much dependent on the crystallization characteristics of the blend and this also affects the blend properties. In order to analyze the effect of the EPDM on the PP crystallization, at different temperatures, Arroyo et al. (2000) calculated the PP crystallinity degree from the crystallization isotherms of the blend with EPDM content. He found, at low EPDM percentages, that the increase of PP crystallinity in the blends was due to two simultaneous phenomena: EPDM particles act as nucleating agents for the PP crystallization, and simultaneously the PP crystallites act as nucleating centers for the polypropylene segments of the EPDM. It was suggested that at low EPDM contents in the blend ($\leq 25\%$), the particles of EPDM act as nucleating agents and co-crystallize with the PP, increasing both the crystallization rate and crystallinity of the PP. However, at higher percentages ($>50\%$), the EPDM obstructs the mobility of PP chains and hence decreases the PP crystallization rate. Martuscelli et al. (1982) also found that EPDM particles act as a nucleating agent for PP, and this nucleation efficiency is strongly dependent on the chemical structure and molecular mass of EPDM.

It is known that a EPDM/PP blend is immiscible at all temperatures, however, Lim et al. (1999) observed a spinodal decomposition (SD) type liquid-liquid phase separation at high temperature in a EPDM/PP blend. This indicated a partially miscible system i.e. the system with lower critical solution temperature (LCST)/upper critical

solution temperature (UCST). The evidence of phase separation by spinodal decomposition (SD) was given by observing structure formation at 130°C. By extrapolation of the data of the apparent diffusion coefficient ($D_{app.}$) vs. temperature, they found that the value of $D_{app.}$ at 130°C is very low. This implies that the liquid-liquid phase separation rate may be negligible at 130°C. On the other hand, the crystallization rate of PP is very high so that the crystallization was completed in about 4 sec. In such cases it is well known that the liquid-liquid phase-separated morphology, i.e. the periodic and interconnected structure, is preserved during the crystallization process. The SEM observations also yielded the same highly interconnected PP phase with unique periodicity. The connectivity of phases is an important morphological feature of SD. At the later stage of liquid-liquid phase separation, the phase connectivity seemed to grow in size while maintaining their connectivity and eventually broke up into macrospheres. These characteristics also agree with Cahn's SD prediction mechanism.

2.6.6 Properties of EPDM/PP blends

The morphology of the blend directly affects the properties and EPDM/PP blends are especially required in the industry for their toughness properties. Thus, most authors examine the effect of the particular morphology, obtained during their experiments, on the properties of the blend. In case of the EPDM/PP blend it has been found that it exhibits many properties better than the parent polymers. The properties of TPEs have been found to be a strong function of dispersed rubber particle size. Various

theories have been proposed to explain the toughening of PP with a dispersed rubbery EPDM phase, including energy absorption by rubber, stress relief by cavitation around rubber particles, crack branching caused by rubber particles, crack termination at rubber particles, crazing promoted by the rubbery phase, shear yielding, and combined crazing and shear yielding.

One of the real possibilities, as discussed previously, is that the EPDM might act as a nucleus for the crystallization of the polypropylene and produce smaller crystallites. A decrease in crystallite size generally increases the notched Izod impact strength. Jang et al. (1985) observed a similar phenomenon for his blends.

Another real possibility is that the EPDM may absorb energy through the formation of crazes. The evidence of stress whitening, in Speri et al's (1975) experiments supports this possibility. They found that the degree of improvement in impact toughness for their experiments was dependent on rubber particle size and distribution. These parameters are internal function of the shear developed during compounding. The study indicated that the highest properties are obtained when the EPDM particle size in the blend is reduced to approximately 0.5 μm and a narrow size distribution is obtained. The addition of potassium titanate fibers further improved the composite mechanical and thermal properties for their blends. The results of D'Orazio (1991) are also in agreement with the above observations. They noticed a 14 times higher impact strength for a blend with 0.4 μm diameter particles than the blend having

0.3 μm diameter particles at 0°C, which showed the values of impact strength just three times higher than that of pure PP at 0°C.

The ductility and toughness of a given system lie in the competition between catastrophic crack propagation and the degree of plastic deformation through crazing and shear yielding. The toughened PP systems with smaller average rubber particle size are thus more ductile and impact resistant. For EPDM-modified PPs, Jang et al. (1985) also found that the optimum average diameter appears to be approximately 0.4 μm . Thus this phase morphology seems to represent a more efficient use of rubber particles in promoting crazes and/or shear bands. They also found that a radial compressive stress produced by the volume shrinkage due to PP crystallization on the rubber particles is greater than the stress due to differential thermal contraction in cooling from solidification temperature to end-use temperatures. Thus the interfacial adhesion between the rubber particles and PP matrix is insufficient to “control” craze propagation or to retard the crack initiation.

As the EPDM composition increases in the blend, Arroyo et al. (2000) found that the stiffness and tensile strength at break of the EPDM/PP blend decreases and elongation at break increases.

Jiang et al. reported that the notched Izod impact strength of PP could be improved by increasing the temperature or by adding EPDM rubber. It decreases the interparticle distance provided the particle size remains unchanged. The critical interparticle distance increases with increasing temperature and ever more dramatically

when the temperature is close to the brittle-tough transition temperature. The graph of critical interparticle distance vs. $T_g - T$ was to be found independent of the matrix material, and suggested that there is a single master curve of critical interparticle distance for toughening crystalline thermoplastic with EPDM.

The addition of a compatibilizer generally increases the properties of the blend. Actually the effectiveness of the compatibilizer can be judged by the increase in the properties of the blend. Kim et al. (1994, 2000) observed an increase in the viscosity and a decrease in the tensile properties of the blend after addition of Na and Zn neutralized ionomers. They also observed an increase in the elongation at break and higher impact strength at -40°C after the addition of 0.5 wt% PP-g-MAH-co-PA 6,6-co-EPDM-g-MAH copolymer.

Pukanszky et al. (1990) tried to determine the compositions required to generate interpenetrating polymer networks (IPN) by investigating the changes in the properties which are also a function of the composition. They explained the two transitions that can be expected: one from continuous PP/dispersed EPDM to IPN and the other from IPN to continuous EPDM/dispersed PP structure. The torque, which is proportional to the viscosity of the blends, and the Young's modulus did not show any sudden transition with composition, thus no indication of IPN formation was found from their behavior. Contrary to the melt viscosity, the flow activation energy showed two transitions, one at 0.2 and another at 0.8 composition of EPDM, indicating an IPN structure. However, these results should be used carefully as the flow activation energy

is difficult to measure and it can be measured only with considerable experimental error. Young's moduli were also calculated by the Lewis-Nielsen equation. The comparison of the measured and calculated values indicated phase inversion up to 0.8 volume fraction EPDM. Tensile yield stress, tensile strength and elongation at break showed IPN structures in between 0.6 to 0.8, 0.25 to 0.75, and 0.2 to 0.8 volume fraction of EPDM, respectively.

The Charpy impact strength increases, and at about 0.25-0.3 volume fraction elastomer content, the specimens stopped breaking, which was observed as one transition in impact strength. However, no sudden change was observed in the impact properties with the composition. Elastomers of lower viscosity were more effective impact modifiers than those with high viscosity. This particular result is in accordance with the results of Vander Sande and Karger-Kocsis (1979, 1984) which indicate that a lower melt viscosity of the elastomer will result in a smaller dispersed particle size and thus higher impact strength.

However, the results of Pukanszky are contradictory both with respect to the structure of the blend and the possible differences between copolymer types. Some properties indicate phase inversion, while others suggest IPN structure. Also, the compositions at which a property change can be observed differ from property to property. Thus the composition range over which IPNs can be observed and phase inversion cannot be estimated from the properties.

TPVs can be prepared from a great number of plastics and elastomers, however, only a limited number of elastomer-plastic combinations give technologically useful blends, even after dynamic vulcanization. To define the practical scope of TPVs that can be prepared, Coran and Patel (1982) studied about 100 elastomer-plastic combinations (based on 11 elastomers and 9 plastics). This was accomplished by an analysis that related mechanical properties of the dynamically vulcanized blends to the characteristics of their elastomeric and plastic components. They selected a few characteristics of the pure rubber and plastic components such as estimated surface energies, crystallinity of the hard phase plastic material and the critical chain length of rubber molecules for entanglement, to evaluate the criteria for selecting the polymer for TPV. Finally they found that the best TPVs can be prepared from the elastomer-plastic in which (a) the surface energies of the plastic and elastomer are matched, (b) the entanglement molecular length of the elastomer is low (high entanglement density), and (c) the plastic is at least 15% crystalline. With these characteristics there is a high probability of success to obtain a TPV of good mechanical integrity and elastic recovery.

The tensile strength of TPV improves continuously as the crosslink density of the rubber phase and PP content in the blend increase. Coran and Patel found that complete vulcanization further improves the mechanical properties of the blend. They found that the tensile strength, which was between 10 to 60 kg/cm² before vulcanization, increased to 60 to 80 kg/cm² at 90 to 96% gel content and increased to about 130 to 300 kg/cm² after complete vulcanization.

The ultimate tensile strength and the ultimate elongation increase with the degree of vulcanization and PP content in the blend. The ultimate elongation was found to increase from 180-200% to 460-560% after vulcanization. Young's modulus can even decrease slightly as a result of vulcanization and increase with PP content in the blend. The improved strength can arise from a more favorable micro-morphology, which may be associated with more highly crosslinked rubber particles.

Only small changes were observed in the stiffness over a wide range of extent of cure. Also, the stiffness, as measured by Young's modulus was found to increase with the differences in surface energy between the two phases.

Only a small amount of vulcanization is required for a large improvement in tension set. Tension set was also found to increase with the PP content in the blend. An increase in the viscosity of the rubber phase, crystallization in the plastic or hard phase, or dissimilarity between the polarity and wetting characteristics of the two phases tends to give a composition of higher shear modulus. Finally, the ultimate mechanical properties (σ_B and ϵ_B) and elastic recovery (inversely measured by tension set) were found to increase with the similarity of the rubber and plastic, as measured by the critical surface tension for melting γ_c . The properties also increased with the crystallinity W_c of the PP phase.

2.6.7 Crosslinking systems

Typical crosslinking agents, for crosslinking the rubber phase, reported in the literature are based on sulfur, peroxides, and ionic curing, all of which have serious

drawbacks during manufacture or with respect to the end use of the resulting products. They often lead to matrix degradation through unwanted side-reactions. Unfortunately dynamic curing, as traditionally practiced, also suffers from the generation of low molecular weight species, involves the use of toxic, noxious, or explosive reagents.

In the case of sulfur crosslinking systems, the crosslinking reactions effected by the sulfur/accelerator or sulfur donor/accelerator system also crosslink the EPDM with a similar selectivity to the phenolic resin system with no problem of degradation. The sulfur-induced crosslinking of the vinyl containing polymers generally involves the formation of mono-, di-, and tri-sulfido bridges between vinyl groups on the polymer backbone, resulting in the vulcanization of the polymer. The sulfide crosslinking imparts greater strength and resiliency to the polymer, allowing for its subsequent use in a variety of demanding applications. However, the polysulfide crosslinkage, i.e. (Sn:n = 2-6)- type linkage, is unstable at the required temperature for the melt-blending process and the molding process of EPDM/PP blends. The sulfur links are capable of exchanging among themselves, a capability that could cause the rubber particle to coalesce into bigger domains which, in turn, can lead to a loss of thermoplastic processibility of the blend. The method also requires the continuous heating of the polymer and is therefore energy intensive. Thus, the sulfur crosslinking system is not suitable for the commercial production of TPVs.

The organic peroxide/coagent crosslink system is the most commonly used and is also very well known. However peroxide also degrades the PP matrix and changes its

mechanical and rheological properties, besides crosslinking EPDM. The mechanism of organic peroxide induced crosslinking involves the generation of highly active radicals that abstract hydrogen atoms not only from the allylic carbons of EPDM but also from the tertiary carbons of PP. This further generates polymer-bound radicals which link together to form covalent carbon-carbon bonds. The formation of the carbon-carbon bonds produces the crosslinking of the polymer necessary to impart greater strength and resiliency to the vulcanized substrate. Organic peroxide crosslinking is typically used when heat age resistance or continuous vulcanization is desired. This process also requires the continuous input of heat energy and thus is not suitable for vulcanization.

The phenolic curatives are favored over sulfur and peroxide cure because the crosslinking reaction of the phenolic resin crosslink systems proceeds at the unsaturated bonds of EPDM without hydrogen radical abstraction (i.e., by addition of the phenolic resin to a carbon of the double bond in EPDM). Thus, this system can be considered to demonstrate a kind of selectivity, among other curatives, with no problem of degradation of PP matrix. Phenolic curative crosslinking gives significant improvement in compression set and oil resistance realized in the cured blends. Morphologically, phenolic and peroxide cure systems give similar dispersed phase morphologies. Following Figure 2.22 gives the general mechanism of crosslinking in EPDM with phenolic curatives,

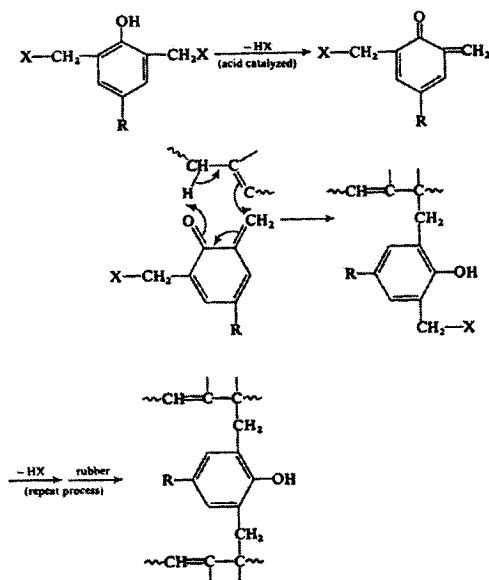


Figure 2.22: Vulcanization by phenolic curative resin

Inoue et al. (1994) carried out the selective crosslinking of EPDM by using *N,N'*-*m*-phenylene-*bis*-maleimide (PM) as a crosslinking agent and 6-ethoxy-2,2,4-trimethyl-1,2-dihydroquinoline or polymerized-(2,2,4-trimethyl-1,2-dihydroquinoline) as an activator. The radicals produced from the system are carbon radicals and, as such, abstract only the hydrogen radical at the allylic positions of the unsaturated elastomers, and not a hydrogen radical at the secondary or tertiary carbons of the polyolefin. This selectively crosslinks the EPDM.

Silanes can also be used to crosslink the EPDM phase. The details of chemistry of silane crosslinking are available in the literature. If done properly the silane crosslinking provides selective crosslinking of the EPDM phase and in addition can give enhanced interaction between the filler materials and the components of the blend, thus further increasing the properties. Unlike other crosslinking agents, silanes are also

known to provide white colored TPVs, which is an additional advantage and quite important for some specific purposes. The silane crosslinked TPVs are also softer and have better surface properties. Despite all of these advantages we will not discuss the silane crosslinking system further in this thesis since an enormous literature on the subject already exists. The readers are advised to refer to the US patents of Medsker et al. (1997) and Umpleby (1989), and also to number of other publications like Pal et al. (1984), Mukhopadhyay et al. (1989), Ghosh et al. (1994, 1999), King et al. (1989) for further details related to this topic.

Thus, the crosslinking system is very important for TPVs. A good choice of crosslinking system can result in materials with special properties, better filler interactions etc. On the other hand, a poor choice of crosslinking system can render the final material useless or even unprocessable due to matrix degradation.

2.7 Conclusions of the literature review

A number of conclusions can be drawn from the literature. The main highlights are listed below:

1. The main mechanism governing phase morphology development in immiscible polymer blends is the result of a competition between droplet breakup and coalescence. The formation of dual phase continuity can be described by percolation concepts.
2. The existing equations for the phase inversion point and the models for predicting the cocontinuous composition range provide some information concerning the

composition around which cocontinuity can be expected. However, all these models lack in their predictive capabilities. Often the models even fail to predict the correct trend with viscosity or elasticity ratio.

3. BET nitrogen adsorption is a powerful, simple, rapid, reproducible and reliable technique for the characterization of cocontinuous polymer blends.
4. Low interfacial tension systems demonstrate the onset of percolation and cocontinuity at lower compositions of minor phase. Cocontinuity is maintained over a wide composition range and the pore size of the blend changes little with increase in minor phase composition. The cocontinuity development takes place through fiber-fiber coalescence.
5. High interfacial tension systems show percolation phenomena and full cocontinuity at a higher composition of minor phase than the low interfacial tension systems. Full continuity is maintained in a narrower composition range and the pore size of the blend increases significantly with minor phase composition. The cocontinuity development takes place by droplet-droplet coalescence.
6. An interfacial modifier shifts the percolation threshold, continuity development and possibly full cocontinuity to higher compositions of the minor phase. In addition, the modifier also hinders coalescence and hence stabilizes the cocontinuous morphologies against annealing.
7. Dual phase continuous structures possess a high interfacial area and thus high interfacial energy. Addition of an interfacial modifier can remarkably reduce the interfacial tension, and minimize the interfacial energy, thus stabilizing the

cocontinuous morphological structure. Experimental results have indicated that mechanical properties can also be notably improved by the addition of an interfacial modifier.

8. Prolonged blending time and annealing can destabilize the cocontinuous morphologies to give dispersed phase morphologies.
9. Non-vulcanized and vulcanized blends of EPDM/PP show a spherical dispersed phase morphology. The particle size and size distribution increases with viscosity ratio.
10. There is a controversy on whether EPDM/PP blends are compatible or incompatible, partially miscible.
11. Rheologically, TPVs display highly pseudoplastic behavior, similar to highly filled polymer composites in shear flow.
12. Morphologically the EPDM/PP TPV shows an inverted matrix type of morphology.
13. Complete vulcanization of EPDM gives a stable phase morphology as it reduces particle-particle coalescence after vulcanization.
14. The crosslinking system should be selective to the elastomer. Non-selectivity of the crosslinking system can degrade the matrix material and thus can alter the morphological and mechanical properties of the blend.
15. A sulfur crosslinking system and organic peroxides are not suitable crosslinking systems due to a number of reasons. Silanes and phenolic curatives show selectivity for crosslinking the elastomer.
16. During the crystallization of PP, EPDM particles act as nuclei for PP crystallites.

17. EPDM/PP blends with compatibilizers show better mechanical properties. Tensile strength at break and stiffness decrease and elongation at break increases with EPDM content.
18. The impact strength of the vulcanized and non-vulcanized EPDM/PP blends increases with EPDM concentration. The highest impact strength can be obtained at between 20 to 40% EPDM composition.
19. The impact strength and ductility increase with decreasing particle size. The most effective particle size to significantly improve the impact strength is around 1 μm for both non-vulcanized and vulcanized blends.
20. Mechanical properties such as impact strength increase dramatically with vulcanization. Thus complete vulcanization of EPDM gives large improvements in mechanical properties.
21. Tensile strength, ultimate tensile strength, ultimate elongation, and tension set increase with degree of vulcanization. The Young's modulus may decrease with degree of vulcanization.

2.8 Limitations of the previous work

From the literature studied so far it is evident that much work has been done in this field. However, many questions remain unanswered. We still do not know the exact role of viscosity ratio, elasticity ratio, and interfacial tension in the formation of cocontinuity. Which of these phenomena ultimately control the formation of

cocontinuity? Which phenomenon dominates the other and under what circumstances? What is the validity of phase inversion models?

Apart from viscosity and elasticity ratio, other parameters like interfacial tension, shear stress, shear rate, time of mixing, temperature etc. are also known to affect the cocontinuous morphologies. Future models for predicting the phase inversion composition or cocontinuous composition range should incorporate these variables. More characterization techniques should be developed for the fast and accurate estimation of cocontinuous morphologies. Also the quantification of suitable structural parameters of cocontinuous structures is needed for correlation with properties.

In the case of TPVs, how does crosslinking affect cocontinuity? How does crosslinking give birth to the inverted matrix type of morphology? Why does the blend adopt an inverted matrix morphology with crosslinking? What is the effect of viscosity ratio on the inverted matrix type of morphology? How are properties affected and by how much?

Apart from the above limitations one also encounters many practical problems which are serious roadblocks in ultimately understanding this and other systems. For example in the EPDM/PP system, is there any method to dissolve PP without affecting EPDM? In addition, new morphological techniques to quantify the cocontinuity and inverted matrix morphologies, especially during and after crosslinking, are needed.

CHAPTER 3

ORGANIZATION OF THE ARTICLES

To achieve the aforementioned objectives we chose three different Mooney viscosity ethylene-propylene-diene terpolymers (EPDM) and two polypropylenes (PP) with very different viscosities. After measuring their rheological properties and the average shear rate under the mixing conditions used, it is found that six different viscosity and elasticity ratios can be generated. In general, four of the viscosity ratios fall in the low to medium range (from 0.7 to 5.0) while the other two are high (11 and 17). The morphology, continuity development and cocontinuity in low to medium viscosity ratio blends is discussed in the first paper, "Continuity development in polymer blends of very low interfacial tension", whilst for high viscosity ratio blends it is discussed in the second paper, "Erosion-controlled continuity development in high viscosity ratio blends of very low interfacial tension".

In the first paper, EPDM morphology development is studied by dissolving the EPDM dispersed phase by cyclohexane at room temperature and by dissolving the PP matrix phase of the irradiation crosslinked blends using hot xylene. The PP phase morphology is investigated by dissolving the EPDM matrix by cyclohexane at room temperature. The micrographs are obtained using scanning electron microscopy and the atomic force microscope. The micrographs demonstrate that the dispersed phase exists in the form of extremely small diameter fibers in the blend. Typically, these fibers have a diameter of about 50–200 nm. These structures are also found to be uniformly

dispersed throughout the matrix. The thread breakup times, estimated using the Tomotika equation for capillary instabilities, are shown to support these findings.

With an increase in composition, these nano-fibers coalesce at crossover points to develop continuity, as typically expected from blends of low interfacial tension. The viscosity ratio does not show any effect on phase size and continuity development. An eight-fold variation in shear stress also does not affect the continuity development; however, it does affect the phase size.

Despite glass transition temperatures which demonstrate these blends to be completely immiscible on cooling from the melt, the system shows several unexpected features, such as: artificially high percolation thresholds, delayed continuity development, achievement of cocontinuity at higher than expected compositions of minor phase, maintenance of cocontinuity over a narrow composition range, and high phase coalescence with composition typical of a partially miscible system. Since the principal morphological features of the blend are developed during melt blending, these results indicate that the blends were partially miscible during melt blending but completely phase separate upon cooling from the melt. It appears that the quenching of the EPDM/PP blends from the melt is clearly rapid enough to preserve the imprint of that partial miscibility on the blend morphology after cooling.

In the second paper, the viscosity ratio is even further increased to 11 and 17. Using similar tactics of morphology investigation developed in the first paper, the high viscosity EPDM dispersed phase is shown to coexist in the form of a variety of unusual

morphological structures including: isolated stable nano-fibers, very large particles, partially coalesced particles, and numerous particles interconnected by nano-fibers. This unusual combination of morphologies leads the blend to a novel cocontinuous structure of partially coalesced particles and particles interconnected by stable fibers.

The second paper also compares and discusses morphology development in the high viscosity ratio blends with the low to medium viscosity ratio blends, already studied in the first paper. The comparison indicates that the high viscosity ratio blends present lower percolation thresholds, rapid continuity development, and achieve cocontinuity at lower than expected compositions of minor phase. These blends maintain cocontinuity over a wider composition range and present an asymmetrical widening in the region of cocontinuity with respect to mid-composition. The characteristic nature of the novel cocontinuous network is shown to be responsible for these phenomena.

The slow surface erosion process of high viscosity EPDM phase is found to be responsible for the generation of this wide variety of morphologies. Typically the time scale for erosion phenomena are so small, that they have defied study in the mixing environment itself and typical blend morphology studies almost always examine the final steady-state morphology obtained after several minutes of mixing. The combination of very low interfacial tension and very high viscosity ratios of these EPDM/PP blends provide a unique opportunity to examine erosion phenomena persisting over longer time scales during melt mixing. For a 17 viscosity ratio blend the

erosion phenomenon is shown to be incomplete even after 30 minutes of melt mixing at low blend concentrations.

In high viscosity ratio blends, the stress transferred by the low viscosity matrix is insufficient to completely deform and disintegrate the high viscosity particles. However, if the stress transferred by the matrix is more than a critical value then the local viscosity of the material on the surface of a large high viscosity particle drops. The shear stress, however, does not get transferred to the core because of the high viscosity of the droplet. Thus, the surface of the particle becomes much less viscous than its core because of the shear thinning of the material. Under such circumstances, the particle can no longer sustain material at the surface and starts giving away this material. The eroded material is shown to form extremely stable nano-fibers because of the ultra-low interfacial tension between the blend components and very high viscosity of the fiber material.

To account for other results, a new erosion mechanism based on collision-separation dynamics is proposed. In this type of erosion the two particles of highly viscous material collide during melt blending and partially penetrate each other, causing partial coalescence at the surface of the particles. However, the particles recoil because of the high viscosity, ultra-low interfacial tension of the blend components, and continued shearing in an internal mixer. Since the particles were coalesced at the surface before separation, the separation draws stable nano-fiber(s) between the particles. Based on increased particle-particle collisions at higher compositions, the

proposed mechanism is shown to dramatically accelerate the erosion process and maintain cocontinuity over prolonged periods of mixing. Thus, the higher concentration blends achieve steady state morphology much more rapidly.

In the third paper, “The influence of dynamic vulcanization on the cocontinuous morphology in EPDM/PP blends” is studied. The cocontinuous morphologies in the 0.7 and 5.0 viscosity ratio blends are crosslinked to 50% and 100% by adding a predetermined quantity of crosslinking agent. The degree of crosslinking achieved in each blend is estimated by measuring the gel content. The morphology of the blend is investigated by applying a novel technique of morphology investigation involving focused ion beam (FIB) etching of the sample surface followed by topological investigation of the sample surface using tapping mode atomic force microscopy (TMAFM). It is shown that the FIB ion etching rate of EPDM and PP is distinctly different. Thus, this treatment leads to a topological contrast between the phases when subsequently analyzed by TMAFM.

Since it is found that the ion etching rates of non-crosslinked and crosslinked EPDM are similar, the non-crosslinked EPDM phase is selectively removed from the sample by solvent dissolution to create an additional topological contrast. This novel combination of techniques allows for the clear distinction of polypropylene as well as non-crosslinked and crosslinked EPDM phases in the blend.

The status of non-crosslinked EPDM is investigated by solvent gravimetry and the phase dimensions of the pores are determined by the BET nitrogen adsorption

technique. The amount of crosslinked phase present in the solvent obtained after extraction of the non-crosslinked EPDM phase is estimated by measuring the weight of the membrane before and after filtration.

The results, surprisingly, indicate that a non-crosslinked co-continuous EPDM phase (α -network) transits to a much finer network of crosslinked EPDM (β -network) due to the dynamic crosslinking of the blends. The micrographs and the sample integrity after gel content measurement suggest a high level of interconnectivity in the β -network. It is suggested that this β -network is produced as a result of the viscosity mismatch between non-crosslinked and crosslinked EPDM created due to crosslinking. As the crosslinked material pulls away from the non-crosslinked material under dynamic melt mixing conditions, it creates a smearing effect. The dynamic crosslinking, therefore, dramatically modifies the cocontinuous morphology.

The initial α -network maintains its continuity and demonstrates a diminished pore size as crosslinking proceeds. For the viscosity ratios studied, it is found that no crosslinked phase exists in the cocontinuous non-crosslinked EPDM phase (α -network). As the crosslinking reaction rate is very high, these results indicate that the crosslinking proceeds initially at the outer envelope of the EPDM phase and works its way towards the center. Based on all these results, the schematics of morphology development in a cocontinuous blend of EPDM/PP with dynamic crosslinking are presented.

CHAPTER 4

CONTINUITY DEVELOPMENT IN POLYMER BLENDS OF VERY LOW INTERFACIAL TENSION

The objective of this first paper is to carry out a detailed morphology study of ethylene-propylene-diene terpolymer/polypropylene (EPDM/PP) blends. In particular, to study the continuity development and cocontinuity in polymer blends of ultra-low interfacial tension. The viscosity and elasticity ratios are varied by melt mixing three different Mooney viscosity EPDM materials and two very different molecular weight homo-polypropylenes in an internal mixer. Miscibility between the blend components is determined using a dynamic mechanical thermal analyzer. The morphology is investigated using a scanning electron microscope after extracting the dispersed phase and by atomic force microscopy. The phase sizes are quantified by image analysis of the micrographs. In addition, matrix dissolution is carried out to determine the three-dimensional structure of the dispersed phase. The continuity development and cocontinuity is determined by solvent gravimetry. Wherever it was necessary to dissolve PP phase without dissolving EPDM phase, the blends were irradiation crosslinked after melt mixing.

This article is submitted to the journal : "*Polymer*"

Continuity Development in Polymer Blends of Very Low Interfacial Tension

Prashant Bhadane¹, Michel Champagne², Michel Huneault², Florin Tofan³,
and Basil D. Favis^{1,*}

¹ CREPEC, Department of Chemical Engineering, École Polytechnique de Montréal,
2900 Édouard Montpetit, P.O. Box 6079, Station Centre-Ville, Montréal, Qué., Canada
H3C 3A7

² Industrial Materials Institute, National Research Council of Canada, 75 de Mortagne
Blvd., Boucherville, Qué., Canada J4B 6Y4

³ Lavergne Group, 8800 Crescent 1, Ville d'Anjou (Montréal), Qué., Canada H1J 1C8

Abstract

Phase continuity development and co-continuous morphologies are highly influenced by the nature of the interface in immiscible polymer blends. Blends of ethylene-propylene-diene terpolymer (EPDM) and polypropylene (PP) possess an interfacial tension of about 0.3 mN/m and provide an interesting model system to study the detailed morphology development in an ultra-low interfacial tension binary system. A variety of blends with viscosity ratios of 0.2 – 4.9 and shear stresses of 11.7 – 231.4 kPa were considered. Using a variety of sophisticated morphology protocols it is shown that at low blend compositions, the dispersed phase actually exists as stable fibers of

*Corresponding author. Tel.: + 1 514 340 4711x4527; fax: + 1 514 340 4159.
E-mail address: basil.favis@polymtl.ca (B.D. Favis).

extremely small diameter of about 50–200 nm and the continuity develops by fiber-fiber coalescence. An analysis using break-up times from Tomotika theory also supports the notion of highly stable dispersed fiber formation. These results challenge the current view of the dispersed phase as small spherical droplets. It is shown, under these conditions, that a 7-fold variation in the viscosity ratio has virtually no influence on % continuity or morphology, while large changes in the matrix viscosity from 11.7 to 90.9 kPa has an important effect on pore diameter. Both sides of the continuity diagram are studied and highly symmetrical continuity behavior is observed with composition. In fact a single master continuity curve is observed for these blends varying in viscosity ratio from 0.7–4.9 and with shear stresses from 11.7–90.9 kPa. Although the glass transition temperatures indicate that these materials are completely immiscible after melt mixing and cooling, it is shown that the blends demonstrate the morphological features of a partially miscible system. These results support a concept that the blend was partially miscible during melt blending, at which time the gross morphological features of the blend were developed, but becomes fully phase separated upon cooling. It appears that the quenching of the EPDM/PP blend from the melt is clearly rapid enough to preserve the imprint of that partial miscibility on the gross blend morphology.

Keywords: Polymer blends, Co-continuous morphology

4.1 Introduction

Today, polypropylene (PP) is produced on a massive scale because of its versatile properties and for years now, the unfavorable low temperature brittleness of

PP has been overcome by blending it with different elastomers. Ethylene-propylene-diene terpolymer (EPDM) has been found to be the most successful elastomer in blending with PP due to: the ultra-low interfacial tension (σ) (≈ 0.3 mN/m at 190°C) [1-6] and its low glass transition temperature (≈ -40 – 50°C) [7-12]. Furthermore, the EPDM can be crosslinked which opens up numerous advantages as a thermoplastic vulcanizate (TPVs) [13-16].

At low compositions in PP and when the viscosity ratio is controlled near unity, the EPDM phase has been reported to form very fine dispersed spherical domains. Number average particle sizes as low as $0.2\ \mu\text{m}$ have been reported in the literature for blends prepared via melt mixing [17-22] making this one of the finest blend morphologies reported in the polymer blend literature.

Many authors have reported the EPDM/PP blends to be immiscible [7,19,23-28], however, the miscibility-immiscibility issue in this blend system is very complex and controversial. In the past, Lohse et al. [26] by small angle neutron scattering (SANS) and more recently Han et al. [28] by determining the solubility parameter through pressure-volume-temperature (P-V-T) properties measurement, demonstrated that unlike atactic-PP (aPP), EPDM is immiscible both in the melt and on cooling from the melt with isotactic-PP (iPP), even when the ethylene content of the elastomer is as low as ca. 8 percent. However, recent similar SANS experiments carried out by Seki et al. [29] with deuterated-EPDM (unlike Lohse who used deuterated-PP) prepared with

metallocene catalyst indicated that these blends are a homogeneous one-phase mixture in the melt.

Chen et al. [8] found EPDM/PP blends to be immiscible below an upper critical solution temperature (UCST) marked by the crystallization temperature curve and above a lower critical solution temperature (LCST) marked by cloud point curve found to be just below the melting point of iPP phase in the blend. Thus, these blends are miscible in the temperature range in between the UCST and LCST. Inaba et al. [30,31] have reported that immiscible EPDM/PP blends phase separate by a spinodal decomposition mechanism above their melting temperature. The crystallization takes place and proceeds in and through PP-rich domains without invoking the long-range rearrangement of PP molecules. These discussions demonstrate the complexity and controversial nature of the miscibility-immiscibility issue in EPDM/PP blends.

Recently, Marin et al. [32] studied the co-continuous morphology development in partially miscible poly(methyl methacrylate) (PMMA)/polycarbonate (PC) blends. Both polymers are amorphous in nature and possess an interfacial tension of 0.6 mN/m. In that work it was shown that because of the partial miscibility the blend demonstrated significantly different morphological features as compared to that reported for fully immiscible blends of low interfacial tension by Li et al. [33] Marin et al. found that these partially miscible blends exhibited very fine dispersed phase morphologies, artificially high percolation thresholds, and attained cocontinuity at higher than expected compositions of the minor phase. Furthermore, these blends demonstrated

significant coalescence effects as a function of dispersed phase composition as compared to the highly stable morphologies observed for fully immiscible binary blends of low interfacial tension. Marin et al. carried out a detailed correction of the phase composition and continuity phenomena by treating the blend as a mixture of PMMA-rich and PC-rich phases. Once these corrections were carried out, the continuity phenomena in terms of percolation onset and attainment of co-continuity fell in line with the expected behavior for a low interfacial tension binary system.

Despite their commercial significance, detailed morphological studies of EPDM/PP blends are lacking in the literature. In particular, continuity development and co-continuity are virtually untreated for this blend system. Furthermore, this system provides an excellent view into the blend morphology development of systems with ultra-low interfacial tension. This paper is the first of a series of studies that will examine the morphology development in EPDM/PP blends in a highly detailed fashion. Future work will involve examination of continuity development and cocontinuity in the high viscosity ratio blends and the relationship of the final cross-linked morphology to the initial non-crosslinked morphological states.

4.2 Experimental procedures

4.2.1 Materials

Three EPDM elastomers with different Mooney viscosities and two different types of PP homopolymers with significantly different melt flow index were used in this study. The materials do not contain any fillers. The ethylene and diene content of all the

grades of EPDM were kept as close as possible to eliminate any effect of these variables on the study. All EPDM grades contain ethylidene norbornene (ENB) as the diene. A small amount (0.5 wt.%) of Irganox B 225 antioxidant was added to the mixture to reduce the oxidative degradation of PP. The further details of the materials are given in Table 4.1.

Table 4.1: Characteristic properties of the materials

Polymer	Supplier	Given name	Molecular weights x 10 ³		Ethylene content (%)	ENB content (%)
			M _n	M _w		
PP	Basell	PP 1	89	288	-	-
PP	Basell	PP 2	166	773	-	-
EPDM	Bayer	EP 1	71.2	141.9	62	4.0
EPDM	Bayer	EP 2	112.4	194	52	4.3
EPDM	Bayer	EP 3	146	241.1	53	4.3

4.2.2 Rheological characterization

The neat EPDM, and PP on mixing with 0.5 wt.% Irganox B 225 were compression molded at 190°C in the form of disks for rheological characterization. The rheological characterization was carried out using a Bohlin constant stress rheometer (CSM) in the dynamic mode. The experiments were performed in parallel plate geometry of 25 mm diameter, at 190°C and under a nitrogen atmosphere. An oscillation mode at 0.1 Hz frequency was used to test the stability of the materials at the test temperature. Both PP homopolymers, after addition of an antioxidant, were found to be stable, however, all the grades of EPDM showed the tendency to crosslink (as marked

by the increase in all the rheological properties over time). Thus, several samples were used to carry out rheological experiments, so as not to exceed the time window revealed by the time sweep test. A stress sweep was then performed from 0.3 to 2420 Pa to determine the region of linear viscoelasticity. The frequency sweep tests were then performed in an experimental window permitted by the time and stress sweep tests.

4.2.3 Melt blending

PP, EPDM, and antioxidant were first dry blended in a beaker and the mixture was then fed all together into the mixing chamber. The two polymers were melt blended together using a Haake Rheomix 600 batch mixer with a Haake system 90 drive, internal mixer equipped with a 69 cm³ chamber and roller-type rotors for 8 minutes at 100 rpm and at 190°C. Under these mixing conditions an average shear rate of 27 sec⁻¹ was estimated using an empirical calibration technique of Marquez et al. [34].

The materials were weighed accurately so that the mixing chamber was filled to approximately 70% of its total volume. At this loading, an optimum interchange between the two chambers of the mixer is observed and there are no stagnant melt areas in the mixer center due to overfilling. The blending was carried out under a nitrogen blanket in order to avoid the degradation of the materials due to environmental oxygen, at the melt blending temperature. Subsequently the torque required to mix the blend compositions was noted. After mixing, the melt was taken out of the mixing chamber very gently but rapidly, and was quenched immediately in cold water to freeze in the morphology generated during melt mixing.

In total four different types of blends over the entire composition range were prepared. The different types of blends prepared together with their various rheological property ratios determined at constant shear rate and at constant shear stress are reported in Table 4.2.

Table 4.2: Rheological property ratios at constant shear rate and constant shear stress

Sr no	Blend components		Blend name	Torque ratio	At const. shear rate		Matrix shear stress (kPa)	At const. shear stress	
	Dispersed phase	Matrix			p^a	ψ^b		p^a	ψ^b
1	EP 1	PP 2	EP 1/PP 2	0.7	0.7	0.5	90.9	0.5	0.7
2	EP 2	PP 2	EP 2/PP 2	1.3	1.5	1.0	90.9	2.0	0.8
3	EP 3	PP 2	EP 3/PP 2	2.0	2.5	2.0	90.9	5.5	0.8
4	EP 1	PP 1	EP 1/PP 1	4.0	5.0	6.5	11.7	12.0	1.0
5	PP 2	EP 1	PP 2/EP 1	1.4	1.5	2.0	69.4	2.5	1.5
6	PP 2	EP 2	PP 2/EP 2	0.8	0.7	1.0	144.7	0.2	1.5
7	PP 2	EP 3	PP 2/EP 3	0.5	0.4	0.5	231.4	-	1.0 ^c
8	PP 1	EP 1	PP 1/EP 1	0.3	0.2	0.2	69.4	-	

^a Viscosity ratio

^b Elasticity ratio

^c by extrapolation of the data

P.S. All the rheological properties are determined at an average shear rate in internal mixer of 27 sec⁻¹.

4.2.4 Irradiation crosslinking

Blends were prepared at four different viscosity ratios over the entire composition range. All these blends, along with the pure materials, were then subjected to γ -irradiation in air with a Cobalt-60 (⁶⁰Co) source, using a commercial carrier type 8900 irradiator with the dose rate of 25 kGy/hr and to an average optimal [35-37] total dose of 154 kGy.

4.2.5 Dynamic mechanical thermal analysis

A dynamic mechanical thermal analyzer (DMTA) model mark V of Rheological Instruments was used to measure the glass transition temperatures (T_g) for the pure EPDM, PP materials, and their blends. The blends were first molded into rectangular samples of approximately 64 x 12 x 2 mm. The samples were then conditioned at 75°C in a vacuum oven for 3 weeks to relieve any internal stresses in the molded samples. Initially the experiments were performed using 3 point bending clamp in a multi-strain single cantilever mode to determine the linear zone and thus the target strain. Based on the results obtained the experiments were then performed in a multi-frequency single cantilever mode at 1 Hz frequency, with the target strain of 0.1%, and at the heating rate of 1°C/min. The peak in loss modulus with the temperature was used for measuring the T_{gs} .

4.2.6 Solvent extraction and gravimetry for % continuity

At least three samples of approximately 8 x 12 x 4 mm, weighing 0.3 to 0.4 g were cut from each of the non-crosslinked blends. These samples were kept in 40 mL of fresh cyclohexane solvent in a centrifuge tube for 48 h at room temperature. The tubes were shaken constantly. The samples were then dried in a vacuum oven at 60°C until a constant weight was obtained. The samples were then subjected to another wash of fresh cyclohexane and again dried to constant weight. This procedure was repeated until the sample weight from two consecutive washes remained unchanged.

The irradiated blends were cut into 3 mm cubes, in total weighing about 0.1 g, to achieve faster dissolution of the PP. These samples were then boiled in 100 mL of xylene for about 45 mins to 1 hr. The samples were then dried in a vacuum oven to constant weight. These well-dried samples were then boiled in fresh xylene and again dried to constant weight. This procedure was repeated until the sample weight from two consecutive washes remained unchanged.

With the help of initial sample weight, the final weight after extraction, the known composition of the sample, and assuming that the blend was completely homogeneous in the composition, the continuity of the respective material in the blend was calculated using following formula,

$$\% \text{ Continuity of A} = \left(\frac{\text{Wt. of A}_{\text{Before Extraction}} - \text{Wt. of A}_{\text{After Extraction}}}{\text{Wt. of A}_{\text{Before Extraction}}} \right) \times 100 \dots\dots\dots (4.1)$$

where ‘A’ represents the component which has been extracted and whose continuity has to be determined. The values reported are the average of at least three measurements done in this way.

4.2.7 Characterization of phase morphology

At least two samples from each blend were cut and microtomed carefully using a glass knife under liquid nitrogen to create a perfectly plane face using a Leica-Jung RM 2065, and 2165 equipped with a Leica LN 21 type cryochamber. The microtomed samples were then subjected to a cyclohexane wash to remove the EPDM phase and were dried completely. The samples were then coated with a gold-palladium alloy, and

the observations were carried out under a Jeol JSM 840 Scanning Electron Microscope (SEM) operated at a voltage of 15 kV.

The SEM micrographs were analyzed by a semiautomatic method of image analysis, consisting of a digitizing table and in-house developed software, described elsewhere [38]. On an average at least 300 diameters were measured per blend sample. The number average diameter (D_n) and the volume average diameter (D_v) were then calculated based on these measurements. Since the microtome does not necessarily cut the dispersed phase at the equator and also to correct for the polydispersity, the Saltikov [39] correction was applied.

The micrographs for the blends containing PP as their dispersed phase were obtained by tapping mode atomic force microscopy (AFM). The blend specimens were first cryo-microtomed and the subsequent observations were carried out with a scanning probe microscope Dimension 3100 with a Nanoscope IIIa controller from Veeco Instruments. Silicon tips, model RTESP from Veeco, with spring constants of 20-80 N/m and resonant frequency of approximately 320 kHz were used. The tip was oscillated at approximately 98% of the resonant frequency and the engagement on the surface was done at 95% of the free oscillation amplitude. Topographical pictures were taken at 95% of the free oscillation amplitude.

4.2.8 BET measurement

A Flowsorb 2300 BET instrument was used to measure the surface area of the specimen. The solvent-extracted porous samples from the solvent gravimetry were cut

into small rod-like pieces, so that they could be fed into the cell used in BET measurements. Prior to testing, exactly 1 mL of nitrogen was introduced into the equipment for calibration purposes. The samples were then analyzed for their total surface area. At least two readings per sample and two samples per blend were analyzed and the average of those readings was taken for further calculations. Now, by considering that the total volume of the pores is equal to that of the extracted phase(V), the total surface area (S) is that of the pore wall, and that the pores are cylindrical in shape, the pore diameter (d) can be readily calculated as,

$$d = 4V/S \dots\dots\dots (4.2)$$

Further details regarding this technique have been described by Li and Favis [40].

4.2.9 Matrix dissolution

4.2.9.1 Complete matrix dissolution

Less than 0.01 g of the 95 EPDM/5 PP samples were cut from the blend and were completely dissolved in 300 mL of pre-filtered cyclohexane solvent. The solution was then filtered using a 0.8 μm filter membrane. Additional fresh pre-filtered cyclohexane solvent was filtered to insure complete removal of the dissolved EPDM phase. The weight of the filter membrane before and after filtration and complete drying were noted.

Similarly, about 0.02 g of the material was cut from 5 EPDM/95 PP irradiated blends. The material was then completely dissolved in about 100 mL of pre-filtered

xylene by boiling for 30 to 45 minutes. The solution was then rapidly filtered at 140°C with the help of 0.8 μm membrane. Additional hot xylene was passed to assure the complete removal of the PP phase. The weight of the filter membrane before and after filtration and complete drying were noted.

Our calculations show that on an average we were able to retain more than 80% of the dispersed phase and only about 1% of the matrix phase on the membrane in all the cases. This amount is more than enough to assess the shape and structure of the dispersed phase.

4.2.9.2 Partial matrix dissolution

On the complete dissolution of the matrix, the individual dispersed phase becomes suspended in the solvent. Occasionally, the very high surface area of the dispersed phase and the tacky nature of the polymers at the experimental conditions (as in this case for EPDM), may lead to the agglomeration of the dispersed phase in solution. The agglomeration makes the identification of the nature of the dispersed phase very difficult. In such cases the partial removal of the matrix from the surface can expose and would prevent the dispersed phase from agglomeration because of the complete removal of the matrix. This technique especially makes sense for the elongated dispersed structures and is complementary to the complete matrix dissolution study.

For the partial matrix dissolution study, the well microtomed samples of the 5 EPDM/95 PP irradiated blends, pure EPDM, and pure PP were immersed in hot xylene

for about 2-5 seconds. That time was found to be just enough for the partial dissolution of the PP matrix. Thus treated samples were rapidly rinsed with cold xylene and later dried in a vacuum oven. The samples were then coated and examined by SEM microscopy.

4.2.9.3 Complete matrix dissolution and freeze drying

In these experiments, initially, small samples were cut from the 30 EPDM/70 PP irradiated blends and 70 EPDM/30 PP non-irradiated blends, the compositions at which the samples present partial continuity. The 30 EPDM/70 PP irradiated blend samples were boiled in xylene to completely remove the PP matrix. Two to three similar washes were given to the sample to assure complete matrix phase removal. After the final xylene wash, the samples were washed several time with cyclohexane. The excess cyclohexane was then removed, keeping only just enough solvent to submerge the sample completely.

In the case of 70 EPDM/30 PP non-irradiated blend samples, the EPDM matrix was completely removed by dissolving it in cyclohexane. After the final solvent wash, the excess cyclohexane was removed, keeping only just enough solvent to submerge the sample completely.

All the above samples were subsequently frozen and freeze-dried completely by applying vacuum and by maintaining the temperature of the samples from -25 to -30°C. These freeze-dried samples were later coated with the gold-palladium alloy and observed under the SEM.

4.3 Results and discussions

4.3.1 Rheology

PP and EPDM are known to follow the Cox-Merz [41] relation [5,42], thus the frequency of the rheometer can easily be converted to the shear rate and the complex viscosity can be treated as a steady shear flow viscosity. Figures 4.1(a) and (b) show the complex viscosity and the storage modulus as a function of shear rate. Figure 4.1(a) illustrates that all the materials are showing shear thinning behavior. EP 1, and PP 1 and 2 demonstrate a Newtonian plateau, but the higher molecular weight EP 2 and 3 show a yield stress. This latter observation is quite common and other authors have also observed similar effects with higher molecular weight polymers and especially with elastomers [33,42]. At the average shear rate of blending, it can be seen that, EP 3 is the most viscous and most elastic of all the polymers. PP 2 is almost as elastic as that of EP 2 but is less viscous than EP 2. PP 1 is the least viscous and elastic of all the neat polymers.

Table 4.2 illustrates the blend rheological properties, based on the neat materials, at both constant shear rate and constant shear stress. In the field of polymer blends, there is still some debate as to whether the rheological property ratios should be calculated at constant shear rate or at constant shear stress since the local shear rate at the surface of the droplet under deformation may be discontinuous (although the velocity may be continuous). The local shearing stress may also be discontinuous, if we take into consideration the slip at the interface. Thus, it may be more precise to compare

the rheological properties at constant shear stress. Comparing the numbers reveal that no matter how the rheological ratios are estimated, the trends are identical.

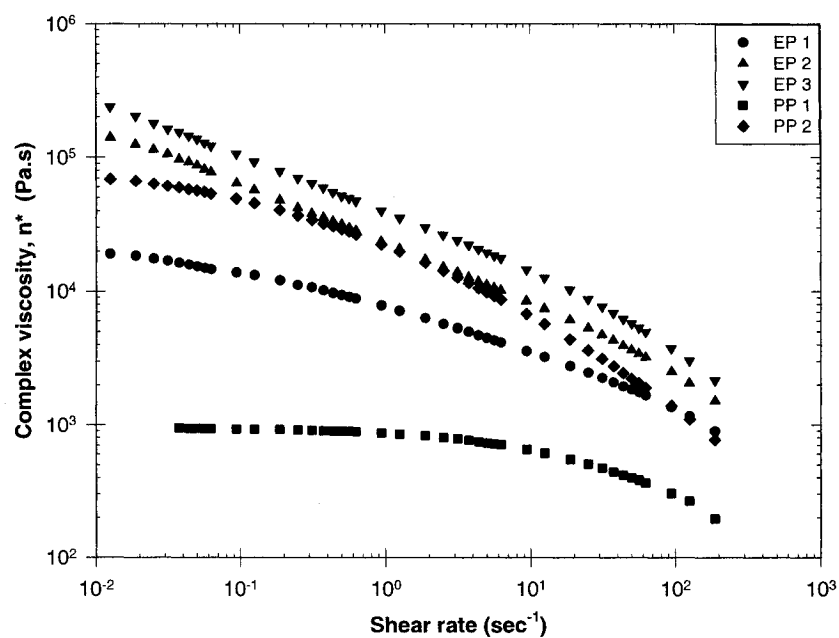


Figure 4.1 (a): Complex viscosity of the pure materials as a function of shear rate at 190°C

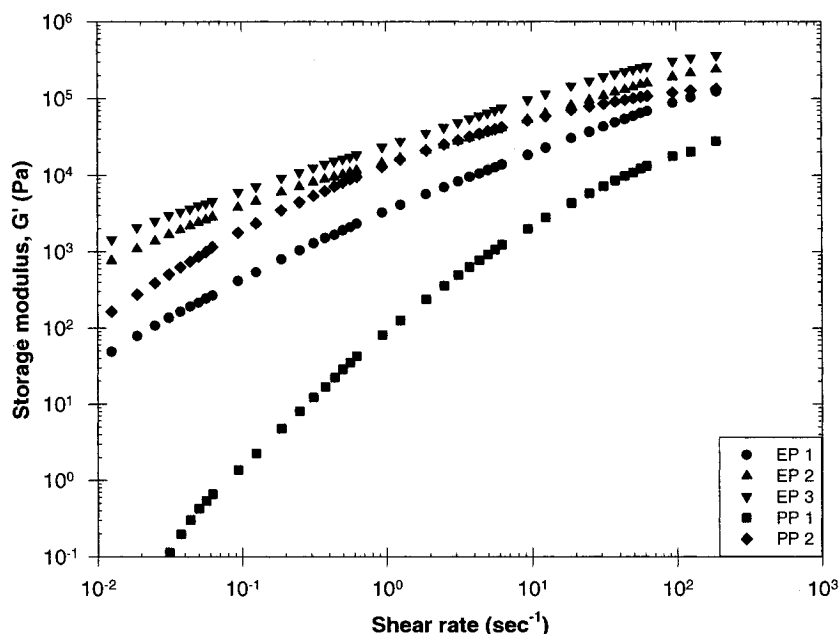


Figure 4.1 (b): Storage modulus of the pure materials as a function of shear rate at 190°C

4.3.2 Interfacial tension and miscibility/immiscibility

The interfacial tension between EPDM and PP is known to be very low and is dependent on ethylene content in EPDM, besides other known variables. The weak optical contrast and low interfacial tension makes the actual measurement of the interfacial tension extremely difficult using common experimental techniques. Interfacial tension values ranging from 0.06 to 0.6 mN/m estimated using the harmonic mean equation [43] and various other techniques can be found in the literature [1-6]. Using our own calculation from the harmonic mean equation and considering other data published in the literature, we estimate the interfacial tension between EPDM and PP to be around 0.3 mN/m at the melt blending temperature of 190°C.

The breaking-thread experiment was also carried out to measure the interfacial tension between these two polymers, however the PP thread in the EPDM matrix did not break up even after several hours. This highly stable thread behavior occurs as a result of the ultra-low interfacial tension between EPDM and PP and can be explained directly from Tomotika theory [44] as outlined in other work [33,45-48]. This result is also a support for the observation of highly stable fibers that will be discussed later in this paper.

As mentioned earlier in the Introduction, the issue of miscibility/immiscibility in this blend system is quite complex and is known to depend on various factors. Thus, it is crucial to determine if the blends in this study show some degree of miscibility between the components. In order to evaluate the miscibility, the T_g s of the lowest molecular weight pure materials and their blends, i.e. of EP 1, PP 1, and their blends, were measured using the DMTA and the results are shown in Figure 4.2. It can be seen that the T_g of PP 1 remains completely unaffected by blending. The T_g of EP 1, however, can be seen to decrease as the composition of EP 1 in the blend decreases. Thus, unlike completely miscible systems in which the blends show a single T_g for both blend components (as indicated by a solid line in Figure 4.2 and predicted using the Fox equation [49]), or for a partially miscible system (e.g. PMMA/PC blends system of Marin et al. [32]) in which the blends show two T_g s, each corresponding to the respective rich blend phases, moving towards the complete miscibility line; the T_g s in EPDM/PP blends remains unchanged for PP, and actually moves away from the line of complete miscibility for the EPDM.

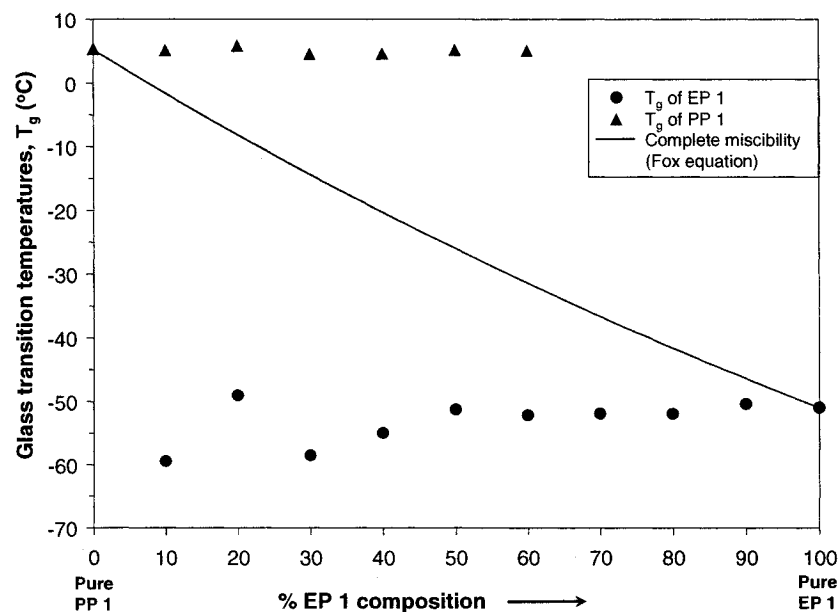


Figure 4.2: Glass transition temperatures for the EP 1/PP 1 blends as a function of EP 1 composition in the blend

Mäder et al. [50] have observed similar phenomenon of T_g depression of styrene-ethylene-butylene-styrene (SEBS), and poly(ethane-*co*-1-octene) (EO) elastomers melt blended with PPs of different stereoregularities. No change in the T_g of any PP was observed on melt blending with an elastomer, however the depression in the T_g of an elastomer was found on melt blending. The effect was more pronounced in the PP with the highest degree of crystallinity, i.e. for iPP, and was attributed to thermally induced internal stress resulting from the differential volume contraction of the two phases during cooling from the melt.

It is important to mention here that improper conditioning of these blends prior to T_g measurement, via DMTA testing, can result in erroneous data. The samples used

in the above tests and shown in Figure 4.2 were conditioned in a vacuum oven for about 3 weeks at 75°C. A shorter conditioning time resulted in lower T_g values for the PP phase. Blends rich in PP showed the greatest decrease in PP's T_g values with the effect becoming progressively less pronounced as the EPDM composition in the blend increased. The T_g values for the EPDM phase, however, did not show any difference on sample conditioning. This decrease in the T_g of the PP phase due to an incomplete conditioning prior to measurement could potentially be erroneously interpreted as a partial miscibility. The relaxation of the frozen-in stresses of the PP phase in the blend, generated during the compression-molding preparation of the samples after blending, thus require long conditioning time.

The results in Figure 4.2, with long conditioning times, clearly demonstrate that the blends with lowest molecular weight EP 1 and PP 1 are completely immiscible and do not show signs of even a partial miscibility at room temperature. By extrapolation, the other higher molecular weight blends would also be expected to show complete immiscibility; as the blending technique and the ethylene content of the EPDM elastomer remains unchanged.

4.3.3 Microstructure of EPDM/PP blends

4.3.3.1 EPDM minor phase

Micrographs of the EPDM minor phase in EP 1/PP 2 blends (viscosity ratio 0.7 and shear stress 90.9 kPa), at various compositions, are shown in Figure 4.3. The minor phase was extracted with cyclohexane. All the micrographs distinctively show a very

clear interface between EPDM and PP, which suggests and supports our previous finding that these blends are completely immiscible at room temperature at all compositions. At 10% EPDM, Figure 4.3(a), ultra-fine nano-scale particles ranging from 50 to 150 nanometers are observed. These structures are even finer than those typically reported in the literature [17-22]. As the concentration of the EPDM phase is increased to 20% it can be seen in Figure 4.3(b) that the shape of the phases appear to be significantly deviating from spherical. At 30% in Figure 4.3(c) this effect becomes much more pronounced. Finally at 50% the blend reaches cocontinuous morphology as evident in Figure 4.3(d). These results clearly pointed to the importance of confirming the shape of the EPDM phase and that work is outlined below.

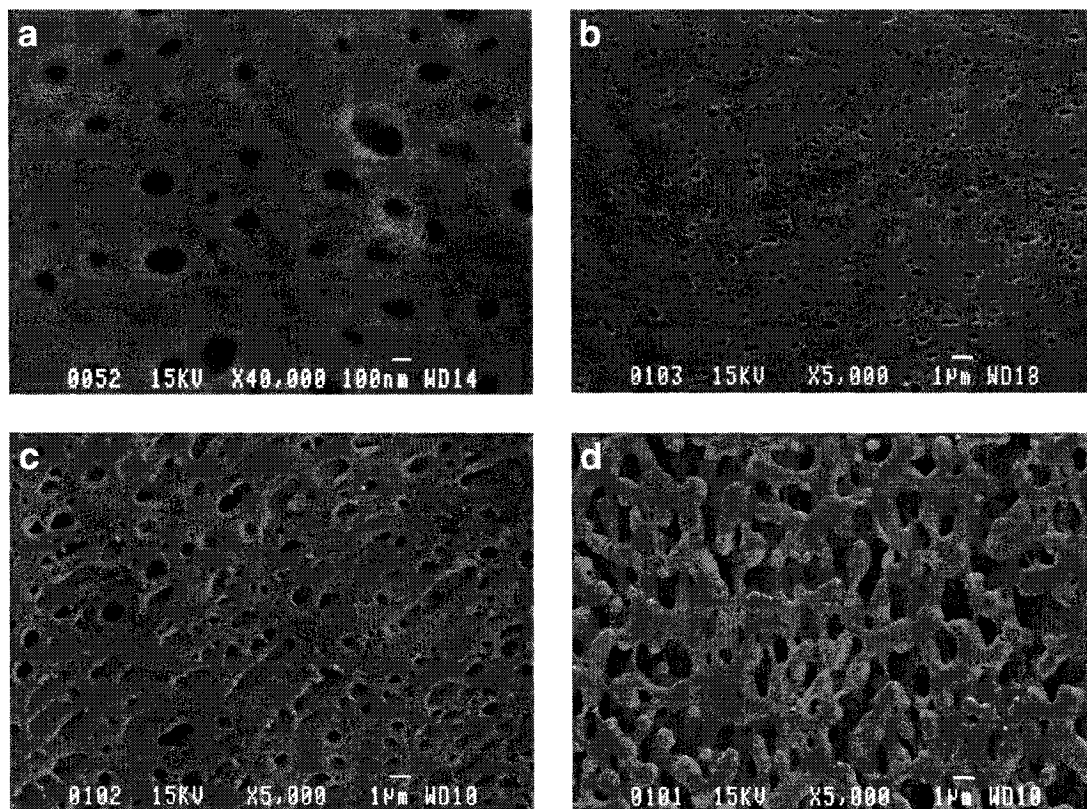


Figure 4.3: EPDM phase morphology development

SEM micrograph (a) 10 EP 1/90 PP 2, (b) 20 EP 1/80 PP 2, (c) 30 EP 1/70 PP 2, and (d) 50 EP 1/50 PP 2

Typically in the literature, low concentrations of dispersed EPDM in PP blends are considered to be composed of spherical droplets dispersed in a PP matrix [18-20,51-54]. However, it is very difficult to infer the shape of the minor phase from 2-dimensional micrographs. In order to assess the shape of the dispersed EPDM, a protocol was developed to selectively remove the PP matrix. This is accomplished by irradiation crosslinking the dispersed EPDM phase followed by dissolution of the PP phase with xylene. Results for the matrix dissolution test for systems EP 1/PP 2 and EP

1/PP 1 at 5 and 30% EPDM composition are shown in Figure 4.4. Note that upon collection of the 5% dispersed EPDM phase on the filter, it is impossible to avoid agglomeration of the EPDM phase. The very high surface area of the dispersed phase, the tacky nature of EPDM, and the high temperatures used for dissolving PP matrix in xylene are some of the reasons behind this agglomeration of the particles. Nevertheless, high magnification micrographs of the agglomerate surface in Figure 4.4(a) and (b) indicate that it is composed of very uniform fibers of EPDM with dimensions in the 100–200 nanometers range. At 30% EPDM, the PP matrix dissolution test results in an intact, non-disintegrated structure clearly possessing a very high level of interconnected fibers for both EP 1/PP 2 and EP 1/PP 1. In all cases in Figure 4.4, the scale of the fiber diameter corresponds closely to that observed in Figure 4.3 for EP 1/PP 2 blends.

In order to further support the observation of EPDM fibers, a partial-PP matrix dissolution was carried out. This allows one to observe the EPDM structure and avoid any EPDM fiber agglomeration. The results of partial matrix dissolution are shown in Figure 4.5 for pure EPDM, pure PP and for the 5 EP 1/95 PP 1 system at two magnifications. The PP 1 system was used here since it was easier to control the partial dissolution experiment. Figures 4.5(c) and (d) demonstrate elongated fibers of the same scale as seen in Figure 4.4(b).

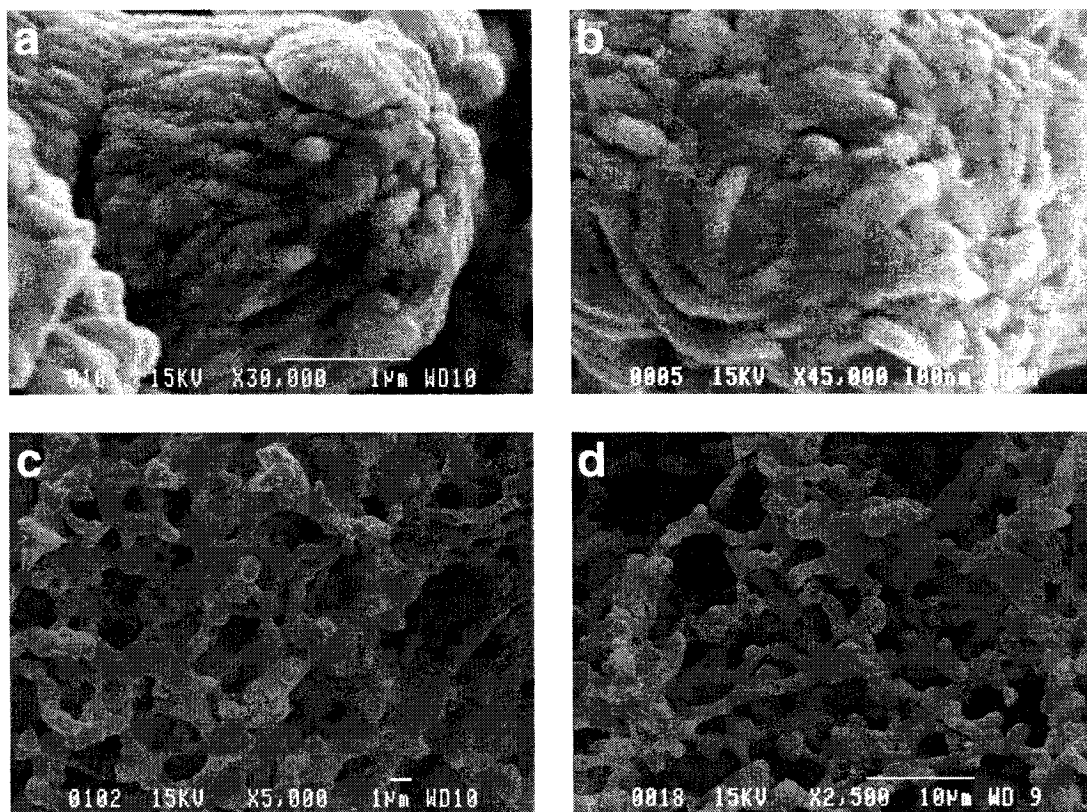


Figure 4.4: SEM micrographs of the dispersed EPDM phase after PP matrix dissolution

SEM micrograph (a) 5 EP 1/95 PP 2, (b) 5 EP 1/95 PP 1, (c) 30 EP 1/70 PP 2, and (d) 30 EP 1/70 PP 1

These results clearly indicate, in the viscosity ratio range used in this work, that the dispersed EPDM phase in EPDM/PP blends forms nano-scale fibers and challenges the current view of EPDM being dispersed as spherical particles in PP [18-20,51-54].

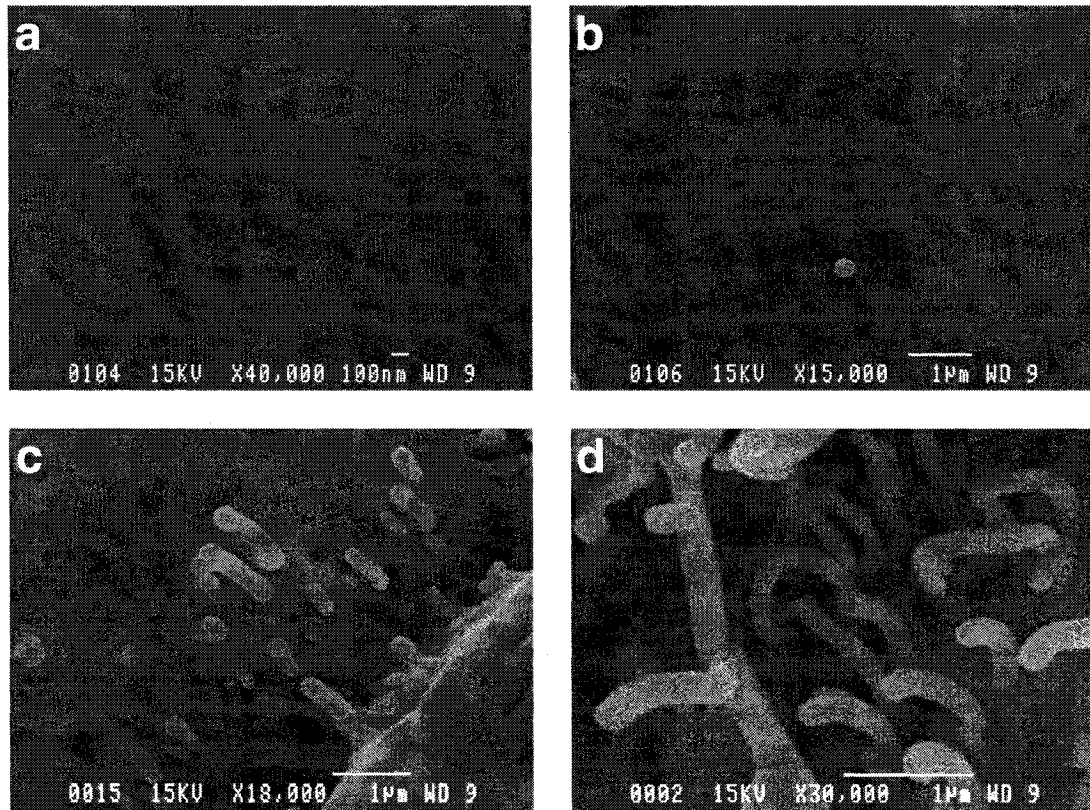


Figure 4.5: SEM micrographs after partial PP matrix dissolution

SEM micrograph (a) Pure EP 1, (b) Pure PP 1, (c) and (d) 5 EP 1/95 PP 1

Tomotika [44] theory also provides theoretical support for this observation. From Tomotika's theory the typical thread breakup time of a Newtonian fluid in the matrix of another Newtonian fluid is given by,

$$t_b = \frac{2\eta_c R_o}{\Omega_m(\lambda_m, p)\sigma} \ln\left(\frac{0.81 R_o}{\alpha_o}\right) \dots\dots\dots (4.3)$$

where, t_b is the thread breakup time, η_c is the viscosity of the continuous (matrix) phase, η_d is the viscosity of the disperse (thread) phase, p is the viscosity ratio (η_d/η_c), R_o is the

initial thread radius, σ is the interfacial tension, $\Omega_m(\lambda_m, p)$ is the complex function of wavelength (λ) and viscosity ratio (p) determined at dominant wavelength (λ_m), and α_o is the original amplitude.

In order to theoretically estimate the breakup time we need to estimate the original amplitude (α_o). Elemans et al. [47] suggested that α_o can be estimated from the equation derived by Khun [55] based on fluctuations of the interface caused by Brownian motion. These are the smallest possible perturbations and are always present on a fluid cylinder. Thus equation 3 can be re-written as,

$$t_b = \frac{\eta_c R_o}{\Omega_m(\lambda_m, p) \sigma} \ln \left(\frac{1.39 \sigma R_o^2}{k T} \right) \dots\dots\dots (4.4)$$

where, k is the Boltzmann constant, and T is the absolute temperature.

The values used for the estimation of the fiber breakup time for both 5 and 10% EPDM in EP 1/PP 2 and EP 1/PP 1 blends are reported in Table 4.3. The actual average diameter values determined by image analysis at those compositions are used in these calculations. The omega function is determined using the equations developed by Tomotika [44] and by inserting the values of $I_n(x)$ and $K_n(x)$ from the tables given by Watson [56], as suggested by Tomotika. The estimated values of the fiber breakup time in Table 4.3 vary from 7 to 15 minutes and support the notion of stable EPDM fiber formation over the melt mixing times used in this work. Note that in order to support the experimental breaking thread experiment on a PP thread in EPDM discussed earlier, the theoretical breakup time for a 30 μ m PP 2 thread in an EP 1 matrix is also

calculated. The extremely long thread breakup times clearly support the experimental observation of no breakup after several hours for this system.

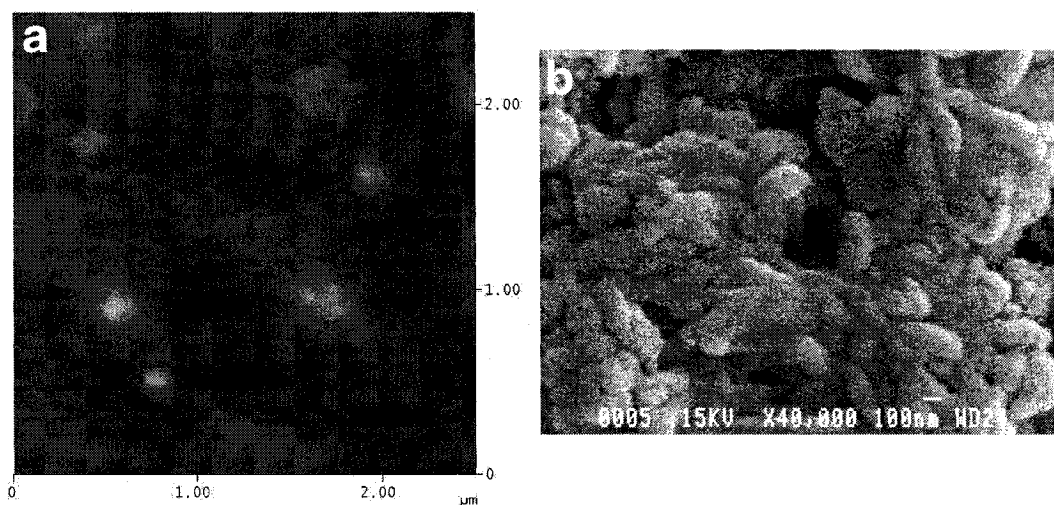
Table 4.3: Estimated fiber breakup times

System	EP 1/PP 2		EP 1/PP 1		Experimental breaking time for PP 2 thread in EP 1 matrix
% EP in the blend	5%	10%	5%	10%	
D_o (μm)	0.11	0.19	0.44	0.46	≈ 30
$\eta_{o,EP}$ (kPa)					30.6
$\eta_{o,PP}$ (kPa)	79.6		0.96		79.6
p	0.38		31.9		2.6
σ (mN/m)					0.3
k ($\text{kg m}^2/\text{s}^2 \text{K}$)					1.38×10^{-23}
T ($^{\circ}\text{C}$)					190
$\Omega_m(\lambda_m p)$	0.173		0.009		0.06
t_b (s)	446	931	651	688	422548
t_b (min)	7.4	15.5	10.9	11.5	7042.5

It is well known that Tomotika theory was developed for Newtonian fluids and does not account for complex viscoelastic effects. However, it has been reported that as particle sizes or fiber diameters approach one micron, viscoelastic effects become negligible [57]. As dispersed structures become very small in size, their surface to volume ratio becomes so large that interfacial mechanisms such as capillary instabilities can be expected to dominate breakup over bulk dominated mechanisms related to viscoelasticity.

4.3.3.2 PP minor phase

Similar studies were carried out to demonstrate the PP microstructure in the EPDM matrix, and the results are shown in Figure 4.6 for the system PP 2/EP 1. Since dissolution of the dispersed PP phase is difficult and because of EPDM matrix swelling (which could alter the blend morphology, especially the phase sizes), atomic force microscopy was used to study the morphology of dispersed PP blends. The AFM micrograph (a) for 10 PP 2/90 EP 1 blend shows that the PP, like EPDM, is also distributed uniformly and finely with size scales ranging from 150-300 nanometers. Moreover, an EPDM matrix dissolution protocol, shown in Figure 4.6(b), confirms that the PP phase is also dispersed in the form of nanometer scale ($\approx 200\text{nm}$ in diameter) fibers. Complete matrix dissolution for the 30 PP 2/70 EP 1 blend, Figure 4.6(c), shows a network of interconnected PP fibers. This result supports the notion, as observed for dispersed EPDM, that PP continuity develops by fiber-fiber coalescence. The similarity of the microstructural results for dispersed EPDM and dispersed PP are not unexpected since the viscosity and elasticity ratios are not greatly different after phase inversion (see Table 4.2). The morphology thus appears to be largely dominated by the low interfacial tension.



Atomic force microscopy

Complete matrix dissolution

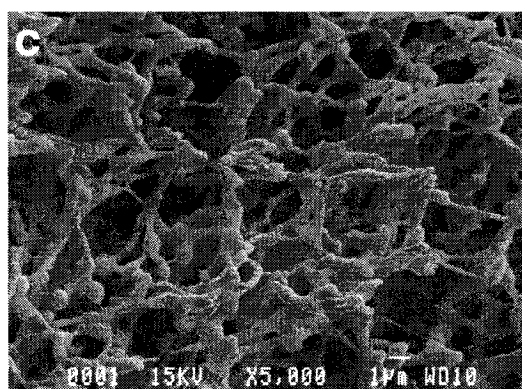
Complete matrix dissolution
with freeze drying

Figure 4.6: PP phase microstructure in EPDM matrix

Micrograph (a) atomic force micrograph of 20 PP 2/80 EP 1 blend;
SEM micrograph of PP dispersed phase after complete EPDM matrix dissolution
in (b) 5 PP 2/95 EP 1 blend, and (c) 30 PP 2/70 EP 1 blend

4.3.4 Effect of EPDM composition on phase size

Figure 4.7 presents the number average and volume average diameters obtained by image analysis as well as the pore diameter obtained by the BET nitrogen adsorption technique as a function of composition for EP 1/PP 2 blends. The system clearly demonstrates high coalescence features as characterized by a 6 to 10 fold increase in the phase sizes. Coalescence on this scale is highly unexpected for such a low interfacial tension system and this will be discussed along with some anomalies in the continuity data later in section 3.7.

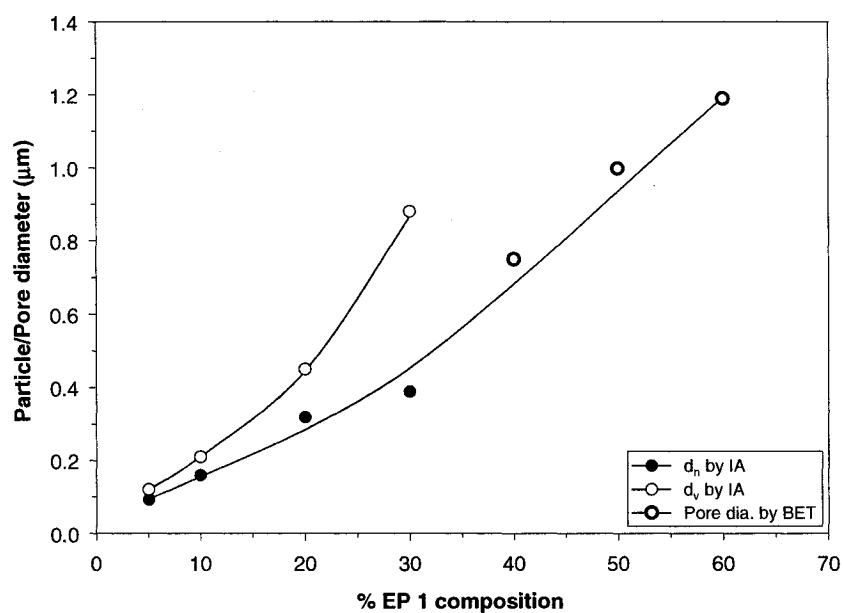


Figure 4.7: Average particle/pore diameters as a function of composition for EP 1/PP 2 blends

4.3.5 Effect of viscosity ratio and matrix viscosity on microstructure

Figure 4.8 demonstrates the effect of viscosity ratio and matrix viscosity on the particle size as a function of EPDM composition. All the blends irrespective of their viscosity ratio and matrix shear stress show a significant increase in particle size with composition as shown in the previous section. The viscosity ratio has little effect on the microstructure, however, an 8-fold decrease in the matrix viscosity, i.e. for EP 1/PP 1 blends, does impact the phase sizes by roughly 3 to 4 times at low compositions of EPDM. The strong phase size increase beyond 20% EPDM for EP 1/PP 1 blends is most likely related to the effect of PP viscosity on EPDM coalescence [58-61]. Note however that the matrix viscosity does not significantly influence the shape of the dispersed phase i.e. the EPDM exists as elongated fibers as already shown in micrograph (b) of Figure 4.4 for the EP 1/PP 1 blend system.

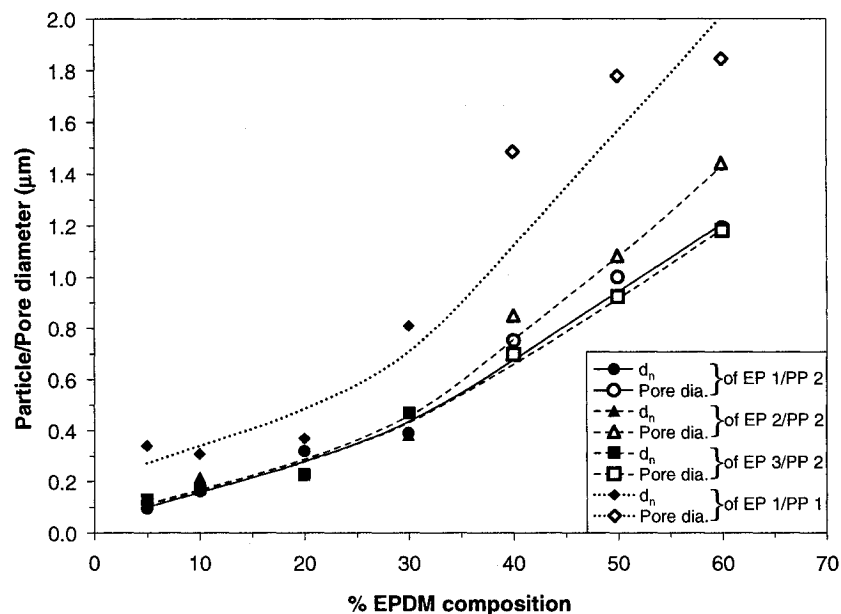


Figure 4.8: Effect of viscosity ratio and shear stress on average particle/pore sizes as a function of composition

4.3.6 Continuity development and cocontinuity

Figure 4.9 presents the complete continuity development and co-continuity data with composition for EPDM/PP blends at all viscosity ratios. The continuity values reported in this diagram are already corrected for the PP solubility in cyclohexane (about 2.6% for PP 1 and 1.4% for PP 2) at room temperature, and EPDM solubility in boiling xylene (about 3.0%). The correction for PP arises due to the fact that commercial PP contains a small atactic portion or low molecular weight chains of PP which are soluble in cyclohexane at room temperature. For EPDM the correction is related to the presence of a small fraction of non-crosslinkable EPDM, and the gel content achieved by irradiation, because of the fact that irradiation also causes chain

scission of EPDM to some degree. These corrections are necessary, especially at the higher concentration of each component where small amounts of solubility of the major component can result in substantial changes in the continuity values of the minor component.

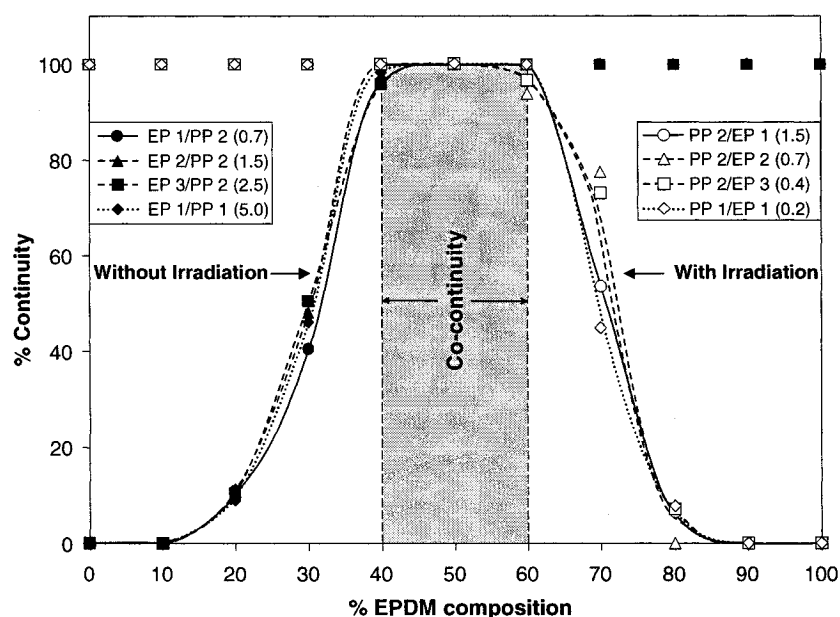


Figure 4.9: Complete continuity development and cocontinuity diagram for EPDM/PP blends system (corrected for PP solubility in cyclohexane at room temperature, and EPDM solubility in xylene)

Figure 4.9 reveals that the continuity development with composition is symmetrical in all EPDM/PP blends studied here. In general, at viscosity ratios between 0.7 and 4.9 and for shear stresses varying from 11.7–90.9 kPa, a virtual single master-curve for continuity development is obtained. There are some differences in the continuity data at 70% EPDM however, the continuity data at that concentration was

particularly challenging to measure due to the combination of crosslinked EPDM matrix swelling and the extreme concentration sensitivity of continuity development. The systems demonstrate high percolation thresholds, gradual continuity development and attain cocontinuity at high compositions of the minor phase. Co-continuity is maintained over a relatively restricted composition range (about 20 composition units). This behavior is highly unexpected from such a low interfacial tension system. Low interfacial tension systems are known to possess very broad regions of cocontinuity [33,45,46]. These anomalies in the continuity data and the higher coalescence already seen in the section 3.4 are explained below.

4.3.7 Morphological characteristics of partial miscibility

The EPDM/PP system according to a definition provided by Li et al. [33] represents a Type I low interfacial tension binary blend. In fact the EPDM/PP system has an even lower interfacial tension than that of the styrene-ethylene-butylene-styrene (SEBS)/high density polyethylene (HDPE) blends system studied by Li et al. This type of system is expected to demonstrate: dispersed phase in the form of very uniform fibers, thus continuity development by fiber-fiber coalescence, very low percolation thresholds and attainment of co-continuity at low compositions. Moreover, they showed that these systems possess a very large composition range for cocontinuity and virtually no dependence of phase size with composition. Although this system demonstrates some of the expected features of a low interfacial tension immiscible binary blend such as ultra-low diameter fiber formation and continuity development via fiber-fiber

coalescence (Figure 4.4–4.6), a number of anomalies are also observed, i.e. the EPDM/PP system shows a dependence of pore size with composition in Figures 4.7 and 4.8; high percolation threshold compositions as shown in Figure 4.9; and a composition range for dual-phase continuity of only 20 composition units. These latter characteristics are more typical of a high interfacial tension blend system.

As mentioned earlier, Marin et al. [32] observed similar tendencies for a low interfacial tension PMMA/PC system. They were able to relate those deviations to the partial miscibility of PMMA/PC. In a detailed study of glass transition temperatures for the PMMA/PC blend they were able to quantitatively estimate the extent of partial miscibility using the Fox equation [49] and correct the gravimetric data by considering the blend as a mixture of a PMMA-rich phase with a PC-rich phase. By correcting the continuity and co-continuity data in this way they were able to demonstrate that indeed the blend showed all the principal features of a low interfacial tension system: very low percolation thresholds and low concentration for the attainment of fully co-continuous structures. They related the increase of phase size with increasing composition to a reduced miscibility of the PMMA/PC system.

The anomalies seen in this research work for EPDM/PP blends closely correspond to the behavior of the partially miscible systems, yet Figure 4.2 demonstrates that these blends are completely immiscible upon cooling from the melt. Unlike partially miscible PMMA/PC system, the main difference in this work, however, is that PP is a crystallizable component. The blends studied in this work thus present the

morphological characteristics of a mixture which was partially miscible during melt blending at which time the gross morphological features are developed. The crystalline nature of PP then drives the system to complete phase separation upon cooling. It appears, however, that the quenching of the EPDM/PP blend from the melt is clearly rapid enough to preserve the imprint of that partial miscibility on the gross blend morphology.

Since the blends completely phase separate upon cooling, the quantitative estimation of the extent of partial miscibility using the Fox equation and subsequent corrections to the gravimetric data in Figure 4.9 are not possible for this EPDM/PP blends system.

4.4 Conclusions

This research work rigorously studies the morphology development, with particular attention to the continuity development and cocontinuity, in ultra-low interfacial tension EPDM/PP blends. The blends with viscosity ratios of 0.2 to 4.9 and shear stresses of 11.7 to 231.4 kPa are considered.

Contrary to the current view of dispersed phase as being in the form of spherical droplets, by the variety of sophisticated morphology protocols and an analysis using break-up times from Tomotika theory, it is demonstrated that the minor phase (of either component) is dispersed in the form of extremely small diameter (50-200 nm) stable fibers. These fibers are shown to coalesce together at crossover points to develop the continuity and cocontinuity as per the expected behavior of a binary compatible system.

The blends demonstrate virtually no effect of 7-fold variation in the viscosity ratio on the phase sizes, shape of the dispersed phase, % continuity, region of cocontinuity and thus also the mechanism of continuity development; however, 8-fold variation in shear stress does affect the particle sizes.

The complete continuity diagram shows very symmetrical continuity development for either of the blend components. The blends present high percolation thresholds, gradual continuity development, and attainment of cocontinuity at much higher compositions of the minor phase. The blends also demonstrate very high coalescence with the composition of the minor phase, for such an ultra-low interfacial tension system. Since the gross morphological features of the blend develops during melt blending, these results indicate that the blends were partially miscible in the melt; however the crystalline nature of PP forced the blends to completely phase separate upon cooling, as shown by the glass transition temperatures of the quenched blend samples. The quenching of the blends from the melt is clearly rapid enough to preserve the imprint of the partial miscibility in the melt on the gross blend morphology.

Acknowledgements

The authors would like to thank Mr. Mike Gallagher of Bayer Inc. for supplying EPDM; Mr. Denis Therrien of Basell Polyolefins Inc. for supplying and measuring the molecular weights of the PP; Prof. Monique Lacroix, of INRS-Institut Armand-Frappier, Université du Québec, for irradiating the blends; Mr. Pierre Sammut, and Ms. Nicole Côté of the Industrial Materials Institute of the National Research Council

of Canada for their kind assistance with DMTA. The authors would also like to thank the whole “Groupe de mélanges polymères” of École Polytechnique de Montréal, especially Nick Virgilio for AFM and Xavier Roy for his kind expertise in freeze drying.

References

1. Mighri F, Huneault M. Can J Chem Eng 2002;80(6):1028-35.
2. Reichart GC, Graessley WW, Register RA, Krishnamoorti R, Lohse DJ. Macromolecules 1997;30:3036-41.
3. Pogodina NV, Chapman BR, Lohse DJ. PMSE preprints 2003;89:421-3.
4. Tsou AH, Lyon MK. ANTEC 2000 Proceedings of the 58th Annual Technical Conference, Society of Plastics Engineers;58(2):2116-9.
5. Chung O, Coran AY, Rubber Chem Technol 1997;70(5):781-97.
6. Hemmati M, Nazokdast H, Shariat Panahi H. J Appl Polym Sci 2001;82(5):1129-37.
7. Yamaguchi M, Miyata H, Nitta K, J Appl Polym Sci 1996;62(1):87-97.
8. Chen CY, Yunus WMdZW, Chiu HW, Kyu T. Polymer 1997;38(17):4433-8.
9. Amash A, Zugenmaier P, J Polym Sci, Polym Phys 1997;35(9):1439-48.
10. Ramanujam A, Kim KJ, Kyu T. Polymer 2000;41:5375-83.
11. Xiao HW, Huang SQ, Jiang T, Cheng AY. J Appl Polym Sci 2002;83:315-22.
12. Zhao R, Dai G. J Appl Polym Sci 2002;86:2486-91.
13. Fischer WK. US Pat 1974;3,806,558.

14. Coran AY, Das B, Patel RP. US Pat 1978;4,130,535.
15. Abdou-Sabet S, Fath MA. US Pat 1982;4,311,628.
16. Coran AY, Patel RP. Rubber Chem Technol 1982;55:116-36.
17. Danesi S, Porter RS. Polymer 1978;19(4):448-57.
18. Karger-Kocsis J, Kallo A, Kuleznev VN. Polymer 1984;25(2):279-86.
19. Yang D, Zhang B, Yang Y, Fang Z, Sun G, Feng Z, Polym Eng Sci 1984;24(8):612-7.
20. Dao KC. Polymer 1984;25(10):1527-33.
21. Jang BZ, Uhlmann DR, Vander Sande JB. J Appl Polym Sci 1985;30(6):2485-504.
22. D'Orazio L, Mancarella C, Martuscelli E. Polymer 1991;32(7):1186-94.
23. Karger-Kocsis J, Kallo A, Szafner A, Bodor G, Senyei Zs. Polymer 1979;20(1):37-43.
24. Martuscelli E, Silvestre C, Abate G. Polymer 1982;23(2):229-37.
25. Martucelli E. Polym Eng Sci 1984;24(8):563-86.
26. Lohse DJ. Polym Eng Sci 1986;26(21):1500-9.
27. Lohse DJ, Wissler GE. J Mater Sci 1991;26(3):743-8.
28. Han SJ, Lohse DJ, Condo PD, Sperling LH. J Polym Sci, Polym Phys 1999;37(20):2835-44.
29. Seki M, Nakano H, Yamauchi S, Suzuki J, Matsushita Y. Macromolecules 1999;32(10):3227-34.
30. Inaba N, Sato K, Suzuki S, Hashimoto T. Macromolecules 1986;19(6):1690-5.
31. Inaba N, Yamada T, Suzuki S, Hashimoto T. Macromolecules 1988;21(2):407-14.

32. Marin N, Favis BD. Polymer 2002;43(17):4723-31.
33. Li J, Ma PL, Favis BD. Macromolecules 2002;35(6):2005-16.
34. Marquez A, Quijano J, Gaulin M. Polym Eng Sci 1996;36(20):2556-83.
35. Zaharescu T, Setnescu R, Jipa S, Setnescu T. J Appl Polym Sci 2000;77:982-7.
36. Kammel G, Wiedenmann R. Siemens Forsch - u Entwickl 1976;5(3):157-62.
37. Vroomen GLM, Visser GW, Gehring J. Rubber World 1991;205(2):23-32.
38. Favis BD, Chalifoux JP. Polym Eng Sci 1987;27(20):1591-1600.
39. Saltikov SA. In: Elias H, editor. Proceedings of the 2nd international congress for stereology. Berlin:Springer-Verlag; 1967. p. 163-73.
40. Li J, Favis BD. Polymer 2001;42(11):5047-53.
41. Cox WP, Merz EH. J Polym Sci 1958;28:619-22.
42. Chung O, Coran AY, White JL. ANTEC 1997 Proceedings of the 55th Annual Technical Conference, Society of Plastics Engineers;55(3):3455-60.
43. Wu S. Polymer Interface and Adhesion, New York:Marcel Dekker Inc, 1982.
44. Tomotika S. Proc R Soc London 1935;A150:322-37.
45. Willemse RC, Posthuma de Boer A, Van Dam J, Gotsis AD. Polymer 1998;39(24):5879-87.
46. Veenstra H, Van Lent BJJ, Van Dam J, Posthuma de Boer A. Polymer 1999;40(24):6661-72.
47. Elemans PHM, Janssen JMH, Meijer HEH, J Rheol 1990;34(8):1311-25.
48. Elmendorp JJ. Polym Eng Sci 1986;26(6):418-26.
49. Fox TG. Bull Am Phys Soc (2) 1956;1:123.

50. Mäder D, Bruch M, Maier R, Stricker F, Mülhaupt R. *Macromolecules* 1999;32(4):1252-9.
51. Thamm RC. *Rubber Chem Technol* 1977;50(1):24-34.
52. Martuscelli E, Silvestre C, Bianchi L. *Polymer* 1983;24(11):1458-68.
53. Karger-Kocsis J, Kiss L, Kuleznev VN. *Polymer Commun* 1984;25(4):122-6.
54. Jang BZ, Uhlmann DR, Vander Sande JB. *J Appl Polym Sci* 1984;29(12):4377-93.
55. Kuhn W. *Kolloid Z* 1953;132:84-99.
56. Watson GN. *A Treatise on the Theory of Bessel Functions*, 2nd ed. Cambridge: University Press, 1966.
57. Van Oene H. *J Colloid Interf Sci* 1972;40(3):448-67.
58. Wildes G, Keskkula H, Paul DR. *Polymer* 1999;40:5609-21.
59. Roland CM, Bohm GGA. *J Polym Sci, Polym Phys* 1984;22(1):79-93.
60. Kressler J, Higashida N, Inoue T, Heckmann W, Seitz F. *Macromolecules* 1993;26(8):2090-4.
61. Fortelny I, Zivny A. *Polymer* 1995;36(21):4113-8.

CHAPTER 5

EROSION-CONTROLLED CONTINUITY

DEVELOPMENT IN HIGH VISCOSITY RATIO BLENDS

OF VERY LOW INTERFACIAL TENSION

The objective of this second paper is to examine morphology development, in particular continuity development and cocontinuity, in high viscosity ratio ethylene-propylene-diene terpolymer/polypropylene (EPDM/PP) blends. In general, blend morphology studies almost always examine the steady-state morphology obtained after several minutes of mixing. The time scales to achieve steady-state morphology are typically so small that they have defied examination of the non-steady-state morphology. High viscosity ratio blends of ultra-low interfacial tension, however, provide a unique opportunity to examine those phenomena.

By melt mixing two EPDM materials with very low viscosity PP, blends having high viscosity ratios of 11 and 17 are made. The same morphology investigation tactics developed in the first paper are applied here. In addition, blends with different composition are melt mixed for prolonged times to examine the erosion phenomena and its effect on continuity.

This article is submitted to the journal : *“Journal of Polymer Science Part B: Polymer Physics”*

Erosion-Controlled Continuity Development in High Viscosity Ratio Blends of Very Low Interfacial Tension

Prashant Bhadane,¹ Michel Champagne,² Michel Huneault,² Florin Tofan,³
and Basil D. Favis¹

¹ CREPEC, Department of Chemical Engineering, École Polytechnique de Montréal,
2900 Édouard Montpetit, P.O. Box 6079, Station Centre-Ville, Montréal, Qué., Canada
H3C 3A7

² Industrial Materials Institute, National Research Council of Canada, 75 de Mortagne
Blvd., Boucherville, Qué., Canada J4B 6Y4

³ Lavergne Group, 8800 Crescent 1, Ville d'Anjou (Montréal), Qué., Canada H1J 1C8

ABSTRACT

This work studies continuity development and cocontinuity in high viscosity ratio EPDM/PP blends. An ultra-low interfacial tension ($\approx 0.3 \text{ mN/m}$) between the blend components together with high viscosity ratios (11 and 17) result in a variety of unusual morphological features including: isolated nanometer diameter fibers, very large particles, partially coalesced particles, and numerous particles interconnected by fibers. This unique combination of morphologies leads the blend to a novel and stable cocontinuous structure of partially coalesced particles and particles interconnected by fibers. Compared to low to medium viscosity ratio EPDM/PP blends, such cocontinuous

Correspondence to: Basil Favis (E-mail: basil.favis@polymtl.ca)

networks demonstrate early percolation thresholds, rapid continuity development, and attain cocontinuity at lower compositions of minor phase.

The slow surface erosion of the high viscosity EPDM phase during melt blending is shown to be responsible for the generation of these unusual morphological structures. Typically the time scale for erosion phenomena are so small, that they have defied study in the mixing environment itself and typical blend morphology studies almost always examine the final steady-state morphology obtained after several minutes of mixing. The combination of very low interfacial tension and very high viscosity ratios of these EPDM/PP systems provide a unique opportunity to examine erosion phenomena persisting over longer time scales during melt mixing. We propose a new concentration-dependent erosion mechanism which is based on particle collision-coalescence-separation dynamics. The proposed conceptual mechanism is shown to dramatically accelerate the erosion process and maintain cocontinuity over prolonged periods of mixing.

Keywords: Blends; Morphology; Polypropylene (PP); Erosion; Co-continuous morphology; High viscosity ratio

5.1 INTRODUCTION

A co-continuous blend morphology is one in which neither of the blend phases can be defined as a matrix or the dispersed phase. It forms highly interconnected and intertwining structures and both the blend phases remain fully continuous throughout the blend. Since co-continuous blends can be prepared for any immiscible polymer pair

and since the phase size can be controlled over many orders of magnitude, this polymer blend structure has been receiving particular attention in the literature. It has the potential for exceptional mechanical¹⁻² and functional properties.³⁻⁵ Some of these applications include: carrier structures for conducting polymers,³ high porosity templates and membranes which can be used to deliver catalysts in the chemical industry; biodegradable scaffolds for use in tissue engineering, drug delivery and as human implant materials.⁶ Despite significant activity in this field in the last several years, a number of fundamental questions remain unresolved. In the past, several authors have studied the effect of variation in the viscosity ratio,⁷⁻¹⁴ elasticity ratio,¹⁵⁻¹⁷ interfacial tension, and type of interface¹⁸ on continuity development and cocontinuity. A number of papers have targeted the development of models to predict the region of dual-phase continuity. A variety of expressions have been proposed based on the viscosity ratio,⁷⁻¹⁴ predicting that the low viscosity material tends to form the matrix, and based on elasticity ratio,¹⁵⁻¹⁷ predicting that the high elasticity material tends to form the matrix. Nevertheless, none of these equations alone appears to be consistently capable of predicting the composition of phase inversion.

Recently, Li et al.¹⁸ published work related to the role of the interface in controlling the formation of cocontinuous morphologies. They defined several different types of blend interfaces and systematically examined their role in the development of cocontinuous morphologies during melt mixing. Using general arguments based on fiber lifetime vs droplet lifetime during melt processing they demonstrated that for a binary compatible interface, typical of low interfacial tension system, the dispersed

phase exists in the form of stable elongated fibers at low composition. The continuity in such a system develops by the coalescence of these fibers at crossover points. Hence, the system demonstrated low percolation thresholds, no coalescence, and very broad regions of cocontinuity. Other authors have also observed similar tendencies for low interfacial tension systems.^{14,19} For a binary incompatible interface, typical of a high interfacial tension system, the dispersed phase was shown to form droplets and the continuity in that case develops by droplet-droplet coalescence. Hence, the system presented high percolation thresholds, high coalescence, and narrower regions of cocontinuity. For the ternary compatibilized interface, continuity develops by reduced droplet-droplet coalescence because of the presence of an interfacial modifier at the interface. In that case, the system demonstrated even higher percolation thresholds and attained cocontinuity at even higher compositions of the minor phase.

In an earlier publication²⁰ we showed that, at 5 and 10% EPDM concentrations, the dispersed phase in an ultra-low interfacial tension EPDM/PP blend system, with low to medium viscosity ratio, exists in the form of extremely small fibers of 50–200 nm. The formation of such a structure was considered as following the trends for a binary compatible-type interface as suggested by Li et al.¹⁸ The blends from that study actually demonstrated a number of morphological features consistent with a partially miscible system,²¹ such as high coalescence, artificially high percolation thresholds, and a narrow composition range for cocontinuity. The results indicate that the EPDM/PP blends in that study were partially miscible in the melt and then fully phase separated upon cooling, as demonstrated by the glass transition temperatures of the quenched

blend samples. Since the dominant morphological features of the blend are established during melt blending, the quenching of the blend from the melt was clearly rapid enough to preserve the imprint of that partial miscibility on the morphology after cooling.

The objective of this study is to build on the previous work and examine the continuity development and co-continuity in very high viscosity ratio blends of EPDM/PP. In this paper it will be shown that the combination of very low interfacial tension ($\approx 0.3 \text{ mN/m}$) and very high viscosity ratios (11 and 17) provide an opportunity to examine erosion phenomena persisting over long time scales during melt mixing. It is well known that multiphase polymer blends undergo complex deformation and disintegration processes during melt mixing. The time scale for these phenomena are typically so small, however, that they have defied study in the mixing environment itself and typical blend morphology studies almost always examine the final steady-state morphology obtained after several minutes of mixing. This very high viscosity ratio, ultra-low interfacial tension system provides the possibility of a unique window into examining those phenomena.

5.2 EXPERIMENTAL PROCEDURES

5.2.1 Materials

In this study, two EPDM materials with different Mooney viscosities and a PP homopolymer with very high melt flow index were used to generate high viscosity ratio blends. Some of the other characteristics of the materials are summarized in Table 5.1.

The various rheological property ratios, calculated at constant shear rate and at constant shear stress, are noted in Table 5.2.

Table 5.1: Characteristic properties of the materials

Polymer	Supplier	Given name	Molecular weights x 10 ³		Ethylene content (%)	ENB content (%)
			M _n	M _w		
PP	Basell	PP 1	89.0	288.0	-	-
EPDM	Bayer	EP 1	71.2	142.0	62	4.0
EPDM	Bayer	EP 2	112.4	194.0	52	4.3
EPDM	Bayer	EP 3	146.0	241.1	53	4.3

Table 5.2: Rheological property ratios at constant shear rate and constant shear stress

Sr no	Blend components		Blend name	Torque ratio	At const. shear rate		Matrix shear stress (kPa)	At const. shear stress	
	Dispersed phase	Matrix			p ^a	ψ ^b		p ^a	ψ ^b
1	EP 2	PP 1	EP 2/PP 1	7.0	11.0	17.0	11.7	74.0	1.5
2	EP 3	PP 1	EP 3/PP 1	10.0	17.0	29.0	11.7	174.0	1.5
3	PP 1	EP 2	PP 1/EP 2	0.1	0.1	0.1	144.7	-	1.0 ^c
4	PP 1	EP 3	PP 1/EP 3	0.1	0.1	0.05	231.4	-	1.0 ^c

^a Viscosity ratio

^b Elasticity ratio

^c by extrapolation of the data

P.S. All the rheological properties are determined at an average shear rate in internal mixer of 26 sec⁻¹.

5.2.2 Rheological characterization

The rheological characterization was carried out using a Bohlin constant stress rheometer (CSM) in the dynamic mode. The experiments were performed in parallel plate geometry of 25 mm diameter, at 190°C and under a nitrogen atmosphere. The

frequency sweep tests were performed in an experimental window permitted by the time and stress sweep test.

5.2.3 Melt blending

PP, EPDM and antioxidant were first dry blended in a beaker and then simultaneously fed into the mixing chamber. The two polymers were melt blended using a Haake Rheomix 600 batch mixer with a Haake system 90 drive for 8 minutes, at 100 rpm, 190°C temperature, and under a nitrogen blanket. This internal mixer is equipped with a 69 cm³ chamber and roller-type rotors. After mixing, the melt was taken out of the chamber very gently but rapidly, and was quenched immediately in cold water to freeze in the morphology generated during mixing.

In total two different types of blends, over the entire composition range, were prepared. The different types of blends prepared as well as their various rheological property ratios (determined at constant shear rate and at constant shear stress) are reported in Table 5.2.

5.2.4 Irradiation crosslinking

A second batch of all these blends, along with the pure materials, were irradiation crosslinked in air with a Cobalt-60 (⁶⁰Co) source, using a commercial carrier type 8900 irradiator with the dose rate of 25 kGy/hr and to an average optimal²²⁻²⁴ total dose of 154 kGy.

5.2.5 Solvent extraction and gravimetry

The samples used for EPDM continuity measurement were extracted using cyclohexane, and the samples used for PP continuity measurement, i.e. the samples taken from irradiation crosslinked blends, were extracted using boiling xylene. The weight of the samples before extraction and after extraction and complete drying were noted. The complete phase removal was assured by comparing the sample weight after each solvent wash.

The continuity of each phase was then measured using the following formula,

$$\% \text{ Continuity of A} = \left(\frac{\text{Wt. of A}_{\text{Before Extraction}} - \text{Wt. of A}_{\text{After Extraction}}}{\text{Wt. of A}_{\text{Before Extraction}}} \right) \times 100 \dots\dots\dots (5.1)$$

where ‘A’ represents the component which has been extracted and whose continuity has to be determined. The values reported are the average of at least three measurements done in this way.

5.2.6 Microtomy, scanning electron microscopy and image analysis

In order to avoid the presence of any air/nitrogen bubbles in these samples, the EPDM/PP blends were gently pressed by compression molding at low pressure at 190°C for 4 minutes. No change in the blend morphology was observed using this protocol. The samples were subsequently microtomed using a glass knife under liquid nitrogen to create a perfectly plane face.

The normal blend samples, i.e. the ones which were not subjected to irradiation, were extracted for EPDM using cyclohexane as the solvent. The extracted and dried samples were then coated with a gold-palladium alloy and micrographs were taken using a Jeol JSM 840 scanning electron microscope (SEM) operated at a voltage of 15 kV.

The SEM micrographs were analyzed using a semi-automatic method of image analysis, explained elsewhere.²⁵ On average at least 300 diameters were measured per blend sample. The number average diameter (d_n) and the volume average diameter (d_v) were then calculated based on these measurements and all the necessary corrections²⁶ were applied.

5.2.7 Pore diameter measurement

The solvent extracted porous samples from the solvent gravimetry were used for measuring the surface area (S) of the specimen. A Flowsorb 2300 BET instrument was used to carry out these measurements. The pore diameter was calculated by assuming that the pores are cylindrical in shape, the total volume of the pores is equal to that of the extracted phase (V), and the total surface area (S) is that of the pore wall. The pore diameter (d) can then be calculated as,

$$d = 4V/S \dots\dots\dots (5.2)$$

Further details regarding this technique have been described by Li and Favis.²⁷

5.2.8 Matrix dissolution

For the complete matrix dissolution study, the samples from 5 EP/95 PP and 30 EP/70 PP irradiation crosslinked blends were boiled in pre-filtered xylene for about 30 to 45 min. The solution was then rapidly filtered at about 140°C using a 0.8 μm filter membrane. Additional hot xylene was filtered to assure the complete removal of the PP phase. For cocontinuous blend samples many more washes were given to assure the complete removal of the PP matrix. The sample was then washed with and transferred to cyclohexane. The sample was subsequently frozen and was freeze dried at -25 to -30°C.

For the partial matrix dissolution study, microtomed samples of the 5–20% EPDM/PP irradiated blends were immersed in hot xylene for about 2 seconds. This time period was found to be just enough for the partial dissolution of the PP matrix. The samples were rapidly removed from hot xylene and were placed in cold xylene, and were subsequently dried.

Subsequently, all samples were coated with the gold-palladium alloy and observed under the SEM.

5.3 RESULTS AND DISCUSSIONS

5.3.1 Rheology

Figures 5.1 (a) and (b) show the complex viscosity and the storage modulus as a function of shear rate for all the materials used in this study. The frequency of the rheometer is directly treated as the shear rate, since these materials are known to follow

the Cox-Merz relation.²⁸⁻³⁰ Figure 5.1 (a) illustrates that the PP homopolymer is significantly less viscous than both EPDM materials at a shear rate of 26 sec^{-1} . This value of the shear rate is determined for the mixing conditions in this study using an empirical calibration technique of Marquez et al.³¹ The EPDM in PP blends thus clearly demonstrate very high viscosity ratios of 11 and 17. Due to its low viscosity, the PP homopolymer exhibits a wide Newtonian plateau. On the other hand, EP 2 and EP 3 elastomers do not demonstrate a Newtonian plateau, but show a yield stress due to the higher molecular weights. All the materials exhibit shear thinning behavior. Thus at an average shear rate of melt mixing it can be seen that, EP 3 is the most viscous and most elastic of all the polymers and PP 1 is the least viscous and elastic polymer of all. Other important rheological ratios calculated at constant shear rate and at constant shear stress are reported in Table 5.2.

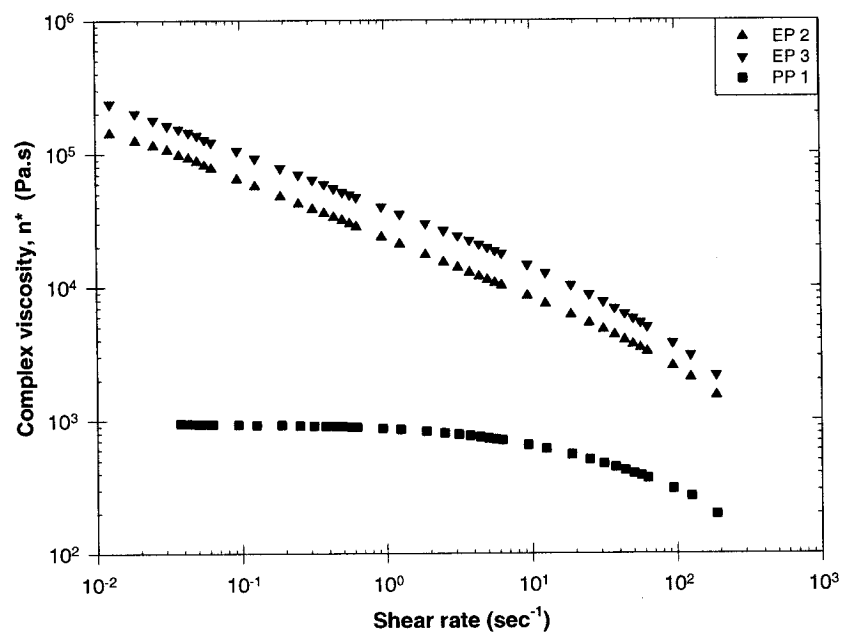


Figure 5.1 (a): Complex viscosity of the pure materials as a function of shear rate at 190°C

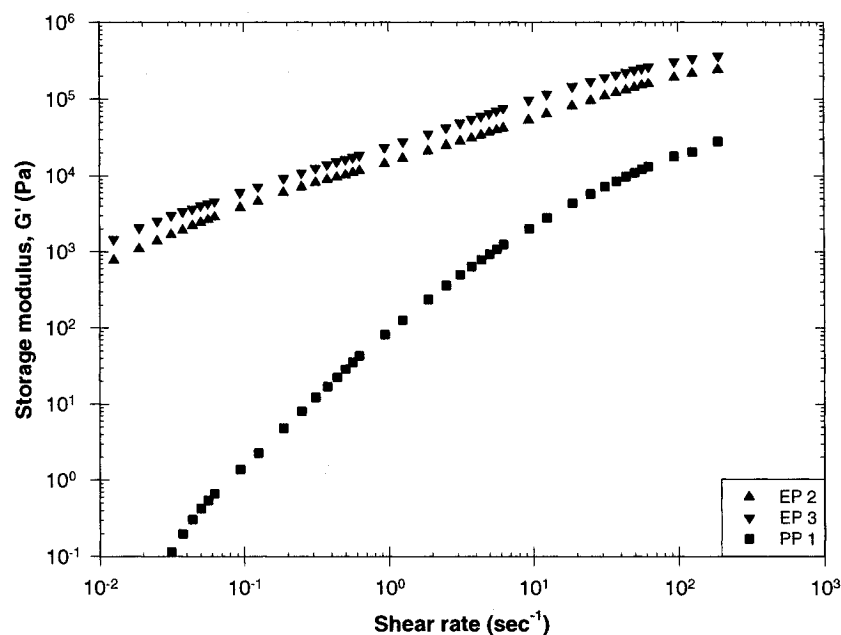


Figure 5.1 (b): Storage modulus of the pure materials as a function of shear rate at 190°C

5.3.2 Continuity development and cocontinuity

Figure 5.2 demonstrates the complete continuity development and cocontinuity diagram for high viscosity ratio EPDM/PP blends. The corrections for PP solubility in cyclohexane at room temperature and for EPDM solubility in boiling xylene after irradiation crosslinking have been applied.²⁰ A reference curve for the low to medium viscosity ratio systems from our previous publication²⁰ is also plotted in Figure 5.2 for comparison purposes.

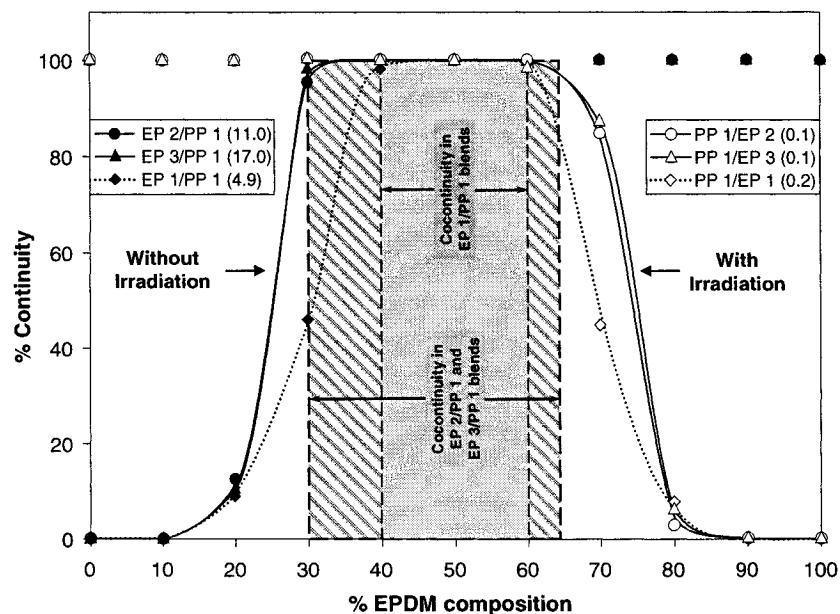


Figure 5.2: Complete continuity development and cocontinuity diagram for EPDM/PP blends system (corrected for PP solubility in cyclohexane at room temperature, and EPDM solubility in xylene)

Figure 5.2 clearly shows that the high viscosity ratio EPDM/PP blends studied in this work are demonstrating a significantly wider range of dual-phase continuity than the low viscosity ratio systems from the previous paper.²⁰ Co-continuity can be seen to extend from 30% to 65% EPDM concentration. The percolation and continuity development for the high viscosity ratio blends is also occurring at significantly lower compositions. Full continuity development for these blends is achieved over a narrower concentration range from 10-30% EPDM. In addition, an overall shift in the region of dual-phase continuity to lower concentrations is also apparent in Figure 5.2 as the curve shows a somewhat asymmetrical shape with respect to the 50% composition point.

A number of these features are highly surprising and are intuitively unexpected. Neither viscosity ratio-based nor elasticity ratio-based phase inversion models are able to explain this behavior since both of those models predict a symmetrical shift in the region of dual-phase continuity to either higher or lower EPDM concentrations respectively. What is observed here is a widening of the region of dual-phase continuity on both sides of the composition diagram. In another study,¹⁸ on the role of the interface on continuity development and cocontinuity it was found that the tendency to form elongated dispersed fibers had a very significant effect on widening the range of dual-phase continuity. Even that model is not respected here since the high viscosity ratio EPDM in PP blends would be expected to have a significantly lower tendency towards fiber formation. Clearly, another mechanism is responsible for this unusual behavior.

5.3.3 Microstructure of highly viscous EPDM in PP matrix

SEM micrographs after EPDM phase extraction with cyclohexane at various compositions are shown for EP 3 in PP 1 blends of viscosity ratio 17 in Figure 5.3. The micrograph (a) for 5 EP 3/95 PP 1 blend shows very large particles of several microns in diameter as well as very small particles of several hundred nanometers. Note also in Figure 5.3(a) the penetration of the large particle by a very small one in the lower left-hand corner. This combination of very large and very small particles is preserved in Figure 5.3(b), but becomes much less evident in 5.3(c) and 5.3(d).

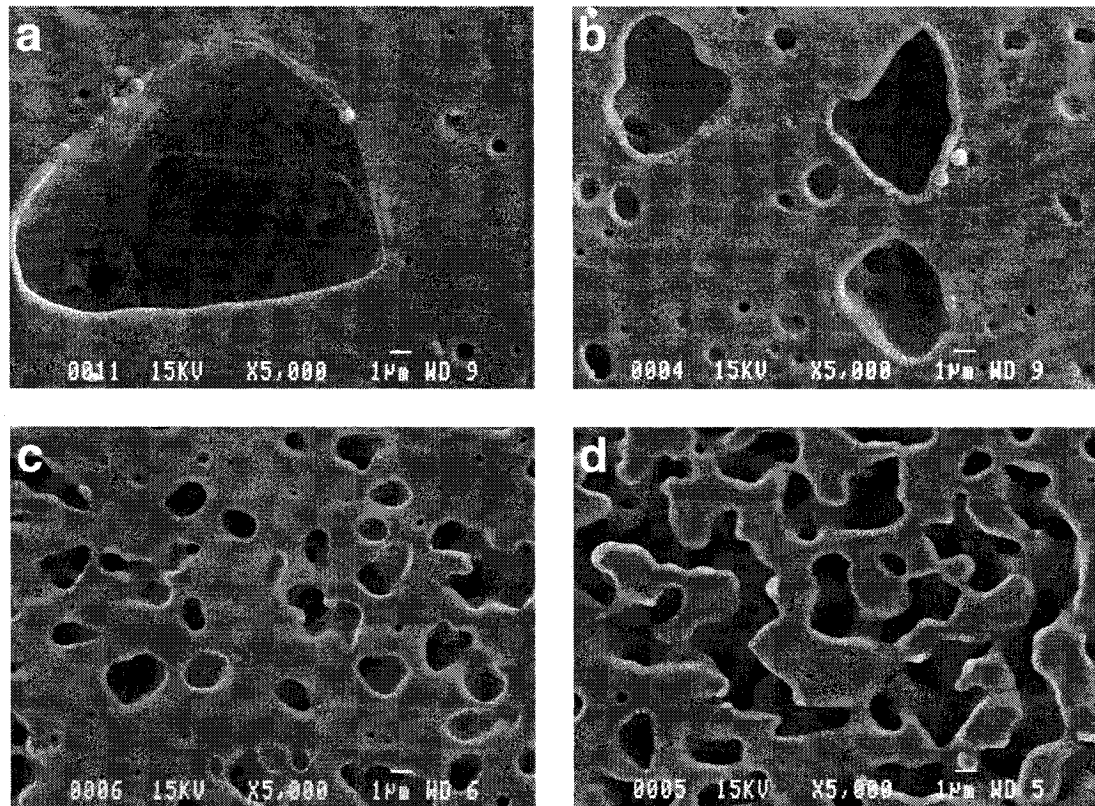


Figure 5.3: EPDM phase morphology development

SEM micrograph (a) 5 EP 3/95 PP 1, (b) 10 EP 3/90 PP 1, (c) 30 EP 3/70 PP 1, and (d) 50 EP 3/50 PP 1

The particle size was quantified by image analysis and the number average (d_n) and volume average (d_v) diameter values for various EPDM concentrations in PP are shown in Figures 5.4(a) and 5.4(b), respectively. Note that d_n is tracking the smallest particles in the system, while d_v tracks the largest ones. The dependence of d_n on EPDM composition for these high viscosity ratio blends shows a strong particle size/composition dependence typical to systems demonstrating significant coalescence.

Again, this is intuitively unexpected since these ultra-low interfacial tension systems would not be expected to demonstrate high rates of coalescence.

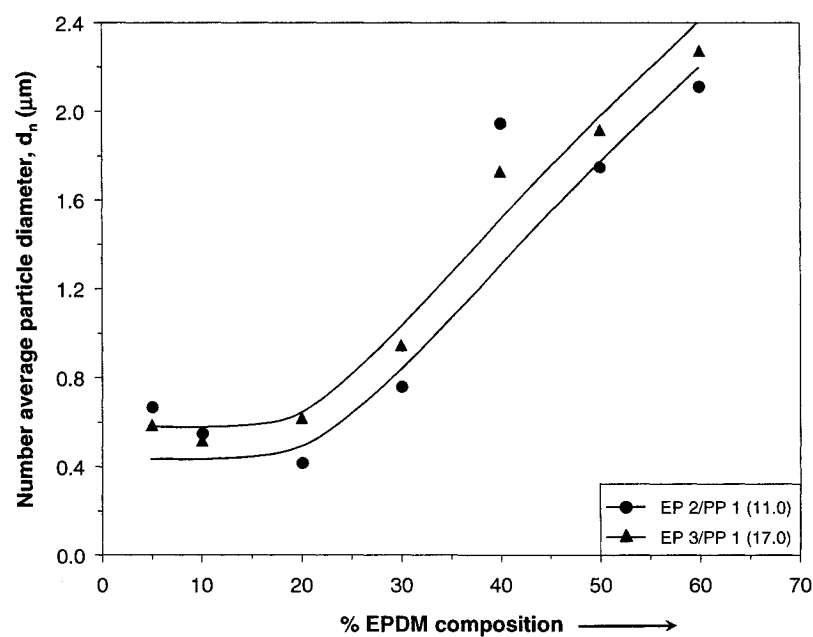


Figure 5.4 (a): Number average particle diameter as a function of EPDM composition in the blend

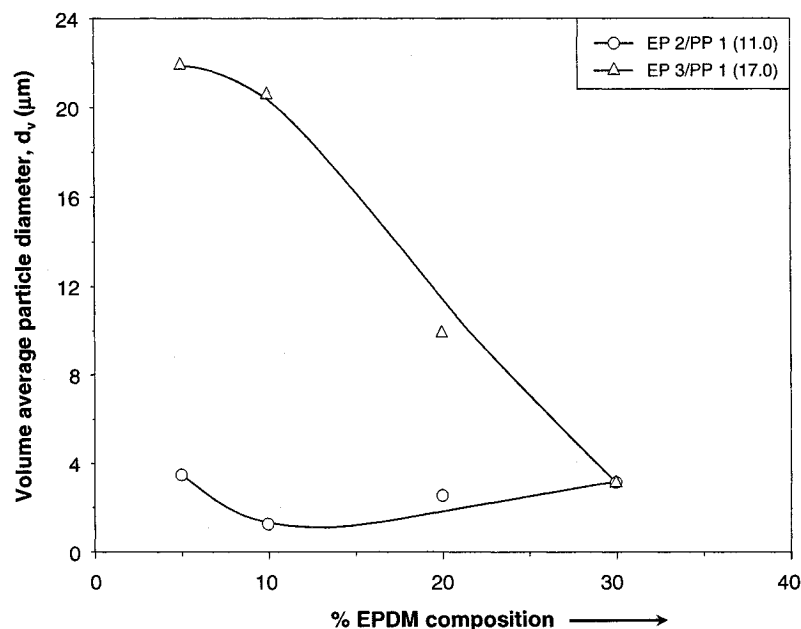


Figure 5.4 (b): Volume average particle diameter as a function of EPDM composition in the blend

5.3.3.1 Erosion phenomenon

The d_v values shown in Figure 5.4(b) illustrate that the d_v value for the 17 viscosity ratio system actually diminishes dramatically with composition. This tendency is a strong indication of the presence of incomplete erosion phenomena related to the breakdown of the EPDM particle. In Figure 5.4(b), the erosion process is almost complete for the blend of viscosity ratio of 11 and, in that case, the reduction of d_v is limited to only a small effect. Figure 5.5 shows the presence of very large particles in the 17 viscosity ratio blend. This figure plots the cumulative volume average diameter as a function of the successive addition of individual particle diameters of increasing value. The number of very large particles clearly decreases as the EPDM concentration

is increased. Additionally, the figure shows the presence of a massive number of very small particles (less than a micron) as compared to the relatively few large particles.

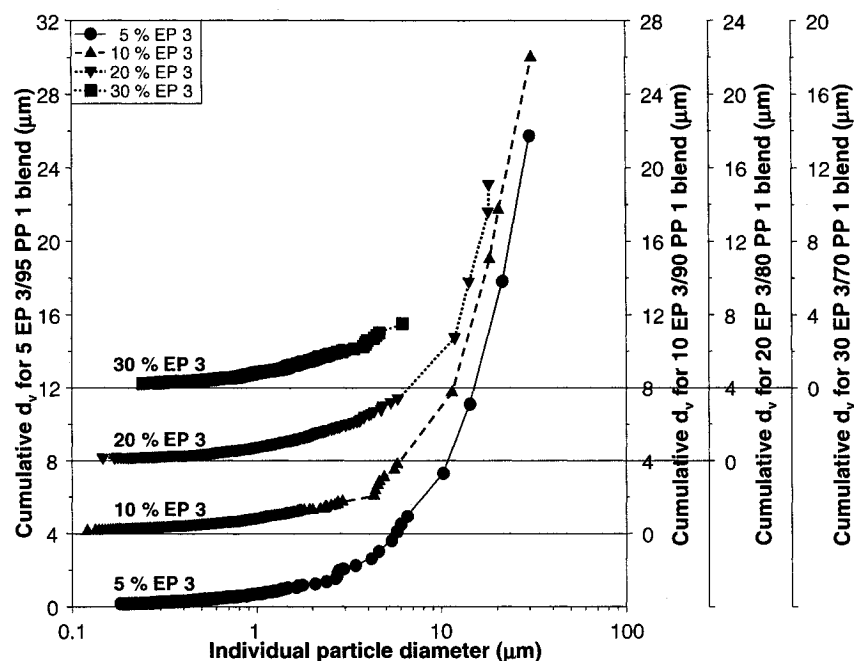
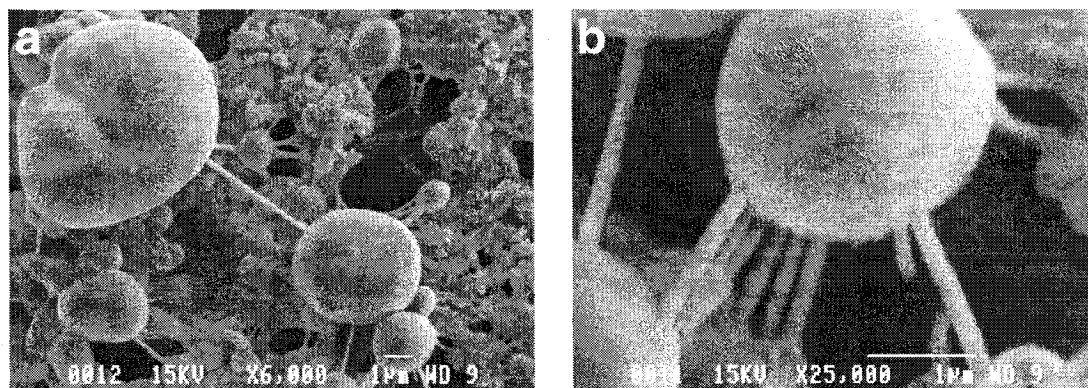


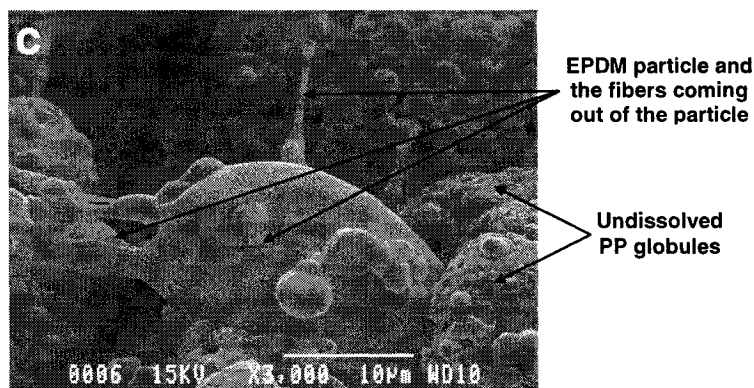
Figure 5.5: Volume average diameter as a function of individual particle diameter at different EPDM compositions in the EP 3/PP 1 blends

It is well known that multiphase polymer blends undergo complex deformation and disintegration processes during melt mixing. The time scale for these phenomena is typically so small, however, that they have defied study in the mixing environment itself and typical blend morphology studies almost always examine the final steady-state morphology obtained after several minutes of mixing. In this work, however, it appears that blends possessing the combination of very low interfacial tension ($\approx 0.3 \text{ mN/m}$) and very high viscosity ratio (17) provide a unique opportunity to examine erosion phenomena persisting over longer time scales in a melt mixing environment.

In order to better understand the nature of the erosion phenomena for these blends, the 17 viscosity ratio EPDM in PP blend was subjected to a matrix dissolution experiment. All the matrix PP was dissolved by immersing the sample in hot xylene and the remaining dispersed phase was collected on a filter membrane and was subsequently examined on the scanning electron microscope. Figures 5.6(a) to (c) give a good indication of the mechanism of erosion in these blends. Throughout the sample large particles are observed to be interconnected via 100-200 nm diameter fibers. Moreover, particles partially coalesced at the interface are also evident. It appears that when EPDM particles collide during mixing they experience a local merging phenomenon and then recoil with a drawn stable fiber between them. These data underline the presence of a collision-dependent mechanism of polymer erosion.



Complete matrix dissolution



Partial matrix dissolution

Figure 5.6: SEM micrographs of the high viscosity dispersed EPDM phase after PP matrix dissolution

Micrographs (a) and (b) on complete matrix dissolution of 5 EP 3/95 PP 1 blend, and micrograph (c) on partial matrix dissolution of 20 EP 3/80 PP 1 blend

These results further suggest that the cocontinuous structure in these high viscosity ratio blends is a network of partially coalesced particles and particles interconnected by fibers. The micrographs obtained on completely dissolving the PP

matrix of a cocontinuous 30 EP 3/70 PP 1 blend are presented in Figure 5.7. Indeed, a highly irregular, intact cocontinuous network of partially coalesced particles is evident. Whenever the particles are quite far from each other, fine fibers can be seen connecting the particles. This unique network of partially coalesced particles and particles interconnected by fibers, thus, also explains the early percolation thresholds, rapid continuity development, the shift in continuity development, and the wide range of co-continuity observed for these high viscosity ratio blends as compared to low viscosity ratio blends (see Figure 5.2).

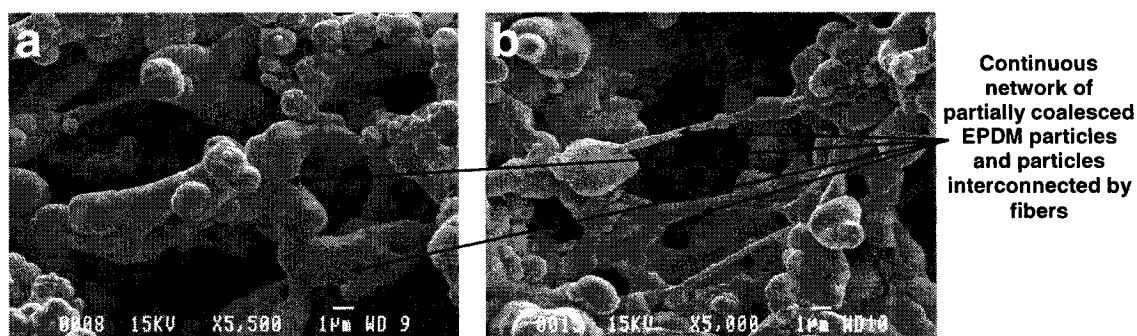


Figure 5.7: SEM micrographs of the continuous network of high viscosity EPDM phase obtained after complete matrix dissolution of the low viscosity PP matrix in 30 EP 3/70 PP 1 blend

In order to further confirm the presence of an erosion process, 5 EP 3/95 PP 1 and 30 EP 3/70 PP 1 blends were melt mixed for different time intervals in an internal mixer and the results obtained are presented in Figure 5.8. The plot clearly shows that the d_v of 5 EP 3/95 PP 1 blend substantially decreases and d_n increases slightly with the increase in mixing time, i.e. the big particles in the blend are slowly disappearing to yield smaller particles. These results reveal that the morphologies generated at low

compositions of EPDM in the blend after 8 min of mixing are not the steady state morphologies and that erosion continues even after 30 minutes of mixing.

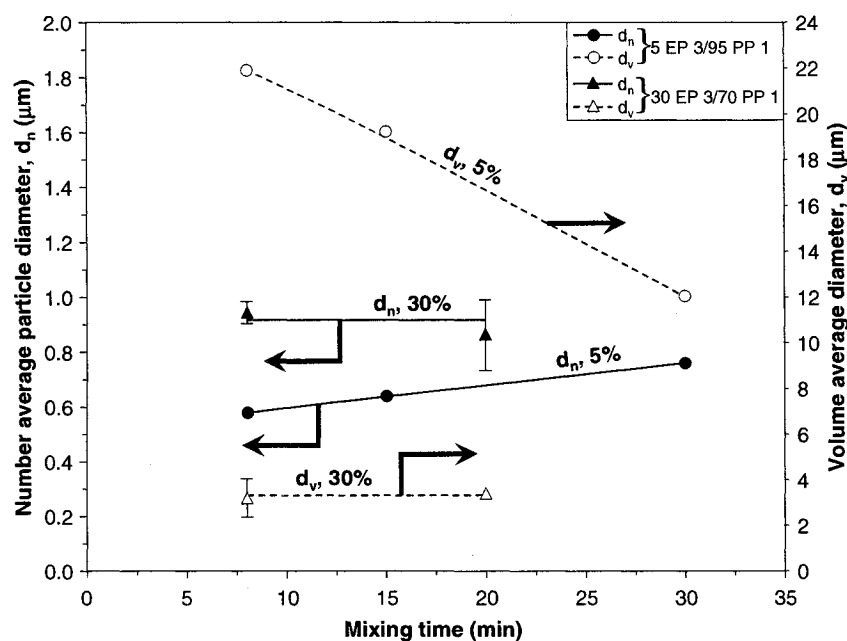


Figure 5.8: Erosion in high viscosity ratio EPDM/PP blends

On the other hand for 30 EP 3/70 PP 1 blend in Figure 5.8, it can be seen that the morphology has already reached a steady state value after 8 min of mixing. The d_n and d_v both remain constant and the blend remains co-continuous as confirmed by solvent gravimetry for the long mixing time. Thus, the slow surface erosion phenomenon is limited to only the lower dispersed phase content blends. The schematics of this process are given in Figure 5.9. A large particle is shown to erode slowly into nanometer diameter fibers. In the literature, Mighri et al.^{32,33} and Lin et al.³⁴ observed similar erosion phenomenon for a high viscosity ratio PC/PE blend system in pure shear flow. By direct observation using a specially designed transparent Couette

device, they observed the slow surface erosion of the high viscosity PC mother drop to give out thin ribbons, sheets and cylinders. They explain that in case of a highly viscous particle, the matrix shear stress is not sufficient to completely deform and break the particle. However, if the forces applied by the matrix on the surface of the droplet are more than a critical value,³⁴ then the local viscosity of the material at the surface decreases. At this point, the droplet can no longer sustain the material at its surface and starts slowly giving away this material, i.e. it starts eroding. In their work they also observed that the interfacial tension plays a much smaller role than elasticity in determining erosion behavior. The surface erosion of the high viscosity ratio EPDM/PP blends in the current study appears to take the form of stable nano-fibers. Unlike the PC/PE system, however, these fibers are extremely stable as a result of the ultra-low interfacial tension between the blend components and also due to the high viscosity of the EPDM phase which resists fiber breakup by capillary instabilities, as already shown in our earlier publication.²⁰

For the mother droplet of EPR in PP matrix with a viscosity ratio of about 10, Mighri et al.³³ observed another novel droplet breakup mechanism. In this other type of mechanism the droplet aligns itself and elongates perpendicular to the flow direction, i.e. in the vorticity direction due to the normal stresses developed inside the droplet. This causes the droplet to strangle in the direction of flow. In this process a waist is formed somewhere near midsection of the deformed droplet and the droplet ultimately breaks up when the ends of highly elongated droplets resolve into slightly different planes. At that point, the relative velocity difference between the particle ends forces it

to be torn apart. The authors observed that the newly formed droplets remain connected to each other by a fine stable fiber. Lin et al.³⁴ observed a similar breakup mechanism for the daughter droplets of about 5 – 20 μm in diameter, formed by the surface erosion of the PC mother droplet. Those structures are conceptually similar to the droplets interconnected by fibers shown in Figure 5.6 of this work.

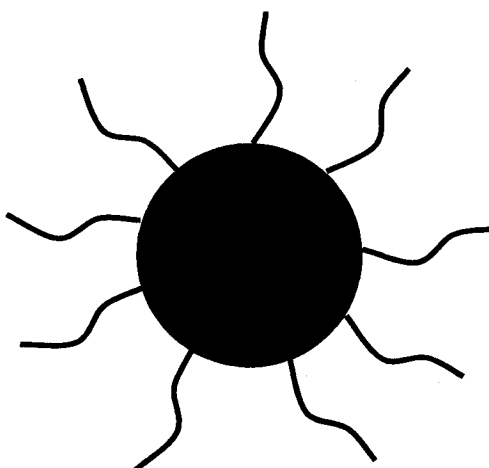


Figure 5.9: Schematics of single high viscosity particle surface erosion process – A big particle eroding to give out nanometer diameter fibers

These mechanisms still do not account for the dramatic decrease in the volume average diameter with composition, and the attainment of an equilibrium morphology, i.e. the particle size and cocontinuity, for 30 EP 3/70 PP 1 blend observed in Figure 5.8. Furthermore, during mixing the nano-fibers interconnecting the particles can break or the partially coalesced particles may separate because of the mixing dynamics. Thus, for a structure to remain cocontinuous at any point of mixing would require the continuous regeneration of the structures seen in Figure 5.6 and 5.7.

To account for these results, here we propose new ‘particle collision-coalescence-separation’ type erosion shown schematically in Figure 5.10. In this type of erosion, first two particles approach each other and the matrix material in-between the particles is drained (schematic 5.10(a)). Ultimately, the particles collide. The collision between these two high viscosity particles results in a partial penetration or coalescence at the interface because of the large volume of interaction in between the particles, as schematically shown in Figure 5.10(b). These two steps are the basic steps of a coalescence process³⁵ in any polymer blend system. However, the high viscosity, high elasticity, and ultra-low interfacial tension between the blend components prevent the complete coalescence of the particles into a single particle. As the particles then rebound, (schematic 5.10(c)), a nano-fiber(s) is generated in between the particles because of the partial coalescence at the interface. By the principle of conservation of volume, the generation of nanofiber(s) actually induces a decrease in the particle sizes, i.e. the particles erode. The rate of erosion by the proposed mechanism can be expected to dramatically increase as the increase in the composition incorporates more and more particles and hence more collisions. Moreover, the mechanism facilitates regeneration of nano-fibers between the particles on breakup under dynamic mixing conditions. Thus, the proposed mechanism explains the decrease in volume average diameter with composition (Figure 5.4(b) and 5.5) and the formation and maintenance of co-continuous morphologies (Figure 5.8). This study thus demonstrates a significant contribution of the particle concentration in the erosion process and its effect on the continuity development in high viscosity ratio blends of ultra-low interfacial tension.

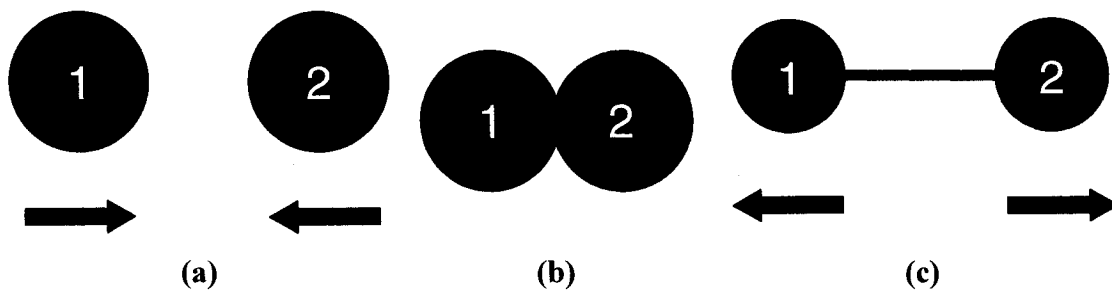


Figure 5.10: Schematics of coalescence based conceptual particle collision-coalescence-separation type erosion of high viscosity EPDM phase

(a) High viscosity particles approaching each other, (b) Only partial coalescence at the interface because of high volume of interaction and high viscosity of the particles, (c) Separation and stable fiber formation in-between the particles

5.4 CONCLUSIONS

This work studies the morphology development, with a particular attention to continuity development and cocontinuity, in high viscosity ratio blends of ultra-low interfacial tension. At low blend compositions, the high viscosity EPDM phase is found to coexist in a variety of unusual morphological structures, which includes: stable isolated nanometer diameter fibers, very large particles, partially coalesced particles, and numerous particles interconnected by nano-fibers. This unusual combination of morphologies leads the blend to a novel cocontinuous structure of partially coalesced particles and particles interconnected by fibers. Consequently, the high viscosity ratio blends demonstrate early percolation thresholds, rapid continuity development, and attain cocontinuity at lower than expected compositions of the minor phase.

It is found that the varieties of morphologies generated are the result of a slow surface erosion process of the high viscosity EPDM phase. For higher EPDM composition blends, we propose a particle collision-coalescence-separation type of erosion that dramatically increases the erosion rate and allow the blends to establish a steady-state morphology.

Acknowledgements

The authors would like to thank Mr. Mike Gallagher of Bayer Inc. for supplying the EPDM; Mr. Denis Therrien of Basell Polyolefins Inc. for supplying and measuring the molecular weights of the PP; Prof. Monique Lacroix, of INRS-Institut Armand-Frappier, Université du Québec, for irradiating the blends. The authors would also like to thank the whole "Groupe de mélanges polymères" of the École Polytechnique de Montréal and especially Xavier Roy for his kind expertise in freeze drying.

REFERENCES AND NOTES

1. Willemse, R.C.; Speijer, A.; Langeraar, A.E.; Posthuma de Boer A. *Polymer* 1999, 40, 6645.
2. Veenstra, H.; Verkooijen, P.C.J.; Van Lent, B.J.J.; Van Dam, J.; Posthuma de Boer, A.; Nijhof, A.P.H.J. *Polymer* 2000, 41, 1817.
3. Gubbels, F.; Jerome, R.; Teyssie, Ph.; Vanlathem, E.; Deltour, R.; Calderone, A.; Parente, V.; Bredas, J.L. *Macromolecules* 1994, 27, 1972.
4. Jacoby, M. *Chem Eng News* 2001, 79, 30.

5. Subramanian, P.M. (E.I. Du Pont de Nemours & Co.). U.S. Patent 4,410,482, October 18, 1983.
6. Favis, B.D.; Sarazin, P.; Li, J.; Zhenhua, Y. (Corporation de École Polytechnique de Montréal). PCT Int Appl WO 2004087797 A1, October 14, 2004.
7. Avgeropoulos, G.N.; Weissert, F.C.; Biddison, P.H.; Bohm, G.G.A. Rubber Chem Technol 1976, 49, 93.
8. Paul, D.R.; Barlow, J.W. J Macromol Sci, Rev Macromol Chem 1980, C18, 109.
9. Jordhamo, G.M.; Manson, J.A.; Sperling, L.H. Polym Eng Sci 1986, 26, 517.
10. Miles, I.S.; Zurek, A. Polym Eng Sci 1988, 28, 796.
11. Lyngaae-Jørgensen, J.; Utracki, L.A. Makromol Chem Macromol Symp 1991, 48-49, 189.
12. Metelkin, V.I.; Blekht, V.S. Kolloid Zh 1984, 46, 476.
13. Utracki, L.A. J Rheol 1991, 35, 1615-1637.
14. Willemse, R.C.; Posthuma de Boer, A.; Van Dam, J.; Gotsis, A.D. Polymer 1998, 39, 5879.
15. Steinmann, S.; Gronski, W.; Friedrich, C. Polymer 2002, 43, 4467.
16. Bourry, D.; Favis, B.D. J Polym Sci Part B: Polym Phys 1998, 36, 1889.
17. Steinmann, S.; Gronski, W.; Friedrich, C. Polymer 2001, 42, 6619.
18. Li, J.; Ma, P.L.; Favis, B.D. Macromolecules 2002, 35, 2005.
19. Veenstra, H.; Van Lent, B.J.J.; Van Dam, J.; Posthuma de Boer, A. Polymer 1999, 40, 6661.

20. Bhadane, P.; Favis, B.D.; Champagne, M.; Huneault, M.; Tofan, F. Submitted to Polymer.
21. Marin, N.; Favis, B.D. Polymer 2002, 43, 4723.
22. Zaharescu, T.; Setnescu, R.; Jipa, S.; Setnescu, T. J Appl Polym Sci 2000, 77, 982.
23. Kammel, G.; Wiedenmann, R. Siemens Forsch - u Entwickl 1976, 5, 157.
24. Vroomen, G.L.M.; Visser, G.W.; Gehring, J. Rubber World 1991, 205, 23.
25. Favis, B.D.; Chalifoux, J.P. Polym Eng Sci 1987, 27, 1591.
26. Saltikov, S.A. In Proceedings of the 2nd International Congress for Stereology; Elias, H., Eds.; Helias: New York, 1967.
27. Li, J.; Favis, B.D. Polymer 2001, 42, 5047.
28. Cox, W.P.; Merz, E.H. J Polym Sci 1958, 28, 619.
29. Chung, O.; Coran, A.Y. Rubber Chem Technol 1997, 70, 781.
30. Chung, O.; Coran, A.Y.; White, J.L. ANTEC 1997 Proceedings of the 55th Annual Technical Conference, Society of Plastics Engineers, 1997, 55, 3455.
31. Marquez, A.; Quijano, J.; Gaulin, M. Polym Eng Sci 1996, 36, 2556.
32. Mighri, F.; Huneault, M. J Rheol 2001, 45, 783.
33. Mighri, F.; Huneault, M. Can J Chem Eng 2002, 80, 1028.
34. Lin, B.; Sundararaj, U.; Mighri, F.; Huneault, M. Polym Eng Sci 2003, 43, 891.
35. Chesters, A.K. Trans IchemE 1991, 69, 259.

CHAPTER 6

THE INFLUENCE OF DYNAMIC VULCANIZATION ON CO-CONTINUOUS MORPHOLOGY IN EPDM/PP BLENDS

The diene monomer in EPDM offers an opportunity to crosslink an elastomer phase in the blend. Extensive studies in chapter 4 and 5 provide comprehensive knowledge of morphology, continuity development and cocontinuity in ethylene-propylene-diene terpolymer/polypropylene (EPDM/PP) blends before crosslinking and, thus, offer highly characterized cocontinuous structures. The objective of this paper is to apply recently developed focused ion beam etching of the sample surface followed by tapping mode atomic force microscopy (FIB/TMAFM) approach to thermoplastic vulcanizates and thereby study the influence of dynamic vulcanization on the phase continuity and cocontinuity in EPDM/PP blends.

Blends having viscosity ratios of 0.7 and 5.0 are dynamically crosslinked to particular levels. The continuity of non-crosslinked EPDM phase is determined using solvent gravimetry. The effect of crosslinking on pore diameter of non-crosslinked EPDM phase is determined by the BET nitrogen adsorption technique. The results strongly indicate that crosslinking dramatically modifies the original cocontinuous microstructure (α -network) and leads to a much finer network of crosslinked elastomer (β -network). During the transition cocontinuous non-crosslinked phase is found to

maintain its cocontinuity. Moreover, the results indicate that the crosslinking proceeds initially at the outer envelope of the EPDM phase and works its way towards the center. Based on high resolution micrographs and other results, schematics of morphology development in cocontinuous EPDM/PP blends with dynamic crosslinking are presented.

This article is submitted to the journal : “*AIChE Journal*”

The Influence of Dynamic Vulcanization on Co-continuous Morphology in EPDM/PP Blends

Prashant Bhadane, Nick Virgilio, and Basil D. Favis

CREPEC, Dept. of Chemical Engineering, École Polytechnique, Montréal, Québec,
H3C 3A7 Canada

Michel Champagne and Michel Huneault

Industrial Materials Institute, National Research Council of Canada, Boucherville,
Québec, J4B 6Y4 Canada

Florin Tofan

Lavergne Group, Montréal, Québec, H1J 1C8 Canada

Abstract

This study examines the effect of dynamic crosslinking on the cocontinuous morphology in ethylene-propylene-diene terpolymer (EPDM)/polypropylene (PP) blends using a novel technique of morphology investigation involving focused ion beam (FIB) etching of the sample surface followed by topological investigation of the sample surface using tapping mode atomic force microscopy (TMAFM). The FIB ion etching rates of EPDM and PP are distinctly different and these differences create a significant topological contrast between the phases when subsequently analyzed by atomic force microscopy. These differences allow for the high resolution observation of dispersed EPDM and phases as small as 100 nanometers are clearly identified. Since it is shown

Correspondence concerning this article should be addressed to B.D. Favis at basil.favis@polymtl.ca.

that the etching rates of non-crosslinked and crosslinked EPDM are similar, it was necessary to selectively remove the non-crosslinked EPDM phase by solvent dissolution. This novel combination of techniques then allows for the clear distinction of polypropylene as well as non-crosslinked and crosslinked EPDM phases in the blend. The high resolution micrographs together with the continuity data, surprisingly, indicate that a non-crosslinked co-continuous EPDM phase (α -network) transits to a much finer network of crosslinked EPDM (β -network) after crosslinking. It is suggested that this β -network is produced as a result of the viscosity mismatch between the non-crosslinked and crosslinked EPDM melt occurring at the outer envelope of the α -network during crosslinking. As the crosslinked material pulls away from the non-crosslinked material under dynamic melt mixing conditions, it creates a smearing effect. It is shown that the initial α -network maintains its continuity and demonstrates a diminished pore diameter as crosslinking proceeds. Furthermore, when the non-crosslinked material is extracted no crosslinked phase is found to be present in the extract. These results strongly indicate that crosslinking dramatically modifies the co-continuous microstructure and that the crosslinking proceeds initially at the outer envelope of the EPDM phase and works its way towards the center.

Keywords: Polymer blends, Co-continuous morphology, Dynamic vulcanization, Thermoplastic vulcanizates, FIB/TMAFM

6.1 Introduction

Despite the major commercial significance of vulcanized ethylene-propylene-diene terpolymer (EPDM)/polypropylene (PP) blends, many fundamental questions related to the influence of crosslinking on the microstructure of these blends have remained unanswered. This is due in large part to the tremendous challenge of differentiating the phases in such a blend system. The very similar chemical nature of EPDM to PP combined with the ultra-low interfacial tension of the blend make it arguably one of the most difficult polymer pairs for morphology characterization in the entire polymer blend literature. Classical techniques such as the selective staining of EPDM by osmium or ruthenium tetroxide with subsequent characterization with Transmission electron microscope (TEM) or Scanning electron microscope (SEM) do not provide effective contrast between the various phases of the thermoplastic vulcanizate. (Abdou-Sabet et al., 1991; Galuska et al., 1997; Chung et al., 2000; Nysten et al., 1999)

More recently, a number of authors have applied Atomic force microscopy (AFM) in various operating modes such as contact (Nysten et al., 1995; Trifonova et al., 1999; Tanem et al., 2003), lateral (friction) (Nysten et al., 1995), tapping (Chung et al., 2001; Tanem et al., 2003; Yerina et al., 2003), and force modulation (Galuska et al., 1997; Nysten et al., 1995, 1999; Ellul et al., 2004) in order to characterize these complex morphologies. For non-crosslinked blends, they were not only able to differentiate between the domains of EPDM and PP but frequently revealed the

complex structure of amorphous and crystalline regions in the elastomer itself. The technique was also shown to be successful in identifying the different fillers, compatibilizers, and the qualitative crosslink density distribution in the blend. Because of the soft EPDM phase and the hard PP phase, contact, lateral (friction) and force modulation modes were found to produce better results than the tapping mode (Galuska et al., 1997; Ellul et al., 2004). Nevertheless, these micrographs still lack quality and do not present convincingly sufficient contrast between non-crosslinked and crosslinked rubber phases in the blend. Further improvement in contrast is necessary in order to understand the mechanism of morphology development in TPVs, as well as the effect of dynamic vulcanization on continuous and co-continuous morphologies.

Recently, Virgilio et al. (2005) demonstrated the applicability of focused ion beam (FIB) preparation followed by tapping mode atomic force microscopy (TMAFM) to analyze model interphase thicknesses in high density polyethylene/polystyrene/poly(methyl methacrylate) (HDPE/PS/PMMA) ternary polymer blends. Those systems were comprised of a polyethylene matrix and a dispersed phase composed of a PS shell and a PMMA core. FIB, most commonly, employs gallium ions with a typical energy of 30 keV. In sample preparation by such technique, a beam scans and gradually etches the selected sample surface due to collision of the ions with the material. It was shown in that work that the three polymer components have different ion beam etching rates, which creates a topological contrast between the phases of the blends when viewed by TMAFM. The contrast levels obtained were so high that this approach allowed for the

estimation of PS interphase thicknesses from 100 to 200 nm depending on the PS/PMMA composition ratio.

A co-continuous blend morphology is one in which neither of the blend phases can be defined as a matrix or the dispersed phase. It forms highly interconnected and intertwining structures and both the blend phases remain fully continuous throughout the blend. Our two previous papers (Bhadane et al., submitted to Polymer and J. Polym. Sci. Part B: Polym. Phys.) examined the detailed morphology, continuity development and cocontinuity in non-crosslinked EPDM/PP blends.

The objective of this work is to apply the FIB/TMAFM approach to thermoplastic vulcanizates and thereby study the effect of dynamic vulcanization on the phase continuity and cocontinuity in EPDM/PP blends.

6.2 Experimental Procedures

More extensive details on materials and various experimental techniques are explained in our earlier publication (Bhadane et al., submitted to Polymer) and should be referred to accordingly.

6.2.1 Materials

In this study, one EPDM and two PP homopolymer with significantly different viscosities were used. The EPDM grade contains ethylidene norbornene (ENB) as the diene. For chemical crosslinking of the EPDM, bromomethylated alkyl phenol-formaldehyde heat reactive resin from Schenectady International Inc., was used in

conjunction with zinc oxide (ZnO) as a hydrogen halide scavenger. Some of the other characteristics of the materials are summarized in Table 6.1.

Table 6.1: Characteristic properties of the materials

Polymer	Supplier	Given name	Molecular weights x 10 ³		Ethylene content (%)	ENB content (%)
			M _n	M _w		
PP	Basell	PP 1	89	288	-	-
PP	Basell	PP 2	166	773	-	-
EPDM	Bayer	EP 1	71.2	141.9	62	4.0

6.2.2 Rheological characterization

The rheological characterization was carried out using a Bohlin constant stress rheometer (CSM) in the dynamic mode. The experiments were performed in parallel plate geometry of 25 mm diameter, at 190°C and under a nitrogen atmosphere. The frequency sweep tests were performed in an experimental window permitted by the time and stress sweep test. More details are given in an earlier publication (Bhadane et al., submitted to Polymer).

6.2.3 Melt blending

PP, EPDM and antioxidant were first dry blended and then fed simultaneously into the mixing chamber. The polymers were melt blended using a Haake Rheomix 600 batch mixer with a Haake system 90 drive. The internal mixer was equipped with a 69 cm³ chamber with roller-type rotors and the blend was mixed for 8 minutes at 100 rpm,

190°C, and under a nitrogen blanket. The materials were weighed accurately such that the mixing chamber was filled to approximately 70% of its total volume.

After 8 minutes of mixing the master batch, a mixture of 50 parts EPDM/50 parts curing resin, was added to achieve the desired degree of gel content. This quantity comprises only 0.5 to 7.0% of the final volume of the blend. At 9 minutes of mixing, 5 parts of ZnO (based on the rubber content (phr)), was added to the mixture and the mixing was continued thereafter for 4 more minutes. After mixing, the melt was taken out of the mixing chamber very gently, but rapidly, and was quenched immediately in cold water to freeze-in the morphology generated during mixing.

Table 6.2: Rheological property ratios at constant shear rate and constant shear stress

Sr no	Blend components		Blend name	Torque ratio	At const. shear rate		Matrix shear stress (kPa)	At const. shear stress	
	Dispersed phase	Matrix			p^a	ψ^b		p^a	ψ^b
1	EP 1	PP 2	EP 1/PP 2	0.7	0.7	0.5	90.9	0.5	0.7
2	EP 1	PP 1	EP 1/PP 1	4.0	5.0	6.5	11.7	12.0	1.0
3	PP 2	EP 1	PP 2/EP 1	1.4	1.4	2.0	69.4	2.5	1.5
4	PP 1	EP 1	PP 1/EP 1	0.3	0.2	0.2	69.4	-	1.0 ^c

^a Viscosity ratio

^b Elasticity ratio

^c by extrapolation of the data

P.S. All the rheological properties are determined at an average shear rate in internal mixer of 27 sec⁻¹.

In total, two different viscosity ratio blends, EP 1/PP 2 and EP 1/PP 1, from 30 to 70% EPDM content (in steps of 10 vol.%) were crosslinked to about 50 and 100% gel content. Using an empirical calibration technique developed by Marquez et al.

(1996) the shear rate for each material in the mixing chamber was determined. The average shear rate for the blend is reported in Table 6.2, along with other important rheological property ratios estimated at the average shear rate and average shear stress of the blend.

6.2.4 Determination of gel content

At least two samples weighing less than 1 g were cut directly from the blend. The sample was then boiled in 100 mL of pre-filtered xylene for 45 to 60 minutes. The solution was then rapidly filtered at 140°C through a 0.8 µm membrane. An additional hot xylene wash was carried out to assure the complete removal of the PP and non-crosslinked EPDM phase. The weight of the filter membrane before, and after filtration and drying was noted. The gel content is determined using the following formula,

$$\% \text{ Gel content} = \left(\frac{\text{Wt. of the sample after extraction}}{\text{Wt. of crosslinkable material in the sample}} \right) \times 100 \dots\dots\dots (6.1)$$

6.2.5 Solvent extraction and gravimetry

The samples used for EPDM continuity measurement were extracted using cyclohexane at room temperature. The weight of the samples before extraction and after extraction and complete drying were noted. The complete phase removal was assured by comparing the sample weight after each solvent wash.

The wash solution was filtered using a membrane. The weight of the membrane before filtration and after complete drying was measured to determine the amount of crosslinked EPDM phase present in the continuous part of non-crosslinked EPDM.

The continuity of non-crosslinked EPDM phase was then measured using the following formula,

$$\% \text{ Continuity} = \left(\frac{\text{Sample wt. before extraction} - \text{Sample wt. after extraction}}{\text{Total wt. of EPDM in the sample}} \right) \times 100 \dots (6.2)$$

The values reported are the average of at least two measurements done in this way.

6.2.6 Focused ion beam (FIB) sample preparation and atomic force microscopy (AFM)

Specimens were first cryomicrotomed using a glass knife under liquid nitrogen to create a perfectly plane face using a Leica-Jung RM 2065, and 2165 equipped with a Leica LN 21 type cryochamber. The samples were then plasma-coated. The focused ion beam (FIB) surface preparation was then performed with a Hitachi FIB-2000A using a 30 keV Ga⁺ beam. The beam current was set at approximately 0.8 nA and the dwell time at 3 μs. A layer of approximately 3-4 μm thick was removed by milling parallel to the observed surface, on an 80 μm x 3-4 μm section, with a fluence rate of approximately 1.8 x 10¹⁵ ions/cm²/s.

The subsequent morphological observation of specimens by AFM was carried out with a scanning probe microscope Dimension 3100 with a Nanoscope IIIa controller from Veeco Instruments. Silicon tips, model RTESP from Veeco, with spring constants of 20-80 N/m and a resonant frequency of approximately 320 kHz were used. The tip was oscillated at approximately 98% of the resonant frequency and the engagement on

the surface was done at 95% of the free oscillation amplitude. Topological pictures were taken at 95% of the free oscillation amplitude. Specimens were fixed on a metallic support using silver glue or graphite tape. More details of the process are given by Virgilio et al. (2005).

6.2.7 BET nitrogen adsorption

The solvent extracted porous samples from the solvent gravimetry were used for measuring the interfacial area (S) of the specimen. A Flowsorb 2300 BET instrument was used to carry out these measurements. The pore diameter was calculated by assuming that the pores are: cylindrical in shape, the total volume of the pores is equal to that of the extracted phase (V), and the total surface area (S) is that of the pore wall. The pore diameter (d) can then be calculated as,

$$d = 4V/S \dots\dots\dots (6.3)$$

Li and Favis (2001) have described further details regarding this technique.

6.3 Results and Discussions

6.3.1 Rheology

Figures 6.1 (a) and (b) present the complex viscosity and the storage modulus as a function of shear rate, respectively, and it can be seen that all the materials are showing Newtonian plateau and shear thinning behavior. PP 2 is the most viscous and elastic, while PP 1 is the least viscous and elastic polymer of all. EP 1 possesses a viscosity and elasticity intermediate to that of PP 1 and PP 2 at an average shear rate of

mixing in the internal mixer of 27 sec^{-1} . The rheological property ratios such as viscosity ratio, torque ratio and elasticity ratio are evaluated at both constant shear rate and at constant shear stress and are shown in Table 6.2.

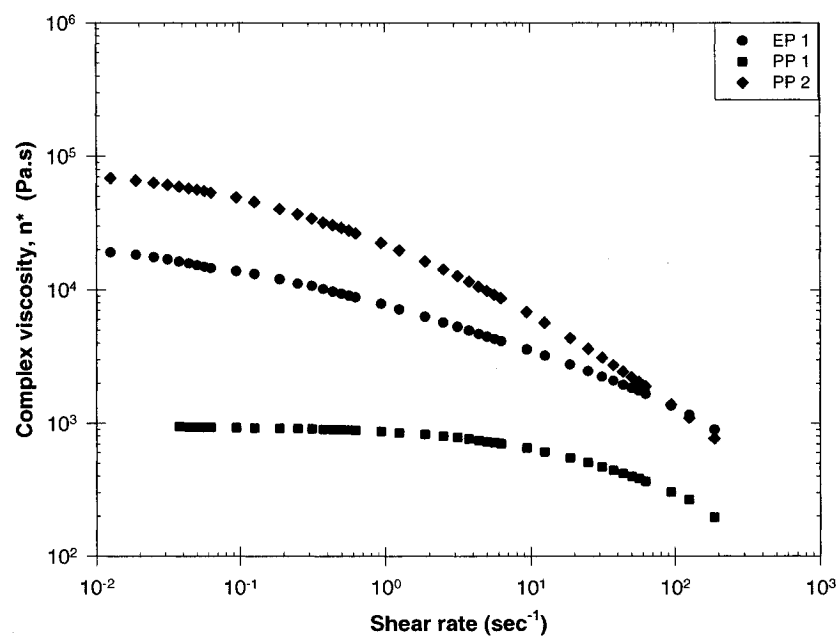


Figure 6.1 (a): Complex viscosity of the pure materials as a function of shear rate at 190°C

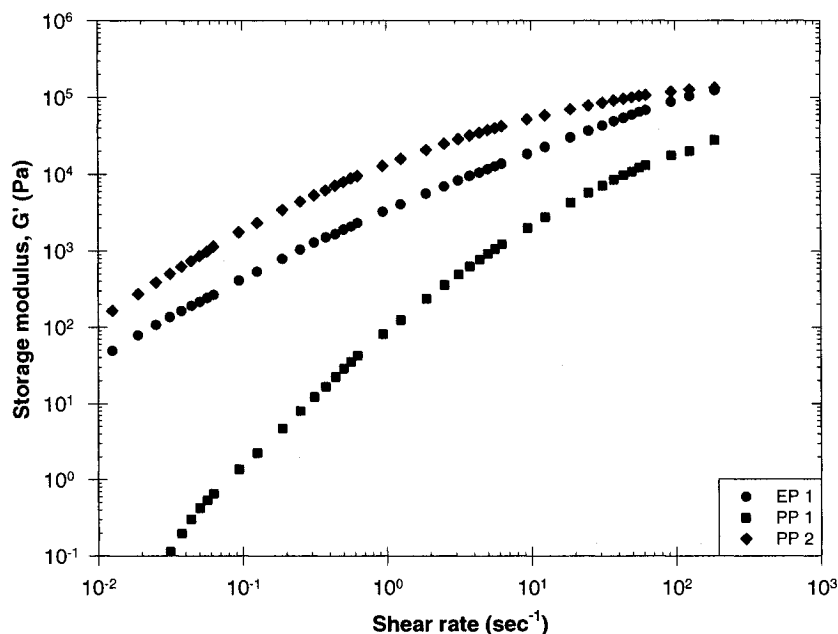


Figure 6.1 (b): Storage modulus of the pure materials as a function of shear rate at 190°C

6.3.2 Chemical crosslinking of EPDM

Figure 6.2 demonstrates the amount of gel content which can be achieved in a 50 EP 1/50 PP 1 blend as a function of crosslinking agent before and after applying corrections. The corrections arise because not all of the EPDM material in the blend is crosslinkable. The amount of non-crosslinkable material is determined as the combined EPDM fraction soluble in acetone and the fraction that remains insoluble in cyclohexane at room temperature. The acetone soluble material is considered as being non-crosslinkable, while the cyclohexane insoluble material is considered as being a polyolefin homopolymer (Abdou-Sabet et al., 1982). Thus for the EP 1 material 0.3% was found to be acetone soluble and about 3.2% was found to be cyclohexane insoluble.

Thus, an average total correction of about 3.5% was applied to determine the accurate gel content of the blends.

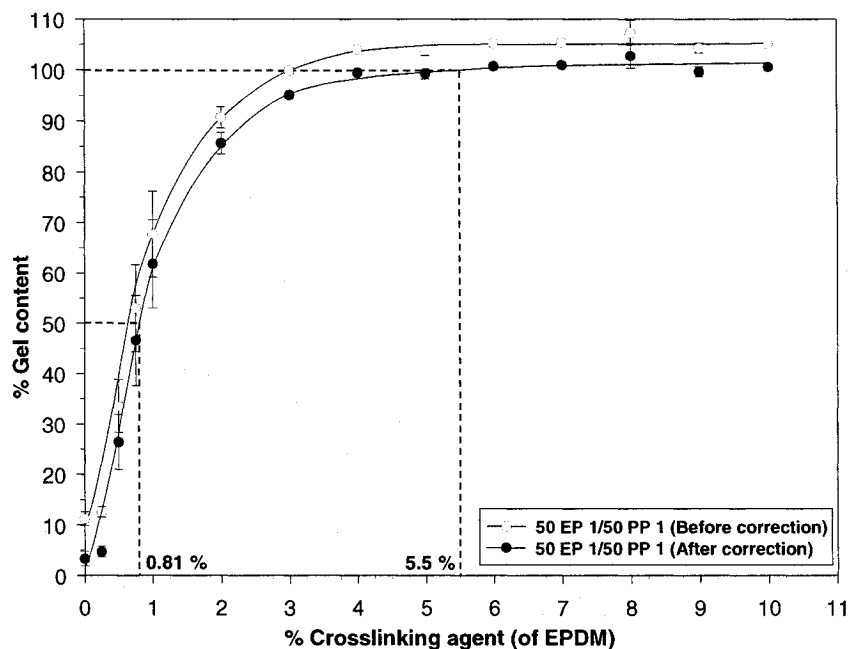


Figure 6.2: Gel content as a function of crosslinking agent

Figure 6.2 indicates that about 0.81%, of crosslinking agent based on the weight of EPDM is required to achieve 50% gel content. Four percent crosslinking agent is required to obtain 100% gel content. In this latter case, in order to assure complete crosslinking, a slight excess, about 5.5% of crosslinking agent was used.

Figure 6.3 shows the amount of gel content achieved for a range of blend compositions. Some difficulty is associated with the precise control of the degree of crosslinking in these systems particularly at lower compositions. This, in part, depends upon the amount of crosslinking agent able to migrate to the EPDM phase without being lost in the PP phase. This consideration clearly is more of a concern at low

compositions. At 50-70% EPDM, however, a good control of % gel content was achieved. During crosslinking, attention also has to be given for signs of degradation of the crosslinking agent. Due to its low viscosity, it has a tendency to migrate towards the wall of the mixer and degrade as a result of the high temperatures of the mixer wall.

Figure 6.3 clearly demonstrates that the vulcanization protocol used here was successful at producing both 50% and 100% crosslinked EPDM phases in two systems of different starting viscosity ratios (EP 1/PP 2 and EP 1/PP 1). Most of the discussion that will follow will concentrate on the 50 EPDM/50 PP blend composition and on how vulcanization influences its co-continuous morphology.

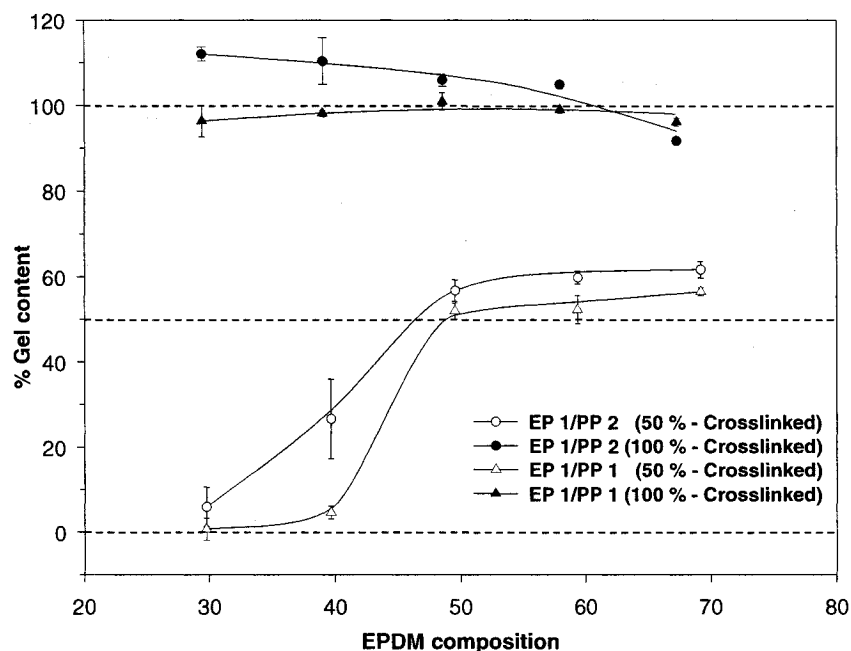


Figure 6.3: Gel content as a function of EPDM composition

6.3.3 Microstructure of crosslinked blends

Figures 6.4(a) and (b) show FIB micrographs after FIB ion etching, but prior to AFM observation. Two samples are shown, 6.4(a) is the surface of EP 1 melt mixed with 5% zinc oxide, 6.4(b) is that of 50 EP 1/50 PP 2 partially crosslinked ($\approx 50\%$) blend containing 5phr zinc oxide. Some white zinc oxide particles are clearly evident in both the micrographs and care was taken in subsequent AFM testing to analyze areas where no zinc oxide particles were present. FIB surface treatment can be seen to provide a very smooth surface for the case of pure EP in 6.4(a), while the treatment leads to a topographical contrast between the EP and PP phases in Figure 6.4(b). Nevertheless, this contrast is still not sufficient to clearly identify each phase and subsequent AFM analysis is necessary.

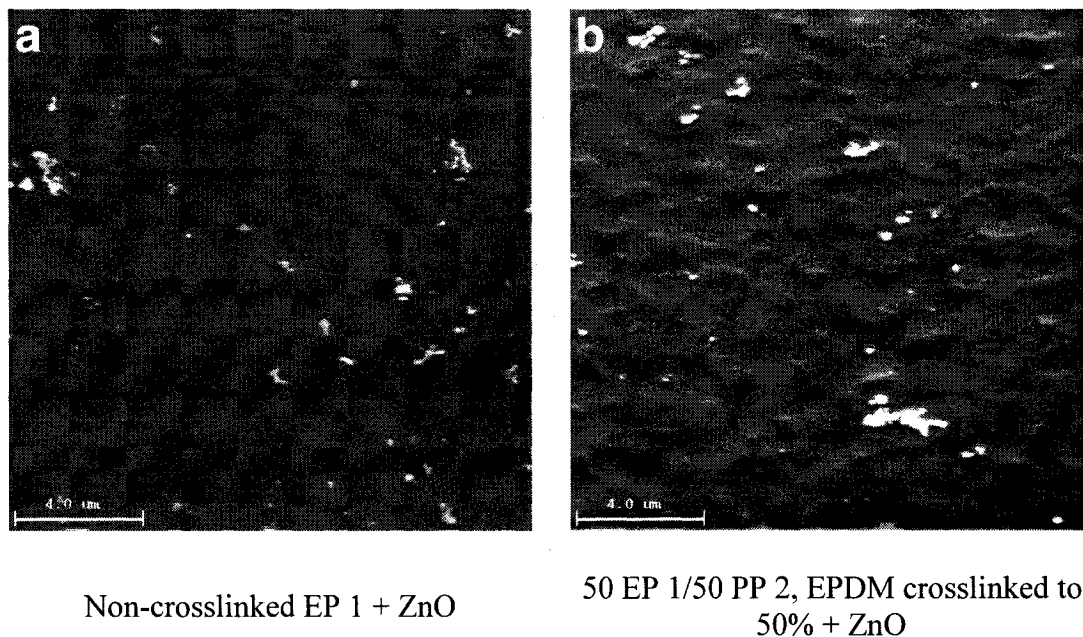


Figure 6.4: FIB micrographs

Figure 6.5 demonstrates the topographical surface image obtained by tapping mode AFM after FIB sample preparation for pure PP 2 (Figure 6.5(a)), 20 EP 1/80 PP 2 non-crosslinked blend (Figure 6.5(b)), and fully crosslinked 20 EP 1/80 PP2 blend (Figure 6.5(c)). As evident in the micrograph 6.5(a) the FIB sample preparation is yielding a very smooth surface for pure polypropylene, and the surface generated remains free from any artifacts. Below the micrograph, a typical surface profile for pure PP 2 demonstrates an average roughness value of less than 2 nm. Micrograph 6.5(b) demonstrates that FIB sample etching is generating an excellent topographical contrast between the PP and non-crosslinked EPDM phase. A very fine and uniform distribution of EP particles with phase sizes ranging from 100 to 500 nm is evident. The capability of combined FIB/AFM is clearly able to resolve the presence of very small EP domains. An earlier publication (Bhadane et al., submitted to Polymer) using SEM analysis demonstrated that these domains are actually ultra-fine stable fibers. There is a good correlation between the phase size observed here and in that previous paper.

The typical surface profile across a particle is shown below the micrograph. It is evident that EPDM is being etched more than PP and that a height difference of about 12 nm exists between the phases. Micrograph 6.5(c) obtained after fully crosslinking the EPDM phase of the blend shown in micrograph 6.5(b), demonstrates similar structures of finely distributed phases in the blend. Figure 6.5(c) also demonstrates the occasional observation of a zinc oxide particle, as expected. Close analysis of 6.5(c) clearly shows that the EPDM phase size has increased and that the phases have taken on a more smeared and distorted appearance. The morphological changes observed in the

crosslinked EPDM phase in Figure 6.5(c) are likely related to the dramatic effect of vulcanization on the viscosity of EPDM and this effect will be discussed in more detail later on in the paper. The surface height profile across a typical crosslinked phase demonstrates that the FIB preparation also etches the crosslinked EPDM more than the PP and a height difference of about 15 nm is observed. This height difference, however is very similar to that observed for non-crosslinked EPDM and indicates that FIB ion etching rates alone are not able to distinguish between crosslinked and non-crosslinked EPDM.

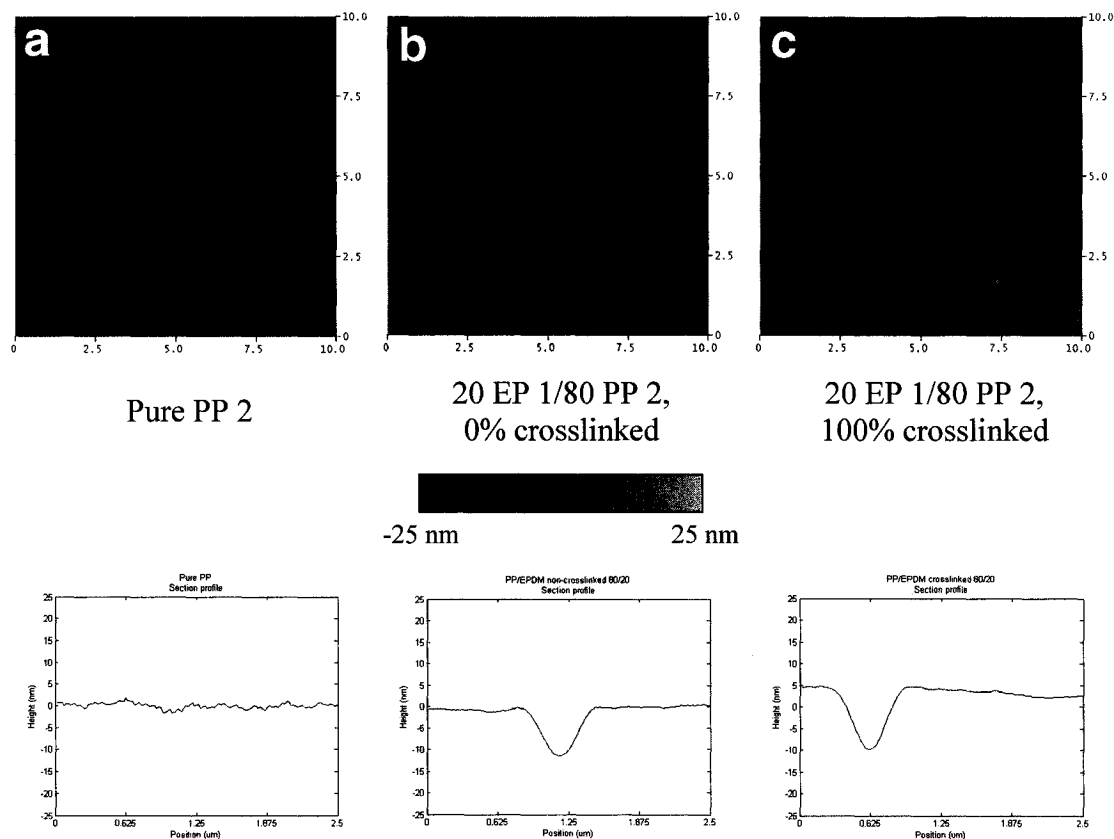


Figure 6.5: AFM micrographs after FIB sample preparation as well as topological height profiles of polypropylene, and non-crosslinked and crosslinked EPDM

Figure 6.6 presents the topological image of the 50 EP 1/50 PP 2 blend obtained by tapping mode AFM after FIB surface treatment. Micrograph 6.6(a) illustrates the structure of the non-crosslinked blend. The EPDM is evident as a red phase corresponding to a topographical valley of about 30nm. Note that although the EPDM appears to be dispersed in this 2D micrograph, it is in fact fully co-continuous as confirmed by the continuity data shown in Figure 6.7(a) and also in a previous publication (Bhadane et al., submitted to Polymer). For the purposes of further

discussion, this co-continuous, non-crosslinked, 50 EPDM/50 PP morphology will be referred to as the “ α -network”.

Micrograph 6.6(b) shows the microstructure in a partially crosslinked ($\approx 50\%$) 50 EP 1/50 PP 2 blend. It can clearly be seen in this micrograph that the non-crosslinked co-continuous system is undergoing significant morphological changes. A much finer, more extensive EPDM network is present. Furthermore, the phases have an even more smeared, more distorted appearance than that observed in Figure 6.5(c).

In order to try to distinguish between non-crosslinked and crosslinked EPDM, the blend preparations used in Figure 6.6(a) and (b) were further subjected to a cyclohexane solvent extraction. Those results are shown in Figure 6.6(d) and (e), respectively. Extracting out the non-crosslinked EPDM creates an additional extreme topological contrast due to the holes left in the sample and the non-crosslinked EPDM phase can be clearly observed in Figure 6.6(e). This non-crosslinked phase bears a close resemblance to the largest phases in micrograph 6.6(a), (b), and (d) and hence it can be inferred that the fine network produced in micrograph 6.6(b) is the crosslinked EPDM. This fine network will be referred to as the β -network in the rest of the discussion. Figure 6.6(e) also shows the presence of a much finer crosslinked phase which is not evident in micrograph 6.6(d). Unfortunately in micrograph 6.6(e), the analysis software tends to ignore comparatively smaller variations in the topography of the sample because of the great depths of pores resulting from the extraction. Hence, the level of network formation is not as evident in micrograph 6.6(e) as in 6.6(b).

Micrograph (c) presents the microstructure of a 100% crosslinked 50 EP 1/50 PP 2 blend. A very fine, extensive β -network is observed. The network is much more highly developed than in Figure 6.6(b) due to the complete crosslinking of the system. The network formation is also confirmed with the results from the gel content measurements for 100% crosslinked blends, i.e. on removal of the non-crosslinked EPDM and PP phases from the blend samples. The remaining crosslinked material remains structurally intact and maintains the original shape of the blend prior to extraction. This clearly supports the concept of network formation. It should be noted that the structural integrity of the crosslinked material after extraction of the PP phase was maintained up to a concentration of 70% EPDM. At that composition and higher, the EPDM disintegrates into a fine powder after PP extraction. Even the 50% crosslinked blend at a composition of 50% EPDM, demonstrates a high level of structural integrity after removal of the non-crosslinked and polypropylene phases. Although this latter sample collapses after drying, this result unambiguously reinforces the concept of network formation as shown in Figures 6.6(b) and (c).

These results indicate for the first time that co-continuous morphologies are dramatically changed as vulcanization proceeds and that a non-crosslinked co-continuous EPDM phase (α -network) transits to a much finer network of crosslinked EPDM (β -network) after crosslinking. Coran et al. (1996) does report a 'network' of vulcanized elastomer but, it is worth understanding here that, unlike the finer β -network evident in Figure 6.6, it was a network formed by physically touching, loosely bound

together vulcanized particles formed at higher compositions of an elastomer ($\approx 80\%$ EPDM).

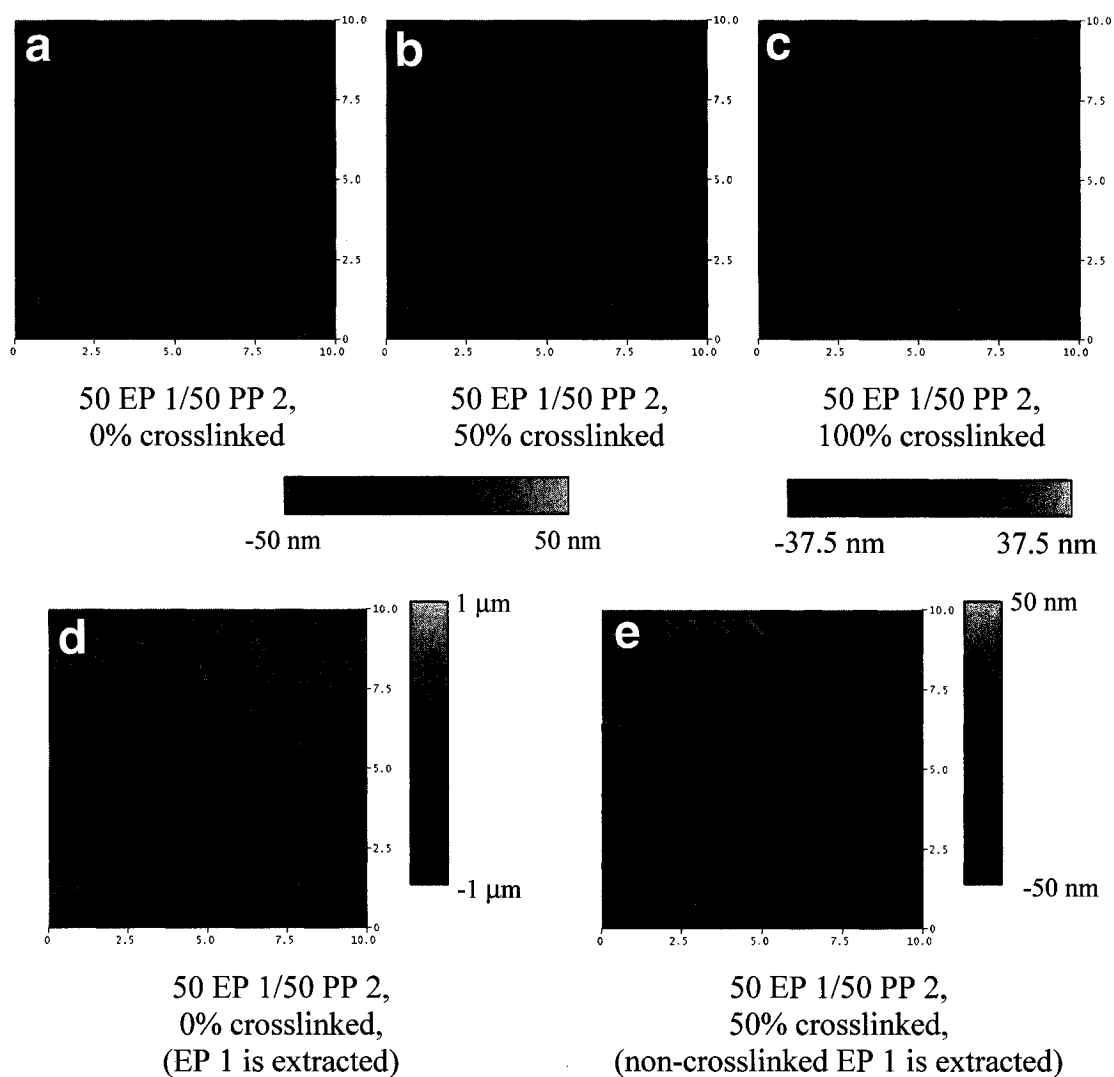


Figure 6.6: AFM micrographs of 50 EP 1/50 PP 2 after FIB sample preparation at 0%, 50% and 100% EPDM crosslinking

6.3.4 Effect of crosslinking on the continuity of non-crosslinked EPDM

In order to develop a better understanding of the structural nature of the non-crosslinked EPDM phase as vulcanization proceeds, the continuity of the non-crosslinked phase was determined. Figures 6.7(a) and (b) demonstrate the percent continuity of the non-crosslinked EPDM phase in the blend at different levels of crosslinking as a function of the total EPDM composition in the blend. Figure 6.7(a) shows that the EPDM phase in the non-crosslinked blend is about 50% continuous at 30% EPDM content in the blend, and reaches co-continuity at a composition of 40% EPDM. When these blends are crosslinked to 100%, the non-crosslinked portion is so small that continuity falls to 0% at all blend compositions. However, Figures 6.7(a) and 6.7(b) show that when the 50 EP 1/50 PP 2 and 50 EP 1/50 PP 1 blends are crosslinked to about 50%, the remaining non-crosslinked EPDM in the blend remains fully extractible. In other words, the remaining non-crosslinked material remains fully continuous even at 50% crosslinking. Note in Figure 6.7(b) that as the EPDM composition is increased to 60 and 70%, continuity actually exceeds 100%. This is due to the difficulty in accurately achieving and estimating a gel content (see error bars in Figure 6.2). A small overestimation of gel content significantly affects the estimation of amount of non-crosslinked material remaining in the blend. As a result, the value of continuity determined based on the non-crosslinked material remaining in the blend after crosslinking, i.e. as in Figure 6.7(b), exceeds the 100% value. In order to verify whether any crosslinked phase was also extracted with the non-crosslinked portion we filtered the cyclohexane solution obtained after extraction using a 0.8 μm membrane.

Figure 6.8 presents the % crosslinked phase retained on the membrane as a function of the composition of total EPDM phase in the blend. The results clearly show that no more than 1% of the dispersed phase is retained on the membrane for all of the compositions studied. Thus, these results show that on crosslinking virtually none of the crosslinked EPDM phase is present in the non-crosslinked EPDM phase.

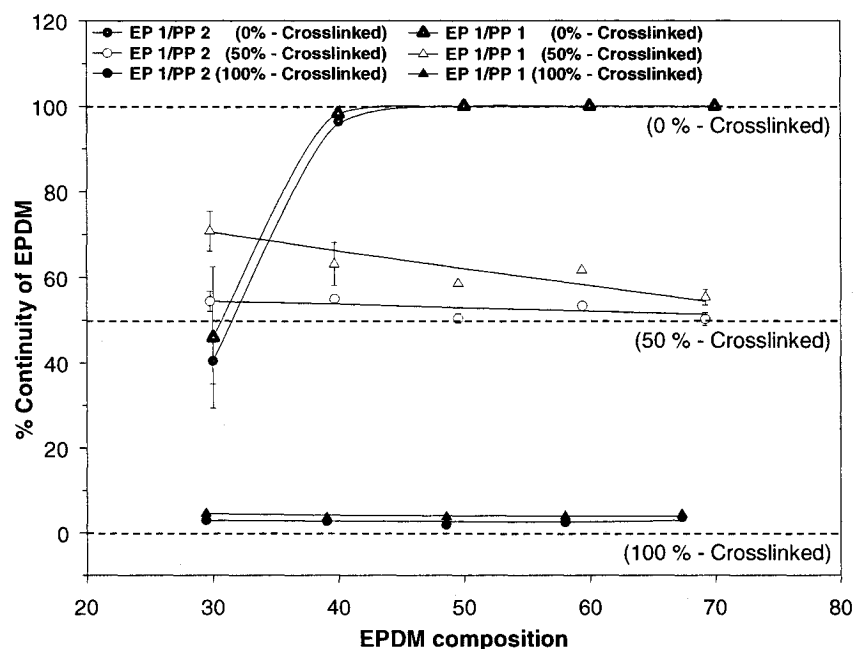


Figure 6.7 (a): Effect of dynamic vulcanization on continuity

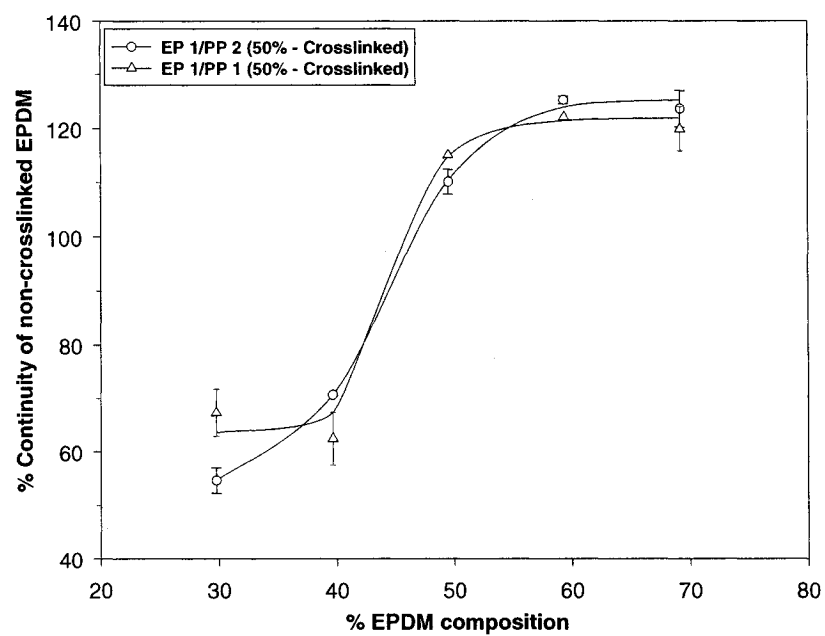


Figure 6.7 (b): Continuity of the non-crosslinked EPDM in the 50% crosslinked blend as a function of EPDM composition

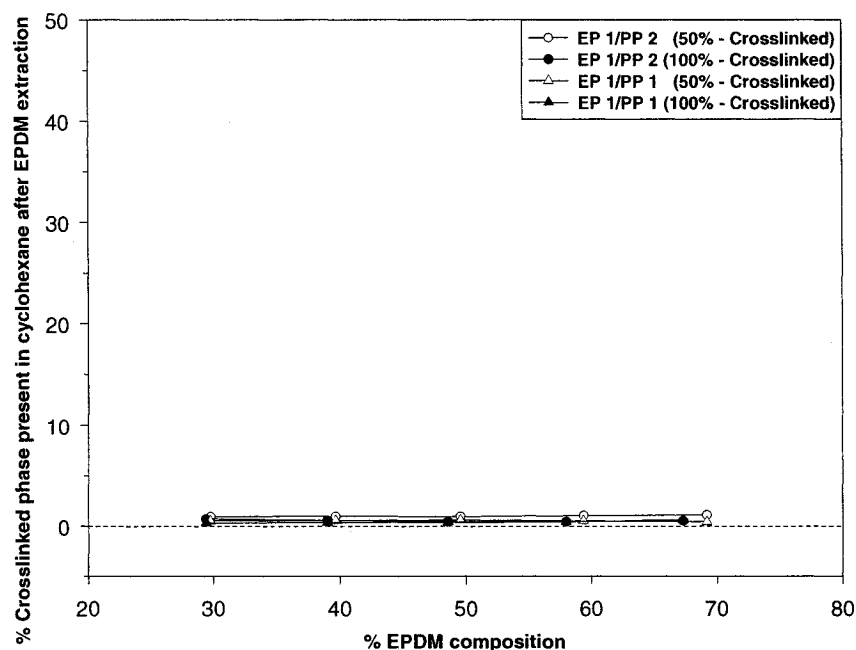


Figure 6.8: Gravimetric analysis of the quantity of crosslinked EPDM material present in the continuous non-crosslinked EPDM

6.3.5 Effect of crosslinking on pore diameter

Since the non-crosslinked portion of EPDM maintains full continuity during the crosslinking process it was decided to determine if crosslinking affects the phase size of this α -network. Figure 6.9 presents the pore diameters of the α -network as a function of the total EPDM composition for the non-crosslinked and partially crosslinked EP 1/PP 1 blends. The results clearly demonstrate that the pore diameter of the α -network is decreasing as the blends are crosslinked. Note that for the 60 and 70% blend concentrations, the samples shrank after removing the non-crosslinked EPDM phase, rendering pore size determination very difficult. The pore size of the EP 1/PP 2 blends

was also examined, however, since the pore sizes are so small in that case the differences fall within the experimental error and limits of the measurement technique.

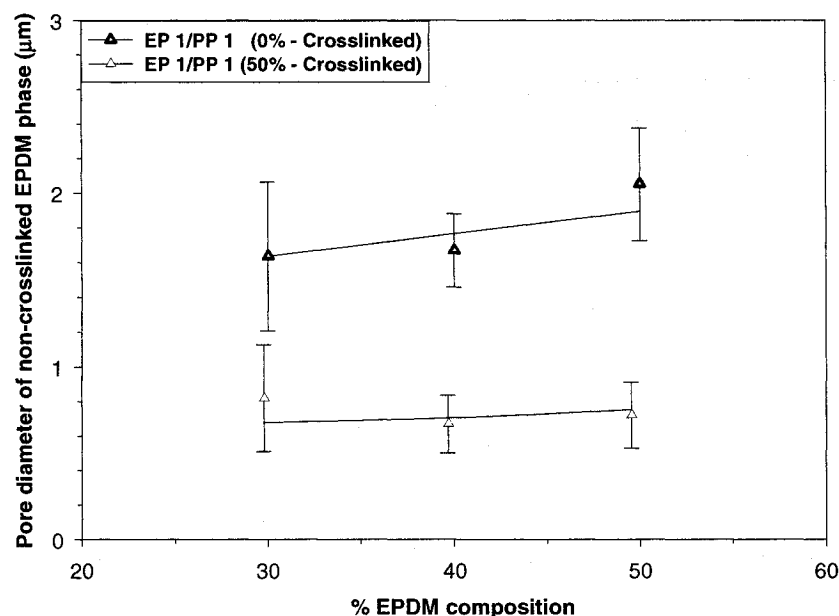


Figure 6.9: Effect of crosslinking on the pore diameter of non-crosslinked EPDM phase from BET

6.3.6 Conceptual mechanism of morphology development in thermoplastic vulcanizates

In this section we will advance a conceptual model of morphology development during the vulcanization of co-continuous structures. Considering that the α -network remains fully continuous even at 50% crosslinking and that the pore size of that network clearly diminishes with time as shown in Figures 6.7 and 6.9, it appears clear that crosslinking starts at the outer envelope of the EPDM phase forming micro-gel particles and works its way towards the center. This concept is supported by the high rates of

reaction of this particular vulcanization protocol. When carrying out the vulcanization experiments, it is noted that the torque of the melt mixer increases almost immediately upon addition of crosslinking agent. Hence it would appear that as soon as the crosslinking agent comes into contact with EPDM, the crosslinking is virtually immediate and a micro-gel is formed. Under dynamic mixing conditions, this micro-gel particle detaches from the α -network due to the viscosity mismatch generated because of the crosslinking and in response to the fluid dynamics occurring during mixing. The micro-gel particle while detaching from the α -network, however, will also pull entangled chains of non-crosslinked EPDM with it, producing a smearing effect and hence resulting in a much finer and more extensive network formation as seen in Figure 6.6.

Figure 6.10 schematically shows the mechanism of a crosslinked β -network formation from the template of a non-crosslinked α -network based on the results from this work. Schematic 6.10(a) shows the α -network, i.e. the coarse cocontinuous network of non-crosslinked EPDM, in a 50 EP/50 PP blend prior to crosslinking. As crosslinking proceeds, in 6.10(b) and (c), the crosslinked material, i.e. β -network, (shown in grey) begins to form at the outer envelope of the EPDM and pulls material away from the main body of the EPDM during mixing, resulting in a much finer network. Ultimately in 6.10(d), all the EPDM has been crosslinked and the co-continuous structure has transited completely from a coarse α -network to a much finer morphology, the fully formed β -network.

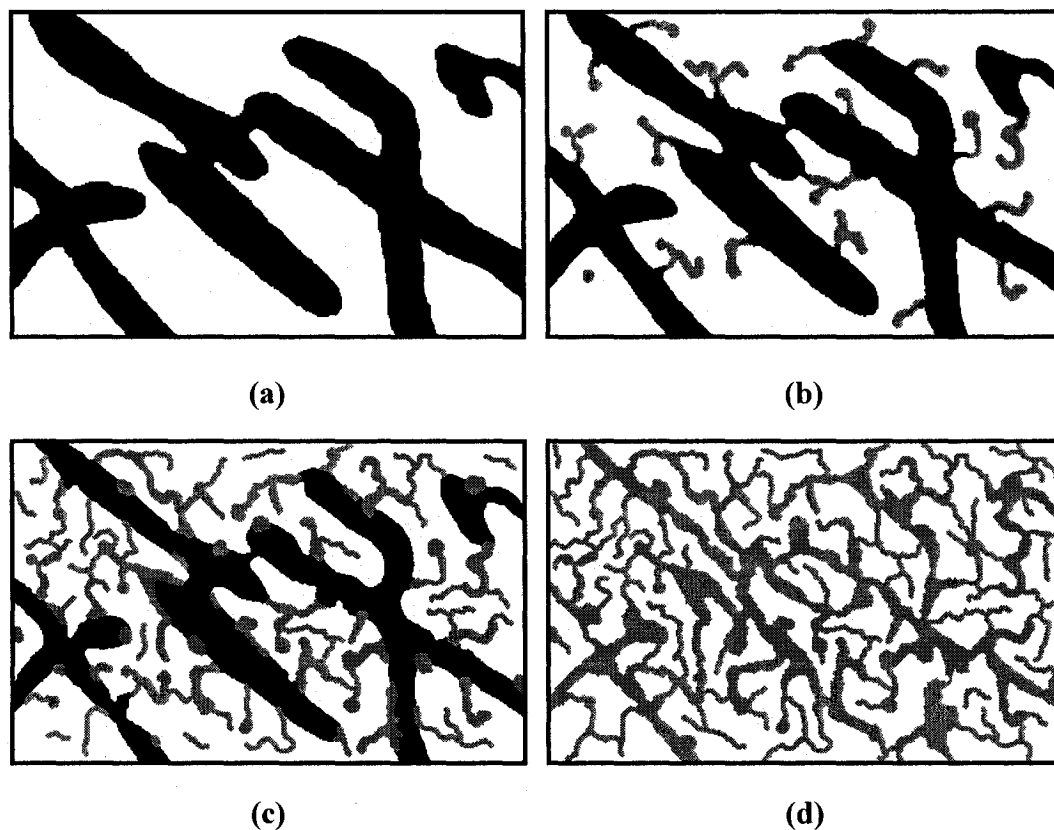


Figure 6.10: Schematics of the morphology development in a cocontinuous blend of EPDM/PP with dynamic crosslinking

**(a) 0% crosslinked, (b) 25% crosslinked (onset of crosslinking),
(c) 50% crosslinked (partial crosslinking), (d) 100% crosslinked**

6.4 Conclusions

This study investigates the influence of dynamic crosslinking on the cocontinuous morphology in EPDM/PP blends. The blends are both partially and fully crosslinked during melt mixing in order to better understand the morphology evolution. The morphology of the blends is investigated by applying a novel technique involving

focused ion beam (FIB) etching of the sample surface followed by topological analysis of the sample surface using tapping mode atomic force microscopy (TMAFM). It is shown that the FIB ion etching rates of EPDM and PP are distinctly different and, thus, leads to a significant topological contrast between the phases when subsequently analyzed by atomic force microscopy. The technique also effectively distinguishes the zinc oxide particles in the blend. The contrast generated due to FIB ion etching is found to be so high that the domains as small as 100 nm in diameter are clearly evident.

Since the FIB ion etching rate for the non-crosslinked and crosslinked EPDM phases was similar, an additional topological contrast is created by dissolving the non-crosslinked EPDM phase of the blend. In this way, the technique is found to effectively distinguish non-crosslinked and crosslinked EPDM phases in the dynamically crosslinked blends. The high resolution micrographs suggest that the dynamic crosslinking of cocontinuous EPDM phase (α -network), surprisingly, leads to the formation of a new much finer network of crosslinked EPDM (β -network). The micrographs combined with the structural integrity of the sample after gel content measurement suggest a high level of interconnectivity in the β -network. As dynamic crosslinking proceeds, the α -network maintains its cocontinuity but decreases in pore diameter. For the viscosity ratios studied, the results indicate that no crosslinked phase exists in the cocontinuous non-crosslinked EPDM phase (α -network). As the crosslinking reaction rate is very high, these results indicate that the crosslinking

proceeds initially at the outer envelope of the EPDM phase and works its way towards the center.

The β -network forms as a result of the viscosity mismatch created due to crosslinking between the non-crosslinked and crosslinked EPDM. The micro-gel particle while detaching from the α -network, however, pulls entangled chains of non-crosslinked EPDM with it, producing a smearing effect and hence resulting in a much finer and more extensive network formation.

Acknowledgements

The authors would like to thank Mr. Mike Gallagher of Bayer Inc. for supplying EPDM; Mr. Denis Therrien of Basell Polyolefins Inc. for supplying and measuring the molecular weights of the PP, and Mr. Terry Stroble of Schenectady International Inc. for supplying phenol-formaldehyde heat reactive curing resin. The authors would also like to thank Professor Gilles L'Espérance of the Center for Characterization and Microscopy of Materials (CM)² and Professor Patrick Desjardins of the Department of Engineering Physics at École Polytechnique de Montréal for the use of the Focused ion beam (FIB) and Atomic force microscope, respectively.

Literature Cited

Abdou-Sabet S, Patel RP. Morphology of elastomeric alloys. Rubber Chem. Technol. 1991;64:769-779.

Galuska AA, Poulter RR, McElrath KO. Force modulation AFM of elastomer blend: morphology, fillers and crosslinking. *Surf. Interface Anal.* 1997;25:418-429.

Chung O, Nadella HP. Phase morphology and cure state characterization of soft thermoplastic vulcanizates (TPVs) by using atomic force microscopy (AFM). ANTEC 2001 Proceedings of the 59th Annual Technical Conference, Society of Plastics Engineers 2001;59:2926-2930.

Nysten B, Ghanem A, Costa J, Legras R. Influence of EP/PP viscosity ratio on the surface morphology and elasticity of injection molded PP/EP. *Polym. Int.* 1999;48:334-338.

Nysten B, Legras R, Costa J. Atomic force microscopy imaging of viscoelastic properties in toughened polypropylene resins. *J. Appl. Phys.* 1995;78:5953-5958.

Trifonova-Van Haeringen D, Schonherr H, Vancso GJ, Vander Does L, Noordermeer JWM., Janssen PJP. Atomic force microscopy of elastomers: morphology, distribution of filler particles, and adhesion using chemically modified tips. *Rubber Chem. Technol.* 1999;72:862-875.

Tanem BS, Kamfjord T, Augestad M, Lovgren TB, Lundquist M. Sample preparation and AFM analysis of heterophase polypropylene systems. *Polymer* 2003;44:4283-4291.

Yerina N, Magonov S. Atomic force microscopy in analysis of rubber materials. *Rubber Chem. Technol.* 2003;76:846-859.

Ellul MD, Tsou AH, Hu W. Crosslink densities and phase morphologies in thermoplastic vulcanizates. *Polymer* 2004;45:3351-3358.

Virgilio N, Favis BD, Pepin M, Desjardins P, L'Esperance G. High contrast imaging of interphases in ternary polymer blends using forced ion beam preparation and atomic force microscopy. *Macromolecules* 2005;38:2368-2375.

Bhadane P, Favis B, Champagne M, Huneault M, Tofan F. Continuity development in polymer blends very low interfacial tension. Submitted to *Polymer*.

Bhadane P, Favis B, Champagne M, Huneault M, Tofan F. Erosion-controlled continuity development in high viscosity ratio blends of very low interfacial tension. Submitted to *J. Polym. Sci. Part B: Polym. Phys.*

Marquez A, Quijano J, Gaulin M. A calibration technique to evaluate the power-law parameters of polymer melts using a torque-rheometer. *Polym. Eng. Sci.* 1996;36:2556-2583.

Li J, Favis BD. Characterizing cocontinuous high density polyethylene/polystyrene blends. *Polymer* 2001;42:5047-5053.

Abdou-Sabet S, Fath MA. Thermoplastic elastomeric blends of olefin rubber and polyolefin resin. U.S. Patent 4,311,628, 1982.

Coran AY, Patel RP. Thermoplastic elastomers based on dynamically vulcanized elastomers – thermoplastic blends. In: Holden G, Legge NR, Quirk RP, Schroeder HE. *Thermoplastic elastomers* (2nd edition). New York: Hanser Publishers, 1996:153-190.

CHAPTER 7

GENERAL DISCUSSIONS

This chapter discusses the problems related to achievement of consistent level of crosslinking in the blends, and the problems related to dynamic crosslinking of the high viscosity ratio blends. The choice of the blend system, the problems related to its characterization and their comparison with the literature has already been done.

7.1 Dynamic crosslinking of the blends

The work of Coran et al. (1978) clearly demonstrates the importance of complete vulcanization of elastomer phase during the preparation of thermoplastic vulcanizates, and is already discussed in Chapter 2. They showed that partial crosslinking provides only the modest improvement in the properties. However, complete crosslinking of the elastomer phase under the dynamic melt mixing conditions is quite tricky. This is because a bromomethylated alkyl phenol-formaldehyde heat reactive resin, used as a crosslinking agent in this work, has a low viscosity and melting point of around 80°C. On its addition to the melt in the mixer at 190°C most of it tends to move towards the wall of the mixer where it eventually degrades because of the high temperature. The degradation was evident by dark brown colored coating formed on inside wall of the mixer. The degradation was even more severe as the amount of crosslinking agent increases. This fact not only makes complete crosslinking of the elastomer phase impossible but even the amount of gel content achieved in the blends under such conditions is inconsistent and is shown in Figure 7.1.

In this work, to solve this problem, a concentrated master batch consisting of 50 parts EPDM and 50 parts curing resin is prepared. The EPDM and curing resins are intimately mixed together by dissolving both the components in cyclohexane at room temperature. The thick films of the solution are made by solvent casting and the solvent is completely removed by applying vacuum. Since the master batch is prepared at room temperature by solution blending, no crosslinking reaction occurs and the complete homogeneity of the mixture can be assured. Unlike on addition of a pure crosslinking agent, on addition of the master batch no thick brown coat was observed inside the mixer wall, which indicates no degradation of the crosslinking agent over the mixer wall. The addition of master batch allows for complete crosslinking of the elastomer phase and the consistent level of gel content is also obtained as shown in Figure 7.1.

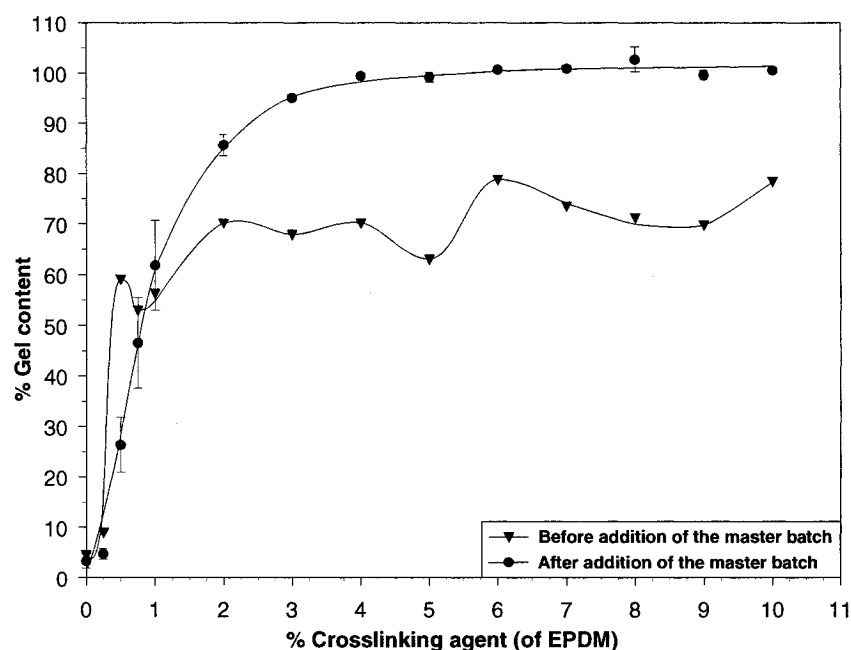


Figure 7.1: Gel content in 50 EP 1/50 PP 2 blend before and after addition of the master batch

Figure 7.1 clearly demonstrate the effectiveness of the master batch in preventing the migration of the crosslinking agent towards the wall of the mixer. Though the master batch of 50 parts EPDM/50 parts curing agent is good enough to solve the aforementioned problems, if required more concentrated master batch can also be prepared by the said procedure.

7.2 Dynamic crosslinking of high viscosity ratio blends

As shown in Chapter 5 EP 3/PP 1 blend has the viscosity ratio of 17. Efforts were taken to carryout dynamic crosslinking studies, similar to one reported in Chapter 6, on this high viscosity ratio blend. The blends were partially and fully crosslinked and the gel content achieved is shown in Figure 7.2.

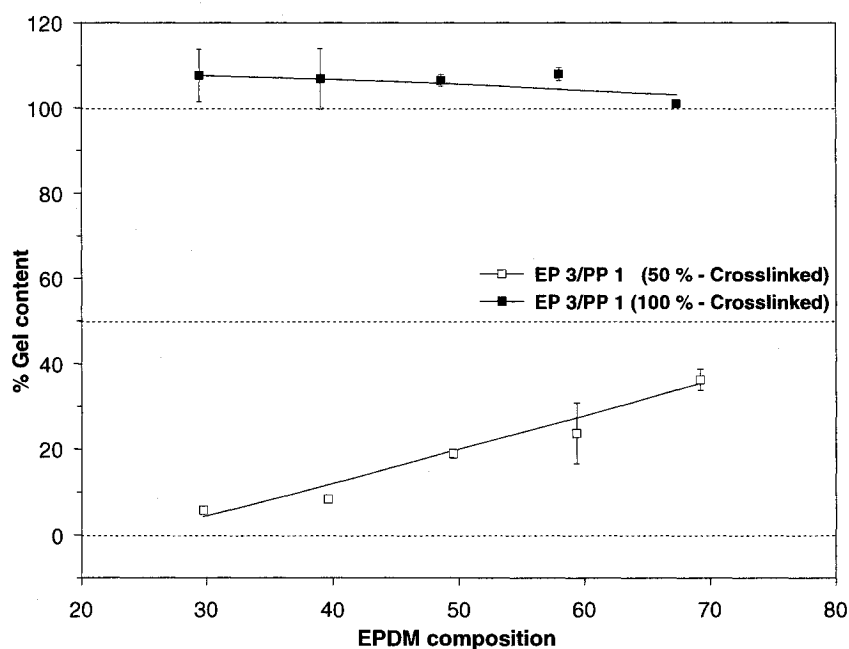


Figure 7.2: Gel content in high viscosity ratio blends

Figure 7.2 shows the difficulty associated with partial crosslinking of the high viscosity ratio blends. Despite the addition of calculated amount of crosslinking agent, the blends have not achieved 50% gel content. The problem was even more significant at lower concentrations, ≈ 5 to 20%, of EPDM. These results are expected since these blends demonstrate erosion phenomena which remain incomplete after 8 minutes of melt mixing (see Chapter 5), the time at which the dynamic crosslinking of the blends is started. Moreover, rate of the crosslinking reaction is very high and therefore the high viscosity master batch added on 8th minute of mixing gets crosslinked even before it is dispersed in the mixture. The fine, unbroken chunks of the master batch were evident all over the blend. The more the composition of EPDM in the blend more effective is the dispersion of the master batch and hence is the increase in gel content, as seen in Figure 7.2. However, the similar problem does not arise when the blends are crosslinked to 100% because of much excess amount of master batch added for crosslinking. Thus, the crosslinked blends of high viscosity ratio demonstrate uneven morphology and further studies are not carried out on these blends.

CHAPTER 8

CONCLUSIONS AND RECOMMENDATIONS

8.1 Conclusions

This thesis studies the morphology, continuity development and cocontinuity in EPDM/PP blends and their thermoplastic vulcanizates in detail. Using the harmonic mean equation, the interfacial tension between EPDM and PP is theoretically estimated to be 0.3 mN/m, at the melt blending temperature of 190°C. The experimental estimation of interfacial tension by the breaking thread method is found to be extremely difficult because of its ultra-low value.

Overall, EPDM/PP blends of viscosity ratios from 0.1 – 17.0, elasticity ratios from 0.1 – 29 and matrix shear stresses from 11.7 – 231.4 kPa are prepared in an internal mixer by melt mixing. The study of the glass transition temperatures of the blends comprising the lowest molecular weight components, i.e. EP 1 and PP 1, were carried out with a dynamic mechanical thermal analyzer. The results show that EPDM/PP blends are completely immiscible over the entire composition range after cooling from the melt. Given that the ethylene content of all EPDM grades used in this work is very similar, by extrapolation all other blends of higher molecular weight materials would be expected to be completely immiscible after cooling from the melt.

The blends in the low to medium, i.e. 0.2 to 5.0, viscosity ratio range demonstrate that the dispersed phase, at low compositions, is distributed very finely and uniformly throughout the matrix material. On average, the phase sizes are estimated to

be 50–200 nm in diameter. Contrary to the current belief that the dispersed phase exists in the form of spherical droplets in this blend system, the matrix dissolution study shows that it, in fact, exists in the form of extremely small diameter stable fibers. The thread breakup times estimated from Tomotika theory by inserting the actual phase sizes of the dispersed phase also support this notion.

With an increase in composition, these fibers coalesce at crossover points to develop continuity and cocontinuity as per the expected behavior of a binary compatible system. The blends demonstrate virtually no effect of a 7-fold variation in the viscosity ratio on the phase sizes, the shape of the dispersed phase, the % continuity, the region of cocontinuity and also on the mechanism of continuity development. However, 8-fold variation in shear stress does affect the particle sizes. Moreover, these blends demonstrate very symmetrical continuity development with respect to the mid-composition.

Despite following many of the features of a binary compatible system, the blends show numerous unexpected features such as: artificially high percolation thresholds, delayed continuity development, cocontinuity at higher than expected compositions of minor phase and hence very narrow range of cocontinuity, and high coalescence with composition. These are features typical of a partially miscible system. Since these dominant morphological features of the blend develop during melt blending, the results suggest that the blends are partially miscible in the melt. Nevertheless, because of the crystalline nature of PP, the partially miscible blends are forced to

completely phase separate upon cooling from the melt as revealed by the glass transition temperatures of the quenched blend samples. The quenching of the blends from the melt is clearly rapid enough to preserve the imprint of that partial miscibility in the melt on the blend morphology after cooling.

An even further increase in the viscosity ratio to 11 and 17, however, does affect all aspects of the blend morphology. In addition to stable isolated nano-fibers, the dispersed phase is found to contain very large particles, partially coalesced particles, and particles interconnected by nano-fibers. This unusual combination of variety of morphologies is found to lead the blends to a novel cocontinuous structure of partially coalesced particles and particles interconnected by stable fibers. The high viscosity ratio blends, therefore, demonstrate early percolation thresholds, rapid continuity development, and attain cocontinuity at lower than expected compositions of minor phase. Compared to low to medium viscosity ratio blends, these blends certainly demonstrate a wider but asymmetrical region of dual-phase continuity.

It is found that the varieties of morphologies generated are the result of a slow surface erosion process of the high viscosity EPDM phase. In this process, the unique combination of ultra-low interfacial tension and high viscosity ratio between the blend components pull long and stable nano-fibers off a high viscosity particle. The morphology at low blend compositions is, thus, a non-steady-state morphology, and the slow surface erosion process remains incomplete even after 30 minutes of melt mixing.

For higher blend compositions, a new concentration dependent erosion mechanism based on particle collision-coalescence-separation dynamics is proposed. Based on increased particle-particle collisions at higher compositions, the proposed mechanism dramatically accelerates the erosion process. The proposed mechanism also results in the coalescence of particles and fiber regeneration between the two particles on breakup under dynamic mixing conditions which help blends maintain cocontinuity over prolonged periods of mixing. The higher composition blends, thus, demonstrate steady-state (at equilibrium) morphologies.

It is found that dynamic crosslinking of the cocontinuous morphologies (α -network) in 0.7 and 5.0 viscosity ratio blends, surprisingly, leads to a new much finer network of crosslinked EPDM (β -network). The morphology in dynamically crosslinked blends is investigated by applying a novel technique involving focused ion beam (FIB) etching of the sample surface followed by topological analysis of the sample surface using tapping mode atomic force microscopy (TMAFM). The FIB ion etching rates of EPDM and PP are found to be distinctly different and, thus, lead to a significant topological contrast between the phases when subsequently analyzed by atomic force microscopy. The contrast generated due to FIB ion etching is found to be so high that the domains as small as 100 nm in diameter are clearly evident. The technique also effectively distinguishes the zinc oxide particles in the blend. However, the FIB ion etching rates of the non-crosslinked and crosslinked EPDM phases were found to be similar, and hence, an additional topological contrast is created by dissolving the non-crosslinked EPDM phase of the blend. In this way, the technique is

found to effectively distinguish non-crosslinked and crosslinked EPDM phases in the dynamically crosslinked blends.

The high resolution micrographs together with the structural integrity of the sample after gel content measurement suggest a high level of interconnectivity in the β -network. As dynamic crosslinking proceeds, the α -network maintains its cocontinuity but decreases in pore diameter. For the viscosity ratios studied, the results indicate that no crosslinked phase exists in the cocontinuous non-crosslinked EPDM phase (α -network). As the crosslinking reaction rate is very high, these results indicate that the crosslinking proceeds initially at the outer envelope of the EPDM phase and works its way towards the center.

The β -network forms as a result of the viscosity mismatch created due to crosslinking between the non-crosslinked and crosslinked EPDM. The micro-gel particle while detaching from the α -network, however, pulls entangled chains of non-crosslinked EPDM with it, producing a smearing effect and hence resulting in a much finer and more extensive network formation.

8.2 Recommendations

Based on the research work carried out here, several recommendations can be made for the future work.

Further evidence should be given for the partial miscibility between EPDM and PP at melt blending temperature. For this purpose, the correct value of χ (interaction parameter) without deuteration effects needs to be measured. As noted by Crist et al.

(1997), it can be done by taking the root mean square average of the two χ values measured separately by deuterating one polymer at a time. Moreover, the blend morphology in the melt should be investigated by collecting a small sample directly from the internal mixer and quenching with liquid nitrogen on the spot.

More evidence of nano-fiber formation, in low to medium viscosity ratio EPDM/PP blends, could be given by removing layer-by-layer material of the sample with focused ion beam and subsequent analysis with SEM or AFM.

At low composition of the dispersed phase in high viscosity ratio EPDM/PP blends, i.e. for the blends for which the erosion phenomena were observed, the time to achieve the equilibrium morphology and the equilibrium morphology itself should be determined. Although the continuity development and morphology of low viscosity PP material in highly viscous EPDM matrices, i.e. in PP 1/EP 2 and PP 1/EP 3 blends, is not expected to be very different from that observed for low to medium viscosity ratio blends, it should be investigated.

On the part of dynamic vulcanizates, the investigation should be carried out to determine the effect of an increase in the degree of vulcanization on partial miscibility between the blend components at melt blending temperature and its role in morphology development in TPVs.

Moreover, the efficacy of the crosslinking agent towards EPDM and PP needs to be determined. The blend morphologies at the very early onset of crosslinking should be determined. This work should be done with very small addition of crosslinking agent,

with different starting morphologies, and also with time by quenching small samples in liquid nitrogen directly from the mixer. Overall, the effect of degree of dynamic vulcanization on different starting morphologies needs to be established.

More efforts are needed to further improve the contrast between non-crosslinked and crosslinked elastomer phase by some new technique or by developing some computer program or method to analyze the data from AFM, which would distinguish the smaller variations in the topography despite the very deep pore in the sample after solvent extraction of the non-crosslinked phase. The form and size of crosslinked and non-crosslinked phases with different degree of crosslinking can also be investigated. To obtain more accurate pore diameter values for dynamically crosslinked blends, the BET measurements should be carried out on freeze dried samples.

The various physical properties, e.g. impact strength, tensile strength, tension set, elongation at break etc, before vulcanization and after dynamic vulcanization should be measured.

One of the important parameters in manufacturing TPVs is the addition sequence of polymers and crosslinking agent. The future work should investigate the different addition sequences and their effect on blend morphology.

The phase sizes and pore diameter values in low interfacial tension systems are known to be insensitive to the viscosity ratio and this was confirmed in this work. Therefore one of the main objectives during this work, to obtain the cocontinuous structure with different pore sizes, remains unaccomplished. The cocontinuous

structures with different pore sizes, however, can be obtained by varying the interfacial tension between the blend components. Thus, different TPVs with higher interfacial tension between the blend components, e.g. Nylon/elastomer, PET/elastomer etc, should be made and thereby the effect of dynamic vulcanization on these different morphologies should be determined.

To obtain the further improvement in properties of TPVs, research should be done on making nanocomposites of TPVs by adding nano-clays, carbon nano-tubes, silica, and various other fillers.

CHAPTER 9

SCIENTIFIC CONTRIBUTIONS

This research work contributes to the field of science, more specifically to the field of polymer blends, in various ways. Several major scientific contributions of this work are listed below,

1. This is the first study to carry out the matrix dissolution experiment in EPDM/PP blend. This is especially significant for blends with minor EPDM phase, where it is impossible to dissolve PP without dissolving EPDM. The matrix dissolution after irradiation crosslinking of EPDM phase has shown various novel and unanticipated morphological structures and their development, in these ultra-low interfacial tension blends.
2. This study for the first time, examines the complete continuity development for EPDM/PP blend systems, i.e. on either side for EPDM and also for PP.
3. Contrary to current knowledge, this work demonstrates that at low to medium viscosity ratios the minor phase in EPDM/PP blends exists in the form of nanometer diameter stable fibers, and thereby the continuity develops by fiber-fiber coalescence. The dispersed phase in high viscosity ratio blends is shown to form varieties of morphologies, which are eventually responsible for early percolation phenomenon and rapid continuity development in these blends.

4. Previous studies demonstrating erosion phenomena in high viscosity ratio blends were carried out on very big particles (typically, 0.5 – 0.7 mm) to enable direct visualization of the mechanism. Such big particles possess about 600 times lower surface to volume ratio when compared to typical blend morphologies. Thus, these mechanisms may exist only during the initial stages of melt mixing. However, this study demonstrates erosion phenomena for much smaller phases in polymer blends in a typical mixing environment.
5. In addition to previously known mechanisms of erosion in high viscosity ratio blends, this study contributes a novel concentration dependent mechanism based on the simple facts during melt mixing and demonstrates its effectiveness in morphology development in high viscosity ratio blends.
6. A new method involving the use of FIB sample etching followed by tapping mode AFM surface analysis is successfully applied to TPVs. After selective dissolution of the non-crosslinked EPDM phase, this technique is shown to effectively distinguish various phases in the blend, especially between the non-crosslinked and crosslinked elastomer phase.
7. The morphology development in dynamically vulcanized TPVs with degree of vulcanization is shown based on the high resolution micrographs and other results.

REFERENCES

- Abdou-Sabet S., Datta S. (2000), Thermoplastic Vulcanizates, in '*Polymer Blends*' Edited by Paul D.R., Bucknall C.B., John Wiley & Sons Inc., Vol. 2: Performance, Ch. 35, 517-555
- Abdou-Sabet S., Fath M.A. (1982). Thermoplastic elastomeric blends of olefin rubber and polyolefin resin. *U.S. Patent* 4,311,628
- Abdou-Sabet S., Patel R.P. (1991). Morphology of elastomeric alloys. *Rubber Chem Tech*, 64:5, 769-779
- Abdou-Sabet S., Puydak R.C., Rader C.P. (1996). Dynamically vulcanized thermoplastic elastomers. *Rubber Chem Tech*, 69:3, 476-494
- Agari Y., Ueda A., Nagai S. (1992). Thermal conductivity of polyethylene/polystyrene blends containing SEBS block copolymer. *J Appl Polym Sci*, 45, 1957-1965
- Amash A., Zugenmaier P. (1997). Dynamic mechanical investigations on drawn samples of isotactic polypropylene/EPM-rubber blend. *J Polym Sci, Part B: Polym Phys*, 35:9, 1439-1448
- Arends C.B. (1992). Percolation in injection molded polymer blends. *Polym Eng Sci*, 32:13, 841-844
- Arns C.H., Knackstedt M.A., Roberts A.P., Pinczewski V.W. (1999). Morphology, cocontinuity, and conductive properties of anisotropic polymer blends. *Macromolecules*, 32, 5964-5966

- Arroyo M., Zitzumbo R., Avalos F. (2000). Composites based on PP/EPDM blends and aramide short fibers. Morphology/behavior relationship. *Polymer*, 41, 6351-6359
- Avgeropoulos G.N., Weissert F.C., Biddison P.H., Bohm G.G.A. (1976). Heterogeneous blends of polymers. Rheology and morphology. *Rubber Chem Tech*, 49:1, 93-104
- Blacher S., Brouers F., Fayt R., Teyssie Ph. (1993). Multifractal analysis. A new method for the characterization of the morphology of multi-component polymer systems. *J Polym Sci, Part B: Polym Phys*, 31, 655-662
- Bourry D., Favis B.D. (1998). Continuity and phase inversion in HDPE/PS blends: influence of interfacial modification and elasticity. *J Polym Sci, Part B: Polym Phys*, 36, 1889-1899.
- Braidwood C.A. (1961). Substituted phenols. *U.S. Patent* 2,972,600
- Brown G.M., Butler J.H. (1997). New method for the characterization of domain morphology of polymer blends using ruthenium tetroxide staining and low voltage scanning electron microscopy (LVSEM). *Polymer*, 38:15, 3937-3945
- Charlesby A., Pinner S.H. (1959). Analysis of the solubility behavior of irradiated polyethylene and other polymers. *Proc R Soc (Lond)*, A 249, 367-386
- Chen C.Y., Yunus W.Md.Z.W., Chiu H.W., Kyu T. (1997). Phase separation behavior in blends of isotactic polypropylene and ethylene-propylene-diene terpolymer. *Polymer*, 38:17, 4433-4438

- Chesters A.K. (1991). The modeling of coalescence processes in fluid-liquid dispersions: a review of current understanding. *Chem Eng Res Des*, 69:A4, 259-270
- Chuai C.Z., Almdal K., Lyngaae-Jørgensen J. (2002). Dual-phase continuity and phase inversion in polycarbonate/polystyrene blends during compounding. *J Mat Sci Letters*, 21, 89-91
- Chung O., Coran A.Y. (1997). The morphology of rubber/plastic blends. *Rubber Chem Tech*, 70:5, 781-797
- Chung O., Coran A.Y. (2002). The effect of dynamic vulcanization on the morphology and mechanical property of rubber/plastic blends. *2002 ANTEC Conference Proceedings*, 60:3, 3192-3196
- Chung O., Coran A.Y., White J.L. (1997). Melt rheology of dynamically vulcanized rubber/plastic blends. *1997 ANTEC Conference Proceedings*, 55:3, 3455-3460
- Chung O., Nadella H.P. (2001). Phase morphology and cure state characterization of soft thermoplastic vulcanizates (TPVs) by using atomic force microscopy (AFM). *2001 ANTEC Conference Proceedings*, 59:3, 2926-2930
- Clough R. (1989), Radiation-resistant Polymers, in '*Encyclopedia of Polymer Science and Engineering*', edited by Mark, Bikales, Overberger, Menges, 2nd ed., New York: Wiley-Interscience, Vol 13, 667-708
- Coran A.Y. (1994), Vulcanization, in '*Science and Technology of Rubbers*', ed. by Mark, Erman, and Eirich, 2nd ed., Academic Press, Ch 7, 339-385

Coran A.Y., Abdou-Sabet S. (2002). Thermoplastic vulcanizates and process for making the same. *U.S. Patent* 6,437,030 B1

Coran A.Y., Das B., Patel R.P. (1978). Elastoplastic compositions of butyl rubber and polyolefin resin. *U.S. Patent* 4,130,534

Coran A.Y., Das B., Patel R.P. (1978). Thermoplastic vulcanizates of olefin rubber and polyolefin resin. *U.S. Patent* 4,130,535

Coran A.Y., Patel R.P. (1980). Rubber-thermoplastic compositions. Part I. EPDM-polypropylene thermoplastic vulcanizates. *Rubber Chem Tech*, 53:1, 141-150

Coran A.Y., Patel R.P. (1980). Rubber-thermoplastic compositions. Part II. NBR-nylon thermoplastic elastomeric compositions. *Rubber Chem Tech*, 53:4, 781-794

Coran A.Y., Patel R.P. (1981). Rubber-thermoplastic compositions. Part III. Predicting elastic moduli of melt mixed rubber-plastic blends. *Rubber Chem Tech*, 54:1, 91-100

Coran A.Y., Patel R.P. (1981). Rubber-thermoplastic compositions. Part IV. Thermoplastic vulcanizates from various rubber-plastic combinations. *Rubber Chem Tech*, 54:4, 892-903

Coran A.Y., Patel R.P. (1982). Rubber-thermoplastic compositions. Part V. selecting polymers for thermoplastic vulcanizates. *Rubber Chem Tech*, 55:1, 116-136

Coran A.Y., Patel R.P. (1982). Rubber-thermoplastic compositions. Part VI. The swelling of vulcanized rubber-plastic compositions in fluids. *Rubber Chem Tech*, 55:4, 1063-1077

Coran A.Y., Patel R.P. (1983). Rubber-thermoplastic compositions. Part VII. Chlorinated polyethylene rubber-nylon compositions. *Rubber Chem Tech*, 56:1, 210-225

Coran A.Y., Patel R.P. (1983). Rubber-thermoplastic compositions. Part VIII. Nitrile rubber polyolefin blends with technological compatibilization. *Rubber Chem Tech*, 56:5, 1045-1060

Coran A.Y., Patel R.P. (1985). Rubber-thermoplastic compositions. Part IX. Blends of dissimilar rubbers and plastics with technological compatibilization. *Rubber Chem Tech*, 58: 5, 1014-1023

Coran A.Y., Patel R.P. (1996), Thermoplastic elastomers based on dynamically vulcanized elastomers – thermoplastic blends, in ‘*Thermoplastic Elastomers*’, ed. by Holden G., Legge N.R., Quirk R.P., Schroeder H.E., 2nd Ed., New York: Hanser Publishers, Ch 7, 153-190

Coulaloglou, C. A., Tavlarides, L. L. (1977). Description of interaction processes in agitated liquid-liquid dispersions. *Chem Eng Sci*, 32, 1289

Cox R.G. (1969). The deformation of a drop in a general time-dependent fluid flow. *J Fluid Mech*, 37:3, 601-623

Cox W.P., Merz E.H. (1958). Correlation of dynamic and steady flow viscosities. *J Polym Sci*, 28, 619-622

- Crist B., Hill M.J. (1997). Recent developments in phase separation of polyolefin melt blends. *J Polm Sci, Part B: Polm Phys*, 35, 2329-2353
- D'Orazio L., Greco R., Martuscelli E., Ragosta G. (1983). Effect of the addition of EPM copolymers on the properties of high density polyethylene/isotactic polypropylene blends: II. morphology and mechanical properties of extruded samples. *Polym Eng Sci*, 23:9, 489-497
- D'Orazio L., Mancarella C., Martuscelli E. (1991). Polypropylene/ethylene-copolypropylene blends: influence of molecular structure and composition of EPR on melt rheology, morphology and impact properties of injection molded samples. *Polymer*, 32:7, 1186-1194
- Danesi S., Porter R.S. (1978). Blends of isotactic polypropylene and ethylene-propylene rubbers: rheology, morphology and mechanics. *Polymer*, 19:4, 448-457
- Dao K.C. (1982). Mechanical properties of polypropylene/crosslinked rubber blends. *J App Polym Sci*, 27, 4799-4806
- Dao K.C. (1984). Rubber phase dispersion in polypropylene. *Polymer*, 25:10, 1527-1533
- Datta S. (2000), Elastomer Blends, in '*Polymer Blends*', edited by Paul D.R., Bucknall C.B., John Wiley & Sons Inc., Vol 2: Performance, Ch 34, 477-515
- de Gennes P.G. (1984). Partially connected systems. *Portgal phys*, 15, 1-2, 83-94.

- Dedecker K., Groeninckx G. (1998). Reactive compatibilization of A/(B/C) polymer blends. Part 1. investigation of the phase morphology development and stabilization. *Polymer*, 39:21, 4985-4992
- Dedecker K., Groeninckx G. (1998). Reactive compatibilization of A/(B/C) polymer blends. Part 2. analysis of the phase inversion region and the cocontinuous phase morphology. *Polymer*, 39:21, 4993-5000
- Dedecker K., Groeninckx G., Inoue T. (1998). Reactive compatibilization of A/(B/C) polymer blends. Part 3. quantitative analysis of the interfacial thickness and the interfacial reaction. *Polymer*, 39:21, 5001-5010
- Dehoff R.L. (1973). Curing agent for epoxy resin comprising a cyclic anhydride treated with an amino alcohol. *U.S. Patent* 3,709,840
- Dharmarajan N.R., Williams M.G., Datta S., Meka P., Srinivas S. (2005). High impact polymer compositions. *U.S. Patent* 2005/0054781 A1
- Einstein A. (1906). A new determination of molecular dimensions. *Ann Physik*, 19, 289
- Elemans P.H.M., Janssen J.M.H., Meijer H.E.H. (1990). The measurement of interfacial tension in polymer/polymer systems: the breaking thread method. *J Rheol*, 34:8, 1311-1325
- Ellul M.D., Patel J., Tinker A.J. (1995). Crosslink densities and phase morphologies in dynamically vulcanized TPEs. *Rubber Chem Tech*, 68:4, 573-584

Ellul M.D., Tsou A.H., Hu W. (2004). Crosslink densities and phase morphologies in thermoplastic vulcanizates. *Polymer*, 45:10, 3351-3358

Elmendorp J.J. (1986). A study on polymer blending microrheology. *Polym Eng Sci*, 26:6, 418-426

Elmendorp J.J., Ven der velt A.K. (1986). A study on polymer blending microrheology: part IV. The influence of coalescence on blend morphology origination. *Polym Eng Sci*, 26:19, 1332-1338

Everaert V., Aerts L., Groeninckx G. (1999). Phase morphology development in immiscible PP/(PS/PPE) blends influence of the melt-viscosity ratio and blend compositions. *Polymer*, 40, 6627-6644

Favis B.D. (1990). The effect of processing parameters on the morphology of an immiscible binary blend. *J App Polym Sci*, 39, 285-300

Favis B.D. (2000), Factors influencing the morphology of immiscible polymer blends in melt processing, in '*Polymer Blends*', edited by Paul D.R., Bucknall C.B., John Wiley & Sons Inc., Vol 1: Formulations, Ch 16, 501-537

Favis B.D., Chalifoux J.P. (1987). The effect of viscosity ratio on the morphology of polypropylene/polycarbonate blends during processing. *Polym Eng Sci*, 27:20, 1591-1600

Favis B.D., Chalifoux J.P. (1988). Influence of composition on the morphology of polypropylene/polycarbonate blends. *Polymer*, 29, 1761-1767

- Favis B.D., Willis J.M. (1990). Phase size/composition dependence in immiscible blends: experimental and theoretical considerations. *J Polym Sci, Part B: Polym Phys*, 28, 2259-2269
- Fayt R., Harrats C., Blacher S., Jerome R., Teyssie Ph. (1993). Stability of cocontinuous phase morphologies in emulsified polyethylene-polystyrene blends. *Polym Mat Sci Eng*, 69, 178-179
- Fischer W.K. (1974). Dynamically partially cured thermoplastic blend of monoolefin copolymer rubber and polyolefin plastic. *U.S. Patent* 3,806,558
- Fischer W.K. (1974). Thermoplastic blend of copolymer rubber and polyolefin plastic. *U.S. Patent* 3,835,201
- Fortelny I., Cerna Z., Binko J., Kovar J. (1993). Anomalous dependence of the size of droplets of dispersed phase on intensity of mixing. *J Appl Polym Sci*, 48, 1731
- Fortelny I., Kovar J. (1989). Droplet size of the minor component in the mixing of melts of immiscible polymers. *Eur Polym J*, 25, 317
- Fortelny I., Kovar J. (1992). Effect of the composition and properties of components on the phase structure of polymer blends. *Eur Polym J*, 28, 85-90
- Fortelny I., Zivny A. (1995). Coalescence in molten quiescent polymer blends. *Polymer*, 36:21, 4113-4118

Fortelny I., Zivny A., Juza J. (1999). Coarsening of the phase structure in immiscible polymer blends. Coalescence or ostwald ripening? *J Polym Sci, Part B: Polym Phys*, 37, 181-187

Fox T.G. (1956). Influence of diluent and of copolymer composition on the glass temperature of a polymer system. *Bull Am Phys Soc*, 2:1, 123

Funada T., Joseph D.D. (2003). Viscoelastic potential flow analysis of capillary instability. *J Non-Newtonian Fluid Mech*, 111, 87-105

Fusco J.V., Robinson S.B., Miller A.L., Miller R.L. (1963). Vulcanization of synthetic rubber with polyhalomethyl phenol substances. *U.S. Patent* 3,093,613

Galloway J.A., Jeon H.K., Bell J.R., Macosko C.W. (2005). Block copolymer compatibilization of cocontinuous polymer blends. *Polymer*, 46, 183-191

Galloway J.A., Koester K.J., Paasch B.J., Macosko C.W. (2004). Effect of sample size on solvent extraction for detecting cocontinuity in polymer blends. *Polymer*, 45, 423-428

Galloway J.A., Macosko C.W. (2004). Comparison of methods for the detection of cocontinuity in poly(ethylene oxide)/polystyrene blends. *Polym Eng Sci*, 44:4, 714-727

Galloway J.A., Montminy M.D., Macosko C.W. (2002). Image analysis for interfacial area and cocontinuity detection in polymer blends. *Polymer*, 43, 4715-4722

Galuska A.A., Poulter R.R., McElrath K.O. (1997). Force modulation AFM of elastomer blend: morphology, fillers and crosslinking. *Surf Interface Anal*, 25, 418-429

Gergen W.P., Lutz R.G., Davison S. (1996), Hydrogenated block copolymers in thermoplastic elastomer interpenetrating polymer networks, in '*Thermoplastic Elastomers*', ed. by Holden G., Legge N.R., Quirk R.P., Schroeder H.E., 2nd Ed., New York: Hanser Publishers

Gessler A.M., Haslett W.H., Roselle N.J. (1962). Process for preparing a vulcanized blend of crystalline polypropylene and chlorinated butyl rubber. *U.S. Patent* 3,037,954

Geuskens G. (1996). Investigation of the morphology of polymer blends by non-conventional techniques. *J Macromol Sci Phys*, B35:3 & 4, 579-590

Ghodgaonkar P.G., Sundararaj U. (1996). Predication of dispersed phase drop diameter in polymer blends: the effect of elasticity. *Polym Eng Sci*, 36:12, 1656-1665

Giller A., Taunus W. (1966). Process for the cross-linking of unsaturated copolymers and ethylene-propylene terpolymers. *U.S. Patent* 3,287,440

Goharpey F., Katbab A.A., Nazockdast H. (2001). Mechanism of morphology development in dynamically cured EPDM/PP TPEs. I. effects of state of cure. *J App Polym Sci*, 81, 2531-2544

Goharpey F., Katbab A.A., Nazockdast H. (2003). Formation of rubber particle agglomerates during morphology development in dynamically crosslinked EPDM/PP thermoplastic elastomers. Part 1: effects of processing and polymer structural parameters. *Rubber Chem Tech*, 76:1, 239-252

Goizueta G., Chiba T., Inoue T. (1992). Phase morphology of polymer blends: scanning electron microscope observation by back scattering from a microtomed and stained surface. *Polymer*, 33:4, 886-888

Goizueta G., Chiba T., Inoue T. (1993), *Polymer*, 34:2, 253-256

Goldin M., Pfeffer R., Shinnar R. (1972). Breakup of a capillary jet of a non-Newtonian fluid having a yield stress. *Chem Eng J*, 4, 8-20

Gonzalez-Nunez R., Favis B.D., Carreau P.J., Lavallee C. (1993). Factors influencing the formation of elongated morphologies in immiscible polymer blends during melt processing. *Polym Eng Sci*, 33:13, 851-859

Grace H.P. (1982). Dispersion phenomena in high viscosity immiscible fluid systems and application of static mixers as dispersion devices in such systems. *Chem Eng Commun*, 14, 225-277

Grigoryeva O.P., Karger-Kocsis J. (2000). Melt grafting of maleic anhydride onto an ethylene-propylene-diene terpolymer (EPDM). *European Polym J*, 36, 1419-1429

Gubbels F., Blacher S., Vanlathem E., Jerome R., Deltour R., Brouers F., Teyssie Ph. (1995). Design of electrical conductive composites: key role of the morphology on the electrical properties of carbon black filled polymer blends. *Macromolecules*, 28, 1559-1566

Gubbels F., Jerome R., Teyssie Ph., Vanlathem E., Deltour R., Calderone A., Parente V., Bredas J.L. (1994). Selective localization of carbon black in immiscible polymer

blends: a useful tool to design electrical conductive composites. *Macromolecules*, 27, 1972-1974

Ha C., Cho Y., Go J., Cho W. (2000). Dynamic mechanical properties of polypropylene-g-maleic anhydride and ethylene-propylene-diene terpolymer blends: effect of blend preparation methods. *J Appl Polym Sci*, 77, 2777-2784

Han S.J., Lohse D.J., Condo P.D., Sperling L.H. (1999). Pressure-volume-temperature properties of polyolefin liquids and their melt miscibility. *J Polym Sci, Part B: Polym Phys*, 37:20, 2835-2844

Han S.J., Lohse D.J., Radosz M., Sperling L.H. (1998). Thermoplastic vulcanizates from isotactic polypropylene and ethylene-propylene-diene terpolymer in supercritical propane: synthesis and morphology. *Macromolecules*, 31, 5407-5414

Harrats C., Blacher S., Fayt R., Jerome R., Teyssie Ph. (1995). Molecular design of multicomponent polymer systems XIX: stability of cocontinuous phase morphologies in low-density polyethylene-polystyrene blends emulsified by block copolymers. *J Polym Sci, Part B: Polym Phys*, 33, 801-811

Harrats C., Fayt R., Jerome R., Blacher S. (2003). Stabilization of a cocontinuous phase morphology by a tapered diblock or triblock copolymer in polystyrene-rich low-density polyethylene/polystyrene blends. *J Polym Sci, Part B: Polym Phys*, 41, 202-216

He J., Bu W., Zeng J. (1997). Co-phase continuity in immiscible binary polymer blends. *Polymer*, 38:26, 6347-6353

- Heeschen W.A. (1995). A quantitative image analysis method for the determination of continuity in polymer blends. *Polymer*, 36:9, 1835-1841
- Hemmati M., Nazokdast H., Shariat Panahi H. (2001). Study on morphology of ternary polymer blends. I. Effect of melt viscosity and interfacial interaction. *J App Polym Sci*, 82:5, 1129-1137
- Hemmati M., Nazokdast H., Shariat Panahi H.(2001). Study on morphology of ternary polymer blends. II. Effect of composition. *J App Polym Sci*, 82:5, 1138-1146
- Ho R.M., Wu C.H., Su A.C. (1990). Morphology of plastic/rubber blends. *Polym Eng Sci*, 30:9, 511-518
- Hobbie E.K., Migler K.B. (1999). Vorticity elongation in polymeric emulsions. *Physical Rev Let*, 82:26, 5393-5396
- Hofmann W. (1967), *Vulcanization and Vulcanizing Agents*, 1st ed, London: Maclaren and sons Ltd
- Holden G. (2000), *Understanding Thermoplastic Elastomers*, Munich: Hanser Publishers
- Holzer R., Taunus O., Mehnert K. (1966). Composition of matter comprising polypropylene and ethylene-propylene copolymer. *U.S. Patent* 3,262,992
- Hsu W.Y., Wu S. (1993). Percolation behavior in morphology and modulus of polymer blends. *Polym Eng Sci*, 33:5, 293-302

Inaba N., Sato K., Suzuki S., Hashimoto T. (1986). Morphology control of binary polymer mixtures by spinodal decomposition and crystallization. 1. principle of method and preliminary results on PP/EPR. *Macromolecules*, 19:6, 1690-1695

Inaba N., Yamada T., Suzuki S., Hashimoto T. (1988). Morphology control of binary polymer mixtures by spinodal decomposition and crystallization. 2. further studies on polypropylene and ethylene-propylene random copolymer. *Macromolecules*, 21:2, 407-414

Inoue T. (1994). Selective crosslinking in polymer blends. I. novel selective crosslink systems for polypropylene/unsaturated elastomer blends. *J Appl Polym Sci*, 54, 709-721

Inoue T., Suzuki T. (1995). Selective crosslinking reaction in polymer blends. III. The effects of the crosslinking of dispersed EPDM particles on the impact behavior of PP/EPDM blends. *J Appl Polym Sci*, 56, 1113-1125

Inoue T., Suzuki T. (1996). Selective crosslinking reaction in polymer blends. IV. The effects on the impact behavior of PP/EPDM blends (2). *J Appl Polym Sci*, 59, 1443-1450

Ishikawa M., Sugimoto M., Inoue T. (1996). Mechanism of toughening for polypropylene blended with ethylene-propylene-diene rubber following selective crosslinking. *J Appl Polym Sci*, 68, 1495-1502

Jacoby M. (2001). Custom-made biomaterials. *Chem Eng News*, 79:6, 30-35

- Jain A.K., Gupta N.K., Nagpal A.K. (2000). Effect of dynamic crosslinking on melt rheological properties of polypropylene/ethylene-propylene-diene rubber blends. *J Appl Polym Sci*, 77, 1488-1505
- Jain A.K., Gupta N.K., Nagpal A.K. (2000). Effect of dynamic crosslinking on impact strength and other mechanical properties of polypropylene/ethylene-propylene-diene rubber blends. *J Appl Polym Sci*, 78, 2089-2103
- Jang B.Z., Uhlmann D.R., Vander Sande J.B. (1984). Crystalline morphology of polypropylene and rubber modified polypropylene. *J App Polym Sci*, 29:12, 4377-4393
- Jang B.Z., Uhlmann D.R., Vander Sande J.B. (1984). The postdispersion coalescence phenomenon in polymer-polymer blends. *Rubber Chem Tech*, 57:2, 291-306
- Jang B.Z., Uhlmann D.R., Vander Sande J.B. (1985). Rubber-toughening in polypropylene. *J App Poly Sci*, 30:6, 2485-2504
- Janssen J.M.H., Meijer H.E.H. (1993). Droplet breakup mechanisms: stepwise equilibrium versus transient dispersion. *J Rheol*, 37, 597
- Jayaraman K., Kolli V.G., Kang S., Kumar S., Ellul M.D. (2004). Shear flow behavior and oil distribution between phases in thermoplastic vulcanizates. *J App Polym Sci*, 93, 113-121
- Jeelani, S.A.K., Heartland, S. (1991). Collision of oscillating liquid drops. *Chem Eng Sci*, 46, 1807

- Jiang W., Liu C., Wang Z., An L., Liang H., Jiang B., Wang X., Zhang H. (1998). Brittle-tough transition in PP/EPDM blends: effects of interparticle distance and temperature. *Polymer*, 39:14, 3285-3288
- Jiang W., Tjong S.C., Li R.K.Y. (2000). Brittle-tough transition in PP/EPDM blends: effects of interparticle distance and tensile deformation speed. *Polymer*, 41, 3479-3482
- Jordhamo G.M., Manson J.A., Sperling L.H. (1986). Phase continuity and inversion in polymer blends and simultaneous interpenetrating networks. *Polym Eng Sci*, 26:8, 517-524
- Kammel G., Wiedenmann R. (1976). Crosslinking of polyethylene/ethylene-propylene terpolymer blends by electron irradiation. *Siemens Forschungs- und Entwicklungsberichte*, 5:3, 157-162
- Karam H.J., Bellinger J.C. (1968). Deformation and breakup of liquid droplets in a simple shear field. *Ind Eng Chem Fundam*, 7, 576
- Karger-Kocsis J., Kallo A., Kuleznev V.N. (1984). Phase structure of impact-modified polypropylene blends. *Polymer*, 25:2, 279-286
- Karger-Kocsis J., Kallo A., Szafner A., Bodor G., Senyei Zs. (1979). Morphological study on the effect of elastomeric impact modifiers in polypropylene systems. *Polymer*, 20:1, 37-43

- Karger-Kocsis J., Kiss L., Kuleznev V.N. (1984). Optical microscopy of phase separation of impact-modified PP blends and PP block copolymers. *Polym Commun*, 25:4, 122-126
- Keskkula H., Paul D.R., Barlow J.W. (1991), Polymer Blends, in '*Encyclopedia of Chemical Technology*', ed. by Kirk R.E., Othmer D.F., Kroschwitz J.I., Howe-Grant M., 4th ed., New York: Wiley, Vol 19, 837-881
- Kim B.C., Hwang S.S., Lim K.Y., Yoon K.J. (2000). Toughening of PP/EPDM blend by compatibilization. *J Appl Polym Sci*, 78, 1267-1274
- Kim Y., Cho W., Ha C., Kim W. (1995). The control of miscibility of PP/EPDM blends by adding ionomers and applying dynamic vulcanization. *Polym Eng Sci*, 35:20, 1592-1599
- Kim Y., Ha C., Kang T., Kim Y., Cho W. (1994). Rheological properties, tensile properties, and morphology of PP/EPDM/ionomer ternary blends. *J App Polym Sci*, 51, 1453-1461
- Kresge E.N. (1978), Rubbery Thermoplastic Blends, in '*Polymer Blends*', ed. by Paul D.R. and Newman S., 1st ed., New York: Academic Press, Vol 2, Ch 20, 293-318
- Kressler J., Higashida N., Inoue T., Heckmann W., Seitz F. (1993), *Macromolecules*, 26:8, 2090-2094
- Kuhn W. (1953). Spontaneous subdivision of fluid in cylindrical form into small spheres. *Kolloid Z*, 132, 84-99

- Kyu T., Ramanujam A., Kim K.J. (1998). Kinetics of vulcanization-induced phase separation in blends of syndiotactic polypropylene/ethylene propylene diene terpolymer. *Polym Mat Sci Eng*, 79, 98-99
- Labardi M., Allegrini M., Marchetti E., Sgarzi P. (1996). Scanning force microscopy of polyolefinic rubbers in homopolypropylene matrices. *J Vac Sci*, B14:2, 1509-1512
- Lee J.K., Han C.D. (1999). Evaluation of a dispersed morphology from a cocontinuous morphology in immiscible polymer blends. *Polymer*, 40, 2521-2536
- Lee J.K., Han C.D. (1999). Evaluation of polymer blend morphology during compounding in an internal mixer. *Polymer*, 40, 6277-6296
- Lee W.K., Yu K.L., Flumerfelt R.W. (1981). *Int J Multiphase Flow*, 7, 385-400
- Legge N.R. (1989). Thermoplastic elastomers-three decades of progress. *Rubber Chem Tech*, 62:3, 529-547
- Levitt L., Macosko C.W., Pearson S.D. (1996). Influence of normal stress difference on polymer drop deformation. *Polym Eng Sci*, 36:12, 1647-1655
- Li J., Favis B.D. (2001). Characterizing cocontinuous high density polyethylene/polystyrene blends. *Polymer*, 42:11, 5047-5053
- Li J., Favis B.D. (2002). Strategies to measure and optimize the migration of the interfacial modifier to the interface in immiscible polymer blends. *Polymer*, 43, 4935-4945

- Li J., Ma P.L., Favis B.D. (2002). The role of the blend interface type on morphology in cocontinuous polymer blend. *Macromolecules*, 35:6, 2005-2016
- Lieberman R.B. (1991), Polypropylene, in 'Encyclopedia of Chemical Technology', ed. by Kirk R.E., Othmer D.F., Kroschwitz J.I., Howe-Grant M., 4th ed., New York: Wiley, Vol 17, 784-819
- Lim S.W., Lee K.H., Lee C.H. (1999). Liquid-liquid phase separation and its effect on crystallization in the extruded polypropylene/ethylene-propylene-rubber blend. *Polymer*, 40, 2837-2844
- Lin B., Mighri F., Huneault M., Sundararaj U. (2003). Parallel breakup of polymer drops under simple shear. *Macromol Rapid Commun*, 24, 783-788
- Lin B., Mighri F., Huneault M., Sundararaj U. (2005). Effect of premade compatibilizer and reactive polymers on polystyrene drop deformation and breakup in simple shear. *Macromolecules*, 38:13, 5609-5616
- Lin B., Sundararaj U. (2001). Visualization of polymer blends processing. *2001 ANTEC Conference Proceedings*, 59:3, 3056-3060
- Lin B., Sundararaj U. (2004). Sheet formation during drop deformation and breakup in polyethylene/polycarbonate systems sheared between parallel plates. *Polymer*, 45, 7605-7613
- Lin B., Sundararaj U., Mighri F., Huneault M. (2002). Visualization of drop breakup in polymer-polymer systems. *2002 ANTEC Conference Proceedings*, 60:2, 1399-1403

- Lin B., Sundararaj U., Mighri F., Huneault M. (2003). Erosion and breakup of polymer drops under simple shear in high viscosity ratio systems. *Polym Eng Sci*, 43:4, 891-904
- Lohse D. J., Wissler G.E. (1991). Compatibility and morphology of blends of isotactic and atactic polypropylene. *J Mat Sci*, 26:3, 743-748
- Lohse D.J. (1986). The melt compatibility of blends of polypropylene and ethylene-propylene copolymers. *Polym Eng Sci*, 26:21, 1500-1509
- Lohse D.J. (2002). Polypropylene blend miscibility: measurement and application. *Polym Preprints*, 43:1, 309-310
- Lohse D.J., Datta S., Kresge E.N. (1991). Graft copolymer compatibilizers for blends of polypropylene and ethylene-propylene copolymers. *Macromolecules*, 24, 561-566
- Lopez-Manchado M.A., Arroyo M. (2001). New development in dynamically cured PP-EPDM blends. *Rubber Chem Tech*, 74, 211-220
- Luciani A., Jarrin J. (1996). Morphology development in immiscible polymer blends. *Polym Eng Sci*, 36:12, 1619-1626
- Luzinov I., Pagnouille C., Jerome R. (2000). Dependence of phase morphology and mechanical properties of PS/SBR/PE ternary blends on composition: transition from core-shell to triple phase cocontinuity structures. *Polymer*, 41, 3381-3389
- Lyngaae-Jørgensen J., Rasmussen K.L., Chtcherbakova E.A., Utracki L.A. (1999). Flow induced deformation of dual-phase continuity in polymer blends and alloys. Part I. *Polym Eng Sci*, 39:6, 1060-1071

- Lyngaae-Jørgensen J., Utracki L.A. (1991). Dual-phase continuity in polymer blends. *Makromol Chem, Macromol Symp*, 48-49, 189-209
- Lyu S., Bates F.S., Macosko C.W. (2000). Coalescence in polymer blends during shearing. *AIChE J*, 46:2, 229-238
- Lyu S., Bates F.S., Macosko C.W. (2002). Modeling of coalescence in polymer blends. *AIChE J*, 48:1, 7-14
- Lyu S., Jones T.D., Bates F.S., Macosko C.W. (2002). Role of block copolymers on suppression of droplet coalescence. *Macromolecules*, 35, 7845-7855
- Macosko C.W. (2000). Morphology development and control in immiscible polymer blends. *Macromol Symp*, 149, 171-184
- Mäder D., Bruch M., Maier R., Stricker F., Mülhaupt R. (1999). Glass transition temperature depression of elastomers blended with poly(propylene)s of different stereoregularities. *Macromolecules*, 32:4, 1252-1259
- Marin N., Favis B.D. (2002). Cocontinuous morphology development in partially miscible PMMA/PC blends. *Polymer*, 43:17, 4723-4731
- Marquez A., Quijano J., Gaulin M. (1996). A calibration technique to evaluate the power-law parameters of polymer melts using a torque-rheometer. *Polym Eng Sci*, 36:20, 2556-2583

Martuscelli E. (1984). Influence of composition, crystallization conditions and melt phase structure on solid morphology, kinetics of crystallization and behavior of binary polymer-polymer blends. *Polym Eng Sci*, 24:8, 563-586

Martuscelli E., Silvestre C., Abate G. (1982). Morphology, crystallization and melting behavior of films of isotactic polypropylene blended with ethylene-propylene copolymers and polyisobutylene. *Polymer*, 23:2, 229-237

Martuscelli E., Silvestre C., Bianchi L. (1983). Properties of thin films of isotactic polypropylene blended with polyisobutylene and ethylene-propylene-diene terpolymer rubbers. *Polymer*, 24:11, 1458-1468

McGinnis V.D. (1989), Cross-linking with Radiation, in '*Encyclopedia of Polymer Science and Engineering*', edited by Mark, Bikales, Overberger, Menges, 2nd ed., New York: Wiley-Interscience, Vol 4, 418-449

McGinnis V.D. (1991), Radiation Curing, in '*Encyclopedia of Chemical Technology*', ed. by Kirk R.E., Othmer D.F., Kroschwitz J.I., Howe-Grant M., 4th Ed., New York: Wiley, Vol 20, 830-859

Mehta S.D., Honnell K.G. (1997). Towards a molecular theory for polyolefin miscibility. *1997 ANTEC Conference Proceedings*, 55, 2648-2652

Mekhilef N., Favis B.D., Carreau P.J. (1997). Morphological stability, interfacial tension, and dual-phase continuity in polystyrene-polyethylene blends. *J Polym Sci, Part B: Polym Phys*, 35, 293-308

- Mekhilef N., Verhoogt H. (1996). Phase inversion and dual-phase continuity in polymer blends: theoretical predications and experimental results. *Polymer*, 37:18, 4069-4077
- Metelkin V.I., Blekht V.S. (1984). Formation of a continuous phase in heterogeneous polymer mixtures. *Colloid J USSR*, 46, 425-429
- Mighri F., Huneault M. (2001). Dispersion visualization of model fluids in a transparent couette flow cell. *J Rheol*, 45:3, 783-797
- Mighri F., Huneault M. (2002). Drop formation and breakup mechanisms in viscoelastic model fluid systems and polymer blends. *Can J Chem Eng*, 80:6, 1028-1035
- Migler K.B. (2000). Droplet vorticity alignment in model polymer blends. *J Rheol*, 44:2, 277-290
- Miles I.S., Zurek A. (1988). Preparation, structure, and properties of two-phase cocontinuous polymer blends. *Polym Eng Sci*, 28:12, 796-805
- Montezinos D., Wells B.G., Burns J.L. (1985). The use of ruthenium in hypochlorite as a stain for polymeric materials. *J Polym Sci, Polym Let Ed*, 23, 421-425
- Morerira A.C.F., Cario F.O., Soares B.G. (2003). Cocontinuous morphologies in polystyrene/ ethylene-vinyl acetate blends: the influence of the processing temperature. *J Appl Polym Sci*, 89, 386-398
- Muralidhar R., Ramakrishna D. (1988). Coalescence phenomena in liquid-liquid dispersions. *Proceedings of the European conference on mixing*, 6th, 213-220

- Noordermeer J.W.M. (1991), Ethylene-Propylene-Diene Rubber, in '*Encyclopedia of Chemical Technology*', ed. by Kirk R.E., Othmer D.F., Kroschwitz J.I., Howe-Grant M., 4th Ed., New York: Wiley, Vol 8, 978-989
- Nysten B., Ghanem A., Costa J., Legras R. (1999). Influence of EP/PP viscosity ratio on the surface morphology and elasticity of injection molded PP/EP. *Polym Int*, 48:4, 334-338
- Nysten B., Legras R., Costa J. (1995). Atomic force microscopy imaging of viscoelastic properties in toughened polypropylene resins. *J Appl Phys*, 78:10, 5953-5958
- Okamoto S., Ishida H. (2001). Nondestructive evaluation of the three-dimensional morphology of polyethylene/polystyrene blends by thermal conductivity. *Macromolecules*, 34, 7392-7402
- Parikh D.R., Edmondson M.S., Smith B.W., Winter J.M., Castille M.J., Magee J.M., Patel R.M., Karajala T.P. (1997). Structure and properties of single site constrained geometry ethylene-propylene-diene (EPDM) elastomers. *1997 ANTEC Conference Proceedings*, 55, 3434-3438
- Paul D.R., Barlow J.W. (1980). Polymer blends (or alloys). *fJ Macrmol Sci – Rev Macromol Chem*, C18:1, 109-168
- Pfau A., Janke A., Heckmann W. (1999). Determination of the bulk structure of technical multiphase polymer systems with AFM: comparative AFM and TEM investigation. *Surf Interface Anal*, 27, 410-417

- Pogodina N.V., Chapman B.R., Lohse D.J. (2003). Rheology of phase-separated ethylene-propylene copolymer-polypropylene blends with dispersion and cocontinuous morphology. *Polym Mat Sci Eng*, 89, 421-422
- Potschke P., Paul D.R. (2003). Formation of co-continuous structures in melt-mixed immiscible polymer blends. *J Macromo Sci, Part C: Polm Rev*, C43:1, 87-141
- Pukanszky B., Tudos F., Kallo A., Bodor G. (1990). Effect of multiple morphology on the properties of polypropylene/ethylene-propylene-diene terpolymer blends. *Polymer*, 30:8, 1407-1413
- Puydak R.C., Hazelton D.R. (1988). New butyl based DVAs act like thermoset rubbers. *Plast Eng*, 44:9, 37-39
- Puydak R.C., Hazelton D.R., Graham B.A., Dharmrajan N.R. (1992). Dynamically vulcanized alloys having improved stiffness/impact balance. *U.S. Patent 5,100,947*
- Puydak R.C., Hazelton D.R., Ouhadi T. (1992). Dynamically vulcanized alloys having two copolymers in the crosslinked phase and a crystalline matrix. *U.S. Patent 5,157,081*
- Quintens D., Groeninckx G., Guest M., Aerts L. (1990). Mechanical behavior related to the phase morphology of PC/SAN polymer blends. *Polym Eng Sci*, 30:22, 1474-1483
- Quintens D., Groeninckx G., Guest M., Aerts L. (1990). Phase morphology coarsening and quantitative morphology characterization of a 60/40 blend of polycarbonate of bisphenol A (PC) and poly(styrene-co-acrylonitrile) (SAN). *Polym Eng Sci*, 30:22, 1484-1490

- Quintens D., Groeninckx G., Guest M., Aerts L. (1991). Phase morphology characterization and ultimate mechanical properties of 60/40 PC/SAN blend: influence of the acrylonitrile content of SAN. *Polym Eng Sci*, 31:16, 1215-1221
- Quintens D., Groeninckx G., Guest M., Aerts L. (1991). Viscoelastic properties related to the phase morphology of 60/40 PC/SAN blend. *Polym Eng Sci*, 31:16, 1207-1214
- Radusch H.J., Merseburg T.P. (1996). Morphologiebildung in dynamisch vulkanisierten PP/EPDM-blends. *KGK Kautschuk Gummi Kunststoffe*, 49:4, 249-257
- Ramakrishna D. (1985), *Rev Chem Eng*, 3, 49
- Ramanujam A., Kim K.J., Kyu T. (2000). Phase diagram, morphology development and vulcanization induced phase separation in blends of syndiotactic polypropylene and ethylene-propylene diene terpolymer. *Polymer*, 41, 5375-5383
- Ray I., Khastgir D. (1993). Correlation between morphology with dynamic mechanical, thermal, physicomechanical properties and electrical conductivity for EVA-LDPE blends. *Polymer*, 34:10, 2030-2037
- Rayleigh L. (1879), *Proc R Soc Lon*, 29, 71-97.
- Rayleigh L. (1892). On the instability of a cylinder of viscous liquid under capillary force. *Phil Mag S 5*, 34:207, 145-154
- Reichart G.C., Graessley W.W., Register R.A., Krishnamoorti R., Lohse D.J. (1997). Anomalous attractive interactions in polypropylene blends. *Macromolecules*, 30, 3036-3041

- Reignier J., Favis B.D., Heuzey M.C. (2003). On the presence of a critical shell volume fraction leading to pseudo-pure droplet behavior in composite droplet polymer blends. *Polymer*, 44, 49-59
- Roland C.M., Bohm G.G.A. (1984). Shear induced coalescence in two phase polymeric systems. I. determination from small angle neutron scattering measurements. *J Polym Sci, Polym Phys Ed.*, 22:1, 79-93
- Rumscheidt F.D., Mason S.G. (1961). Particle motions in sheared suspensions XII. Deformation and burst of fluid drops in shear and hyperbolic flow. *J Colloid Sci*, 16, 238-261
- Saltikov S.A. (1967), *Proceedings of the 2nd International Congress for Stereology*, New York: Helias
- Sanchez I.C., Stone M.T. (2000), Statistical Thermodynamics of Polymer Solutions and Blends, in '*Polymer Blends*', edited by Paul D.R., Bucknall C.B., John Wiley & Sons Inc., Vol 1: Formulation, Ch 2, 15-53
- Sarazin P., Favis B.D. (2003). Morphology control in cocontinuous poly(L-lactide)/polystyrene blends: route towards highly structured and interconnected porosity in poly(L-lactide) materials. *Biomacromolecules*, 4:6, 1669-1679
- Sarazin P., Favis B.D. (2005). Influence of temperature-induced coalescence effects on cocontinuous morphology in poly(ϵ -caprolactone)/polystyrene blends. *Polymer*, 46:16, 5966-5978

- Sarazin P., Roy X., Favis B.D. (2004). Controlled preparations and properties of porous poly(L-lactide) obtained from a cocontinuous blends of two biodegradable polymers. *Biomaterials*, 25:28, 5965-5978
- Scott C.E., Macosko C.W. (1994). Morphology development during reactive and non-reactive blending of an ethylene-propylene rubber with two thermoplastic matrices. *Polymer*, 35:25, 5422-5433
- Scott C.E., Macosko C.W. (1995). Morphology development during the initial stages of polymer-polymer blending. *Polymer*, 36:3, 461-470
- Seki M., Nakano H., Yamauchi S., Suzuki J., Matsushita Y. (1999). Miscibility of isotactic polypropylene/ethylene-propylene random copolymer binary blends. *Macromolecules*, 32:10, 3227-3234
- Seki M., Yamauchi S., Matsushita Y. (1999). Miscibility and crystallization kinetics for the blend of isotactic polypropylene/ethylene-propylene random copolymer. *J Phy Chem Solids*, 60, 1333-1336
- Shariatpanahi H., Nazokdast H., Dabir B., Sadaghiani K., Hemmati M. (2002). Relationship between interfacial tension and dispersed-phase particle size in polymer blends. I. PP/EPDM *J App Polym Sci*, 86, 3148-3159
- Smoluchowski M. (1917), *Z Physik Chem*, 92, 129
- Speri W.M., Patrick G.R. (1975). Fiber reinforced rubber modified polypropylene. *Polym Eng Sci*, 15:9, 668-672

- Stauffer D. (1985), *Introduction to Percolation Theory*, London: Taylor and Francis
- Steinmann S., Gronski W., Friedrich C. (2001). Cocontinuous polymer blends: influence of viscosity and elasticity ratios of the constituent polymers on phase inversion. *Polymer*, 42:15, 6619-6629
- Steinmann S., Gronski W., Friedrich C. (2002). Influence of selective filling on rheological properties and phase inversion of two-phase polymer blends. *Polymer*, 43:16, 4467-4477
- Steinmann S., Gronski W., Friedrich C. (2002). Quantitative rheological evaluation of phase inversion in two-phase polymer blends with cocontinuous morphology. *Rheol Acta*, 41, 77-86
- Stone H.A., Bentley B.J., Leal L.G. (1986). An experimental study of transient effects in breakup of viscous drops. *J Fluid Mech*, 173, 131-158
- Subramanian P.M. (1983). Process for making laminar articles of polyolefin and a condensation polymer. *U.S. Patent* 4,410,482
- Subramanian P.M. (1985). Permeability barriers by controlled morphology of polymer blends. *Polym Eng Sci*, 25:8, 483-487
- Subramanian P.M. (1987). Laminar morphology in polymer blends: structure and properties. *Polym Eng Sci*, 27:9, 663-668
- Subramanian P.M. (1987). Poly(ethylene terephthalate) blends for permeability barrier applications. *Polym Eng Sci*, 27:20, 1574-1581

Sundararaj U., Dori Y., Macosko C.W. (1995). Sheet formation in immiscible polymer blends: model experiments on initial blend morphology. *Polymer*, 36:10, 1957-1968

Sundararaj U., Macosko C.W. (1995). Drop breakup and coalescence in polymer blends: the effects of concentration and compatibilization. *Macromolecules*, 28, 2647-2657

Sundararaj U., Macosko C.W., Nakayama A., Inoue T. (1995). Milligrams to kilograms: an evaluation of mixers for reactive polymer blending. *Polym Eng Sci*, 35:1, 100-114

Sundararaj U., Macosko C.W., Shih C. (1996). Evidence for inversion of phase continuity during morphology development in polymer blending. *Poly Eng Sci*, 36:13, 1769-1781

Tanem B.S., Kamfjord T., Augestad M., Lovgren T.B., Lundquist M. (2003). Sample preparation and AFM analysis of heterophase polypropylene systems. *Polymer*, 44:15, 4283-4291

Taylor G.I. (1932). The viscosity of a fluid containing small drops of another fluid. *Proc R Soc Lon*, A138, 41

Taylor G.I. (1934). The formation of emulsions in definable fields of flow. *Proc R Soc Lon*, A146, 501

Thamm R.C. (1977). Phase morphology of high impact strength blends of EPDM and polypropylene. Knit-line behavior. *Rubber Chem Tech*, 50:1, 24-34

- Tokita N. (1977). Analysis of morphology formation in elastomer blends. *Rubber Chem Tech*, 50, 292-300
- Tomasetti E., Nysten B., Rouxhet P.G., Poleunis C., Bertrand P., Legras R. (1999). Surface characterization of polypropylene/(ethylene-propylene) copolymer blends (PP/EP): application to injection molded systems. *Surf Interface Anal*, 27, 735-742
- Tomotika S. (1935). On the instability of a cylindrical thread of a viscous liquid surrounded by another viscous fluid. *Proc R Soc Lon*, A150, 322-337
- Trifonova-Van Haeringen D., Schonherr H., Vancso G.J., Vander Does L., Noordermeer J.W.M., Janssen P.J.P. (1999). Atomic force microscopy of elastomers: morphology, distribution of filler particles, and adhesion using chemically modified tips. *Rubber Chem Tech*, 72:5, 862-875
- Tsou A.H. (2001). Polymer blend morphology by dynamic AFM. *2001 ANTEC Conference Proceedings*, 59:2, 1956-1960
- Tsou A.H., Lyon M.K. (2000). Interfacial tensions in polyolefin blends. *2000 ANTEC Conference Proceedings*, 58:2, 2116-2119
- Tsou A.H., Soeda Y., Hara Y. (2004). A method for controlling dispersion size of elastomer in thermoplastic elastomer composition. *Eur Patent* 081107 A1
- Tsou A.H., Soeda Y., Wang H.C., Measmer M.B. (2004). Thermoplastic elastomer composition having viscosity-enhanced and vulcanized elastomer dispersions. *Eur Patent* 081099 A1

Tsou A.H., Westwood A.D., Schulze J.S., Herbert E.G. (2004). Cure state distributions in rubbers by dynamic nano-indentation. *Rubber Chem Tech*, 77, 678-690

Tsou A.H., Zhang G.E., Boyce M.C. (2002). Filler phase distribution in elastomer blends. *2002 ANTEC Conference Proceedings*, 60:3, 3197-3201

Tsujimoto M., Miyake S. (1994). Thermoplastic elastomer composition. *Eur Patent* 0651009 A1

Utracki L.A. (1989), *Polymer Alloys and Blends: Thermodynamics and Rheology*, Hanser Publishers

Utracki L.A. (1991). On the viscosity-concentration dependence of immiscible polymer blends. *J Rheol*, 35, 1615-1637

Van Den Berg J.H.M., Beulen J.W., Duynstee E.F.J., Nelissen H.L. (1984). Model vulcanization of EPDM compounds-part I: structure determination of vulcanization products from ethylidene norbornane. *Rubber Chem Tech*, 57:2, 265-274

Van Den Berg J.H.M., Beulen J.W., Hacking J.M.H., Duynstee E.F.J. (1984). Model vulcanization of EPDM compounds-part II: influence of temperature and time on the vulcanization products from ethylidene norbornane. *Rubber Chem Tech*, 57:4, 725-734

Van Duin M. (2000). The chemistry of phenol-formaldehyde resin crosslinking of EPDM as studied with low-molecular-weight models: part II. formation of inert species, crosslink precursors and crosslinks. *Rubber Chem Tech*, 73:4, 706-719

- Van Duin M., Keijzer Henk A.E. (1998). Chemistry of phenol-formaldehyde resin crosslinking of EPDM. *Polym Mat Sci Eng*, 79, 100-101
- Van Oene H. (1972). Modes of dispersion of viscoelastic fluids in flow. *J Colloid Interface Sci*, 40:3, 448-467
- Varanasi P.P., Ryan M.E., Stroeve P. (1994). Experimental study on the breakup of model viscoelastic drops in uniform shear flow. *Ind Eng Chem Res*, 33, 1858-1866
- Veenstra H., Hoogvliet R.M., Norder B., Posthuma de Boer A. (1998). Microphase separation and rheology of a semi-crystalline poly(ether-ester) multi-block copolymers. *J Polym Sci, Part B: Polym Phys*, 36, 1795-1804
- Veenstra H., Norder B., Van Dam J., Posthuma de Boer A. (1999). Stability of cocontinuous polystyrene/poly(ether-ester) blends in shear flow. *Polymer*, 40, 5223-5226
- Veenstra H., Van Dam J., Posthuma de Boer A. (1999). Formation and stability of cocontinuous blends with a poly(ether-ester) block copolymer around its order-disorder temperature. *Polymer*, 40, 1119-1130
- Veenstra H., Van Dam J., Posthuma de Boer A. (2000). On the coarsening of cocontinuous morphologies in polymer blends: effect of interfacial tension, viscosity and physical crosslinks. *Polymer*, 41, 3037-3045

- Veenstra H., Van Lent B.J.J., Van Dam J., Posthuma de Boer A. (1999). Cocontinuous morphologies in polymer blends with SEBS block copolymers. *Polymer*, 40:24, 6661-6672
- Veenstra H., Verkooijen P.C.J., Van Lent B.J.J., Van Dam J., Posthuma de Boer A., Nijhof A.P.H.J. (2000). On the mechanical properties of cocontinuous polymer blends: experimental and modeling. *Polymer*, 41:5, 1817-1826
- Virgilio N., Favis B.D., Pepin M., Desjardins P., L'Esperance G. (2005). High contrast imaging of interphases in ternary polymer blends using forced ion beam preparation and atomic force microscopy. *Macromolecules*, 38:6, 2368-2375
- Vroomen G.L.M., Visser G.W., Gehring J. (1991). Electron beam curing of EPDM. *Rubber World*, 205:2, 23-32
- Wang J., Tung J.F., Ahmad Fuad M.Y., Hornsby P.R. (1996). Microstructure and mechanical properties of ternary phase polypropylene/elastomer/magnesium hydroxide fire retardant compositions. *J Appl Polym Sci*, 60, 1425-1437
- Watson G.N. (1966), *A Treatise on the Theory of Bessel Functions*, 2nd ed., Cambridge: University Press
- Weis C., Leukel J., Borkenstein K., Maier D., Gronski W., Friedrich C., Honerkamp J. (1998). Morphological and rheological detection of the phase inversion of PMMA/PS polymer blends. *J Polym Bull*, 40, 235-241

Wildes G., Keskkula H., Paul D.R. (1999). Coalescence in PC/SAN blends: effect of reactive compatibilization and matrix phase viscosity. *Polymer*, 40, 5609-5621

Willemse R.C. (1999). Cocontinuous morphologies in polymer blends: stability. *Polymer*, 40, 2175-2178

Willemse R.C., Posthuma de Boer A., Van Dam J., Gotsis A.D. (1998). Cocontinuous morphologies in polymer blends: a new model. *Polymer*, 39:24, 5879-5887

Willemse R.C., Posthuma de Boer A., Van Dam J., Gotsis A.D. (1999). Cocontinuous morphologies in polymer blends: the influence of the interfacial tension. *Polymer*, 40, 827-834

Willemse R.C., Ramaker E.J.J., Van Dam J., Posthuma de Boer A. (1999). Coarsening in molten quiescent polymer blends: the role of the initial morphology. *Polym Eng Sci*, 39:9, 1717-1725

Willemse R.C., Ramaker E.J.J., Van Dam J., Posthuma de Boer A. (1999). Morphology development in immiscible polymer blends: initial blend morphology and phase dimensions. *Polymer*, 40:24, 6651-6659

Willemse R.C., Speijer A., Langeraar A.E., Posthuma de Boer A. (1999). Tensile moduli of cocontinuous polymer blends. *Polymer*, 40:24, 6645-6650

Willis J.M., Caldas V., Favis B.D. (1991). Processing-morphology relationships of compatibilized polyolefin/polyamide blends. *J Mat Sci*, 26, 4742-4750

- Willis J.M., Favis B.D., Lavallee C. (1993). The influence of interfacial interactions on the morphology and thermal properties of binary polymer blends. *J Mat Sci*, 28, 1749-1757
- Wu S. (1982), *Polymer Interface and Adhesion*, New York: Marcel Dekker Inc.
- Wu S. (1985). Phase structure and adhesion in polymer blends: a criterion for rubber toughening. *Polymer*, 26:12, 1855-1863
- Xiao H., Huang S., Jiang T., Cheng A. (2002). Miscibility of blends of ethylene-propylene-diene terpolymer and polypropylene. *J App Polym Sci*, 83, 315-322
- Yamaguchi M., Miyata H., Nitta K. (1996). Compatibility of binary blends of polypropylene with ethylene- α -olefin copolymer. *J App Polym Sci*, 62:1, 87-97
- Yang D., Zhang B., Yang Y., Fang Z., Sun G., Feng Z (1984). Morphology and properties of blends of polypropylene with ethylene-propylene rubber. *Polym Eng Sci*, 24:8, 612-617
- Yerina N., Magonov S. (2003). Atomic force microscopy in analysis of rubber materials. *Rubber Chem Tech*, 76:4, 846-859
- Yuan Z., Favis B.D. (2005). Coarsening of immiscible cocontinuous blends during quiescent annealing. *AIChE J*, 51:1, 271-280
- Zaharescu T., Setnescu R., Jipa S., Setnescu T. (2000). Radiation processing of polyolefin blends. I. crosslinking of EPDM-PP blends. *J App Polym Sci*, 77, 982-987

Zhao R., Dai G. (2002). Mechanical property and morphology comparison between the two blends poly(propylene)/ethylene-propylene-diene monomer elastomer and poly(propylene)/maleic anhydride-g-ethylene-propylene-diene monomer. *J App Polym Sci*, 86, 2486-2491

Zhu S., Chan C. (1998). Transition of phase continuity induced by crosslinking and interfacial reaction during reactive processing of compatibilized PVC/SBR blends. *Polymer*, 39:26, 7023-7032

Ziff, R. M. (1986). Kinetics of polymer degradation. *Macromolecules*, 19, 2513-2519

ANNEX I

DETERMINATION OF THE AVERAGE SHEAR RATE IN AN INTERNAL MIXER

The purpose of this annex is to show how to estimate the average shear rate for the blend materials in an internal Haake mixer. The average values of the shear rate determined by using this procedure have been used throughout this thesis. Based on these shear rate values, other rheological ratios (e.g. the viscosity ratio, elasticity ratio etc.) have been calculated.

A.I.1 Theory

This calibration technique has been developed by Marquez et al. (1996). It is based on the hypothesis that the mixing chamber of an internal mixer can be represented by two adjacent coaxial cylinder viscometers. The rollers are simulated as uniform cylinders as shown in Figure A.I.1.

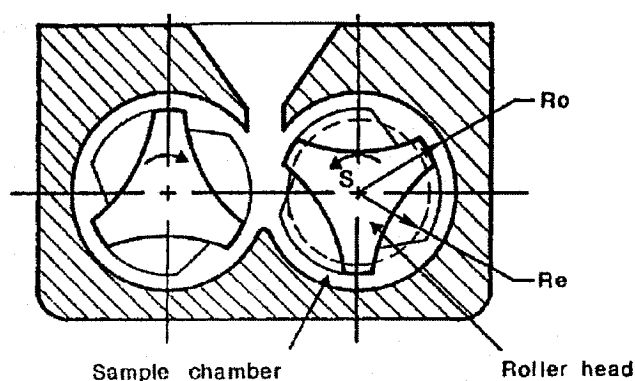


Figure A.I.1 Representation of the coaxial cylinders assumption for the measuring head. (Marquez et al., 1996)

Considering that polymer materials are in a power-law region at the blending shear rate, we have:

$$\sigma = \eta \dot{\gamma} \dots\dots\dots (A.I.1)$$

$$\eta = m \dot{\gamma}^{n-1} \dots\dots\dots (A.I.2)$$

where, σ is the shear stress, $\dot{\gamma}$ is the shear rate, η is the viscosity, and m and n are the consistency and flow indexes, respectively.

The total torque (M_T) measured by an instrument can be written as,

$$M_T = C(n) \cdot m \cdot S_1^n \dots\dots\dots (A.I.3)$$

$$\text{with, } C(n) = 2\pi L R_o^2 \left[\frac{2}{n(\alpha^{-2/n} - 1)} \right]^n (1 + b^{n+1}) \dots\dots\dots (A.I.4)$$

where, S_i is the angular velocity of the respective rotors, b is the relative speed between the two rotors (S_2/S_1), R_o is the outside radius of the rotors, and L is the length of the mixing chamber. The coefficient α is the ratio between the equivalent inner radius R_e and outside radius R_o .

Thus, the average shear rate of the material in mixing chamber can be calculated from the following equation,

$$\dot{\gamma}_{r,\theta} = \frac{2S_1 \alpha^{1/n}}{n(1 - \alpha^{2/n})} \dots\dots\dots (A.I.5)$$

Finally, the average viscosity of the melt can be obtained by the relation,

$$\eta = \frac{\sigma_{r\theta}}{\dot{\gamma}_{r\theta}} = m \left[\frac{2S_1 \alpha^{1/n}}{n(1 - \alpha^{2/n})} \right]^{n-1} \dots\dots\dots (A.I.6)$$

Thus, the variables $C(n)$, m , n , and α need to be determined. The parameter α is used to take into account the irregularity of the roller geometry and its influence on the flow behavior of the processed melts. Thus, it is an adjustable parameter which depends on each individual material and its value should be chosen to obtain a good correspondence between the values of viscosity obtained from the internal mixer to that obtained from conventional rheometer.

From equation A.I.3 we can see that a plot of $\log M_T$ with $\log S_l$ yields the values of n in the slope. The value of $C(n) \cdot m$ can be obtained from the ordinate at $S_l = 1$.

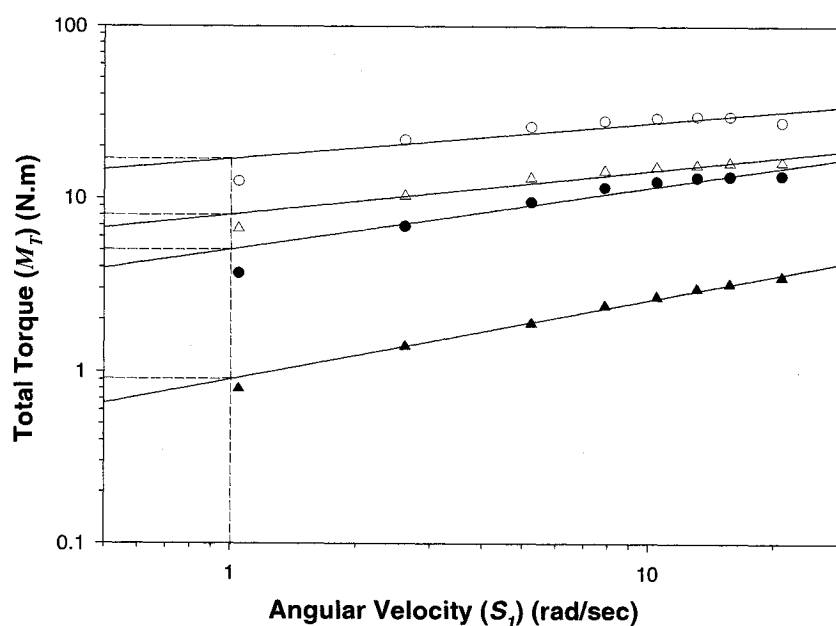
A.I.2 Calculations

To determine the value of $C(n) \cdot m$ and n , the various materials used in this thesis were melt blended in an internal Haake mixer at different rotor speeds and the corresponding torque values are noted. The results are given in the following Table A.I.1.

Table A.I.1 Total torque values for the pure materials at different rotor speeds

Angular velocity (S_I)		Mean total torque (M_T) (N.m)			
RPM	rad/sec	EP 1	EP 3	PP 1	PP 2
10	1.05	3.7	12.6	0.8	6.7
25	2.62	6.9	21.8	1.4	10.3
50	5.24	9.5	26.1	1.9	13.1
75	7.86	11.6	28.3	2.4	14.4
100	10.48	12.5	29.3	2.7	15.1
125	13.10	13.2	29.9	3.0	15.5
150	15.71	13.4	29.9	3.2	16.0
200	20.95	13.6	27.8	3.5	16.1

The above data is plotted in the following plot of $\log M_T$ vs $\log S_I$.

**Figure A.I.2 Plot of Total torque (M_T) vs Angular velocity (S_I) (rad/sec)**

The values of $C(n) \cdot m$ and n obtained from the above plot are listed in the following Table A.I.2.

Table A.I.2 Material characteristics

Materials	n	$C(n) \cdot m$ at $S_I = 1$	α
EP 1	0.3581	5.039	0.732
EP 3	0.2096	16.87	0.755
PP 1	0.4571	0.9029	0.658
PP 2	0.2526	8.026	0.715

Now, for each material we need to choose the value of α in between 0 and 1, such that the best correspondence between the values calculated from the data obtained on internal mixer using equation A.I.5 and A.I.6 and the values obtained from rheometer are obtained. The chosen values of α for each material are listed above in Table A.I.2. The calculated values of shear rate and viscosity are plotted along with the values of the shear rate and complex viscosity obtained from the rheometer in the following Figure A.I.3

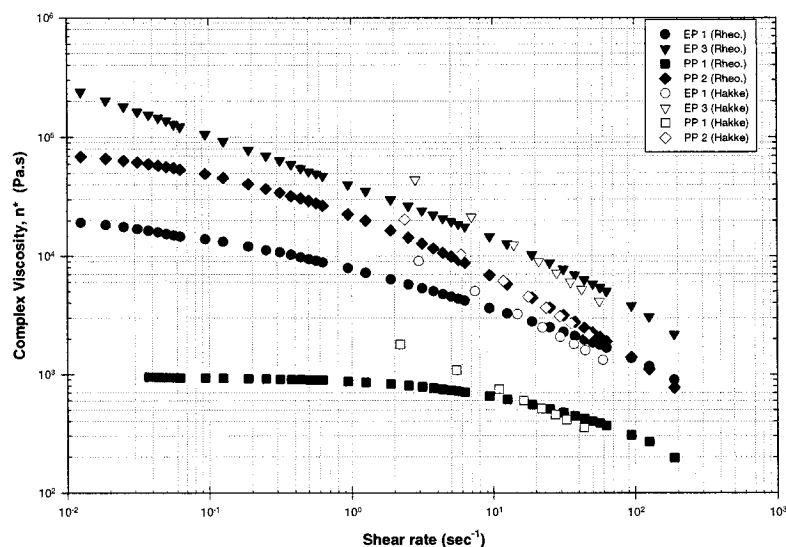


Figure A.I.3 Correspondence between the calculated values of viscosity and shear rate to the values obtained from the Bohlin (CSM) rheometer

It can be seen in the above figure that the data fits very well considering the values of the various variables listed in Table A.I.2. The values of shear rate at the actual rotor speed used to carry out melt blending in this thesis, i.e. 100 rpm, are determined using equation A.I.5. These values are listed in the following Table A.I.3.

Table A.I.3 Estimated shear rate of the materials in the Haake internal mixer at a rotor speed of 100 rpm

Materials	EP 1	EP 3	PP 1	PP 2
Shear rate (s ⁻¹)	30	28	22	24

ANNEX II

THEORETICAL ESTIMATION OF THE INTERFACIAL TENSION

The purpose of this annex is to illustrate the calculations for the theoretical estimation of interfacial tension between EPDM and PP at the melt blending temperature of 190°C.

An experimental determination of the interfacial tension between EPDM and PP using the 'Breaking thread method' was unsuccessful because of its ultra-low value and hence very long breakup times required. The interfacial tension can be determined theoretically, using 'Harmonic mean' equation. The harmonic mean equation for the estimation of the interfacial tension can be written as follows,

$$\gamma_{12} = \gamma_1 + \gamma_2 - \frac{4 \gamma_1^d \gamma_2^d}{\gamma_1^d + \gamma_2^d} - \frac{4 \gamma_1^p \gamma_2^p}{\gamma_1^p + \gamma_2^p} \dots\dots\dots (A.II.1)$$

where, γ_{12} is the interfacial tension between the components; γ_i is the surface tension, γ_i^d is the surface tension due to dispersion (nonpolar) forces, and γ_i^p is the surface tension due to polar forces for component 'i'.

From the theory of fractional polarity, the surface tension of the polymer is the sum of the surface tension due to nonpolar and polar interactions. Thus,

$$\gamma = \gamma^d + \gamma^p \dots\dots\dots (A.II.2)$$

The surface tension due to polar interactions (γ^p) can be determined from the polarity (x^p) of the polymer using the following equation,

$$\gamma^p = x^p \times \gamma_{\text{polyethylene}} \dots\dots\dots (A.II.3)$$

The surface tension (γ) for a random copolymer usually follows the linear relationship,

$$\gamma = x_1 \gamma_1 + x_2 \gamma_2 \dots\dots\dots (A.II.4)$$

where, γ_i is the surface tension and x_i is the mole fraction of component ‘i’.

All of the above equations and variable values are taken from the book “Polymer Interface and Adhesion” by Souheng Wu.

The EPDM used in this work is a random copolymer of ethylene, propylene, and diene. Thus, its surface tension is obtained using equation A.II.3. The average ethylene, propylene, and diene content of the various grades of EPDM used in this work is given in the following Table A.II.1

Table A.II.1. Average composition of the EPDM polymer

Material	Ethylene content (%)	Propylene content (%)	Diene content (%)
EP 1	62.0	34.0	4.0
EP 2	52.0	43.7	4.3
EP 3	53.0	42.7	4.3
Average	55.7	40.1	4.2

The surface tension values at 180°C, the change in surface tension with temperature, and the polarity of polypropylene and polyethylene are listed in Table A.II.2. The values of the surface tension at a melt blending temperature of 190°C are obtained by extrapolating the data. The value of the surface tension for EPDM is estimated based on its average composition obtained from Table A.II.1 and using equation A.II.3. In addition, the surface tension values due to nonpolar and polar interactions, estimated using equations A.II.2 and A.II.3 are also listed in Table A.II.2.

Table A.II.2. Estimation of the surface tension and its polar and nonpolar fractions

	γ at 180°C (mN/m)	$-(d\gamma/dT)$ (mN/m°C)	γ at 190°C (mN/m)	Polarity (x^p)	γ^p	γ^d
Polypropylene	20.8	0.058	20.22	0.020	0.519	19.701
Polyethylene	26.5	0.057	25.93	0		
EPDM			22.55		0.208	22.342

Now, substituting all the estimated values in the harmonic mean equation (A.II.1), we obtain the value of the interfacial tension between EPDM and PP, at the melt blending temperature of 190°C, to be 0.3 mN/m. This value of interfacial tension between EPDM and PP corresponds very well with the values estimated by various other authors, as already mentioned in Chapter 4.

ANNEX III

DETERMINATION OF THE CRYSTALLINITY OF POLYPROPYLENE

The purpose of this annex is to determine the crystallinity of commercial polypropylene materials used in this thesis.

For these measurements the samples were cut from the blend of PP with 0.5 wt.% antioxidant Irganox B 225. The blending was carried out in an internal mixer at 190°C, 100 rpm and for 8 minutes. The blending was carried out in order to determine the crystallinity of materials with the same thermal history as that of the other blends.

The measurements were done using a Perkin Elmer thermal analysis system, Pyris I. The blend sample weight was in the range of 5 to 10 mg. A heating rate of 10°C/min was applied from 50°C to 220°C.

The degree of crystallinity (X_c) of the PP was calculated as follows,

$$X_c = \frac{\Delta H_f}{\Delta H_f^o} \dots\dots\dots (A.III.1)$$

Where, ΔH_f denotes the measured enthalpy of melting or fusion, and ΔH_f^o denotes the enthalpy for 100% crystalline PP (165 ± 18 J/g is usually reported in the literature). Thus the measured values of enthalpies (ΔH_f , enthalpy of melting or fusion, and ΔH_c , enthalpy of crystallization) and crystallinity are listed in the following Table A.III.1.

Table A.III.1 Crystallinity of polypropylene

Sr. No.	Materials	Sample Wt. (mg)	ΔH_f (J/g)	ΔH_c (J/g)	Crystallinity X_c (%)
1	PP 1 + Irganox	8.98	81.228	87.321	50.0
2	PP 2 + Irganox	5.37	78.227	83.013	48.0

ANNEX IV

IRRADIATION CROSSLINKING OF THE POLYMERS

The objective of this annex is to provide more information on irradiation of the polymers, their responses to irradiation, and to show how the particular technique is exploited in this thesis and can be used in the future for morphology investigations in the field of polymer blends.

A.IV.1 Introduction and Theory

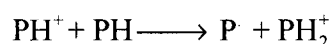
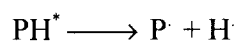
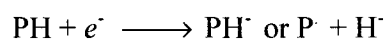
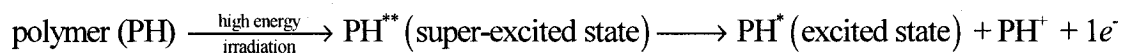
The effect of electromagnetic radiation on polymers was studied quite thoroughly in the past and is very well known to the scientific community. The interaction of electromagnetic radiation with polymeric materials is known to form three-dimensional network structures which generally improve the overall physical or chemical properties of the original substrate. The crosslinking reaction can be induced by non-particulate radiations, such as microwave, infrared, light energies, X rays, and gamma rays or particulate radiations, such as alpha particles, beta particles, high energy electrons, protons, deuterons, neutrons, etc. The most common sources of radiation for commercial crosslinking include cobalt 60 (^{60}Co), low and high-energy electron accelerators, light energy (ultraviolet-visible), infrared sources of energy, and plasma or glow discharge energy sources (microwave or radio-frequency range). In particular, radioisotope sources (^{60}Co) are advantageous, as they produce gamma rays with high penetration capabilities in the energy range of 1.17-1.33 MeV.

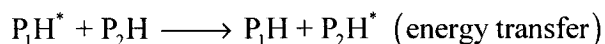
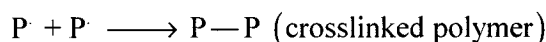
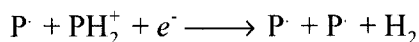
Not all polymers self crosslink in response to high-energy electromagnetic radiation. The response of the polymer also depends on the medium used to carry out irradiation. Some polymers crosslink in inert atmosphere while others degrade, if the irradiation is carried out in air, i.e. in the presence of oxygen. In general, polymers can be divided into two categories, one which mainly crosslinks and the other which mainly degrades as a result of electromagnetic radiations. General mechanisms of crosslinking and chain scission (degradation) are described in the next section.

The amount of crosslinking achieved or the extent of chain scission obtained in any polymer depends on many factors including the material itself, the type of radiation used, the dose rate of radiation, temperature of irradiation, the medium in which the radiation is carried out (i.e. inert or in air), and most importantly on the total radiation dose.

A.IV.2 Theories of crosslinking by radiation

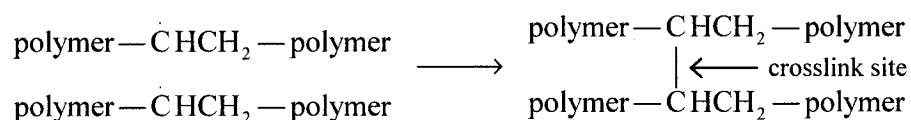
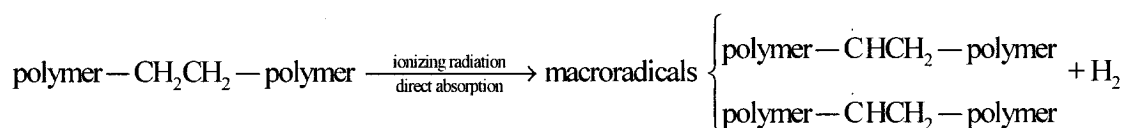
The mechanism of crosslinking by radiation is either free radical or ionic. Crosslinking by interaction with high-energy (ionizing) radiation sources occurs through both of these mechanisms.



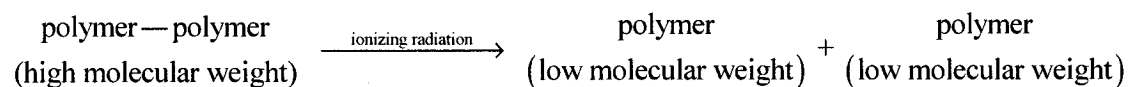


Or, in more general terms,

Crosslinking:



Scission:



Free radical intermediates, complex network structures, and various types of unsaturation sites have been observed directly by electron spin resonance, solid-state nuclear magnetic resonance, and infrared techniques. The approximate time frame for radiation-induced reactions to occur is between 10^{-18} and 10^{-2} s.

The degradation of irradiated materials often continues, in storage or in use, long after the material is removed from the radiation environment. This effect is due to

continuing free-radical mediated oxidation. This induced degradation can be very large in certain materials. However, it is not observed in comparable samples that had not been exposed to the radiation. This post-irradiation reaction is initiated by reactive intermediates formed in the course of the irradiation. It frequently involves migration of long-lived radicals from crystalline regions to amorphous regions where they can subsequently react. Significant post-irradiation oxidation effects may take place over weeks or years, and may result in degradation that is much more extensive than that which occurred immediately after irradiation. The occurrence and magnitude of post-irradiation effects are strongly material dependent. Materials, free of crystalline regions or those, which are effectively stabilized against oxidation, are much less prone to post-irradiation effects.

A.IV.3 Application of irradiation crosslinking in morphology investigation

Many of the morphology characterization techniques in the field of polymer blends, e.g. matrix dissolution, solvent gravimetry etc., frequently require the use of selective solvents for the blend components. If the blending polymers are very different in nature, i.e. usually systems with high interfacial tension, then sometimes it is easy to find selective solvents for each of the polymers in the blend. However, in most cases it is impossible to dissolve either of the phases in the blend without dissolving the other. Thus, finding a selective solvent for both the blend components remains a big hurdle in morphology investigation.

As discussed throughout this thesis, EPDM and PP are very alike, as evidenced by their ultra-low interfacial tension. In EPDM/PP blends, EPDM can be selectively dissolved during the morphology investigation of the blend. However, it is impossible to find a solvent to dissolve PP without dissolving EPDM. Because of their similar nature it is also quite difficult to find another property which could be exploited for studying the morphology of the blend and thus, to date, researchers in the field have been successful in investigating only a part of the blend morphology. To fully investigate the blend morphology it is absolutely necessary to find a way to dissolve the PP phase in the blend without affecting the morphology of the EPDM phase generated during melt blending.

On investigation we found that EPDM and PP respond very differently to irradiation. EPDM is a polymer, which mainly self-crosslinks and PP is a material, which undergoes mainly chain scission reaction when the irradiation is carried out in air. PP self-crosslinks, if the irradiation is carried out in an inert atmosphere.^{34,35} Thus, if the blend of EPDM and PP obtained after melt mixing and quenching is irradiated to the correct radiation dose, then we can crosslink the EPDM phase without affecting its morphology generated during melt blending. The PP phase in the blend will degrade as a result of irradiation, which is even better since it will eventually allow for better, faster and easier dissolution of the PP from the blend sample.

Once the EPDM phase is crosslinked one should be able to dissolve PP without dissolving EPDM, as it is then in the form of an insoluble gel. Subsequent

investigations can be carried out on this gel to reveal the details of the morphology of the blend. Additionally, the dissolution of PP will also enable investigation of its continuity development in the EPDM matrix by the solvent gravimetry technique.

It has been found in the literature that the critical gelation of EPDM begins at the total radiation dose of 60 kGy, and the optimum crosslinking of EPDM can be obtained near the total radiation dose of 150 kGy. Thus, all the blends at all the viscosity ratios are subjected to γ -irradiation in air with a ^{60}Co source, using a commercial carrier type 8900 irradiator with the dose rate of 25 kGy/hr and to an average optimal total dose of 154 kGy.

The gel content achieved in EPDM by irradiation is then determined and is listed in the Table A.VI.2 of Annex–VI. PP is found to dissolve completely in boiling xylene. The continuity of PP is also determined and the results, without correction of total EPDM gel content, are shown in Figure A.VI.3. Those with the correction are shown in Figure A.VI.4. The micrographs of EPDM gel forming dispersed and cocontinuous structures obtained on PP matrix dissolution are already shown in chapter 4 and 5 of this thesis.

All these results demonstrate that this technique can be successfully employed for the complete morphology investigation of EPDM/PP polymer blends. This technique, thus, enables one to dissolve a blend component without affecting the morphology of the other blend component generated during melt blending. Depending on the response of the material to various high-energy electromagnetic radiations,

already mentioned in the section A.IV.1, the technique can be utilized to overcome the difficulties of finding selective solvents for the complete morphology investigation of these polymer blends.

ANNEX V

INVESTIGATION OF THE PP DISPERSED PHASE MORPHOLOGY IN AN EPDM MATRIX

The purpose of this annex is to summarize the work done for investigating the PP morphology developed in an EPDM matrix for different viscosity ratio blends. However, these results were not included in the main body of this thesis because of unsatisfactory results. The reasons for failure, suggestions to obtain better results, and the limitations of the techniques used are appropriately discussed.

A.V.1 Dispersed phase dissolution and SEM microscopy

Since, the EPDM dispersed phase dissolution from the PP matrix and subsequent scanning electron microscopy of such samples yielded good results, initially, the same procedure was employed for investigating the PP dispersed phase morphology. Thus, in order to dissolve the PP phase, the samples were directly cut from the irradiation crosslinked blends. The necessity for crosslinking the blends by irradiation is already discussed in Annex-IV.

The cut samples were cryo-microtomed to obtain a good flat surface. The microtomed samples were then boiled in xylene for about 45 mins to dissolve the PP phase and were then dried completely in the vacuum oven. The samples were then coated with a gold-palladium alloy and the SEM micrographs were obtained at different

blend compositions for different viscosity ratio blends. The results are shown in the following Figures A.V.1-A.V.6.

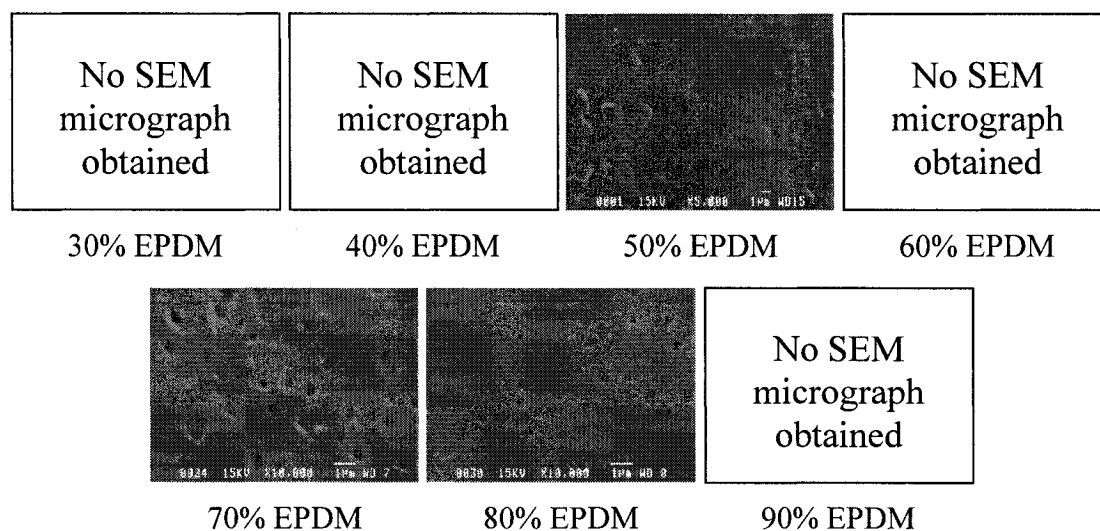


Figure A.V.1 SEM micrographs of PP 2/EP 1 (1.5) blend systems

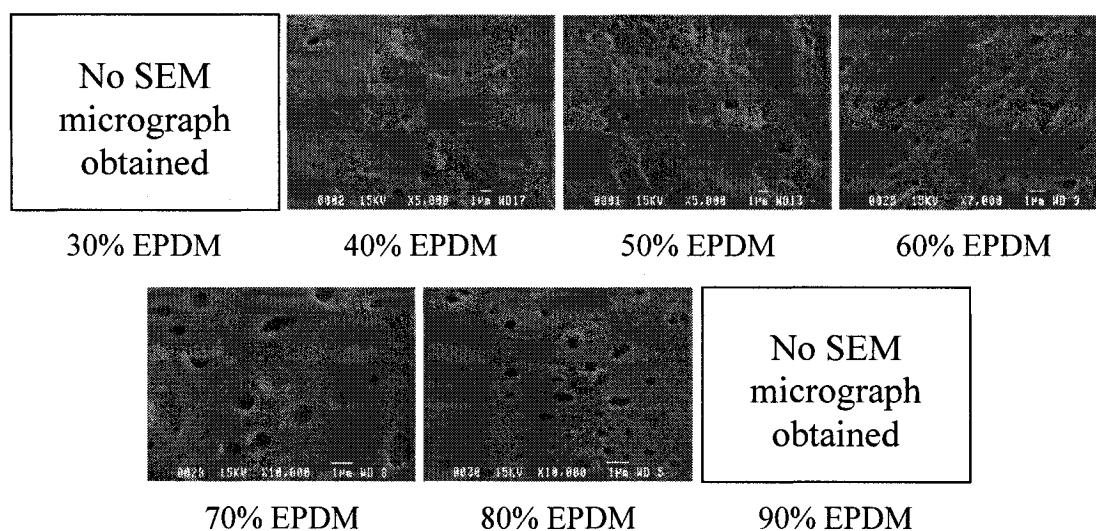


Figure A.V.2 SEM micrographs of PP 2/EP 2 (0.7) blend systems

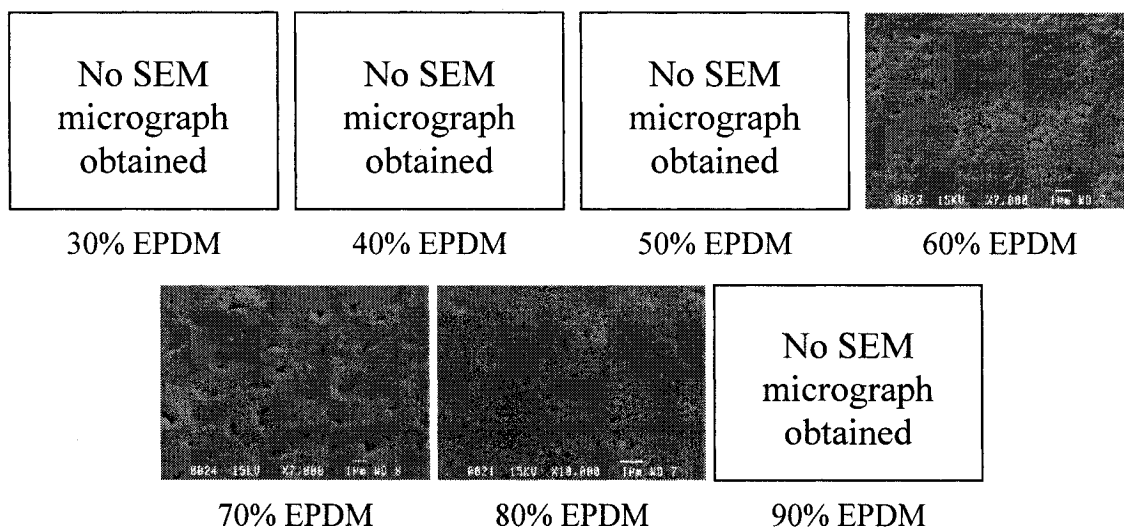


Figure A.V.3 SEM micrographs of PP 2/EP 3 (0.4) blend systems

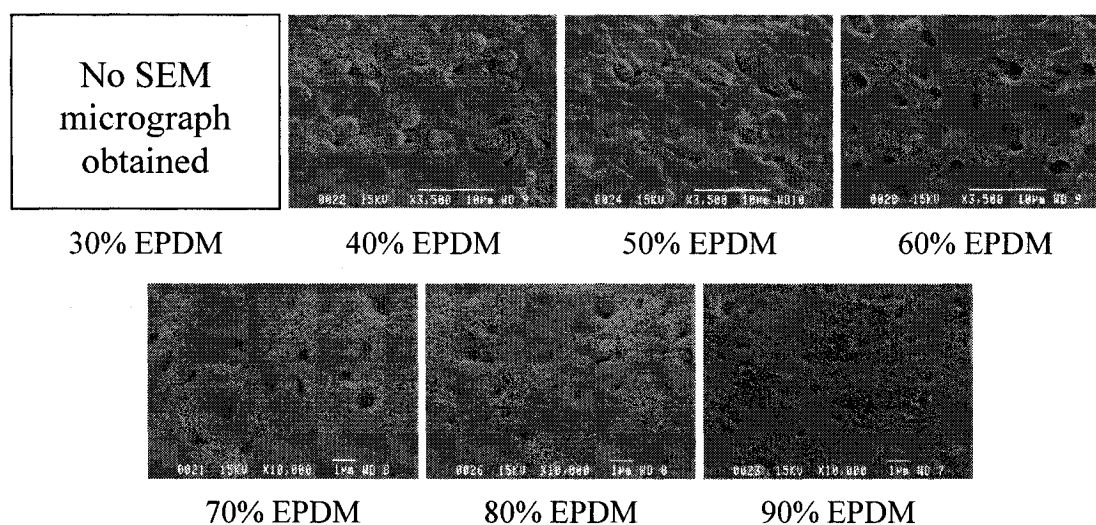


Figure A.V.4 SEM micrographs of PP 1/EP 1 (0.2) blend systems

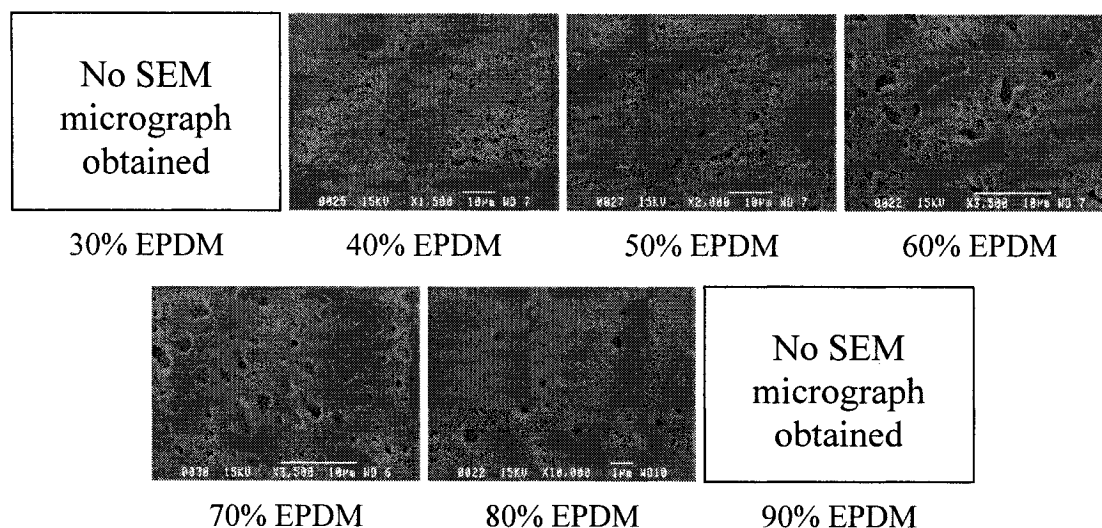


Figure A.V.5 SEM micrographs of PP 1/EP 2 (0.1) blend systems

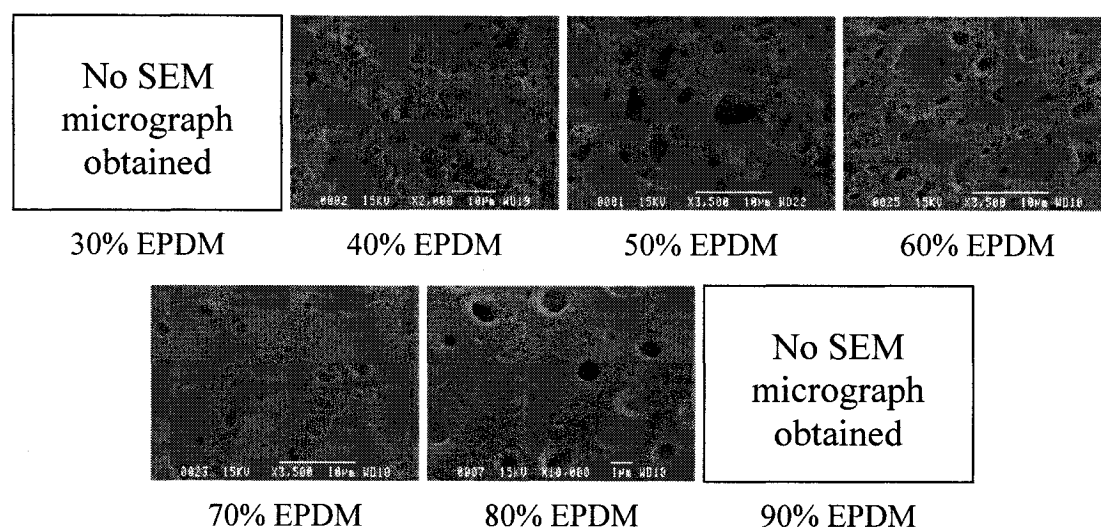


Figure A.V.6 SEM micrographs of PP 1/EP 3 (0.1) blend systems

The above micrographs show that, at low compositions, the PP minor phase is very finely distributed, usually about 200 to 800 nanometers, in the EPDM matrix. Because of the high viscosity matrix, the particle sizes are also quite similar. Though good micrographs are obtained quite a few times, it can also be noted that some of the

micrographs are not clearly showing the morphology, especially those in the mid composition range displaying cocontinuous structures. These micrographs show somewhat collapsed cocontinuous structures.

This collapse and deformation in the morphology can be explained by the physical observations carried out during the PP dissolution and vacuum drying of the sample. It was noted during the experiment that although the crosslinked EPDM matrix does not dissolve in xylene, it does swell in it. These swollen structures on vacuum drying were found to shrink below their original dimensions. This shrinking was more significant in cocontinuous samples because of the pores generated on complete dissolution of the cocontinuous PP phase. Though this phenomenon is acceptable for % continuity measurement, since it only produces larger error bars, it is not acceptable for the characterization of morphology as it affects the phase dimensions. Therefore, these results were not included in this thesis.

Nevertheless these results are not completely useless either, they did teach us a valuable lesson which was utilized during the matrix dissolution study of cocontinuous samples. On matrix dissolution, those cocontinuous samples were freeze dried instead of normal vacuum drying. This helped preserve the shape of the cocontinuous structure instead of its collapse as seen in the above micrographs on normal vacuum drying. Similarly, the freeze drying for the above samples can be expected to yield better results, however, this work has not been carried out.

Some of the above micrographs showed a somewhat grainy structure on the EPDM surface. This is due to the re-crystallization of dissolved PP back on the EPDM surface and is not due to the adverse effect of solvent on the EPDM phase. This fact can be confirmed from the following micrograph in Figure A.V.7, where no such grainy structure is evident after a similar solvent treatment on irradiation crosslinked pure EPDM material.

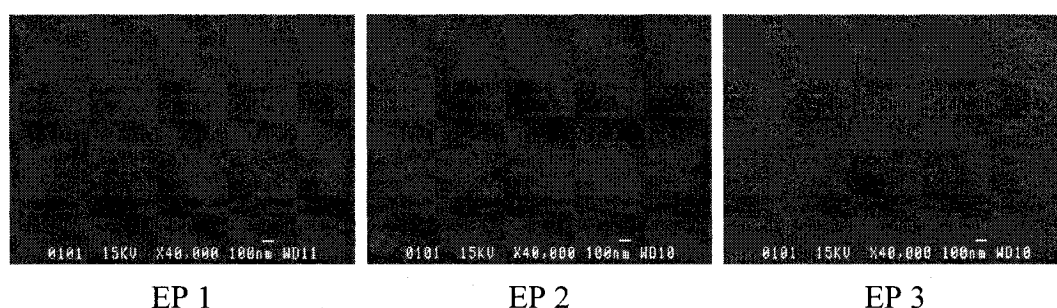


Figure A.V.7 SEM micrographs of pure EPDM after subsection to xylene for more than 45 mins

A.V.2 Solvent etching

In order to obtain better contrast between EPDM and PP another technique of solvent etching was used. In principle, as the contrast between the different blend phases will be obtained due to the differences between the etching rates of materials, there is no need for irradiation crosslinking of the blends. Therefore, the normal blends, ones without irradiation crosslinking, were employed for these experiments. In this technique well cryo-microtomed blend samples were etched by the mixture of solvents (potassium permanganate and sulfuric acid) for about 20 minutes. The etched samples were then dried and coated with a gold-palladium alloy. Subsequently, SEM

observations were carried out. The results are shown in the Figure A.V.8-A.V.13 with different blend compositions and at different viscosity ratios.

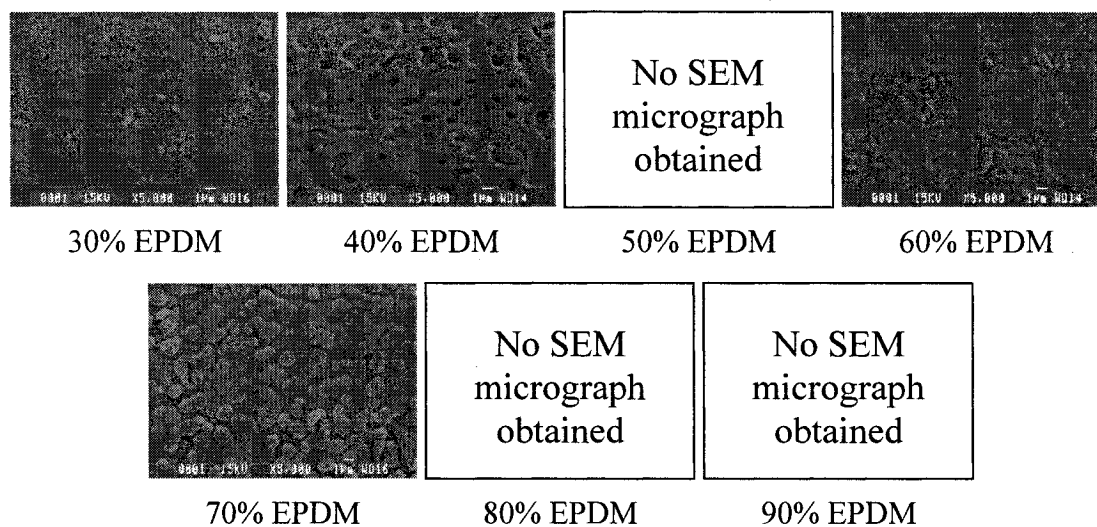


Figure A.V.8 SEM micrographs of PP 2/EP 1 (1.5) blend systems

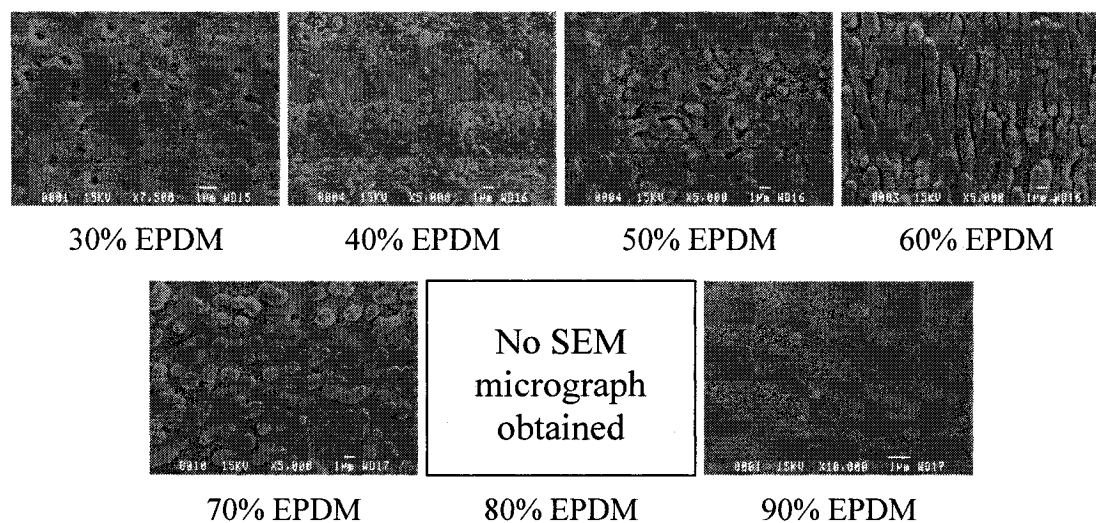


Figure A.V.9 SEM micrographs of PP 2/EP 2 (0.7) blend systems

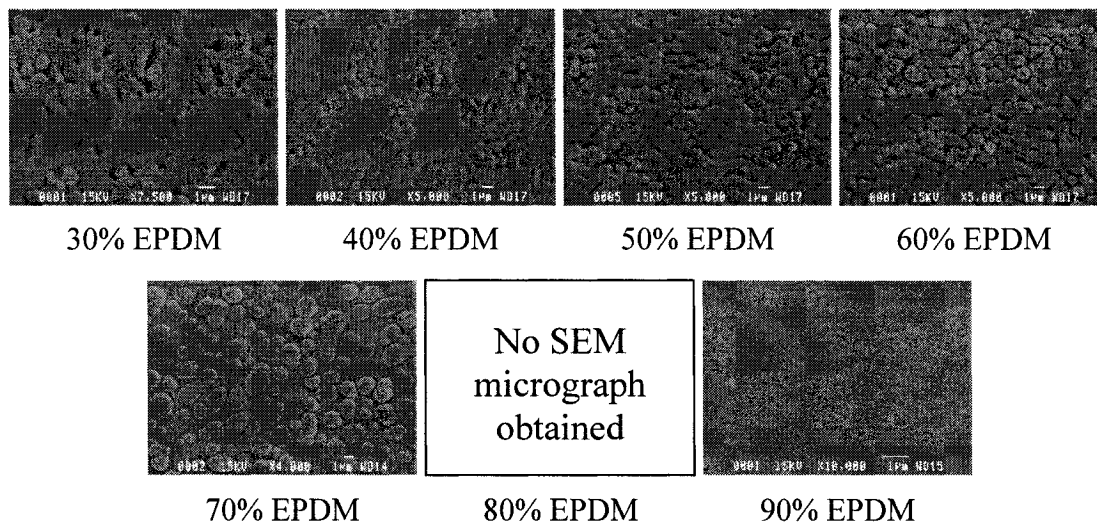


Figure A.V.10 SEM micrographs of PP 2/EP 3 (0.4) blend systems

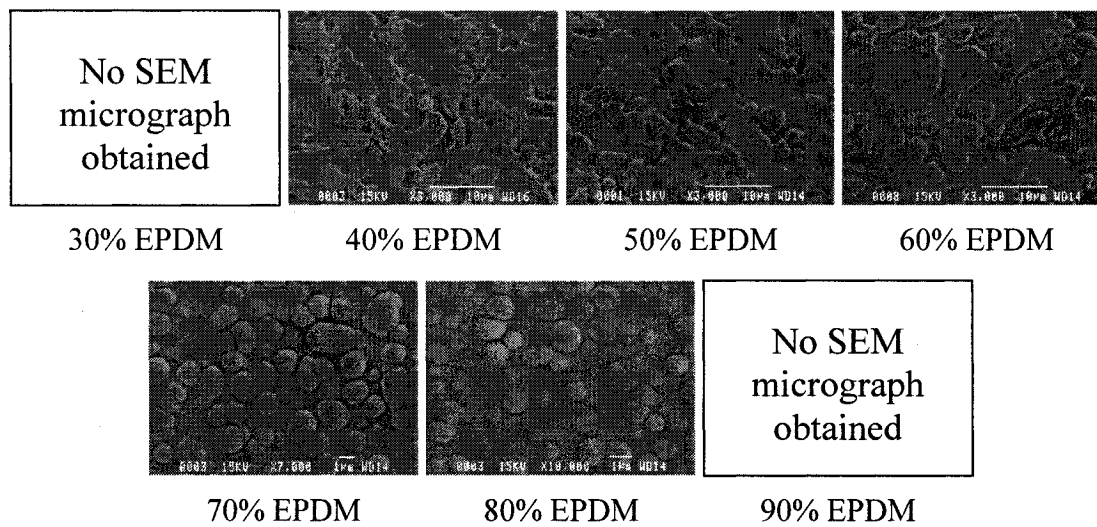


Figure A.V.11 SEM micrographs of PP 1/EP 1 (0.2) blend systems

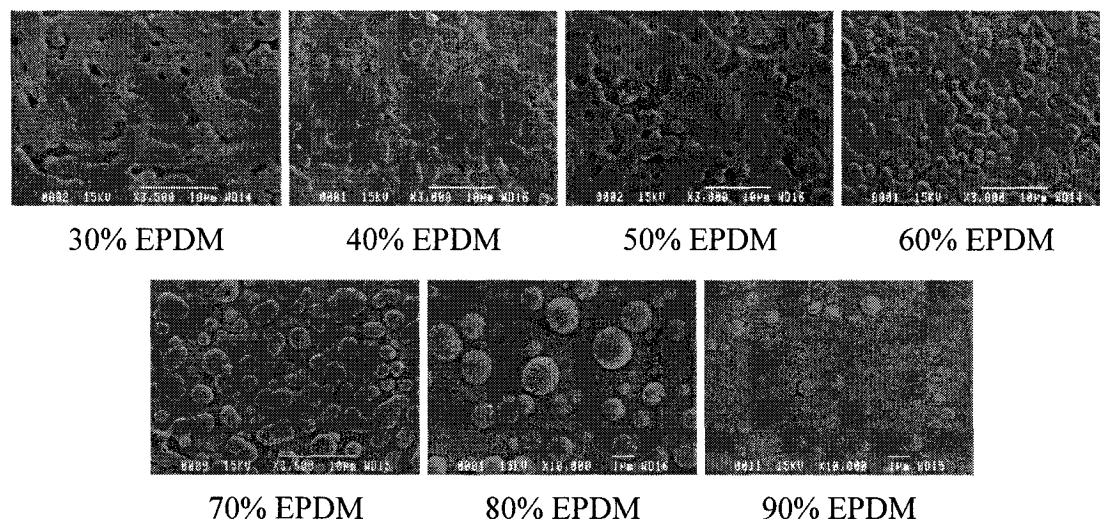


Figure A.V.12 SEM micrographs of PP 1/EP 2 (0.1) blend systems

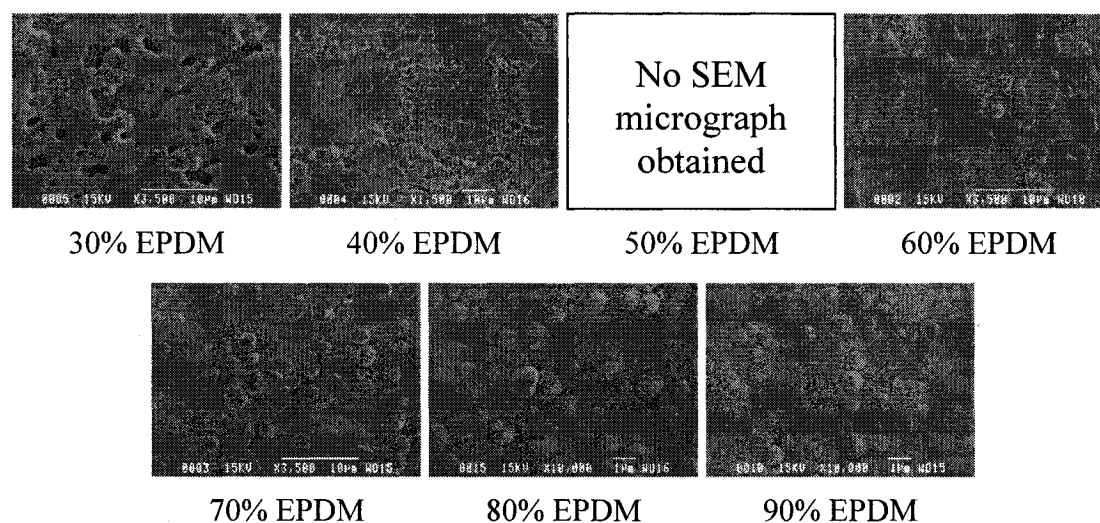


Figure A.V.13 SEM micrographs of PP 1/EP 3 (0.1) blend systems

As evident from the above figures, the etching rate of EPDM is more than PP. Thus, at higher compositions of EPDM, the dispersed domains of PP are evident. Conversely, deeper holes of EPDM are evident at lower compositions of EPDM. It can be seen that, at lower compositions of PP, the dispersed phase is distributed in very fine domains. It is also evident that no appropriate micrographs were obtained at lower

compositions of PP for many different viscosity ratio blends. This is thought to be because of higher etching rates and the very small domain sizes of PP. Thus, very low etching times were tried, but not much success was obtained.

In general, these micrographs tend to deceive the observer into concluding that the minor phase is dispersed in spherical domains. We have already shown in Chapter 4 that the dispersed phase in these blends is in the form of stable fibers of extremely small diameter. Moreover, these micrographs also show larger dispersed phase sizes than previously seen in the dispersed phase dissolved SEM micrographs and compared to the phase sizes found by AFM. The quite round shape of the domains evident in the micrographs is thought to be the result of the gradual removal of the material at the interface as the etching progresses. More details can be explained by following the schematics in Figure A.V.14,

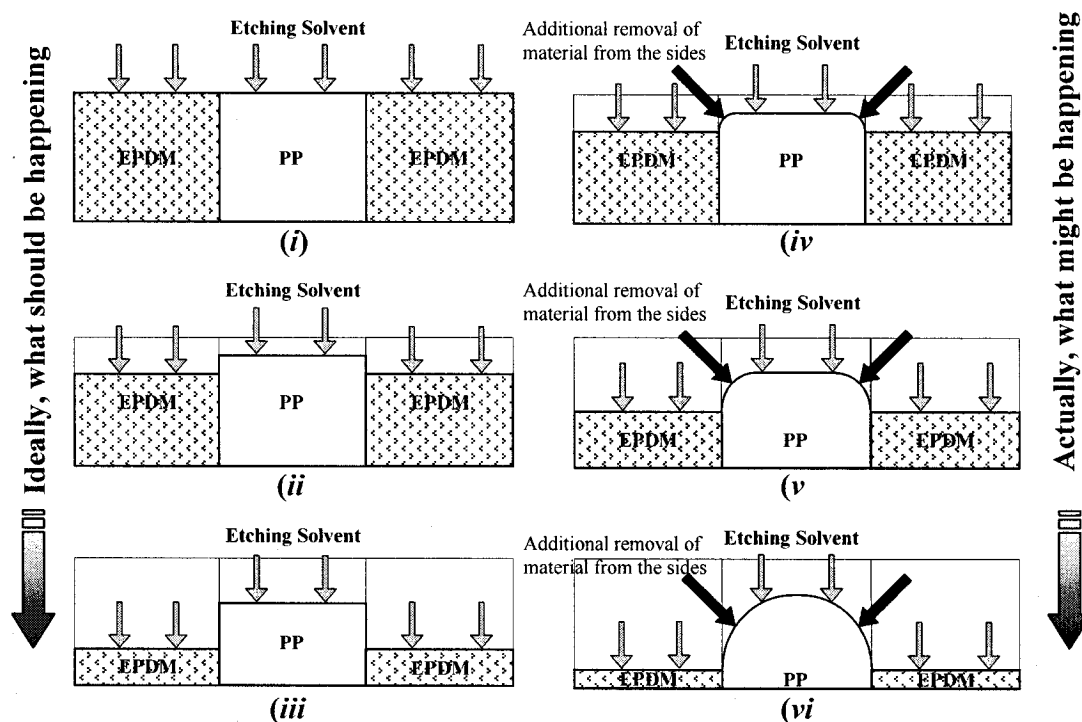


Figure A.V.14 Schematics of solvent etching process

As shown in the above schematic (i), on cryo-microtoming both the surfaces, i.e. of EPDM and PP, are perfectly plane. As the surface is exposed to the etching solvent; the solvent starts depleting the material at the surface with different rates, as shown in schematic (ii). In general, with more time of exposure, more material is supposed to be removed from the surface and better topographical contrast should result, as shown in schematic (iii). Schematics (i)-(iii), however, explain an ideal process of etching, or a general concept of etching process. In fact, as the etching gradually progresses, the corner or the interface of the slower depleting polymer, i.e. PP in this case, also gets exposed to the solvent, as shown in schematic (iv). Thus, the etching solvent can be expected to remove the material also from newly exposed corners of the dispersed

phase, shown by dark black arrows in the schematics. As the etching progresses, more and more corner surface is available for the etching solvent, as shown in schematic (v). Thus, with time, more material is expected to be removed from the interface between the dispersed droplets and matrix, giving a spherical shape to the slowly etching domains, as shown in schematic (vi). Now, if the domains are supposedly very fine in diameter, as in our case, even a little etching at the freshly exposed interface would easily give a spherical look to the dispersed domains, as evident in all solvent etched micrographs of Figure A.V.8 – 13. Thus, these are the limitations of the solvent etching process and it is suggested that the results from such studies should be used with great caution.

Nevertheless, the solvent etched micrograph through Figure A.V.8 – 13 do show some very nice cocontinuous structures. Occasionally, the micrographs show elongated fiber-like structures and the formation of cocontinuous structures by coalescence of fibers, which supports the findings in this thesis.

ANNEX VI

ESTIMATION AND APPLICATION OF CORRECTIONS

The purpose of this annex is to explain the necessity of various corrections applied throughout this thesis and to calculate and list them together.

A.VI.1 PP solubility in cyclohexane at room temperature

Compared to polyethylene, polypropylene only has an additional pendent methyl (CH_3) group associated with every other carbon atom. Based on the location of this group along the backbone chain, polypropylene can form various stereoisomers such as isotactic (crystalline), syndiotactic (crystalline), and atactic (amorphous). Today, commercially produced polypropylene grades mostly contain the crystalline isotactic polypropylene. However even with the use of very sophisticated catalysts, these grades do contain a little amorphous atactic polypropylene.

Ethylene-propylene-diene terpolymer is a random copolymer of ethylene, propylene and a small amount of diene to facilitate crosslinking. The ethylene segments of the copolymer form an amorphous portion and polypropylene segments form a crystalline portion. This combination of amorphous and crystalline nature within a molecule itself provides an elastomeric nature to this random copolymer. With almost the same base molecular composition EPDM and PP have many similar physical and chemical characteristics. The solvents for both of the polymers (depending upon the stereo-regularity for PP) are also more or less same, EPDM being more easily soluble

than PP. There is no solvent to selectively dissolve PP without dissolving EPDM. One cannot selectively dissolve EPDM without dissolving an atactic portion in the PP.

Cyclohexane is a very good known solvent for EPDM at room temperature, but as mentioned earlier, it also does dissolve the atactic portion of PP. Thus during the continuity measurements of EPDM in the PP matrix, the values of EPDM continuity should be corrected by excluding the amount of atactic polypropylene dissolved during such measurements. These measurements are especially important at low compositions of EPDM, i.e. from about 5 to 30% EPDM content, where a small dissolution of PP significantly affects the continuity values of EPDM. Figure A.VI.1 shows the values of EPDM continuity obtained without applying any such corrections for all the blends studied in this thesis.

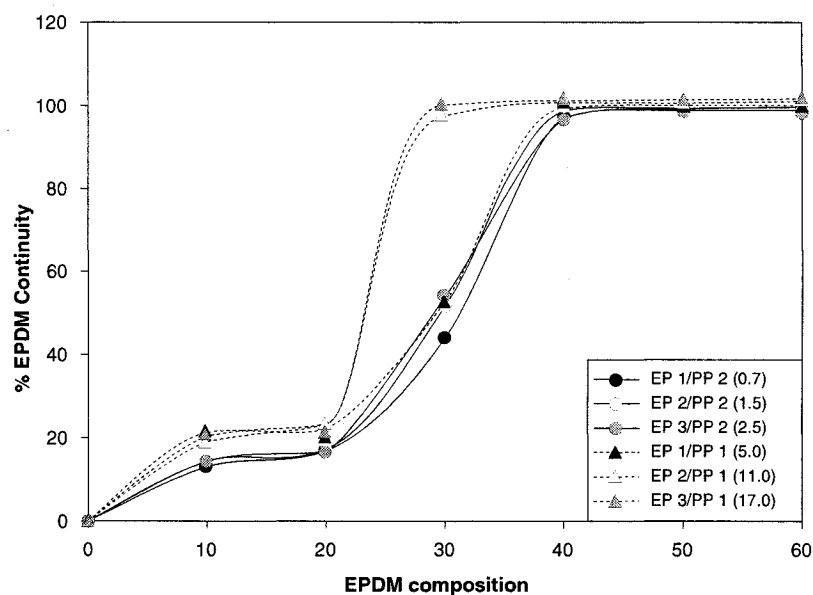


Figure A.VI.1 Non-corrected EPDM continuity development diagram

As evident from the above figure, the EPDM phase presents unusual continuity development features, e.g. very low percolation thresholds for continuity development, quite high values of continuity at low compositions of EPDM, and more than 100% continuity at higher compositions of EPDM.

To correct this diagram for the solubility of PP in cyclohexane at room temperature, initially, pure PP was subjected to an identical thermal history as the other blends, i.e. it was melt mixed with 0.05 wt.% Irganox for 8 min. at 100 rpm in an internal mixer. On completing the blending the material was quenched immediately in cold water. Then, about 1 g of material was taken and cut into small pieces, to provide more solvent-material interaction area, which would be the case in many blends after extracting partly continuous or cocontinuous EPDM phase. These pieces were weighed accurately and subjected to a cyclohexane wash at room temperature for about 48 h. The pieces were then dried at about 60°C in vacuum oven until constant weight was obtained. The samples were then subjected to another wash of fresh cyclohexane solvent and were again dried to constant weight. This procedure was repeated until the sample weight from two consecutive washes remained unchanged. Then, PP solubility in cyclohexane is calculated by using the following formula,

$$\%PP \text{ solubility} = \frac{wt.before \text{ dissolution} - wt.after \text{ dissolution}}{wt.before \text{ dissolution}} \times 100 \dots\dots\dots (A.VI.1)$$

Table A.VI.1 lists these corrections and Figure A.VI.2 presents the EPDM continuity development diagram after excluding the weight of PP dissolved in cyclohexane during the EPDM continuity measurement.

Table A.VI.1 Solubility of PP in cyclohexane at room temperature

Materials	Solubility in cyclohexane (%)
PP 1	2.6
PP 2	1.4

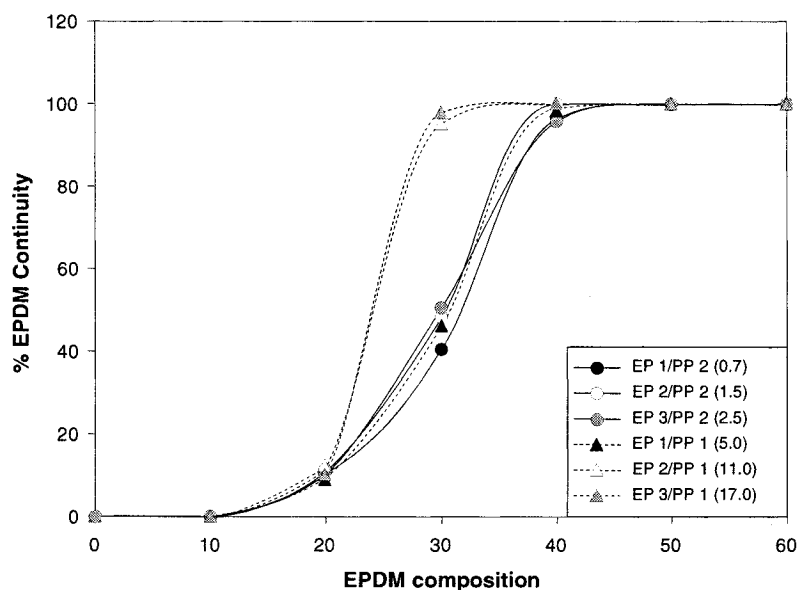
**Figure A.VI.2 Corrected EPDM continuity development diagram**

Figure A.VI.2 demonstrates that the EPDM continuity values at low compositions of EPDM diminish considerably. One obtains a smoother continuity development curve and also accurate cocontinuity values of about 100% at higher compositions of EPDM.

A.VI.2 Determination of gel content of irradiation crosslinked EPDM and the subsequent corrections for PP continuity development

As mentioned earlier, there is no solvent which dissolves PP without dissolving EPDM. Thus it becomes impossible to determine the PP continuity development in the

EPDM matrix by solvent gravimetry. To overcome this difficulty, in this thesis we irradiation crosslink the EPDM phase in the blend. Since all EPDM contains a small amount of non-crosslinkable material and as the irradiation also leads to a chain scission reaction, 100% crosslinking of the EPDM cannot be achieved. Thus, the gel content achieved by irradiation should be measured and accordingly the corrections should be applied to the PP continuity development curve. Figure A.VI.3 shows the non-corrected PP continuity development diagram for all the blends.

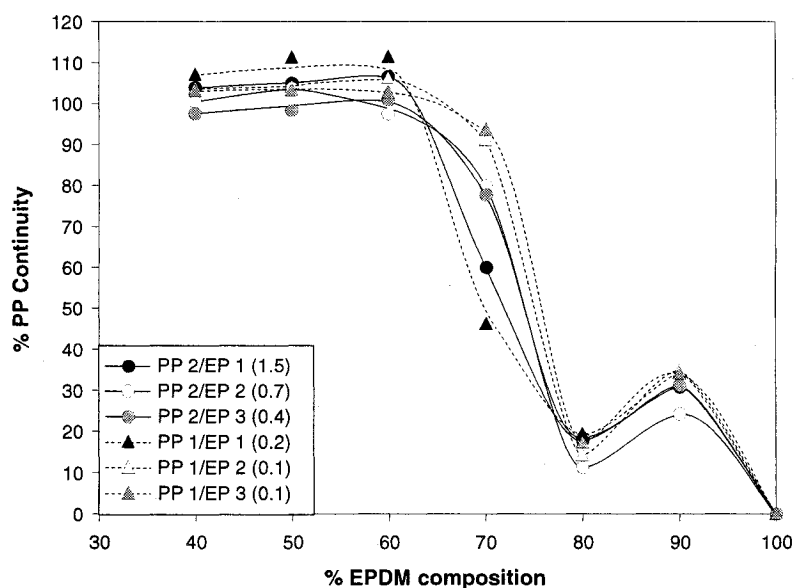


Figure A.VI.3 Non-corrected PP continuity development diagram

In order to determine the gel content of the irradiated EPDM, all the different types of pure EPDM materials used in this work were irradiated together with the blends. Then about 1 g of pure EPDM material was cut from the blend in the form of small pieces and these pieces were boiled in 100 mL of xylene for about 60 mins. After,

the pieces were immediately removed from the solvent and were dried to constant weight in the vacuum oven. The pieces were then boiled again in 100 mL of fresh xylene and were dried again to constant weight. This procedure was repeated until the sample weight from two consecutive washes remained unchanged. The gel content is calculated from the weight of the sample before and after solvent extraction. Table A.VI.2 lists the gel content determined by this process for all the EPDM materials. As evident from the table, on average about 97% of EPDM has been successfully crosslinked and on average about 3% of the EPDM remains soluble in boiling xylene. Thus the values for the PP continuity development were subsequently corrected, and the corrected PP continuity development diagram is shown in Figure A.VI.4.

Table A.VI.2 EPDM gel content on irradiation

Materials	Avg. gel content (%)
EP 1	97.4
EP 2	97.6
EP 3	96.3

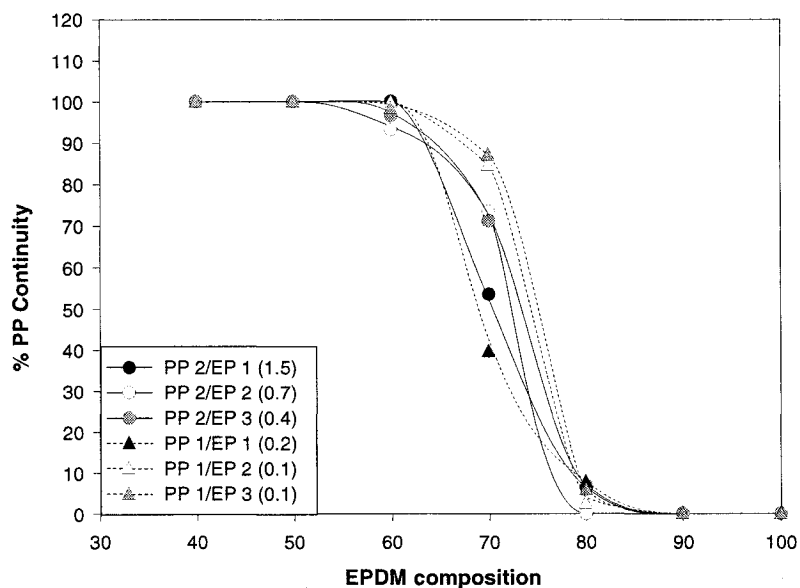


Figure A.VI.4 Corrected PP continuity development diagram

From the above figure it can be seen that the PP continuity values, especially at low compositions of PP, diminish considerably. Thus we obtain a smoother continuity development curve, and accurate cocontinuity values at higher compositions of PP.

A.VI.3 Determination of the percentage of non-crosslinkable material in EPDM

All commercial grade EPDM materials contain a small fraction of non-crosslinkable material in them. This fraction may consist of some very low molecular weight EPDM, some polyolefin homopolymer or some impurities in the material. Thus, the amount of crosslinkable EPDM available in the pure EPDM material actually decreases and this affects the calculations of the final gel content in these materials. Thus it is very important to know the amount of non-crosslinkable material in each of

the EPDM grades used in this thesis. Accordingly, the corrections were applied while determining the gel content for the chemically crosslinked blends.

To determine these corrections the weight fraction of the acetone soluble portion and the weight fraction of the cyclohexane insoluble portion in each of the EPDM materials used at room temperature should be measured.

A.VI.3.1 Acetone soluble portion of EPDM

To determine the acetone soluble portion of EPDM, about 1 g of material from each EPDM grade was taken and was cut into several small pieces. These pieces were then immersed in about 40 mL of acetone at room temperature for 48 h. The pieces were then dried in a vacuum oven to constant weight. Thereafter, the materials were subjected to another wash of acetone and were again dried to constant weight. This procedure was repeated until the sample weight from two consecutive washes remained unchanged. Based on the initial and final sample weights, the average acetone soluble fraction of each EPDM grade was calculated and is noted in Table A.VI.3.

A.VI.3.2 Cyclohexane insoluble portion of EPDM

To determine the cyclohexane insoluble portion of EPDM about 0.1 g of EPDM material was dissolved in about 200 mL of pre-filtered cyclohexane. The solution was then filtered by using a 0.8 μm pore diameter filter membrane. Afterwards, the membrane was dried to constant weight. By measuring the weight of the membrane before and after filtration, the average cyclohexane insoluble portion of EPDM was calculated and is listed in Table A.VI.3

Table A.VI.3 Average non-crosslinkable material in EPDM

Materials	Avg. acetone soluble portion (%)	Avg. cyclohexane insoluble portion (%)	Total avg. non-crosslinkable EPDM material (%)
EP 1	0.30	3.20	3.50
EP 2	0.14	0.50	0.64
EP 3	0.10	0.90	1.00